学位論文

Entangled Spin-Pseudospin Phenomena in the Bilayer Quantum Hall Systems

（二層量子ホール系におけるエンタングルドスピン・擬スピン現象）

平成 26 年 4 月博士（理学）申請

東京大学大学院理学系研究科

物理学専攻

濱　祐介

Abstract

We investigate the entangled spin-pseudospin phenomena in the bilayer quantum Hall systems, triggered by the Nambu-Goldstone mode. They are essentially new phenomena which cannot be described solely by spin or pseudospin degrees of freedom.

First, we present a systematic method to determine the symmetry breaking pattern and to derive an effective Hamiltonian for the Nambu-Goldstone modes in the total filling factor $\nu = 2$ bilayer quantum Hall systems. We then investigate the dispersion relations and the coherence lengths of the Nambu-Goldstone modes, particularly with a careful analysis in the canted antiferromagnetic phase in the $\nu = 2$ bilayer quantum Hall systems. To explore possible emergence of gapless modes and the associated interlayer phase coherence, we analyze the dispersion relations in the limit of zero tunneling energy. We find one gapless mode with the linear dispersion relation in the canted antiferromagnetic phase.

Secondly, we investigate the mechanism of interlayer phase coherence induced by the Nambu-Goldstone mode with a linear dispersion, the associated Josephson supercurrent, and its effect on the Hall resistance in the bilayer quantum Hall systems by employing the Grassmannian formalism. We show that the entangled spin-pseudospin phase coherence develops in the canted antiferromagnetic phase, while pure pseudospin phase coherence develops at $\nu = 1$. The Hall resistance in the canted antiferromagnetic phase is predicted to become anomalous precisely as in the $\nu = 1$ bilayer systems in the counterflow and drag experiments. Furthermore, in the canted antiferromagnetic phase it is shown that the total current flowing in the bilayer systems is a supercurrent carrying solely spins in the counterflow geometry: All these phenomena in the canted antiferromagnetic phase occur only in density-imbalanced configurations.

Contents

Chapter 1

Introduction

1.1 Spin and Pseudospin Degrees of Freedom

Spin is the fundamental degree of freedom in the quantum theory. It provides enormously rich phenomena such as ferromagnet [1, 2], spin Hall effect [3]-[7], and anomalous Hall effect [8]. Furthermore, in the recent years, the new type of engineering called spintronics is actively investigated [9, 10]. Spintronics is an attempt to use both spin and charge degrees of freedom, where the spin acts as an information carrier, and to construct the devices using its coherence. It has functional advantages over the conventional electronics, where the charge degree of freedom has been only used. Many attempts have been conducted, for instance, the study of long-range spin current using the proximity effect between ferromagnet and superconductivity [11], the current carried by magnons [12], and furthermore, the manipulation of nuclear spins in the semiconductor quantum Hall (QH) systems [13, 14].

By adding another type of physical degree of freedom called *pseudospin*, which plays an equivalent role to spin, the systems show much richer physics. For example, xthe pseudospin in a bilayer QH systems as a bilayer semiconductor, is the layer degree of freedom, whereas the pseudospin in monolayer graphene is the valley degree of freedom, which are the two inequivalent corners of the first Brillouin zone. Also, the pseudospin in iron phthalocyanine (FePc) on Au(111) is the orbital degree of freedom. These examples are listed in Table 1.1.

What is remarkable is that the systems possessing both spin and pseudospin exhibit the properties which cannot be described only in terms of spin and pseudospin. As seen in Table 1.1, SU(4) quantum Hall ferromagnet in monolayer graphene is the ground state, where the four energy levels are degenerated owing to the Landau filling factor, and SU(4) isospin (spin-valley) direction is spontaneously polarized [15]-[18]. SU(4) Kondo effect occurs due to the SU(4) symmetry of the Hamiltonian in the system, which leads to much higher Kondo temperature compared to the one in spin SU(2) Kondo effect [19]. The spin Josephson supercurrent will be discussed in detail in chapter 5 of this thesis. When such phenomena are realized, it seems that spin and pseudospin are coupled in complete harmony, and behave as a new type of physical degree of freedom, the *entangled spin-pseudospin*.

As seen in Table 1.1, the entangled spin-pseudospin phenomena can be seen in many systems, showing various novel phenomena. The physical systems showing the interplay between the spin and layer can also be seen in many other strongly correlated systems, for instance, bilayer

System	Pseudospin	Entangled spin-pseudospin phenomena
Bilayer QH system	Layer	Spin Josephson supercurrent
Monolayer graphene	Valley	SU(4) QH ferromagnet
Iron phthalocyanine (FePc) on Au(111)	Orbital	SU(4) Kondo effect

Table. 1.1 Examples of the entangled spin-pseudospin phenomena in various systems possessing spin and pseudospin degrees of freedom.

graphene [39, 40, 41], bilayer systems of ultracold atoms [42, 43], and neutron spin systems in the neutron star forming the alternative layer structure [44, 45]. Taking together, it is interesting to study the mechanism of entangled spin-pseudospin phenomena as a universal problem of quantum many-body problems in strongly correlated systems.

1.2 Physics of Bilayer Quantum Hall systems

In this thesis, we investigate the entangled spin-pseudospin phenomena in the bilayer QH systems, especially triggered by the Nambu-Goldstone (NG) mode as an SU(4) isospin wave. We show schematic illustration of the bilayer QH system in Fig. 1.1. This is because, as we explain later on, the QH systems present various rich and beautiful phenomena induced by the NG mode, which are well worth studying theoretically, and furthermore, there is much possibility to be tested experimentally. Moreover, both theoretical and experimental developments of recent related topics, such as topological insulators [20]-[32] and QH effect in graphene [33]-[38], are still being made. Based on these facts, the bilayer QH system can be considered as one of the most suitable system to study the entangled spin-pseudospin phenomena.

As is well known, QH effect is one of the great discoveries of macroscopic quantum phenomena in the two-dimensional electron systems [114, 115], which can be compared with the discovery of superconductivity. It is not only interesting in the condensed matter physics, but also deeply connected to the concepts developed in particle and nuclear physics [59], for example, the emergence of the skyrmion excitations [46], which leads to the realization of nontrivial spin texture and electron density modulation [47]-[53].

Particularly, physics of the bilayer QH systems are enormously rich owing to the intralayer and interlayer phase coherence controlled by the interplay between the spin and the layer (pseudospin) degrees of freedom [59, 60]. The interlayer phase coherence is a novel phenomenon in the bilayer QH systems [54, 55, 59, 67], where it is enhanced in the zero tunneling gap limit, $\Delta_{\rm SAS} \to 0$. For instance, at the filling factor $\nu = 1$ there arises a unique phase, the spin-ferromagnet and pseudospin-ferromagnet phase, which has been studied well both theoretically and experimentally. One of the most interesting phenomena is the Josephson tunneling between the two layers [62]-[68], whose first experimental indication was obtained in Ref. [70]. Quite recently, careful experiments [71]-[73] were performed to explore the condition for the tunneling current to be dissipationless.

Other examples are the anomalous behavior of the Hall resistance reported in counterflow experiments [74, 75] and in drag experiments [76, 77]. They are triggered by the Josephson supercurrent within each layer [78, 79]. These phenomena are triggered by the NG mode

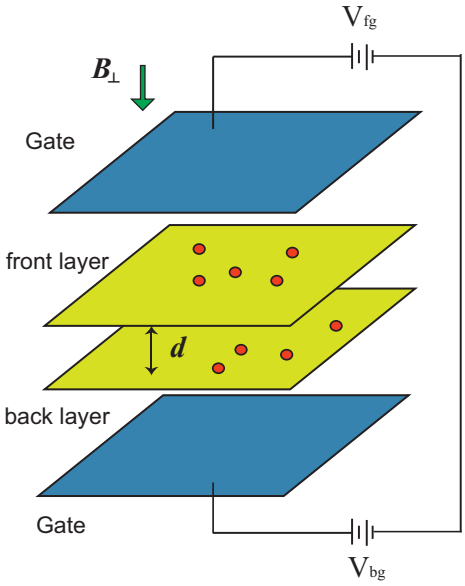

Si-GaAs		15nm
AlGaAs		40nm
AlGaAs		6nm
AlGaAs		200nm
AlGaAs		50nm
GaAs	front layer	20nm
AlGaAs		2.2nm
GaAs	back layer	20nm
AlGaAs		20nm
Ga/AlGaAs Superlattice		400nm
GaAs		50nm
n^+- GaAs Substrate		

Fig. 1.1 The schematic illustration of the bilayer QH systems. This figure is adapted from Refs. [59, 125]. Here we note that the figure on the right-hand side originates from the wafer; R195, K. Muraki NTT-BRL.

describing a pseudospin wave. Here we show the experimental data due to [74, 75, 76, 77] in Figs. 1.2-1.5, and summarize the content of these data since they are important data, motivating the works of this thesis. Let us focus on the region where the total filling factor ν takes 1 in Figs. 1.2-1.5, since the aim of these experiments is to study the QH effects in bilayer systems at $\nu = 1$ where the interlayer phase coherence is spontaneously developed. To do this, the Hall and diagonal resistances were measured under various geometries, as shown in Fig. 1.6. There are three types of geometries, the standard geometry, the counterflow geometry, and the drag geometry. In the standard geometry, the same amount of the currents with the same direction are applied to both layers [Fig. 1.6 (a)]. In the counterflow geometry, the currents are applied to both layers, with the same amount but in the opposite direction [Fig. 1.6 (b)]. In the drag geometry, the current is applied to one of the layers [Fig. 1.6 (c)]. The striking behaviors of the QH effects can be seen clearly in the counterflow (the bottom part of Fig. 1.2 or the right part of Fig. 1.3) and the drag geometry shown in Fig. 1.4. These three figures were obtained in the systems where the electron density in the front layer is equal to the one in the back layer (density-balanced configuration). The results shown in Fig. 1.5 are the Hall resistances in the drag geometry in the density-imbalanced configuration. We denote the electron density in the front layer as $\rho_0^{\rm f}$ whereas that in the back layer as $\rho_0^{\rm b}$.

First, let us take a look at the data of the counterflow geometry shown in the bottom part of Fig. 1.2 or 1.3 at $\nu = 1$. What is interesting is that not only the diagonal resistivity R_{xx} but also the Hall resistivity R_{xy} vanish. On the other hand, in the drag geometry shown in Fig. 1.4, even though the current is injected to the back layer and the Hall voltage or the Hall resistance is measured in the front layer, the non-vanishing Hall voltage or Hall resistance are detected (the configuration B in Fig. 1.4). Moreover, it has been reported in

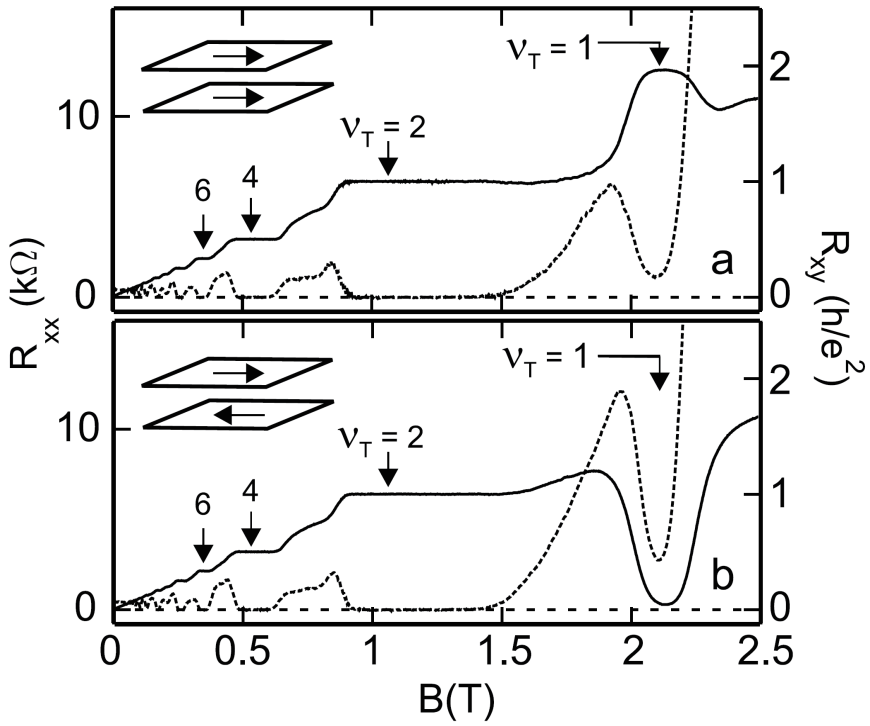

Fig. 1.2 The experimental data for the longitudinal and Hall resistance versus the magnetic field (or the total filling factor ν). The experiment was conducted in the condition $T = 50$ mK, $\rho_0^{\rm f} = \rho_0^{\rm b} = 2.54 \times 10^{10}$ cm^{-2}, and $\Delta_{\rm SAS} \sim 0.1$ mK. The top figure is the data in the standard geometry, while the bottom figure is the one in the counterflow geometry. This figure is taken from [74].

Ref. [76] that the Hall voltage measured in the configuration B and D, where the Hall voltage was measured in the layer with the current injection, were equivalent. By taking account of these experimental results, it can be considered that when the interlayer phase coherence is spontaneously developed in the bilayer QH systems, the Hall voltage in one layer becomes equivalent to the one in the other layer, as we discuss again in section 3.4 and subsection 5.2.1.

To understand the physics of bilayer QH systems in the presence of the interlayer phase coherence, there is a description due to the exciton condensate [68, 69, 136]. In this description, it is considered that supercurrent generated by the exciton condensate flows so that the Hall voltages in the front and back layer become equivalent. Although this description provides simply the explanation of the realization of the two Hall voltages becoming equivalent, it still remains as the picture for the explanation for the experimental results at this stage. On the other hand, Ezawa et al., have established the quantitative description at $\nu = 1$ based on the noncommutative quantum theory [59, 101, 102, 103, 134], by constructing the effective theory of the interlayer phase field and the canonical conjugate density-imbalanced field as a NG mode, which is responsible for the creation of the interlayer phase coherence [78, 79]. They analyzed the QH effect in the presence of the interlayer phase coherence, and calculated the Hall resistivity in a concrete mathematical formalism.

On the other hand, the phases arising at $\nu = 2$ are quite nontrivial. According to the one-

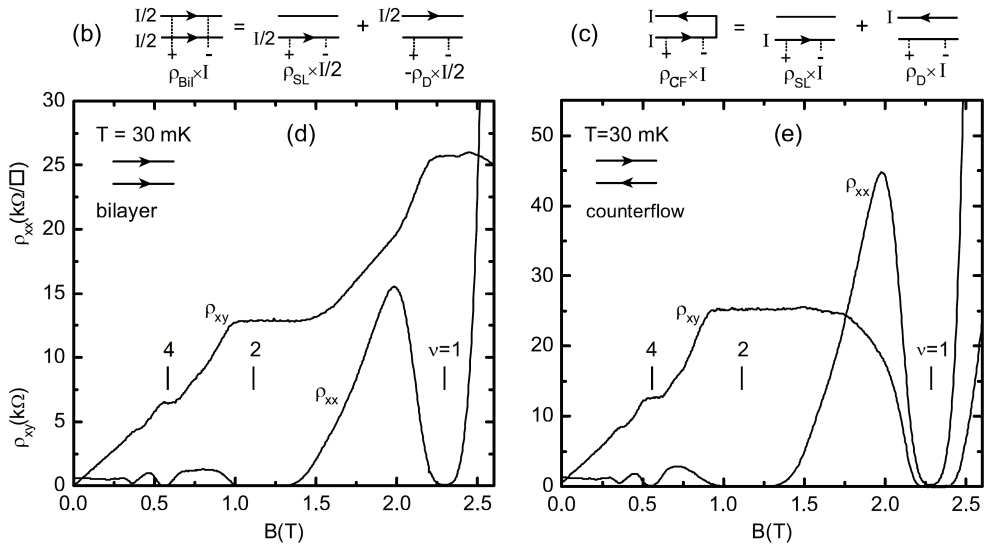

Fig. 1.3 The experimental data for the longitudinal and Hall resistance versus the magnetic field (or the total filling factor ν). The experiment was conducted in the condition $T = 30$ mK and $\rho_0^{\rm f} = \rho_0^{\rm b} = 2.75 \times 10^{10}$ cm^{-2}. The left figure is the data in the standard geometry. On the other hand, the right figure is the data in the counterflow geometry. This figure is taken from [75].

body picture we expect to have two phases depending on the relative strength between the Zeeman gap $\Delta_{\rm Z}$ and the tunneling gap $\Delta_{\rm SAS}$. One is the spin-ferromagnet and pseudospins-inglet phase (abridged as the spin phase) for $\Delta_{\rm Z} > \Delta_{\rm SAS}$; the other is the spin-singlet and pseudospin ferromagnet phase (abridged as the pseudospin phase) for $\Delta_{\rm SAS} > \Delta_{\rm Z}$. Interestingly, at $\nu = 2$ a canted antiferromagnetic phase (abridged as the CAF phase) emerges as an intermediate phase of the spin and pseudospin phase. This is a novel phase where the spin direction is canted coherently and makes antiferromagnetic correlations between the two layers [80, 81]. The previous authors investigated the phase diagram in terms of $\Delta_{\rm SAS}$-d plane (d denotes the layer separation), and the dispersions of intersubband spin-density-wave excitations in the time-dependent Hartree-Fock method [80, 81]. They suggested that the emergence of the CAF phase is due to the softening of the spin collective modes. Later on, various theoretical studies for $\nu = 2$ QH states have been done [82]-[90].

The experimental evidence of the CAF phase was first suggested by Pellegrini et al., using inelastic light scattering spectroscopy [91, 92]. They have investigated the softening of the spin excitation mode, and its relation to the quantum phase transition. Subsequently, the experimental study for the $\nu = 2$ bilayer system as well as the verification of the existence of the CAF phase were obtained through capacitance spectroscopy and magnetotransport measurements [93]-[98]. The ground state structure of the $\nu = 2$ bilayer QH systems has been investigated based on the SU(4) formalism [99]-[104]. The expectation values of the SU(4) isospin operators are the order parameters, in terms of which an anisotropic SU(4) nonlinear sigma model has been derived to describe low-energy coherent phenomena [99].

The effective Hamiltonian for the NG modes has not been derived before. Although there

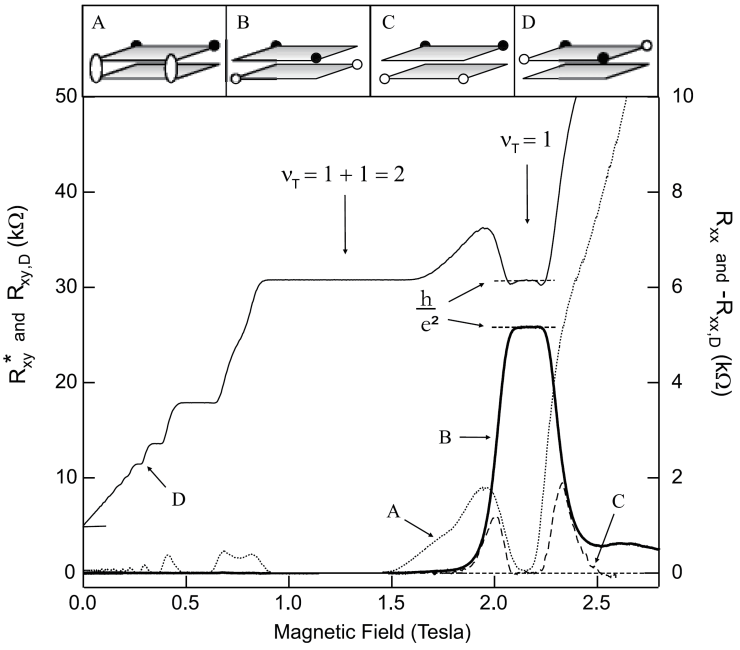

Fig. 1.4 The experimental data for the longitudinal and Hall resistance versus the magnetic field (or the total filling factor ν) in the drag geometry. The open circles denote the current injection whereas the solid circles the voltage measurement. The curve A denotes R_{xx} in the configuration where current was injected in both layers. The curves B and C denote R_{xy} and R_{xx}, respectively, in the configuration where the current was injected in the layer opposite to the one where the voltage measurement was performed. The curve D denotes R_{xy} in the configuration where current injection and voltage measurement was performed in the same layer. The experiment was conducted in the condition $\rho_0^{\rm f} = \rho_0^{\rm b} = 2.6 \times 10^{10}$ cm^{-2}, and $\Delta_{\rm SAS} \sim 0.1$ mK. This figure is taken from [76].

are some results with the use of Grassmannian fields in the spin and pseudospin phases [99], no attempts have been made in the CAF phase. On the other hand, experimentally, a role of a NG mode has been suggested by nuclear magnetic resonance in the CAF phase [105, 106, 107, 125].

It is an urgent and intriguing problem what kind of NG modes emerges in the CAF phase, since if gapless modes emerge in the CAF phase as well as in the $\nu = 1$ bilayer QH system, the possibility of the entangled spin-pseudospin phenomena, owing to the interlayer phase coherence is thoroughly expected.

1.3 Outline

In this thesis, we study the effective theories for NG modes and the associated Josephson supercurrent in $\nu = 2$ bilayer QH systems to explore the entangled spin-pseudospin phenomena in the bilayer QH systems. We do these by extending the theory established by Ezawa et al., [78, 79] based on the noncommutative quantum theory [59, 101, 102, 103, 134] to $\nu = 2$. We do not follow the physical picture of exciton condensation. The reason is that since this description remains rather qualitative for the explanation of the experimental results, it is not clear how to apply it to obtain quantitative results in the case of a complicated ground state structure

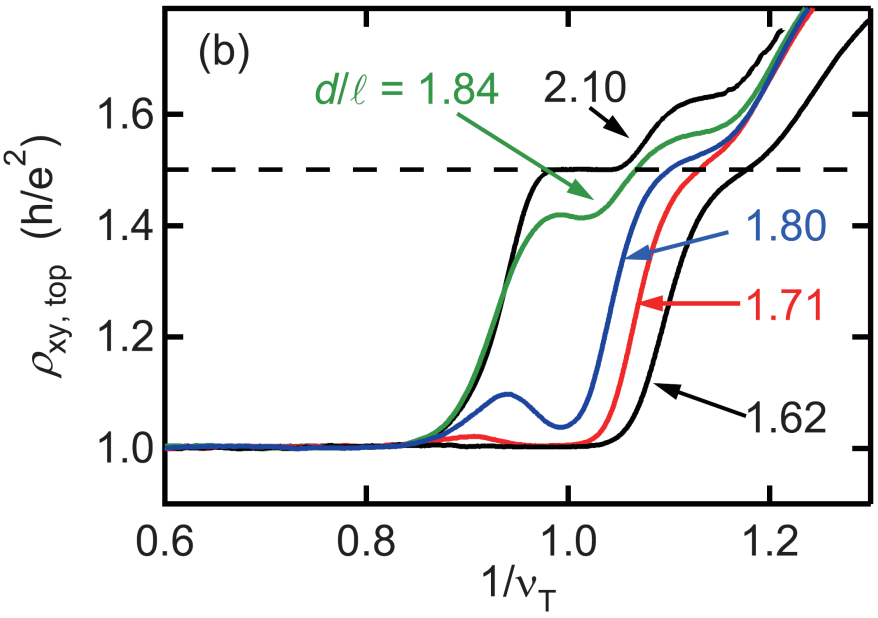

Fig. 1.5 The experimental data for the longitudinal and Hall resistance versus the total filling factor ν in the drag geometry. The experiment was conducted in the condition $\rho_0^{\rm f} : \rho_0^{\rm b} = 2 : 1$. As d/l_B increases, the Hall resistance in the front layer $R_{xy}^{\rm f}$ changes from $R_{\rm K}$ to $3R_{\rm K}/2$, since the QH state changes from $\nu = 1$ bilayer QH state to $\nu_{\rm f} = 2/3$ monolayer QH state. This figure is taken from [77].

at $\nu = 2$. Indeed, the extension of the description of the exciton condensation to $\nu = 2$ has not been established yet. On the other hand, the theory established in [59, 101, 102, 103, 134] can be applied not only to $\nu = 1$ but also to $\nu = 2$. By taking account of the difference of the ground state structure such as the expectation values of the SU(4) isospins, we can clearly extend the theory for $\nu = 1$ constructed in [78, 79] to $\nu = 2$. In this way, we can construct the effective theory for NG modes at $\nu = 2$, described in terms of the interlayer phase field ϑ and the canonical conjugate field σ. Then the development of the interlayer phase coherence and the associated QH effects can be clearly understood. In addition, the SU(4) formalism used in [59, 101, 102, 103, 134] enables us to construct the entangled spin-pseudospin phenomena shown in chapter 5. The construction of the effective theory of the NG mode is also supportable from the experimental point of view, since the existence of the NG mode in the CAF phase has been pointed out from the experimental results of nuclear spin relaxation using the resistively-detected nuclear-magnetic-resonance (RD-NMR) in Refs. [105, 106, 107, 125]. As a result, we have derived the new phenomena in the CAF phase such as entangled spin-pseudospin phase coherence, the associated QH effects, and spin Josephson supercurrent. These phenomena have not been observed yet, since they are all realized at the density-imbalanced configuration, whereas the experimental data for $\nu = 2$ QH effects shown in Figs. 1.2-1.4 are the data in the density-balanced configuration.

We first develop a generic formalism to determine the symmetry breaking pattern and to derive the effective Hamiltonian for the NG modes in $\nu = 1$ and 2 bilayer QH systems. The

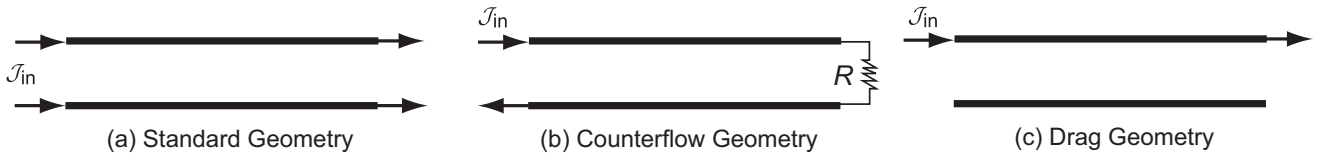

Fig. 1.6 The schematic illustrations of the in-plane current in three different geometries. (a) In the standard geometry, the current injected to front layer flow in same direction with same amount with the one flow in the back layer. (b) In the counterflow geometry, the current injected to the front layer flow with same amount but in opposite direction to the one flow in the back layer. Consequently, the net current becomes zero. (c) In the drag geometry, the current is injected only to the one of the layer. This figure is adapted from Ref. [59].

symmetry breaking pattern for $\nu = 1$ reads

$$\mathrm{SU}(4) \to \mathrm{U}(3), \tag{1.1}$$

and there appear six NG modes, while for $\nu = 2$

$$\mathrm{SU}(4) \to \mathrm{U}(1) \otimes \mathrm{SU}(2) \otimes \mathrm{SU}(2), \tag{1.2}$$

and eight NG modes emerge in each phase; the spin phase, the pseudospin phase, and the CAF phase. The corresponding NG modes in the two phases (spin/CAF or pseudspin/CAF) match smoothly at the phase boundary. All the modes are actually gapped except along the phase boundaries due to explicit symmetry breaking terms. It is important if gapless modes emerge in the limit $\Delta_{\mathrm{Z}} \to 0$ or $\Delta_{\mathrm{SAS}} \to 0$, where the spin coherence or the interlayer coherence is enhanced. Gapless modes are genuine NG modes associated with spontaneous symmetry breaking. Naturally we have gapless modes in the spin phase as $\Delta_{\mathrm{Z}} \to 0$ and in the pseudospin phase as $\Delta_{\mathrm{SAS}} \to 0$. We find one gapless mode with the linear dispersion relation in the CAF phase as $\Delta_{\mathrm{SAS}} \to 0$.

We then investigate the interlayer phase coherence, the associated NG modes, its effective Hamiltonian, the Josephson supercurrent provoked by these NG modes, and its effect on the Hall resistance in the bilayer QH system at $\nu = 1, 2$, by employing the Grassmannian formalism.

This thesis is organized as follows [Fig. 1.7]:

- In chapter 2, we first overview the quantum mechanical theory of QH effect in the monolayer systems. The key concept to understand the QH effect is the Landau quantization. We also overview the physics of bilayer QH system. The new physical quantities such as pseudospin, interlayer tunneling energy, and the imbalanced parameter and bias voltage are introduced. We also present an overview of Landau level projection formalism and SU(4) effective Hamiltonian, which is the basic Hamiltonian for NG modes.
- In chapter 3, we study the NG-mode spectrum and the associated Josephson supercurrent in $\nu = 1$ bilayer QH systems. We first review the ground state structure in $\nu = 1$. By taking account of them, we derive an effective Hamiltonian for the NG modes. We

introduce a complex-projective (CP^3) field to analyze the $\nu = 1$ bilayer QH systems. The CP^3 field emerges when composite bosons undergo Bose-Einstein condensation [59]. We then discuss the SU(4) symmetry breaking pattern and make perturbative analysis of the NG-mode spectrum, such as the dispersion relations and the coherence lengths. We study the dispersions and the coherence length in the limit $\Delta_{\rm SAS} \to 0$, to explore a possible emergence of the interlayer phase coherence. We find that the NG mode as a pseudospin wave mode has linear dispersion relation and its coherence length diverges in the zero tunneling gap limit. All the other modes are gapped.

We next analyze the nonperturbative phase coherent phenomena developed by the NG mode having linear dispersion, where the phase field $\vartheta(\mathbf{x})$ is essentially classical and may become large, which is necessary to analyze the associated Josephson supercurrent. We then show that the Josephson supercurrent flows within the layer when there is inhomogeneity in $\vartheta(\mathbf{x})$. We show the anomalous behavior of the Hall resistivity in the counterflow and drag geometries, which was also studied in [78]. Finally, we compare our results with the experimental data obtained in [74, 75, 76, 77].

- In chapter 4, where the main results of this thesis are shown, we study the NG-mode spectrum and the associated Josephson supercurrent in $\nu = 2$ bilayer QH systems. We begin from reviewing the ground state structure in $\nu = 2$ based on Ref. [104]. There are three phases; the spin phase, the pseudospin phase, and the CAF phase. Then we discuss the SU(4) symmetry breaking pattern and the NG-mode spectrum, such as the dispersion relations and the coherence lengths for all three phases. There are two approaches for doing this; the Grassmannian formalism and the nonlinear representation [130, 131]. In this chapter we adopt the Grassmannian formalism since one-body states occupied by the electrons and the emergence of the associated excitation modes can be seen clearly. Furthermore, it provides us with a clear physical picture and enables us to describe nonperturbative phase coherent phenomena in the bilayer QH systems. The analysis in terms of the nonlinear representation is discussed in Appendix C. The basic field in $\nu = 2$ is the Grassmannian field consisting of two CP^3 fields. In particular, we carefully investigate NG-mode spectrum in the CAF phase. We study the dispersions and the coherence lengths in the limit $\Delta_{\rm SAS} \to 0$, to explore a possible emergence of the interlayer phase coherence in the CAF phase. We find one coherent mode having the linear dispersion with divergent coherence length.
- In chapter 5, we analyze the nonperturbative phase coherent phenomena developed by the NG mode having a linear dispersion, described in terms of the density difference field $\sigma(\boldsymbol{x})$ and its canonical conjugate field $\vartheta(\mathbf{x})$, by retaining solely this gapless mode. We show that the entangled spin-pseudospin phase coherence is developed by this phase field, and R-spin operators play the key role for the creation of entangled spin-pseudospin phase coherence. We also study the associated Josephson supercurrent. We then study the QH effect in the presence of the Josephson supercurrent, concretely, its effect on the Hall resistivity in each layer in the counterflow and drag geometries. The derivation of the basic formulas for the currents in the QH systems from the quantum-mechanical theory in the noncummutative geometry is shown. The Josephson supercurrent in the

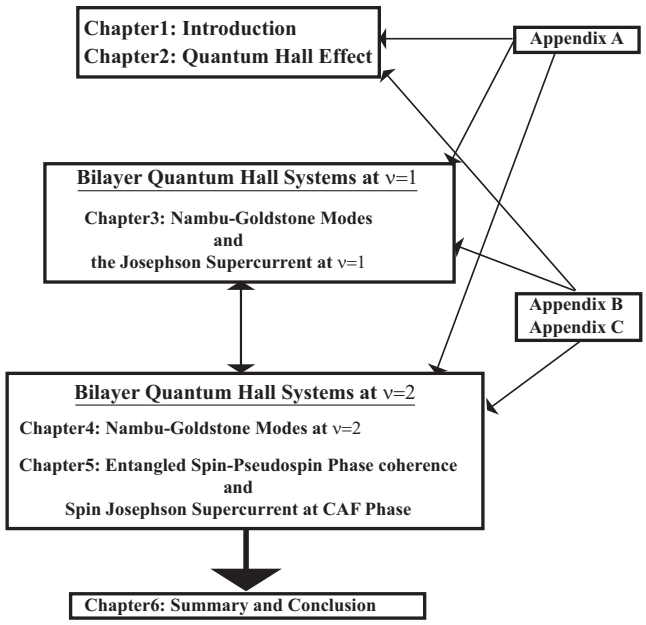

Fig. 1.7 The content of this thesis. It consists of six chapters.

CAF phase leads to the same formula of the anomalous Hall resistivity for the counterflow and drag geometries as the one at $\nu = 1$. Interestingly, the total current flowing in the CAF phase is a Josephson supercurrent carrying solely spins in the counterflow geometry. We also remark that the Josephson supercurrent flows both in the balanced and imbalanced systems at $\nu = 1$ but only in imbalanced systems at $\nu = 2$. We note that the impurity effect is not included in this thesis, when we discuss the QH effect.

- In chapter 6, we summarize our results and discuss future problems.
- In appendices, we present the basic physical quantities and their numerical values in QH systems, the wave functions in the symmetric gauge, the properties of group SU(4), quantum theory in noncommutative geometry, and the calculation of NG modes in the nonlinear representation.

Several remarks are in order here. (i) The summation is taken for indices denoting spatial coordinates and SU(4) isospins, which are repeated twice. (ii) We call the current carried by the interlayer phase field as " Josephson supercurrent". This terminology is motivated by the fact that this current is induced to decrease the phase difference, just like the dc-Josephson effect in the usual superconductivity, (iii) We only discuss the integer bilayer (or monolayer) QH systems, concretely at the total filling factor $\nu = 1$ or 2. (iv) In our calculation the impurity potential is not included, although it is responsible for formating the plateau.

We make further comments on remarks (ii) and (iii). We would like to focus on rich and interesting phenomena owing to the collective excitation modes possessing spin or pseudospin in integer QH systems, simply by neglecting the impurity effects which generate the Hall plateau. There are two reasons. One is that so far in quantum theory [59, 101, 102, 103, 134], it is possible to make a mathematically rigorous treatment to derive an effective Hamiltonian

for NG modes only in the absence of impurities. Second is that the phenomena which we have studied in this thesis may be expected to be realized even if impurities are included and the Hall plateau is generated, just as various intralayer coherent phenomena hold experimentally in the monolayer systems with impurities. Indeed, various interlayer coherent phenomena intrinsic to the bilayer systems are known experimentally to emerge in samples with impurities.

(v) Sections 4.2 through 4.6 in chapter 4, chapter 5, and Appendix C, are the original part of this thesis, the NG modes in $\nu = 2$ bilayer QH systems, the entangled spin-pseudospin phase coherence, the Josephson supercurrent and the associated QH effects, the spin Josephson supercurrent in the CAF phase, and the calculation of NG modes in the nonlinear representation. They are written based on author's papers [108, 109, 110, 111], which were collaborated with Dr. Yoshimasa Hidaka, Prof. George Tsitsishvili, and Prof. Zyun F. Ezawa. In order to understand our original part well, in chapter 3 we present the discussions on the NG mode and the Josephson supercurrent in the $\nu = 1$ bilayer QH systems, based on the previous works, in particular [59, 74, 75, 76, 77, 78, 79]. It is because the works of the QH effects in the presence of the entangled spin-pseudospin phase coherence in the CAF phase are motivated by the QH effects in the presence of the interlayer phase coherence at $\nu = 1$.

Chapter 2

Quantum Hall Effect

In the classical Hall effect, the Hall resistivity shows a linear behavior as a function of the external magnetic field. What has been found experimentally in the 20th century, was, however, totally different behavior. When a high magnetic field is applied to the two-dimensional electron systems, the diagonal resistivity vanishes, and at the same time, the Hall resistivity is quantized as 1/(filling factor) times the von Klitzing constant $R_{\mathrm{K}} = h/e^2$, with formating the plateau. This is called the quantum Hall (QH) effect. In this chapter, we review the basic features of monolayer and bilayer QH systems. The key concept for understanding the QH effect is the Landau quantization.

This chapter is organized as follows. In section 2.1 we review the quantum mechanical theory for monolayer quantum Hall systems. Then we review the basic features of the bilayer QH systems in section 2.2. The description of this chapter is based on [54, 57, 58, 59, 61]

2.1 Quantum Hall Effect in the Monolayer Systems

2.1.1 Classical Hall Effect and Quantum Hall Effect

Classical Hall Effect

We consider the motion of electrons according to the classical electrodynamics. When the electrons are moving with velocity $\boldsymbol{v}$ in an two-dimensional xy plane in the presence of a magnetic field $\boldsymbol{B} = (0, 0, -B_\perp)$ with $B_\perp > 0$, applied to the z direction, and an electric field $\boldsymbol{E}$ applied perpendicular to $\boldsymbol{B}$, the equation of motion for electron with mass M is given by

$$M\frac{d\boldsymbol{v}}{dt} = -e(\boldsymbol{E} + \boldsymbol{v} \times \boldsymbol{B}). \tag{2.1}$$

At first, let us consider the electron motion without the electric field. As is well known, electron shows a circular movement which is called the cyclotron motion, where the frequency is given by $\omega_{\mathrm{c}} = eB_\perp/M$. By decomposing the coordinate of the electron into the central and relative coordinate as $\boldsymbol{x} = \boldsymbol{X} + \boldsymbol{R}$, and denoting the radius of the cyclotron motion as R_0, the motion of electron is expressed as

$$\boldsymbol{x} = (x, y) = (X, Y) + R_0\left(\cos\omega_{\mathrm{c}}t, \sin\omega_{\mathrm{c}}t\right). \tag{2.2}$$

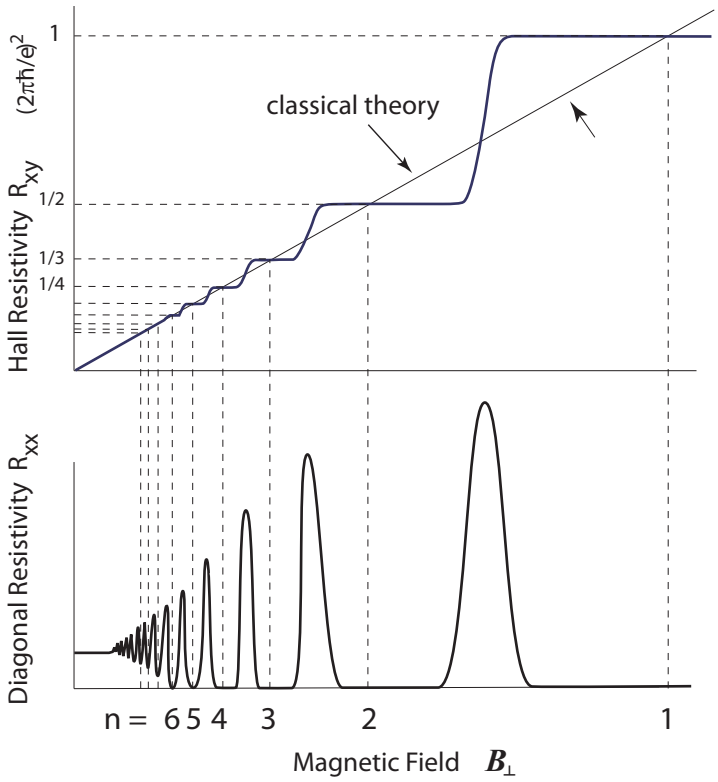

Fig. 2.1 The schematic illustration of the integer QH effect. According to the classical Hall effect, the Hall resistivity R_{xy} is proportional to the magnetic field $B_\perp$ with the vanishing diagonal resistivity R_{xx}, as indicated by thin line. However in a actual systems where an high magnetic field applied, the Hall and diagonal resistivity, R_{xy} and R_{xx} show drastically different behavior (the solid lines); the Hall resistivity R_{xy} is quantized with formating an series of plateau, whereas the diagonal resistivity R_{xx} vanishes with the Schubnikov-de Haas oscillations. This figure is taken from [59].

We next consider the case where the electric field is also applied to the system. The velocity of the electron becomes

$$\boldsymbol{v} = \left(-\frac{E_y}{B_\perp}, \frac{E_x}{B_\perp}, 0\right) + R_0\omega_{\rm c}\left(-\sin\omega_{\rm c}t, \cos\omega_{\rm c}t, 0\right). \tag{2.3}$$

The new type of velocity with the magnitude $|\boldsymbol{E}|/B_\perp$ arises due to the presence of the electric field. It is called the drift velocity. The motion of electron is given by the sum of drift and cyclotron motion. We see that the current $\boldsymbol{\mathcal{J}}$ flows in a direction perpendicular to the electric field $\boldsymbol{E}$. This is due to the Lorentz force $e(\boldsymbol{v}\times\boldsymbol{B})$.

From now on, we consider the static current, $d\boldsymbol{v}/dt = 0$, flowing in the system with homogeneous density $\rho(\boldsymbol{x}) = \rho_0$. Then the electric current $\boldsymbol{\mathcal{J}} = -e\rho_0\boldsymbol{v}$ is expressed in terms of the magnetic and electric field as

$$\boldsymbol{\mathcal{J}} = (\mathcal{J}_x, \mathcal{J}_y) = \left(\frac{e\rho_0}{B_\perp}E_y, -\frac{e\rho_0}{B_\perp}E_x\right). \tag{2.4}$$

Since the electric current only exists in the xy plane, the electric field $\boldsymbol{E}$ and current $\boldsymbol{\mathcal{J}}$ satisfy the relations,

$$\boldsymbol{E} = \boldsymbol{R}\boldsymbol{\mathcal{J}}, \tag{2.5}$$

or writing explicitly,

$$E_x = R_{xx}\mathcal{J}_x + R_{xy}\mathcal{J}_y, \qquad E_y = R_{yx}\mathcal{J}_x + R_{yy}\mathcal{J}_y, \tag{2.6}$$

with $R_{xx} = R_{yy}$ and $R_{xy} = -R_{yx}$. $\boldsymbol{R}$ is called the resistivity tensor. Comparing (2.4) and (2.6), we obtain

$$R_{xx} = R_{yy} = 0, \quad R_{xy} = -R_{yx} = -\frac{B_\perp}{e\rho_0}. \tag{2.7}$$

Consequently, the resistivity R_{xy} $(= -R_{yx})$ is proportional to the magnetic field $B_\perp$, as shown in Fig. 2.1.

Experimentally, as shown in Fig. 2.2, the Hall resistivity and the diagonal resistivity are measured in the following way; we apply homogeneous current $J_{\rm tot}$ to the system along the x axis, and measure V_x and V_y. Here we denote the distance between electrode 1 and 2 by L, and the width of the sample by W. The electric current density $\boldsymbol{\mathcal{J}}$ and the electric field $\boldsymbol{E}$ are given by

$$\begin{aligned} &\mathcal{J}_x = \frac{J_{\rm tot}}{W}, \quad \mathcal{J}_y = 0, \\ &E_x = \frac{V_{12}}{L} = \frac{V_x}{L}, \quad E_y = \frac{V_{13}}{W} = \frac{V_y}{W}, \end{aligned} \tag{2.8}$$

where we have taken the current flowing into the x direction. Then, when E_x and E_y are measured, the Hall and diagonal resistivity are determined from the equations

$$R_{\rm Hall} \equiv \left|\frac{E_y}{\mathcal{J}_x}\right| (= |R_{xy}| = |R_{yx}|), \quad R_{xx} \equiv \frac{E_x}{\mathcal{J}_x}. \tag{2.9}$$

Quantum Hall Effect

In the previous argument, we have shown that the Hall resistivity is a linear function of the perpendicular magnetic field $B_\perp$ in an homogeneous density ρ_0. However, strikingly different behavior has been discovered experimentally. As shown in Fig. 2.1, it shows the following two intriguing features and is called the QH effect:

(i) the Hall resistivity is quantized as

$$R_{\rm Hall} = \frac{R_K}{\nu}, \tag{2.10}$$

with $R_K = h/e^2 \approx 25812.807\Omega$, which is called the von Klitzing constant. ν is called the Landau filling factor, whose meaning will be discussed in detail later on. Roughly speaking,

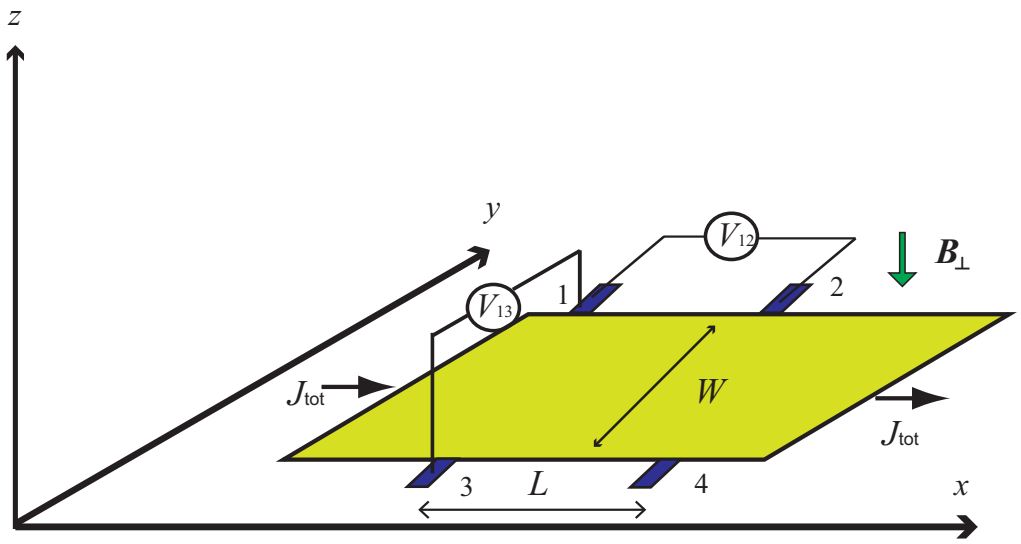

Fig. 2.2 The schematic illustration on the measurement of the Hall and diagonal resistivity $R_{\rm Hall}$ and R_{xx}, respectively. By injecting the homogeneous electric current $J_{\rm tot}$, we measure $V_{12} = V_x = E_x/L$ and $V_{13} = V_y = E_y/W$. Then the Hall and diagonal resistivity are determined from the relations $R_{\rm Hall} = |E_y/\mathcal{J}_x|$ $(= |R_{xy}| = |R_{yx}|)$ and $R_{xx} = E_x/\mathcal{J}_x$. This figure is adapted from Ref. [58].

it describes the number of occupied Landau levels and characterizes the quantum Hall state. Moreover, the flat region is formed with a focus on the filling factor for each value, and as a result, a series of plateau is created.

(ii) The diagonal resistivity vanishes at the magnetic field taking the value of the filling factor ν, with the Schubnikov-de Haas oscillations.

Historically the classical Hall effect was investigated in [112]. Then about hundred years later, the quantum theory of the Hall effect has been studied by Ando [113]. Subsequently, the integer QH effect was discovered by von Klitzing experimentally in 1980 [114], and soon later, the experimental discovery of the fractional QH effect was done by Tsui, Strormer and Gossard in 1982 [115], and the theoretical explanation were given by Laughlin [116, 117]. Jain introduced the concept called composite fermion in order to understand the physics of fractional QH systems [118] (for fractional QH effect, see also [54, 119]). On the other hand, Halperin studied the edge effect of the QH systems [120], and subsequently, the QH effect was studied from the topological point of view with the formula called the TKNN invariant [121, 122]. Haldane has studied the QH effect without Landau levels in the two-dimensional lattice systems [123]. With these studies as a starting point, the study of condensed matter physics from the topological point of view has made a great progress. Furthermore, previous studies led to the birth of topological insulator with time-reversal symmetry (quantum spin Hall systems), where gapless helical edge states exist, and is distinguished from the ordinary insulator [20]-[32]. Another important topic related to the development of the QH physics is the discovery of the unconventional QH effect in graphene [33]-[38]. Its off-diagonal resistivity

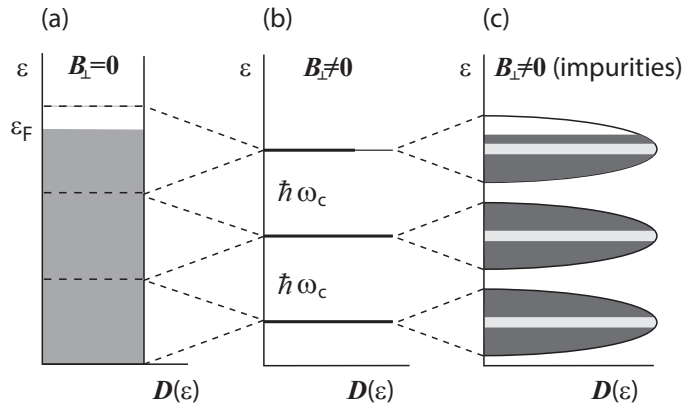

Fig. 2.3 The energy spectrum of the electrons in the two-dimensional system. Due to the Fermi statics, one electron can only occupy one quantum state, or more precisely, two electrons with different spin components can occupy an one-energy levels. (a) When $B_\perp = 0$, the density of states shows continuous spectrum. All the energetic states up to the state with Fermi energy are occupied. The density of state is $D(\epsilon) = M/2\pi\hbar^2$, which is constant. Taking account of spin degres of freedom, it becomes $D(\epsilon) = M\pi\hbar^2$. (b) When the magnetic field is applied ($B_\perp \neq 0$), the Landau levels are created, and the density of states becomes discrete spectrum, $D(\epsilon) = \rho_{\rm DS}\delta(\epsilon - E_N)$, with $\rho_{\rm DS} = 1/2\pi l_B^2$, which is nothing but the density of Landau sites, and $E_N = N\hbar\omega_{\rm c} + (1/2)\hbar\omega_{\rm c}$, the Nth Landau level. (c) In actual samples, the Landau levels are broaden since some electrons are trapped by the impurity potential. The dark shaded region represent the localized states, where as light shaded region represents the extended states. The Hall plateau is formed due to this impurity effect. This figure is taken from [59].

is given by $R_{xy} = \pm 4e^2/h(N + 1/2)$, where N is the Landau level index, and the Landau level in graphene is proportional to $\sqrt{N}$. The factor 4 corresponds to the internal degree of freedom for electrons, spin and valley. Compared to the conventional one, the term $\pm 2e^2/h$ arises since the zeroth Landau level is the half-filled state. The QH effect in graphene is induced by the massless Dirac fermions exhibiting the linear dispersion.

2.1.2 Two-dimensional Electrons in Monolayer Systems

The two-dimensional electron system is realized by the GaAs/AlGaAs hetero-junction by using the molecular beam epitaxy. Between these two semiconductors where the thickness is about $20 \sim 100$ $\mathring{A}$, there exists potential $V(z)$ which attracts the electrons to the surface, and the one-body energy of electron in the z direction is quantized. When the energy difference between the ground state and first excited state is large enough compared to the thermal and interaction energy, the electrons remain in the ground state, and therefore the motion of electrons in the z direction is inactive and electrons are trapped into the two-dimensional xy plane.

In this chapter, we consider the free electron gas for the simplicity, and introduce the Coulomb interactions in subsection 2.2.4. The density of states for the free electrons in two

dimension without electromagnetic field is given by

$$D(\epsilon)d\epsilon = \frac{M}{2\pi\hbar^2}, \tag{2.11}$$

with M the effective (band) mass for electron. It is a constant in the two-dimensional system as shown in Fig. 2.3 (a). Electrons occupy the state up to the Fermi level with the energy $\epsilon_{\rm F}$, which is determined by the electron density ρ_0 and the density of state (2.11) as

$$\epsilon_{\rm F} = \frac{2\pi\hbar^2}{M}\int_0^{\epsilon_{\rm F}} D(\epsilon)d\epsilon = \frac{2\pi\hbar^2}{M}\rho_0. \tag{2.12}$$

Here we have ignored the spin degrees of freedom. When they are taken into account, the density of states for free electrons becomes twice larger than (2.11). The two-dimensional electrons show the continuous spectrum.

In the field theoretical representation, we denote the electron field operator as $\Psi(\boldsymbol{x}) = (\psi_\uparrow(\boldsymbol{x}), \psi_\downarrow(\boldsymbol{x}))$, where $\uparrow$ represents the up-spin whereas $\downarrow$ the down-spin. The physical operators in this system are density operator and spin operators. They are expressed as a bilinear combinations of $\Psi(\boldsymbol{x})$, given by

$$\rho_x(\boldsymbol{x}) = \Psi^\dagger(\boldsymbol{x})\Psi(\boldsymbol{x}) = \sum_{\alpha=\uparrow,\downarrow}\psi_\alpha^\dagger(\boldsymbol{x})\psi_\alpha(\boldsymbol{x}) = \rho_\uparrow(\boldsymbol{x}) + \rho_\downarrow(\boldsymbol{x}), \tag{2.13}$$

$$S_x(\boldsymbol{x}) = \Psi^\dagger(\boldsymbol{x})\frac{\tau_x}{2}\Psi(\boldsymbol{x}) = \frac{1}{2}(\psi_\uparrow^\dagger(\boldsymbol{x})\psi_\downarrow(\boldsymbol{x}) + \psi_\downarrow^\dagger(\boldsymbol{x})\psi_\uparrow(\boldsymbol{x})), \tag{2.14}$$

$$S_y(\boldsymbol{x}) = \Psi^\dagger(\boldsymbol{x})\frac{\tau_y}{2}\Psi(\boldsymbol{x}) = \frac{1}{2i}(\psi_\uparrow^\dagger(\boldsymbol{x})\psi_\downarrow(\boldsymbol{x}) - \psi_\downarrow^\dagger(\boldsymbol{x})\psi_\uparrow(\boldsymbol{x})), \tag{2.15}$$

$$S_z(\boldsymbol{x}) = \Psi^\dagger(\boldsymbol{x})\frac{\tau_z}{2}\Psi(\boldsymbol{x}) = \frac{1}{2}(\psi_\uparrow^\dagger(\boldsymbol{x})\psi_\uparrow(\boldsymbol{x}) - \psi_\downarrow^\dagger(\boldsymbol{x})\psi_\downarrow(\boldsymbol{x})) = \frac{1}{2}(\rho_\uparrow(\boldsymbol{x}) - \rho_\downarrow(\boldsymbol{x})), \tag{2.16}$$

where $\rho_{\uparrow(\downarrow)}(\boldsymbol{x})$ describes the electron density with up (down) spin, and τ_a are the Pauli matrices,

$$\tau_x = \begin{pmatrix} 0 & 1 \\ 1 & 0 \end{pmatrix}, \quad \tau_y = \begin{pmatrix} 0 & -i \\ i & 0 \end{pmatrix}, \quad \tau_z = \begin{pmatrix} 1 & 0 \\ 0 & -1 \end{pmatrix}. \tag{2.17}$$

The spin operators $S_a(\boldsymbol{x})$ satisfy the SU(2) algebra

$$[S_a(\boldsymbol{x}), S_b(\boldsymbol{y})] = i\epsilon_{abc}S_c(\boldsymbol{y})\delta(\boldsymbol{x}-\boldsymbol{y}), \tag{2.18}$$

where ϵ_{abc} is the SU(2) structure constant. The above algebra is derived from the anti-commutation relation $\{\psi_\alpha(\boldsymbol{x}), \psi_\beta(\boldsymbol{y})\} = i\delta_{\alpha\beta}\delta(\boldsymbol{x}-\boldsymbol{y})$. The total one-body Hamiltonian in this system consists of the kinetic term $H_{\rm K}$ and the Zeeman term $H_{\rm Z}$,

$$H = H_{\rm K} + H_{\rm Z}, \tag{2.19}$$

with

$$H_{\mathrm{K}} = \frac{1}{2M} \sum_{\alpha=\uparrow,\downarrow} \int d^2x \psi_\alpha^\dagger(\boldsymbol{x}) \left(-i\hbar\boldsymbol{\nabla} + e\boldsymbol{A}(\boldsymbol{x})\right)^2 \psi_\alpha(\boldsymbol{x}), \tag{2.20}$$

$$H_{\mathrm{Z}} = -\frac{\Delta_{\mathrm{Z}}}{2} \int d^2x \left(\rho_\uparrow(\boldsymbol{x}) - \rho_\downarrow(\boldsymbol{x})\right) = -\Delta_{\mathrm{Z}} \int d^2x S_z(\boldsymbol{x}), \tag{2.21}$$

where $\boldsymbol{A}(\boldsymbol{x})$ is the vector potential for the magnetic field, and is the Δ_{Z} is the Zeeman gap,

$$\Delta_{\mathrm{Z}} = |g^* \mu_{\mathrm{B}} B|. \tag{2.22}$$

Here g^* is the g-factor in a semiconductor, which is about $g^* \approx -0.44$ in the GaAs semiconductor. It becomes much smaller compared to the one in the vacuum $g^* = 2$ due to its band structure (see also Appendix A.1).

2.1.3 Landau Quantization

We consider quantum mechanical motion of the electrons in the two-dimensional system with the external magnetic field. Here we present the argument based on the first quantization. The kinetic Hamiltonian in such a system is given by

$$H_{\mathrm{K}} = \frac{1}{2M} \left(\Pi_x^2 + \Pi_y^2\right), \tag{2.23}$$

where the covariant momentum Π_i with $i = x, y$ is given by

$$\Pi_x \equiv -i\hbar\partial_x + eA_x, \quad \Pi_y \equiv -i\hbar\partial_y + eA_y, \tag{2.24}$$

with A_i being the vector potential. It generates the magnetic field $\boldsymbol{B} = (0, 0, -B_\perp)$ as

$$B_\perp = -\epsilon_{jk}\partial_j A_k. \tag{2.25}$$

By taking account the fact that the electrons have cyclotron motion, we decompose the coordinate $\boldsymbol{x} = (x, y)$ into the guiding-center $\boldsymbol{X} = (X, Y)$ and the relative coordinate $\boldsymbol{R} = (R_x, R_y)$ as

$$x \equiv X + R_x \quad y \equiv Y + R_y, \tag{2.26}$$

$$R_x = -\frac{\Pi_y}{eB_\perp}, \quad R_y = \frac{\Pi_x}{eB_\perp}. \tag{2.27}$$

The guiding-center and relative coordinate satisfy the commutation relations

$$\begin{aligned} [X, Y] = -il_B^2, \quad [\Pi_x, \Pi_y] = i\frac{\hbar^2}{l_B^2}, \\ [X, \Pi_x] = [X, \Pi_y] = [Y, \Pi_x] = [Y, \Pi_y] = 0. \end{aligned} \tag{2.28}$$

We see that the guiding center (X, Y) and the covariant momentum (Π_x, Π_y) or the relative coordinate (R_x, R_y), are independent variables. Furthermore, the coordinate with different components do not commute, which is totally different from the ordinary quantum theory, where the coordinate and momentum make the canonical conjugates.

Here we have introduced the quantity

$$l_B = \sqrt{\frac{\hbar}{eB_\perp}}. \tag{2.29}$$

This is called the *magnetic length*. It gives the fundamental scale to the QH systems. The corresponding Coulomb energy $E_{\rm C}^0$ is

$$E_{\rm C}^0 = \frac{e^2}{4\pi\epsilon l_B}, \tag{2.30}$$

where ϵ is the background dielectric constant in GaAs semiconductors. The physical quantities having the dimension of length and energy are expressed in the unit of l_B and $E_{\rm C}^0$. For the typical values, see Appendix A.1.

We analyze the equations of motion for the guiding center (X, Y) and the relative coordinate (R_x, R_y) to see the quantum mechanical motion of the electrons. First, from the Hamiltonian (2.23) and the commutation relations (2.28), the Heisenberg equations of motion for the guinding center are given by,

$$\frac{d\boldsymbol{X}}{dt} = \frac{d\boldsymbol{Y}}{dt} = 0. \tag{2.31}$$

Therefore, no motion of electron exists for the guinding center and stays at the initial coordinate. The guiding center represents the central coordinate of the cyclotron motion. However, from (2.28), we see that a striking difference between the classical and quantum mechanical motion; there is an uncertainty for the guiding-center coordinate (X, Y). The position (X, Y) cannot be determined at least with the area $2\pi l_B^2$.

We next consider the equations of motion for the relative coordinate $\boldsymbol{R}$. By applying the same analysis given for the guinding center, we obtain the Heisenberg equations of motions

$$\frac{dR_x}{dt} = \omega_{\rm c} R_y, \quad \frac{dR_y}{dt} = -\omega_{\rm c} R_x, \tag{2.32}$$

where $\omega_{\rm c}$ is the cyclotron frequency $\omega_{\rm c} = eB_\perp/M$. By denoting the integration constants for $R_{x,y}$ as $R_{x,y}^0$, and introducing the complex variable $R \equiv R_x + iR_y$, the solution for (2.32) becomes

$$R(t) = R^0 e^{-i\omega_{\rm c} t} \tag{2.33}$$

where $R^0 = R_x^0 + iR_y^0$. As in the case of the classical one (2.2) or as shown in Fig. 2.4 (a), the relative coordinate $\boldsymbol{R}$ makes cyclotron motion around the guiding-center coordinate $\boldsymbol{X}$ with the cyclotron frequency $\omega_{\rm c}$. Note that, however, the quantum mechanical cyclotron motion

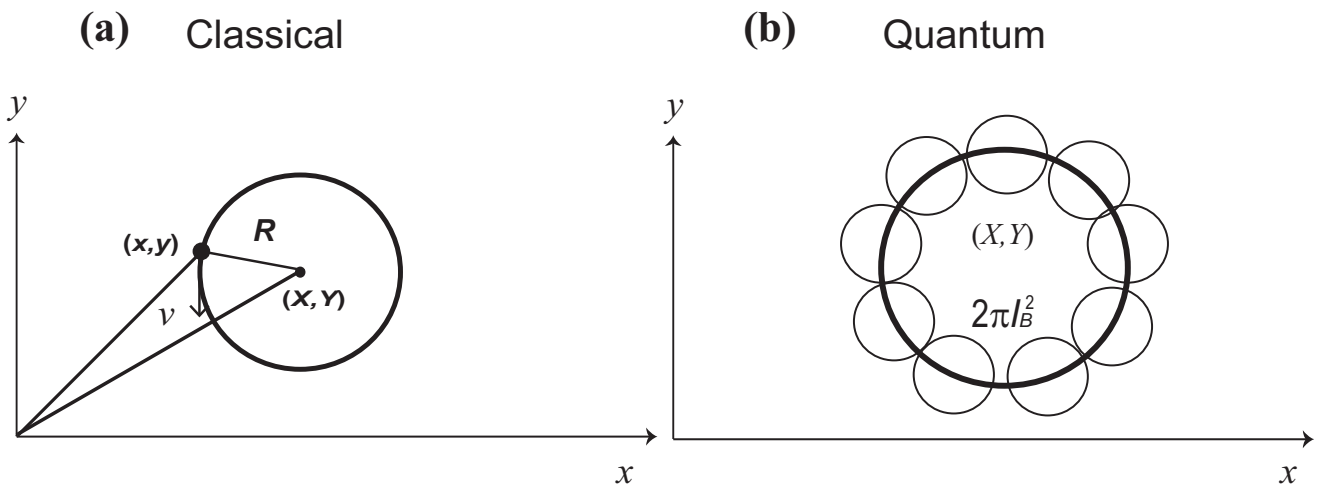

Fig. 2.4 Cyclotron motions for electrons. (a) In the classical theory, the electrons makes cyclotron motion around the guiding center $\boldsymbol{X}$ and the relative coordinate $\boldsymbol{R}$ shows the circular motion with the cyclotron frequency $\omega_c = \hbar/Ml_B^2 = eB_\perp/M$. (b) In the quantum theory, although electrons make cyclotron motion around the guiding center as in the case of classical ones, the big difference is that the guiding-center coordinates X and Y do not commute, and therefore, the electron position has minimum uncertainty with the area $2\pi l_B^2$. It moves as forming concentric circular. This figure is adapted from [59].

for the electron is completely different from the classical one, due to the uncertainty of the guiding-center coordinate $\boldsymbol{X}$, as shown in Fig. 2.4 (b).

We next derive the energy spectrum of the electrons. From (2.28) we see that there are two independent canonical conjugate coordinates, (X, Y) and (R_x, R_y). Thus, we can introduce two pairs of annihilation and creation operators similar to the ones in harmonic oscillator,

$$a = \frac{l_B}{\sqrt{2}\hbar}(\Pi_x + i\Pi_y), \quad a^\dagger = \frac{l_B}{\sqrt{2}\hbar}(\Pi_x - i\Pi_y)), \tag{2.34}$$

$$b = \frac{1}{\sqrt{2}l_B}(X - iY), \quad b^\dagger = \frac{1}{\sqrt{2}l_B}(X + iY), \tag{2.35}$$

and from (2.28), they satisfy the commutation relation

$$[a, a^\dagger] = [b, b^\dagger] = 1, \tag{2.36}$$

with all others being zero. From the creation operators $a^\dagger$ and $b^\dagger$, we construct the quantum states

$$|N, n\rangle = \sqrt{\frac{1}{N!n!}}(a^\dagger)^N(b^\dagger)^n|0\rangle, \quad a|0\rangle = b|0\rangle = 0, \tag{2.37}$$

and due to (2.36), these states $|N, n\rangle$ satisfy the orthonormal completeness condition

$$\langle N', n'|N, n\rangle = \delta_{NN'}\delta_{nn'}, \quad \sum_{n,N} |N, n\rangle\langle N, n| = \mathbf{1}. \tag{2.38}$$

By using the creation and annihilation operators a and $a^\dagger$, the kinetic Hamiltonian (2.23) is described as

$$H_{\mathrm{K}} = \hbar\omega_{\mathrm{c}}\left(a^\dagger a + \frac{1}{2}\right), \tag{2.39}$$

and therefore, the energy levels of the state $|N, n\rangle$ becomes

$$E_N = \hbar\omega_{\mathrm{c}}\left(N + \frac{1}{2}\right). \tag{2.40}$$

The energy spectrum (2.40) is called the Landau level[*1]. Here the energy $\hbar\omega_{\mathrm{c}}/2$ in (2.40) represents the zero-point energy. The energy spectrum becomes discrete in the presence of the magnetic field as shown in Fig. 2.3 (b). Here we note that in the real samples, there are impurities. Then some electrons are trapped by these impurities, and the Landau levels are broaden. As shown in Fig. 2.3 (c), they are divided into the localized states which are represented as the dark shaded region and the extended states, represented as the shaded region. As a result, the Hall plateau is created.

When we include the Zeeman effect, the energy spectrum (2.40) becomes

$$E_N = \hbar\omega_{\mathrm{c}}\left(N + \frac{1}{2}\right) \pm \frac{\Delta_{\mathrm{Z}}}{2}. \tag{2.41}$$

Thus, one Landau level is separated into two energy levels, having the same Landau index.

For each Landau level there exists a degeneracy called the Landau site in the Nth Landau level. In other words, when there are N_Φ Landau sites for each Landau level, there are N_Φ degenerated states, $|N, 0\rangle$, $|N, 1\rangle$, $\ldots$, $|N, N_\Phi\rangle$, for each Landau level, which are created by the operator $b^\dagger$ from the vacuum $|0\rangle$. As we see from (2.35), the guiding-center coordinate contains the information of the Landau site.

We calculate the number of Landau sites or the degeneracy in each Landau level. As we have discussed previously, the energy spectrum of the electrons without external magnetic field is continuous, where the density of states is constant, $D(\epsilon) = M/2\pi\hbar^2$. When the magnetic field is applied, the energy spectrum becomes discrete, which is nothing but the series of Landau levels. The degeneracy of the energy of the states for electrons are bundled into each Landau level with the width $\hbar\omega_{\mathrm{C}}$. Therefore, the density of Landau sites (the number of quantum states per unit area for each Landau level) ρ_Φ is

$$\rho_\Phi = \hbar\omega_{\mathrm{C}} \times \left(\frac{M}{2\pi\hbar^2}\right) = \frac{1}{2\pi l_B^2}, \tag{2.42}$$

which indicates that one Landau site occupies the area $2\pi l_B^2$. The density of Landau sites ρ_Φ

[*1] We use the italic index N for the Landau level index, while the regular style index N for group index.

can also be written by using the Dirac flux quantum $\Phi_{\rm D} \equiv 2\pi\hbar/e$ as

$$\rho_\Phi = \frac{eB_\perp}{2\pi\hbar} = \frac{B_\perp}{\Phi_{\rm D}}. \tag{2.43}$$

We can also express that the density of the states is equal to the number of Dirac flux quantum, which pierce the unit area in the system. One Landau site attaches one Dirac flux quantam.

By using the density of Landau sites ρ_Φ, the Landau level filling factor is defined by

$$\nu = \frac{\rho_0}{\rho_\Phi} = 2\pi l_B^2 \rho_0 = \frac{2\pi\hbar\rho_0}{eB_\perp}. \tag{2.44}$$

It represents the number of Dirac flux quantam attached to one electron. For example $\nu = 2$ QH state is the state which is occupied by the $N = 0$ Landau levels with both up and down spin, and the corresponding energy given by $\hbar\omega_{\rm c}/2 - \Delta{\rm Z}/2$ and $\hbar\omega_{\rm c}/2 + \Delta{\rm Z}/2$, respectively. In this case, two electrons occupy one Landau site. On the other hand, in the $\nu = 1$ QH state, $N = 0$ Landau levels with all the same spin component are occupied, where the energy level is given by $\hbar\omega_{\rm c}/2 - \Delta{\rm Z}/2$. One electron is occupying one Landau site.

2.1.4 Quantum Hall Effect

As we have seen in the previous argument, quantum mechanically, an electron makes cyclotron motion around the guiding center in the presence of the magnetic field. When the electric field is also applied into the system, the drift motion and the corresponding electric current are induced. It is the *Hall current*.

The kinetic Hamiltonian in the presence of the constant magnetic and electric field is given by

$$H = \frac{1}{2M}(\Pi_x^2 + \Pi_y^2) + exE_x + eyE_y. \tag{2.45}$$

We analyze the problem in the Landau gauge instead of symmetric gauge, since the angular momentum for the z component does not conserve anymore due to the electric field[*2]. The gauge potential in this gauge is given by

$$A_x = B_\perp y, \quad A_y = 0, \tag{2.46}$$

and correspondingly, the covariant momentum becomes

$$\Pi_x = -i\hbar\frac{\partial}{\partial x} + \frac{\hbar}{l_B^2}y, \quad \Pi_y = -i\hbar\frac{\partial}{\partial y}. \tag{2.47}$$

From now on we consider the system where the electric field applied to the y direction. Then

[*2] For the discussion of symmetric gauge, see Appendix A.2.

by denoting $p_i = -i\hbar\partial_i$ and setting $E_x = 0, E_y = E$, the Schrödinger equation is given by

$$\left[\frac{(p_x + eBy)^2}{2M} + \frac{p_y^2}{2M} + eEy\right]\chi_N^{\mathrm{E}}(\boldsymbol{x}) = E(k_x)\chi_N^{\mathrm{E}}(\boldsymbol{x}). \tag{2.48}$$

Since the Hamiltonian in (2.48) does not contain the variable x, it represents the momentum conservation in the x direction, and therefore, the wave function $\chi_N^{\mathrm{E}}(\boldsymbol{x})$ can be written in the form $\chi_N^{\mathrm{E}}(\boldsymbol{x}) = e^{ik_x x}\chi_N^{\mathrm{E}}(y)$. Furthermore, we see that the Hamiltonian is equivalent to that for the harmonic oscillator. It can be rewritten in the form

$$H = \frac{p_y^2}{2M} + \frac{M\omega_{\mathrm{c}}^2}{2}(y - \bar{y}^E)^2 + e\bar{y}^E E + \frac{(eEl_B)^2}{2\hbar\omega_{\mathrm{c}}}, \tag{2.49}$$

with $\bar{y}^E = -k_x l_B^2 - \frac{eE}{\hbar\omega_{\mathrm{c}}}l_B^2$. Therefore the wave function in the presence of the electric field is

$$\chi_N^{\mathrm{E}}(\boldsymbol{x}) = \left(\frac{1}{\pi}\right)^{\frac{1}{4}}\left(\frac{1}{2^N N! l_B}\right)^{\frac{1}{2}}\exp(ik_x x)\exp\left[-\frac{(y-\bar{y}^E)^2}{2l_B^2}\right]H_N\left(\frac{y-\bar{y}^E}{l_B}\right), \tag{2.50}$$

where $H_N(x)$ is the Hermite polynomial,

$$H_N(x) = (-1)^N\exp(x^2)\frac{d^N}{dx^N}\exp(-x^2). \tag{2.51}$$

The eigenvalue of the energy for (2.50) is given by

$$E(k_x) = \hbar\omega_{\mathrm{c}}\left(N + \frac{1}{2}\right) - eEl_B^2 k_x - \frac{M}{2}\left(\frac{E}{B}\right)^2. \tag{2.52}$$

The first term in (2.52) describes the kinetic energy due to the cyclotron motion, the second term the potential energy due to the electric field, and the third term representing the kinetic energy with the drift velocity E/B. Especially, in the lowest Landau level we have

$$\chi_0^{\mathrm{E}}(\boldsymbol{x}) = \left(\frac{1}{\sqrt{\pi}l_B}\right)^{\frac{1}{2}}\exp(ik_x x)\exp\left[-\frac{(y-\bar{y}^E)^2}{2l_B^2}\right]. \tag{2.53}$$

We evaluate current density $\mathcal{J}_k(\boldsymbol{x})$ in the system with the homogeneous electron density ρ_0 in the lowest Landau level. By using the covariant momentum (2.47) and denoting the electric current for one electron as J_k, the relation between the current J_k and the current density $\mathcal{J}_k(\boldsymbol{x})$ is given by

$$\langle J_k\rangle_E = \int d^2x\chi_0^{\mathrm{E}*}(\boldsymbol{x})P_k\chi_0^{\mathrm{E}}(\boldsymbol{x}) = \int d^2x\langle\mathcal{J}_k(\boldsymbol{x})\rangle_E, \tag{2.54}$$

with

$$\langle \mathcal{J}_x(\boldsymbol{x})\rangle_E = \frac{eE}{B_\perp}|\chi_k^E(\boldsymbol{x})|^2 - \frac{e\hbar}{\sqrt{\pi}Ml_B^3}(y-\bar{y}^E)\exp\left[-\frac{(y-\bar{y}^E)^2}{l_B^2}\right],$$
$$\langle \mathcal{J}_y(\boldsymbol{x})\rangle_E = 0. \tag{2.55}$$

By performing the spatial integral in (2.54) with using (2.55), the expectation value for the current J_k becomes

$$\langle J_k\rangle_E = \int dy \langle \mathcal{J}_x\rangle_E = \frac{eE}{B_\perp}. \tag{2.56}$$

Thus, in the system with homogeneous density, the current density becomes

$$\langle \mathcal{J}_x\rangle_E = \frac{e\rho_0}{B_\perp}E, \tag{2.57}$$

which agrees with (2.4). The above result can be also obtained from the equations of motion for the guiding center,

$$i\hbar\frac{dX}{dt} = -\frac{i\hbar}{B_\perp}E_y = -\frac{i\hbar}{B_\perp}E, \quad i\hbar\frac{dY}{dt} = \frac{i\hbar}{B_\perp}E_x = 0. \tag{2.58}$$

By using the above equations, we obtain

$$\langle \mathcal{J}_x\rangle_E = -e\rho_0\left\langle\frac{dX}{dt}\right\rangle_E = \frac{e\rho_0}{B_\perp}E, \quad \langle \mathcal{J}_y\rangle_E = -e\rho_0\left\langle\frac{dY}{dt}\right\rangle_E = 0. \tag{2.59}$$

The drift velocity of the electron is due to the motion of the guiding center.

In a quantum state where the electron density is homogeneous, and moreover, the (lowest) Landau level is completely filled, we have $\rho(\boldsymbol{x}) = \rho_0 = \nu/2\pi l_B^2$, and the current density (2.57) becomes

$$\mathcal{J}_x^{\rm tot} = \nu\frac{e^2}{h}E. \tag{2.60}$$

2.2 Bilayer Quantum Hall Systems

QH systems composed of two layers are called the *bilayer QH systems*. We call these two layers as front and back layers. The Hall current in the bilayer QH system is given by

$$\mathcal{J}_i = \sum_{\alpha=\mathrm{f,b}} \mathcal{J}_i^{\alpha} = \frac{e^2\nu}{2\pi\hbar}\epsilon_{ij}E_j, \tag{2.61}$$

where $\nu = 2\pi l_B^2\rho_0$ is the total filling factor as the bilayer system with the total electron density, $\rho_0 = \rho_0^{\mathrm{f}} + \rho_0^{\mathrm{b}}$, and E_y^{Hall} is the electric field of the "bilayer" system. A big difference between the bilayer system and the monolayer system is the addition of a new internal degree of freedom, the layer degree of freedom, or, *pseudospin*. The integer ν QH states in bilayer systems are realized by the electrons possessing the pseudospin, and the bilayer system as a total system, where the electrons in the front and back layers are strongly correlated, shows the QH effect as if it were the monolayer system. Since electrons in the front and back layers are indistinguishable, we treat the electrons in the bilayer QH systems as the two-dimensional electrons having pseudospin internal degree of freedom. In Fig. 2.5, we show the schematic illustrations of the $\nu = 1$ bilayer QH states. They represent electrons with magnetic flux attached. Here σ_0 is the variable defined by

$$\sigma_0 \equiv \frac{\rho_0^{\mathrm{f}} - \rho_0^{\mathrm{b}}}{\rho_0^{\mathrm{f}} + \rho_0^{\mathrm{b}}}, \tag{2.62}$$

where $\rho_0^{\mathrm{f(b)}}$ denotes the electron density in the front (back) layer. The variable σ_0 describes the difference of the electron densities between front and back layers. It is called the density-imbalanced parameter.

What we can observe are the electron densities for the front and back layer ρ_0^{f} and ρ_0^{b}, which are an average of the number of electrons in the front (back) layer), by injecting the current to each layer. We shown the schematic illustration of the electric circuit in the bilayer QH systems in Fig. 2.6.

The variable z does not appear in the algebraic structure and the electrons in the bilayer QH systems satisfy the commutation relation $[X, Y] = -il_B^2$. On the other hand, the layer separation d appears in the Coulomb Hamiltonian between the electron in the front layer and the one in the back layer (see Eq. (2.105)).

The realization of QH state is determined by the competition between the intra and interlayer Coulomb energy and the tunneling gap Δ_{SAS}, or more accurately, by the ratios $\Delta_{\mathrm{SAS}}/E_{\mathrm{C}}^0$ and d/l_B. We present the diagonal resistivity and the phase diagrams as $\Delta_{\mathrm{SAS}}/E_{\mathrm{C}}^0$-$d/l_B$ plane in the bilayer QH system in Fig. 2.7. Moreover, the bilayer QH state is stable against the alteration of the density difference between two layers, or namely the imbalanced parameter σ_0, as is shown in the experimental data Fig. 2.8. It represents the data for the Hall resistances in the total filling factor $\nu = 2/3$, 1, and 2 bilayer systems. Here n_{t}, n_{f}, and n_{b} denotes the total electron density, the electron density in the front layer, and the electron density in the

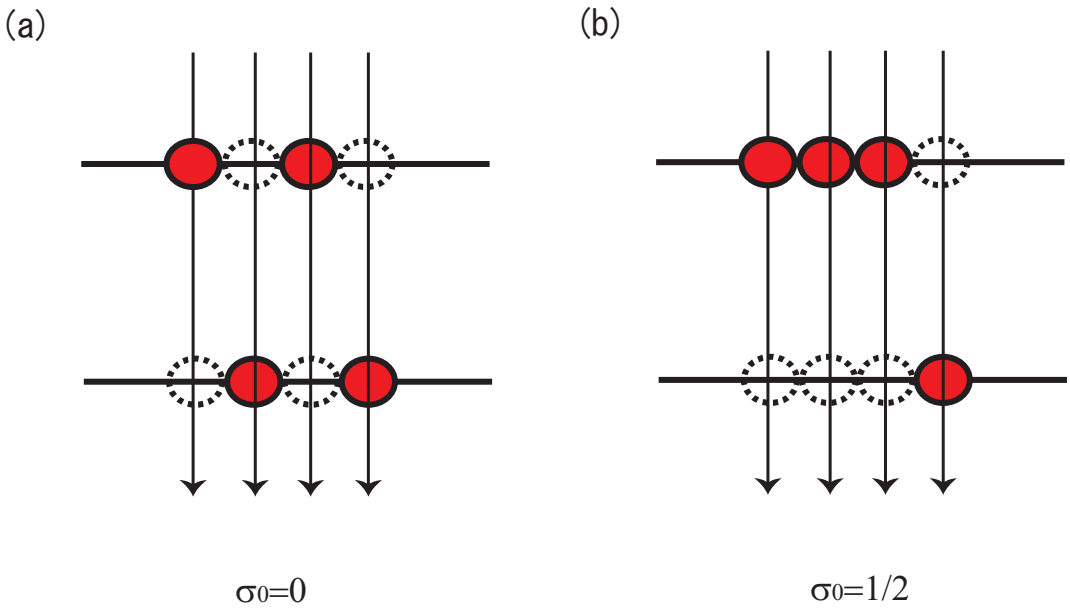

Fig. 2.5 The schematic illustrations of $\nu = 1$ QH states. Here all electrons are in the up-spin states are denoted by red disks, while an arrow indicated one unit of magnetic flux. In the bilayer QH systems, electrons in both the front and back layers are attached to magnetic flux indicated by an arrow. (a) $\nu = 1$ QH state at $\sigma_0 = 0$. (b) $\nu = 1$ QH state at $\sigma_0 = 1/2$. This figure is adapted from [59].

back layer, respectively[*3]. We see that the Hall resistances is stabilized under the change of the difference between electron-density in the front and that in the back layer.

There arises various basic quantities which do not exist in monolayer systems; for instance, the layer separation d, the interlayer Coulomb interactions $\sim e^2/4\pi\epsilon d$ and the tunneling interaction energy ($\sim \Delta_{\rm SAS}$). Each Landau level now possesses four energy levels, and by the competition among the above quantities, it leads to the realization of various QH states.

The electron number densities in the two layers can be independently controlled by applying the bias voltages. In other words, the filling factor for each layer $\nu^{\rm f(b)} = (1 \pm \sigma_0)\nu/2$ can be controlled by the bias voltage under the condition $\nu^{\rm f} + \nu^{\rm b} = \nu$.

Therefore physics of bilayer QH systems becomes extensively rich compared to the monolayer one.

2.2.1 Two-Dimensional Electrons in Bilayer QH Systems and Pseudospin

Electrons in Bilayer QH Systems

The electron field $\psi_\alpha(\boldsymbol{x})$ has now two types of index, the spin index $(\uparrow, \downarrow)$, and the pseudospin index (f,b). It is convenient to combine these two types of index, and consider the electron field with four components, $\Psi(\boldsymbol{x}) = (\psi_{\rm f\uparrow}(\boldsymbol{x}), \psi_{\rm f\downarrow}(\boldsymbol{x}), \psi_{\rm b\uparrow}(\boldsymbol{x}), \psi_{\rm b\downarrow}(\boldsymbol{x}))$. We call this four internal

[*3] In this thesis, we use the notations ρ_0, $\rho_0^{\rm f}$, and $\rho_0^{\rm b}$, as the total electron density, the electron density in the front layer, and the electron density in the back layer, respectively

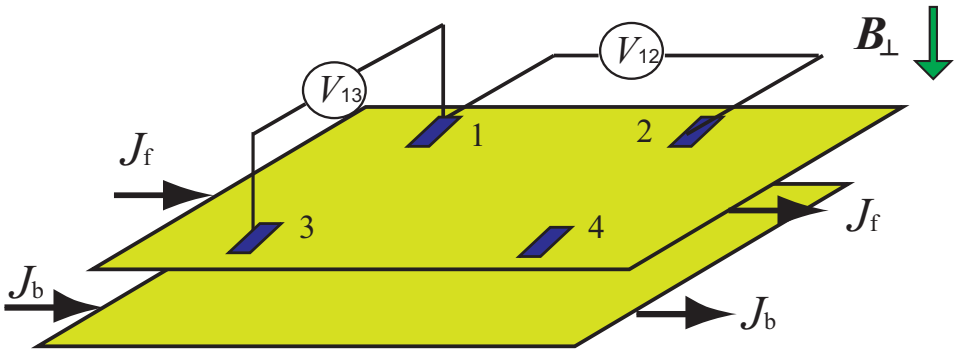

Fig. 2.6 The schematic illustrations of the Hall currents in the bilayer QH systems. The currents are injected in each layer independently. Then the diagonal and Hall resistivity for single layer, for example front layer, are measured. This figure is adapted from Ref. [59].

degrees of freedom, the SU(4) isospin.

There are two types of basis which generate the SU(4) algebra, the Hermitian matrices λ_a ($a = 1, \ldots, 15$), or $\tau_a^{\rm spin}$, $\tau_a^{\rm ppin}$, and $\tau_a^{\rm spin} \cdot \tau_b^{\rm ppin}$ with $a, b = 1, 2, 3$. Their explicit form is given in Appendix A.3. Here by denoting the Pauli matrices as τ_a, we use the basis (A.27)-(A.29), or

$$\tau_a^{\rm spin} = \begin{pmatrix} \tau_a & 0 \\ 0 & \tau_a \end{pmatrix}, \tag{2.63}$$

$$\tau_x^{\rm ppin} = \begin{pmatrix} 0 & \mathbf{1}_2 \\ \mathbf{1}_2 & 0 \end{pmatrix}, \quad \tau_y^{\rm ppin} = \begin{pmatrix} 0 & -i\mathbf{1}_2 \\ i\mathbf{1}_2 & 0 \end{pmatrix}, \quad \tau_z^{\rm ppin} = \begin{pmatrix} \mathbf{1}_2 & 0 \\ 0 & -\mathbf{1}_2 \end{pmatrix}, \tag{2.64}$$

$$\tau_a^{\rm spin}\tau_x^{\rm ppin} = \begin{pmatrix} 0 & \tau_a \\ \tau_a & 0 \end{pmatrix}, \quad \tau_a^{\rm spin}\tau_y^{\rm ppin} = \begin{pmatrix} 0 & -i\tau_a \\ i\tau_a & 0 \end{pmatrix}, \quad \tau_a^{\rm spin}\tau_z^{\rm ppin} = \begin{pmatrix} \tau_a & 0 \\ 0 & -\tau_a \end{pmatrix}, \tag{2.65}$$

for the rest of the argument in this section, since the physical operators are directly described with the bilinear combinations of $\psi(\boldsymbol{x})$ and $\psi^\dagger(\boldsymbol{x})$ generated by these basis. There are 16 physical operators in this system, associated with U(1) and SU(4) generators,

$$\begin{aligned} \rho(\boldsymbol{x}) &= \Psi^\dagger(\boldsymbol{x})\Psi(\boldsymbol{x}), \quad S_a(\boldsymbol{x}) = \frac{1}{2}\Psi^\dagger(\boldsymbol{x})\tau_a^{\rm spin}\Psi(\boldsymbol{x}), \\ P_a(\boldsymbol{x}) &= \frac{1}{2}\Psi^\dagger(\boldsymbol{x})\tau_a^{\rm ppin}\Psi(\boldsymbol{x}), \quad R_{ab}(\boldsymbol{x}) = \frac{1}{2}\Psi^\dagger(\boldsymbol{x})\tau_a^{\rm spin}\tau_b^{\rm ppin}\Psi(\boldsymbol{x}), \end{aligned} \tag{2.66}$$

where ρ is the total electron density, S_a describes the total spin, P_a represents the pseudospin operator, which will be discussed later in details. Here the generators $\tau_a^{\rm spin}$ and $\tau_a^{\rm ppin}$ denote those for spin and pseudospin operators, respectively. (We use the same notation as given in [59, 108, 109, 110, 111].) The operator R_{ab} are the peculiar operators of SU(4), which do not exist in $\mathrm{SU}_{\rm spin}(2) \times \mathrm{SU}_{\rm ppin}(2)$. It has both spin and pseudospin index, and transforms as a spin under $\mathrm{SU}_{\rm spin}(2)$ and as a pseudospin under $\mathrm{SU}_{\rm ppin}(2)$. We call it the R-spin operator. It plays an essential role in the realization of the CAF phase in $\nu = 2$, which is discussed in chapter

4. Furthermore, it plays an important role for the emergence of the entangled spin-pseudospin phenomena in the bilayer QH systems.

From now on, we study $\nu = 1$ bilayer systems with spin degrees of freedom frozen to see clearly the role of the pseudospin.

We briefly show the one-body Hamiltonian of the bilayer QH systems. First, the kinetic term in the bilayer QH systems is given by

$$H_{\rm K} = \frac{1}{2M}\sum_{\alpha={\rm f,b}}\int d^2x\psi^\dagger_\alpha(\boldsymbol{x})(\Pi_x - i\Pi_y)(\Pi_x + i\Pi_y)\psi_\alpha(\boldsymbol{x}) + \frac{N}{2}\hbar\omega, \tag{2.67}$$

where $\psi_\alpha(\boldsymbol{x})$ denotes the electron field at layer α $(=\mathrm{f,b})$, and the covariant momentum is $\Pi_k = -i\hbar\partial_k + eA_k$ with $k = 1, 2$.

Besides the kinetic term (2.67), the one-body Hamiltonian for the electrons in the bilayer systems contains the Zeeman term, the *tunneling interaction term*, and the *bias term*. The details of them will be discussed later on. The tunneling interaction and bias terms are the new terms which arise from the addition of the pseudospin. They are summarized as the pseudo-Zeeman term. Combining the Zeeman and pseudo-Zeeman terms we have

$$H_{\rm ZpZ} = -\int d^2x(\Delta_{\rm Z}S_z + \Delta_{\rm SAS}P_x + \Delta_{\rm bias}P_z), \tag{2.68}$$

with the Zeeman gap $\Delta_{\rm Z}$, the tunneling gap $\Delta_{\rm SAS}$, and the bias voltage $\Delta_{\rm bias} = eV_{\rm bias}$.

The total one-body Hamiltonian is

$$H = H_{\rm K} + H_{\rm ZpZ}. \tag{2.69}$$

Pseudospin

In $\nu = 1$ with spin frozen, the electron has two components, $\Psi = (\psi_{\rm f}, \psi_{\rm b})$, and the pseudospin density operator is expressed as

$$P_x(\boldsymbol{x}) = \Psi^\dagger(\boldsymbol{x})\frac{\tau_x}{2}\Psi(\boldsymbol{x}) = \frac{1}{2}(\psi^\dagger_{\rm f}(\boldsymbol{x})\psi_{\rm b}(\boldsymbol{x}) + \psi^\dagger_{\rm b}(\boldsymbol{x})\psi_{\rm f}(\boldsymbol{x})), \tag{2.70}$$

$$P_y(\boldsymbol{x}) = \Psi^\dagger(\boldsymbol{x})\frac{\tau_y}{2}\Psi(\boldsymbol{x}) = \frac{1}{2i}(\psi^\dagger_{\rm f}(\boldsymbol{x})\psi_{\rm b}(\boldsymbol{x}) - \psi^\dagger_{\rm b}(\boldsymbol{x})\psi_{\rm f}(\boldsymbol{x})), \tag{2.71}$$

$$P_z(\boldsymbol{x}) = \Psi^\dagger(\boldsymbol{x})\frac{\tau_z}{2}\Psi(\boldsymbol{x}) = \frac{1}{2}(\psi^\dagger_{\rm f}(\boldsymbol{x})\psi_{\rm f}(\boldsymbol{x}) - \psi^\dagger_{\rm b}(\boldsymbol{x})\psi_{\rm b}(\boldsymbol{x})) = \frac{1}{2}(\rho_{\rm f}(\boldsymbol{x}) - \rho_{\rm b}(\boldsymbol{x})), \tag{2.72}$$

with τ_a the Pauli matrices, and $\rho_\alpha(\boldsymbol{x}) = \psi^\dagger_\alpha(\boldsymbol{x})\psi_\alpha(\boldsymbol{x})$ with α =f,b, describing the electron density in layer α. Pseudospin operators satisfy the SU(2) algebra

$$[P_a(\boldsymbol{x}), P_b(\boldsymbol{y})] = i\epsilon_{abc}P_c(\boldsymbol{y})\delta(\boldsymbol{x} - \boldsymbol{y}). \tag{2.73}$$

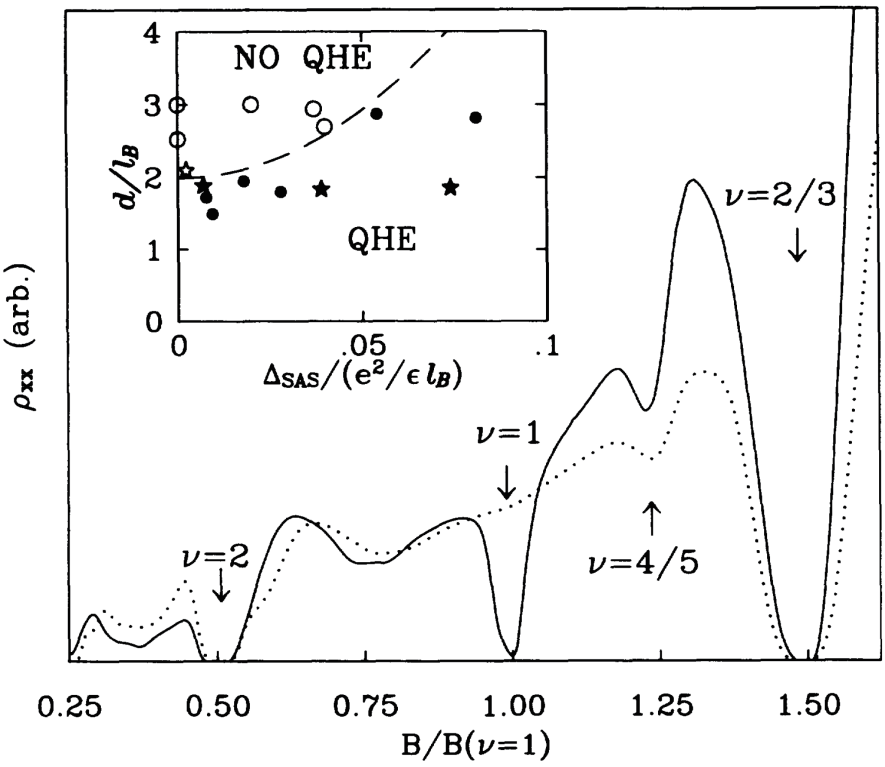

Fig. 2.7 The experimental data for the diagonal resistance versus the magnetic field. The solid line represents the data for the sample with the barrier thickness $d_b = 31\mathring{A}$ while the dotted line represents the one for the sample with the barrier thickness $d_b = 40\mathring{A}$. The filling factor $\nu = 1$ bilayer QH state is realized only for sample with narrower barrier thickness. The inset is the phase diagram in terms of d/l_B and $\Delta_{\rm SAS}/E_{\rm C}^0$, showing whether the bilayer electronic state is in $\nu = 1$ bilayer QH state or not. The interlayer coherence is considered to be developed at $\Delta_{\rm SAS}/E_{\rm C}^0 \to 0$ with d/l_B smaller then 2. This figure is taken from [56].

By using $P_{x,y}$, we introduce the raising and lowering operators for pseudospin as

$$P^+(\boldsymbol{x}) \equiv P_x(\boldsymbol{x}) + iP_y(\boldsymbol{x}) = \psi_{\rm f}^\dagger(\boldsymbol{x})\psi_{\rm b}(\boldsymbol{x}), \quad P^-(\boldsymbol{x}) \equiv P_x(\boldsymbol{x}) - iP_y(\boldsymbol{x}) = \psi_{\rm b}^\dagger(\boldsymbol{x})\psi_{\rm f}(\boldsymbol{x}). \quad (2.74)$$

Let us consider the physical meaning of the pseudospin operators. At first, from (2.72), we see that $2P_z$ implies the density difference between the two layers. It corresponds to the density difference between the electrons with different spins $2S_z$ in the case of spin operator. The meaning of $P_{x,y}$ become clear by using the operators (2.74) as follows. From (2.74), we see that the operator $P^+(\boldsymbol{x})[P^-(\boldsymbol{x})]$ transfers one electron at $\boldsymbol{x}$ in the back (front) layer to the front (back) layer. They correspond to the spin operator $S^+(\boldsymbol{x})[S^-(\boldsymbol{x})]$, which flips down (up) spin to up (down) spin. We see that the pseudospin plays essentially an equivalent role as the spin, although its physical meaning is different. It can be considered that up-spin corresponds to the front layer whereas down-spin corresponds to the back layer.

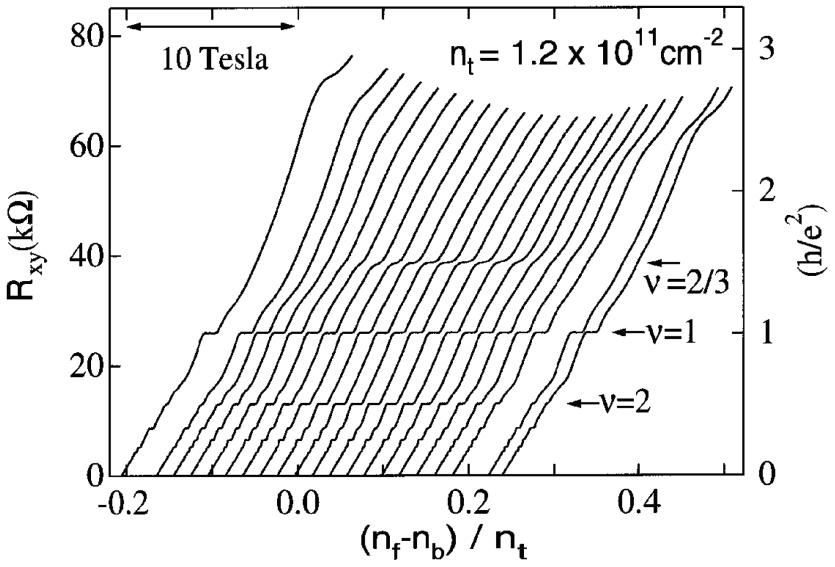

Fig. 2.8 The experimental data for the Hall resistance of $\nu = 2/3, 1, 2$ bilayer QH state. The QH states are realized for the various values of the imbalanced parameter σ_0. This figure is taken from [93].

2.2.2 Tunneling Gap and Tunneling Interaction Term

We first consider the case when the electron density in the front layer is equal to the one in the back layer ($\rho^{\rm f} = \rho^{\rm b}$), which we call the density-balanced configuration. When the two layers become close enough, then the wave function of electron in one layer starts to overlap with the wave function of electron in the other layer, and makes tunneling between two layers. Then there arise two energy levels called the symmetric and antisymmetric state. The ground state is a symmetric state whereas the excited state is an antisymmetric state. The symmetric and antisymmetric field operators, $\psi_{\rm S}$ and $\psi_{\rm A}$ are described in terms of $\psi_{\rm f,b}(\boldsymbol{x})$ as

$$\psi_{\rm S}(\boldsymbol{x}) = \frac{\psi_{\rm f}(\boldsymbol{x}) + \psi_{\rm b}(\boldsymbol{x})}{\sqrt{2}}, \quad \psi_{\rm A}(\boldsymbol{x}) = \frac{\psi_{\rm f}(\boldsymbol{x}) - \psi_{\rm b}(\boldsymbol{x})}{\sqrt{2}}. \tag{2.75}$$

By using (2.75), the pseudospin operators (2.72) can be written in the form

$$P_x(\boldsymbol{x}) = \frac{1}{2}(\psi_{\rm S}^\dagger(\boldsymbol{x})\psi_{\rm S}(\boldsymbol{x}) - \psi_{\rm A}^\dagger(\boldsymbol{x})\psi_{\rm A}(\boldsymbol{x})) = \frac{1}{2}(\rho_{\rm S}(\boldsymbol{x}) - \rho_{\rm A}(\boldsymbol{x})), \tag{2.76}$$

$$P_y(\boldsymbol{x}) = \frac{i}{2}(\psi_{\rm S}^\dagger(\boldsymbol{x})\psi_{\rm A}(\boldsymbol{x}) - \psi_{\rm A}^\dagger(\boldsymbol{x})\psi_{\rm S}(\boldsymbol{x})), \tag{2.77}$$

$$P_z(\boldsymbol{x}) = \frac{1}{2}(\psi_{\rm S}^\dagger(\boldsymbol{x})\psi_{\rm A}(\boldsymbol{x}) + \psi_{\rm A}^\dagger(\boldsymbol{x})\psi_{\rm S}(\boldsymbol{x})). \tag{2.78}$$

As shown in Fig. 2.9 (a), the energy gap between these two states is called the *tunneling gap* denoting $\Delta_{\rm SAS}$. The typical values of $\Delta_{\rm SAS}$ are shown in Appendix A.1.

As in the case of the Zeeman term, the emergence of the tunneling gap $\Delta_{\rm SAS}$ between the

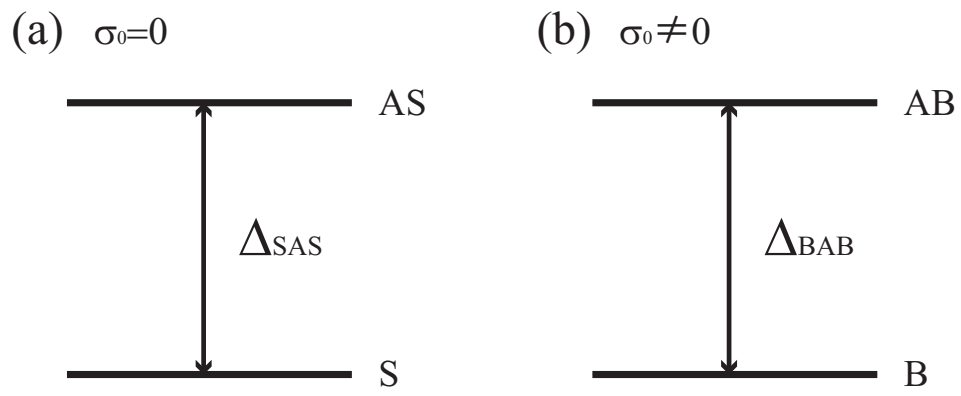

Fig. 2.9 The schematic illustrations of one-body energy levels of electrons in a bilayer QH systems. There arise two energy levels. (a) For balanced configuration $\rho^{\mathrm{f}} = \rho^{\mathrm{b}}$, the ground state is the symmetric state whereas the excited state is the antisymmetric state. The tunneling gap Δ_{SAS} is the energy gap between the symmetric state and the antisymmetric state. (b) When the bias voltage Δ_{bias} is applied, the electrons form the imbalanced configuration $\rho^{\mathrm{f}} \neq \rho^{\mathrm{b}}$. Then the symmetric state and the antisymmetric state turn into the bonding state and the antibonding state, respectively. The energy gap between these two states is $\Delta_{\mathrm{BAB}} = \sqrt{\Delta_{\mathrm{SAS}}^2 + \Delta_{\mathrm{bias}}^2}$.

two states is expressed by the tunneling interaction term. The corresponding Hamiltonian is represented as the difference between the electron number of symmetric and antisymmetric states N^{S} and N^{A},

$$H_{\mathrm{T}} = -\frac{1}{2}\Delta_{\mathrm{SAS}}(N^{\mathrm{S}} - N^{\mathrm{A}}) = \frac{1}{2}\Delta_{\mathrm{SAS}} \int d^2x(\psi_{\mathrm{A}}^\dagger \psi_{\mathrm{A}} - \psi_{\mathrm{S}}^\dagger \psi_{\mathrm{S}}). \tag{2.79}$$

Using (2.76), the tunneling interaction term can also be written in terms of the pseudospin operator as

$$H_{\mathrm{T}} = -\Delta_{\mathrm{SAS}} \int d^2x P_x(\boldsymbol{x}). \tag{2.80}$$

2.2.3 Bias Term and the Imbalanced Parameter

In the bilayer QH systems, the electron densities in the different layers are independently controlled by the bias voltages. As a result, we can create the situation such that the electron density in the front layer is inequivalent to the one in the back layer ($\rho^{\mathrm{f}} \neq \rho^{\mathrm{b}}$), which we call density-imbalanced configuration. The creation of density-imbalanced configuration is expressed by the bias term,

$$H_{\mathrm{bias}} = -\frac{1}{2}\Delta_{\mathrm{bias}}(N^{\mathrm{f}} - N^{\mathrm{b}}) = -\Delta_{\mathrm{bias}} \int d^2x P_z(\boldsymbol{x}). \tag{2.81}$$

By adding the tunneling interaction term (2.80) to the above bias terms, it is organized as the pseudo-Zeeman term

$$H_{\rm pZ} \equiv H_{\rm T} + H_{\rm bias} = \frac{1}{2}\int d^2x \begin{pmatrix} \psi_{\rm f}^\dagger \\ \psi_{\rm b}^\dagger \end{pmatrix}^\dagger \begin{pmatrix} -\Delta_{\rm bias} & -\Delta_{\rm SAS} \\ -\Delta_{\rm SAS} & \Delta_{\rm bias} \end{pmatrix} \begin{pmatrix} \psi_{\rm f} \\ \psi_{\rm b} \end{pmatrix}$$
$$= -\int d^2x(\Delta_{\rm SAS}P_x(\boldsymbol{x}) + \Delta_{\rm bias}P_z(\boldsymbol{x})) = -\int d^2x \boldsymbol{\Delta}_{\rm PZ}\cdot\boldsymbol{\mathcal{P}}. \tag{2.82}$$

Here $\boldsymbol{\Delta}_{\rm PZ} = (\Delta_{\rm SAS}, 0, \Delta_{\rm bias})$ and $\boldsymbol{\mathcal{P}} = (P_x, P_y, P_z)$. We call $\boldsymbol{\Delta}_{\rm PZ}$ the pseudo-Zeeman field, which has the magnitude $\Delta_{\rm BAB} = \sqrt{\Delta_{\rm SAS}^2 + \Delta_{\rm bias}^2}$. We see that when the system is in the balanced configuration, $\Delta_{\rm bias} = 0$, the pseudomagnetic field points to the x axis, and correspondingly, the pseudospin is polarized into the x axis. When the bias parameter becomes finite, it leads to the imbalanced configuration. Then the psedospin starts to be tilted and to be polarized into the z direction.

In order to describe the density-imbalanced configuration, there is a convenient variable called the imbalance parameter σ_0. This is defined as the normalized density difference between the front and back layers, taking its value from -1 to 1. It is described in terms of $\rho_0^{\rm f,b}$ as (2.62), or

$$\sigma_0 = \frac{\rho_0^{\rm f} - \rho_0^{\rm b}}{\rho_0^{\rm f} + \rho_0^{\rm b}}. \tag{2.83}$$

As we see later in chapter 3 and 5, the interlayer phase coherent phenomena are described in terms of this imbalance parameter and its conjugate phase.

The pseudospin configuration in the ground state is expressed in terms of the imbalance parameter σ_0. To see this, we introduce the normalized pseudospin operator $\mathcal{P}_a$ defined by $P_a = \rho_\phi \mathcal{P}_a$. The normalized pseudospin operator $\mathcal{P}_a$ in the ground state is represented by

$$\mathcal{P}_x^0 = \frac{\sqrt{1-\sigma_0^2}}{2}, \qquad \mathcal{P}_y^0 = 0, \qquad \mathcal{P}_z^0 = \frac{\sigma_0}{2}. \tag{2.84}$$

By substituting (2.84) into the pseudo-Zeeman term (2.82), and minimize this Hamiltonian with respect to σ_0, we obtain the relation

$$\Delta_{\rm bias} = \frac{\sigma_0}{\sqrt{1-\sigma_0^2}}\Delta_{\rm SAS}. \tag{2.85}$$

Then by using the above relation, the pseudospin-Zeeman term is expressed in terms of $\Delta_{\rm BAB}$ by diagonalizing the 2×2 matrix in (2.82). It is diagonalized as

$$\frac{1}{\sqrt{2}}\begin{pmatrix} \sqrt{1+\sigma_0} & \sqrt{1-\sigma_0} \\ \sqrt{1-\sigma_0} & -\sqrt{1+\sigma_0} \end{pmatrix}^\dagger \begin{pmatrix} -\Delta_{\rm bias} & -\Delta_{\rm SAS} \\ -\Delta_{\rm SAS} & \Delta_{\rm bias} \end{pmatrix} \begin{pmatrix} \sqrt{1+\sigma_0} & \sqrt{1-\sigma_0} \\ \sqrt{1-\sigma_0} & -\sqrt{1+\sigma_0} \end{pmatrix}$$
$$= \begin{pmatrix} -\Delta_{\rm BAB} & 0 \\ 0 & \Delta_{\rm BAB} \end{pmatrix}. \tag{2.86}$$

Let us introduce the new basis, the bonding and antibonding states,

$$\psi_{\mathrm{B}}(\boldsymbol{x}) = \sqrt{\frac{1+\sigma_0}{2}}\psi_{\mathrm{f}}(\boldsymbol{x}) + \sqrt{\frac{1-\sigma_0}{2}}\psi_{\mathrm{b}}(\boldsymbol{x}), \quad \psi_{\mathrm{A}}(\boldsymbol{x}) = \sqrt{\frac{1-\sigma_0}{2}}\psi_{\mathrm{f}}(\boldsymbol{x}) - \sqrt{\frac{1+\sigma_0}{2}}\psi_{\mathrm{b}}(\boldsymbol{x}), \tag{2.87}$$

which correspond to the symmetric and antisymmetric state in the imbalanced configuration, respectively. Then the pseudo-Zeeman term (2.82) are described in terms of the bonding and antibonding operators (2.87) as a diagonalized form

$$H_{\mathrm{pZ}} = \frac{1}{2}\Delta_{\mathrm{BAB}} \int d^2x \left(\psi_{\mathrm{A}}^\dagger(\boldsymbol{x})\psi_{\mathrm{A}}(\boldsymbol{x}) - \psi_{\mathrm{B}}^\dagger(\boldsymbol{x})\psi_{\mathrm{B}}(\boldsymbol{x}) \right). \tag{2.88}$$

The energy gap Δ_{BAB} is a one-body energy gap between the bonding and antibonding states, presented in Fig. 2.9 (b).

Experimentally, the tunneling gap is measured by the minimum value of the difference between the densities in the bonding state and anti-bonding state, which is determined by the Fourier analysis of Schbnikov-de Haas oscillations (see for example [124, 125]).

2.2.4 Landau-Level Projection Formalism and SU(4) Effective Hamiltonian

QH state is realized by applying the high magnetic field to the two-dimensional electron systems. When the magnetic field is large enough, for example, about 10 [T], the cyclotron energy $\hbar\omega_{\mathrm{c}}$ becomes larger than the Coulomb energy E_{C}^0 (see Appendix A.1). Thus, the excitations across the Landau levels become suppressed, and electrons are confined to a single Landau level. Here we investigate the electrons in the QH systems confined to the lowest-Landau level. Such electrons are constructed by the lowest-Landau level projection formalism [127, 128].

As we have seen, electrons in the lowest-Landau level are labeled by the Landau site $|0, n\rangle$, or

$$|0, n\rangle = \frac{1}{\sqrt{n!}}(b^\dagger)^n|0\rangle, \quad n = 0, 1, \ldots N_\Phi - 1, \quad b|0\rangle = 0, \tag{2.89}$$

where b and $b^\dagger$ obeying the commutation relation $[b, b^\dagger] = 1$. They assign the Landau site $|0, n\rangle$. The quantum states $|n\rangle$ satisfy the completeness condition

$$\sum_n |n\rangle\langle n| = 1. \tag{2.90}$$

The creation and annihilation operators b and $b^\dagger$ are related to the guiding-center coordinate as Eq. (2.35), or

$$b = \frac{1}{\sqrt{2}l_B}(X - iY), \quad b^\dagger = \frac{1}{\sqrt{2}l_B}(X + iY), \tag{2.91}$$

obeying the commutation relation

$$[X, Y] = -il_B^2. \tag{2.92}$$

On the other hand, the other creation and annihilation operators, a and $a^\dagger$, designate the Landau-level index, and are related to the relative coordinate (R_x, R_y). Therefore since the Landau-level index is fixed, especially to $N = 0$, and the relative coordinate is independent variable from the guiding-center coordinate, as shown in Eq. (2.92), the position of electrons confined to the lowest-Landau level is practically described by the guiding-center. Such electrons are expressed by some sort of lattice theory labeled by the Landau-site index n with minimum certainty $2\pi l_B^2$, implying that the position of electrons cannot be precisely determined. What is observed experimentally, on the other hand, is the classical fields which is an function of the position $\boldsymbol{x} = \boldsymbol{X} + \boldsymbol{R}$. Since our goal is to evaluate the classical fields $f(\boldsymbol{x})$, we must have some prescriptions so that the corresponding physical operators, for instance the electron density operator and SU(4) isospin operator, are constructed in terms of the noncommutative quantum theory characterized by (2.92). Here we briefly present the quantum theory in the noncommutative plane (2.92) and the corresponding prescription given by Refs. [59, 101, 102, 103, 134]. Then by following their formalisms, we show the effective Hamiltonian for NG modes (2.141). For the details of the formalism and the derivation of the effective Hamiltonian for NG modes, see Appendix B. We note that some formulas are written repeatedly with ones given in Appendix B, so that readers can understand the essence of the the lowest-Landau level projection formalism and see the detailed derivation in Appendix B.

The electron field operator projected to the Nth Landau-level is given by (B.30), or

$$\Psi_{N,\mu}(\boldsymbol{x}) = \sum_n \langle \boldsymbol{x}|N, n\rangle c_{N,\mu}(n), \tag{2.93}$$

where μ denotes the index for isospin. Here we note that a summation is not taken for the Landau-index N. The creation and annihilation operators $c_{N,\mu}(n)$ and $c^\dagger_{N,\mu}(n)$ satisfy the anticommutation relation $\{c_{N,\mu}(n), c_{N,\nu}(m)\} = \delta_{nm}\delta_{\mu\nu}$. We next construct the density and SU(4) isospin operators projected to the Nth Landau level, since the physical operators in the QH systems are expressed in terms of them. They are

$$\rho_N(\boldsymbol{x}) = \Psi^\dagger_{N,\mu}(\boldsymbol{x})\Psi_{N,\mu}(\boldsymbol{x}), \quad I_{N,a}(\boldsymbol{x}) = \Psi^\dagger_{N,\mu}(\boldsymbol{x})\left(\frac{\lambda_a}{2}\right)_{\mu\nu}\Psi_{N,\nu}(\boldsymbol{x}), \tag{2.94}$$

with λ_a the SU(N) generators. The Fourier transformation of operators (2.94) are

$$\rho_N(\boldsymbol{q}) = F_N(\boldsymbol{q})\hat{\rho}(\boldsymbol{q}), \qquad I_{N,a}(\boldsymbol{q}) = F_N(\boldsymbol{q})\hat{I}_a(\boldsymbol{q}) \tag{2.95}$$

where

$$\hat{\rho}(\boldsymbol{q}) = \frac{1}{2\pi}\langle n|e^{-i\boldsymbol{q}\boldsymbol{X}}|m\rangle\rho(m,n), \quad \hat{I}_a(\boldsymbol{q}) = \frac{1}{2\pi}\langle n|e^{-i\boldsymbol{q}\boldsymbol{X}}|m\rangle I_a(m,n), \tag{2.96}$$

$$\rho(m,n) = c^\dagger_{N,\mu}(n)c_{N,\mu}(m), \quad I_a(m,n) = c^\dagger_{N,\mu}(n)\left(\frac{\lambda_a}{2}\right)_{\mu\nu} c_{N,\nu}(m). \tag{2.97}$$

and

$$F_N(\boldsymbol{q}) = \langle N|e^{-i\boldsymbol{q}\boldsymbol{R}}|N\rangle = L_N\left(\frac{l_B^2\boldsymbol{q}^2}{2}\right)e^{-\frac{l_B^2\boldsymbol{q}^2}{4}}, \tag{2.98}$$

with $L_N(x)$ being the Laguerre polynomial. Eqs. (2.96) and (2.98) are called the bare density operators and the Landau-level form factor, respectively. In particular, for the lowest Landau level $N = 0$ it becomes

$$F_0(\boldsymbol{q}) = e^{-\frac{l_B^2\boldsymbol{q}^2}{4}}. \tag{2.99}$$

The bare density operators (2.96) satisfy the algebra (B.36), or

$$\begin{aligned}
[\hat{\rho}(\boldsymbol{p}),\hat{\rho}(\boldsymbol{q})] &= \frac{i}{\pi}\hat{\rho}(\boldsymbol{p}+\boldsymbol{q})\sin\left(\frac{l_B^2}{2}\boldsymbol{p}\wedge\boldsymbol{q}\right),\\
\left[\hat{\rho}(\boldsymbol{p}),\hat{I}_a(\boldsymbol{q})\right] &= \frac{i}{\pi}\hat{I}_a(\boldsymbol{p}+\boldsymbol{q})\sin\left(\frac{l_B^2}{2}\boldsymbol{p}\wedge\boldsymbol{q}\right),\\
\left[\hat{I}_a(\boldsymbol{p}),\hat{I}_b(\boldsymbol{q})\right] &= \frac{i}{2\pi}f_{abc}\hat{I}_c(\boldsymbol{p}+\boldsymbol{q})\cos\left(\frac{l_B^2}{2}\boldsymbol{p}\wedge\boldsymbol{q}\right) + \frac{i}{2\pi}d_{abc}\hat{I}_c(\boldsymbol{p}+\boldsymbol{q})\sin\left(\frac{l_B^2}{2}\boldsymbol{p}\wedge\boldsymbol{q}\right)\\
&\quad + \frac{i}{2\pi N}\delta_{ab}\hat{\rho}(\boldsymbol{p}+\boldsymbol{q})\sin\left(\frac{l_B^2}{2}\boldsymbol{p}\wedge\boldsymbol{q}\right),
\end{aligned} \tag{2.100}$$

where f_{abc} and d_{abc} are the structure constants for SU(N) algebra. We call the algebra (2.100) the W_∞(N) algebra [102, 103, 134]. In the Landau-level projection formalism, the Hamiltonian of the systems is expressed in terms of the bare density or the isospins. Then the dynamics for the physical operators is represented by the Heisenberg equation of motion

$$i\hbar\frac{d}{dt}O_N = [O_N, H_N], \tag{2.101}$$

where O_N and H_N are the projected operator and Hamiltonian to the Nth Landau level, respectively, expressed in terms of the the bare density or the isospins, which is calculated by using the algebras (2.100). The electric current is calculated in this procedure, which is shown in chapter 5.

Finally, we go on to derive the effective Hamiltonian for the NG modes. First, we summarize the terms of the Hamiltonian in the bilayer QH systems. The total Hamiltonian in the bilayer QH systems is given by

$$H = H_{\mathrm{K}} + H_{\mathrm{C}} + H_{\mathrm{ZpZ}} = H_{\mathrm{K}} + H_{\mathrm{C}}^{+} + H_{\mathrm{C}}^{-} + H_{\mathrm{ZpZ}}, \tag{2.102}$$

where H_{ZpZ} is composed of the Zeeman term, the tunneling interaction term, and the bias term given by (2.68) or

$$H_{\mathrm{ZpZ}} = -\int d^2x(\Delta_{\mathrm{Z}} S_z + \Delta_{\mathrm{SAS}} P_x + \Delta_{\mathrm{bias}} P_z), \tag{2.103}$$

and the Coulomb term

$$H_{\mathrm{C}} = \frac{1}{2}\sum_{\alpha,\beta=\mathrm{f,b}} \int d^2x d^2x' V^{\alpha\beta}(\boldsymbol{x}-\boldsymbol{x}')\rho^{\alpha}(\boldsymbol{x})\rho^{\beta}(\boldsymbol{x}'), \tag{2.104}$$

where $\rho^{\alpha}(\boldsymbol{x}) = \rho^{\dagger}_{\alpha}(\boldsymbol{x})\rho_{\alpha}(\boldsymbol{x})$ is the electron density in layer α, and the Coulomb potentials $V^{\alpha\beta}(\boldsymbol{x})$ are given by

$$\begin{aligned} V^{\mathrm{ff}}(\boldsymbol{x}) = V^{\mathrm{ff}}(\boldsymbol{x}) \equiv V(\boldsymbol{x}) &= \frac{e^2}{4\pi\epsilon|\boldsymbol{x}|}, \\ V^{\mathrm{fb}}(\boldsymbol{x}) = V^{\mathrm{bf}}(\boldsymbol{x}) \equiv V^{\mathrm{d}}(\boldsymbol{x}) &= \frac{e^2}{4\pi\epsilon\sqrt{|\boldsymbol{x}|^2+d^2}}. \end{aligned} \tag{2.105}$$

For later convenience, we introduce the potentials and their Fourier transformation,

$$\begin{aligned} V^{\pm}(\boldsymbol{x}) &= \frac{1}{2}[V(\boldsymbol{x}) \pm V^{\mathrm{d}}(\boldsymbol{x})], \\ V(\boldsymbol{q}) = \frac{e^2}{4\pi\epsilon|\boldsymbol{q}|},\ V^{\mathrm{d}}(\boldsymbol{q}) &= \frac{e^2}{4\pi\epsilon|\boldsymbol{q}|}e^{-\boldsymbol{q}d},\ V^{\pm}(\boldsymbol{q}) = \frac{e^2}{8\pi\epsilon|\boldsymbol{q}|}(1\pm e^{-\boldsymbol{q}d}). \end{aligned} \tag{2.106}$$

The Coulomb interaction (2.104) is decomposed into the SU(4)-invariant and SU(4)-noninvariant terms

$$H^{+}_{\mathrm{C}} = \frac{1}{2}\int d^2x d^2y V^{+}(\boldsymbol{x}-\boldsymbol{y})\rho(\boldsymbol{x})\rho(\boldsymbol{y}) = \pi\int d^2q \rho(-\boldsymbol{q})V^{+}(\boldsymbol{q})\rho(\boldsymbol{q}), \tag{2.107}$$

$$H^{-}_{\mathrm{C}} = 2\int d^2x d^2y V^{-}(\boldsymbol{x}-\boldsymbol{y})P_z(\boldsymbol{x})P_z(\boldsymbol{y}) = 4\pi\int d^2q P_z(-\boldsymbol{q})V^{-}(\boldsymbol{q})P_z(\boldsymbol{q}), \tag{2.108}$$

where

$$V^{\pm}(\boldsymbol{x}) = \frac{e^2}{8\pi\epsilon}\left(\frac{1}{|\boldsymbol{x}|} \pm \frac{1}{\sqrt{|\boldsymbol{x}|^2+d^2}}\right), \tag{2.109}$$

with the layer separation d. Here we used the subscript $+$ for the SU(4)-invariant, while for the SU(4)-noninvariant, we used the subscript $-$.

Since the Landau level is quenched to the lowest-Landau level, the kinetic term becomes just a constant, and can be neglected. The actual total Hamiltonian is composed of the Coulomb terms, and the Zeeman and pseudo-Zeeman terms. The SU(4)-invariant term H^{+}_{C} becomes the dominant among the other terms, which are SU(4) non-invariant, and therefore, they can be regarded as perturbation terms. Thus, it is enough to consider that the system has (approximate) SU(4) symmetry. Thus, we use the SU(4) formalism to investigate the physics of bilayer QH systems. As we show in the chapter 3, 4 and 5, the results obtained

from the SU(4) formalism seems to have good qualitative agreements with the experimental results, where R-spin operator plays a role, which does not exist in the $\mathrm{SU}(2)_{\mathrm{spin}} \times \mathrm{SU}(2)_{\mathrm{ppin}}$, especially in the canted antiferromagnetic phase. Indeed, we can see clearly the mechanism of entangled spin-pseudospin phenomena by adopting the SU(4) formalism.

We next show the Coulomb Hamiltonian projected to the lowest Landau level. First for the monolayer SU(N) QH systems, the Coulomb interaction in the field-theoretical representation is given by

$$H_{\mathrm{C}} = \frac{1}{2}\int d^2x d^2x' \rho(\boldsymbol{x}) V(\boldsymbol{x}-\boldsymbol{x}')\rho(\boldsymbol{x}') = \pi \int d^2q V(\boldsymbol{q})\rho(-\boldsymbol{q})\rho(\boldsymbol{q}), \tag{2.110}$$

where the Coulomb potential $V(\boldsymbol{x})$ and its Fourier transformation $V(\boldsymbol{q})$ given by

$$V(\boldsymbol{x}) = \frac{e^2}{4\pi\epsilon|\boldsymbol{x}|}, \qquad V(\boldsymbol{q}) = \int \frac{d^2x}{2\pi}\frac{e^2}{4\pi\epsilon|\boldsymbol{x}|}e^{-i\boldsymbol{q}\boldsymbol{x}} = \frac{e^2}{4\pi\epsilon|\boldsymbol{q}|}, \tag{2.111}$$

respectively. The Coulomb interaction takes place just in the single layer. By using (2.110) and the bare density operator (2.94) with $N = 0$, we have

$$H_{\mathrm{C}} = \pi \int d^2q V(\boldsymbol{q})\left(F_0(-\boldsymbol{q})\hat{\rho}(-\boldsymbol{q})\right)\left(F_0(\boldsymbol{q})\hat{\rho}(\boldsymbol{q})\right) = \pi \int d^2q V_{\mathrm{D}}(\boldsymbol{q})\hat{\rho}(-\boldsymbol{q})\hat{\rho}(\boldsymbol{q}), \tag{2.112}$$

where

$$V_{\mathrm{D}}(\boldsymbol{q}) \equiv V_0^{\mathrm{eff}}(\boldsymbol{q}) = V(\boldsymbol{q})F_0(-\boldsymbol{q})F_0(\boldsymbol{q}) = \frac{e^2}{4\pi\epsilon|\boldsymbol{q}|}e^{-\frac{l_B^2\boldsymbol{q}^2}{2}}. \tag{2.113}$$

In the real space, it is described in terms of the modified Bessel function $I_0(x)$ as

$$V_{\mathrm{D}}(\boldsymbol{x}) = \frac{e^2\sqrt{2\pi}}{8\pi\epsilon l_B} I_0\left(\frac{\boldsymbol{x}^2}{4l_B^2}\right) e^{-\frac{\boldsymbol{x}^2}{4l_B^2}}. \tag{2.114}$$

The potential (2.113) is the effective Coulomb interaction in the lowest-Landau level. We analyze the Coulomb interaction among the electrons in the lowest-Landau level given by (2.113). In (2.112), we omitted the Landau-level index $N = 0$ from the bare density operators. Hereafter we omit the index $N = 0$ from the bare density operators.

In the short distance limit $|\boldsymbol{x}| \to 0$, we have

$$V_{\mathrm{D}}(\boldsymbol{x}) \to \frac{e^2\sqrt{2\pi}}{8\pi\epsilon l_B} = \sqrt{\frac{\pi}{2}}E_{\mathrm{C}}^0, \tag{2.115}$$

describing the non-locality of the electrons in the lowest-Landau level, whereas in the long distance limit $|\boldsymbol{x}| \to \infty$, (2.114) becomes

$$V_{\mathrm{D}}(\boldsymbol{x}) \to \frac{e^2}{4\pi\epsilon|\boldsymbol{x}|}, \tag{2.116}$$

which is the ordinary Coulomb potential.

The projected Coulomb Hamiltonian in the bilayer QH systems is given by

$$H_{\mathrm{C}} = \pi \int d^2q V_{\mathrm{D}}^{+}(\boldsymbol{q})\hat{\rho}(-\boldsymbol{q})\hat{\rho}(\boldsymbol{q}) + 4\pi \int d^2q V_{\mathrm{D}}^{-}(\boldsymbol{q})\hat{P}_z(-\boldsymbol{q})\hat{P}_z(\boldsymbol{q}), \tag{2.117}$$

where the potentials $V_{\mathrm{D}}^{\pm}(\boldsymbol{q})$ are

$$V_{\mathrm{D}}^{\pm}(\boldsymbol{q}) = \frac{e^2}{8\pi\epsilon|\boldsymbol{q}|}\left(1 \pm e^{-|\boldsymbol{q}|d}\right) e^{-\frac{1}{2}l_B^2\boldsymbol{q}^2}. \tag{2.118}$$

In the real space, they become

$$V_{\mathrm{D}}^{\pm}(\boldsymbol{x}) = \frac{e^2\sqrt{2\pi}}{16\pi\epsilon l_B} I_0\left(\frac{\boldsymbol{x}^2}{4l_B^2}\right) e^{-\frac{\boldsymbol{x}^2}{4l_B^2}} \pm \frac{e^2}{8\pi\epsilon}\int_0^\infty e^{-\frac{1}{2}l_B^2\boldsymbol{k}^2 - kd} J_0\left(k|\boldsymbol{x}|\right), \tag{2.119}$$

with $J_0(x)$ the Bessel function of the first kind.

We consider the classical Coulomb Hamiltonian. It is given by [101, 102, 103]

$$H^{\mathrm{cl}} = \langle\chi|H_{\mathrm{C}}|\chi\rangle = H_{\mathrm{D}}^{\mathrm{cl}} + H_{\mathrm{X}}^{\mathrm{cl}}. \tag{2.120}$$

The classical Coulomb Hamiltonian is decomposed into the direct and exchange forms. First, for the monolayer systems, the direct and exchange forms are

$$H_{\mathrm{D}}^{\mathrm{cl}} = \pi \int d^2q V_{\mathrm{D}}(\boldsymbol{q})\hat{\rho}^{\mathrm{cl}}(-\boldsymbol{q})\hat{\rho}^{\mathrm{cl}}(\boldsymbol{q}), \tag{2.121}$$

$$H_{\mathrm{X}}^{\mathrm{cl}} = -\pi \int d^2k V_{\mathrm{X}}(\boldsymbol{k})\left[\hat{I}_a^{\mathrm{cl}}(-\boldsymbol{k})\hat{I}_a^{\mathrm{cl}}(\boldsymbol{k}) + \frac{1}{2N}\hat{\rho}^{\mathrm{cl}}(-\boldsymbol{k})\hat{\rho}^{\mathrm{cl}}(\boldsymbol{k})\right], \tag{2.122}$$

where V_{X} is the exchange potential,

$$V_{\mathrm{X}}(\boldsymbol{q}) = \frac{l_B^2}{\pi}\int d^2k e^{-il_B^2\boldsymbol{p}\wedge\boldsymbol{k}} V_{\mathrm{D}}(\boldsymbol{k}), \quad V_{\mathrm{X}}(\boldsymbol{x}) = \frac{1}{2\pi}\int d^2p e^{i\boldsymbol{p}\boldsymbol{x}} V_{\mathrm{X}}(\boldsymbol{p}), \tag{2.123}$$

which become

$$V_{\mathrm{X}}(\boldsymbol{q}) = \frac{e^2\sqrt{2\pi}l_B}{4\pi\epsilon} I_0\left(\frac{l_B^2\boldsymbol{p}^2}{4}\right) e^{-\frac{l_B^2\boldsymbol{p}^2}{4}}, \quad V_{\mathrm{X}}(\boldsymbol{x}) = 2V(\boldsymbol{x}) e^{-\frac{\boldsymbol{x}^2}{2l_B^2}}, \tag{2.124}$$

for the lowest-Landau level. We see that when all the spins are polarized into the same direction, the spin configuration $\hat{I}_a^{\mathrm{cl}}(\boldsymbol{k})$ becomes homogeneous, implying $\hat{I}_a^{\mathrm{cl}}(\boldsymbol{k}) \propto \delta(\boldsymbol{k})$. Moreover, the exchange potential $V_{\mathrm{X}}(\boldsymbol{k})$ takes maximum at $\boldsymbol{k} = 0$. Therefore, the Coulomb Hamiltonian is minimized when all the spins align in the same direction, and consequently, the exchange term plays the key role for the spontaneous symmetry breaking.

The direct and exchange forms of bilayer QH systems are

$$H_{\rm D}^{\rm cl} = \pi \int d^2q V_{\rm D}^{+}(\boldsymbol{q})\hat{\rho}^{\rm cl}(-\boldsymbol{q})\hat{\rho}^{\rm cl}(\boldsymbol{q}) + 4\pi \int d^2q V_{\rm D}^{-}(\boldsymbol{q})\hat{P}_z^{\rm cl}(-\boldsymbol{q})\hat{P}_z^{\rm cl}(\boldsymbol{q}), \tag{2.125}$$

$$\begin{aligned} H_{\rm X}^{\rm cl} = &-\frac{\pi}{2}\int d^2p V_X^d(\boldsymbol{p})[\hat{S}_a^{\rm cl}(-\boldsymbol{p})\hat{S}_a^{\rm cl}(\boldsymbol{p}) + \hat{P}_a^{\rm cl}(-\boldsymbol{p})\hat{P}_a^{\rm cl}(\boldsymbol{p}) + \hat{R}_{ab}^{\rm cl}(-\boldsymbol{p})\hat{R}_{ab}^{\rm cl}(\boldsymbol{p})] \\ &- \pi \int d^2p V_X^{-}(\boldsymbol{p})[\hat{S}_a^{\rm cl}(-\boldsymbol{p})\hat{S}_a^{\rm cl}(\boldsymbol{p}) + \hat{P}_z^{\rm cl}(-\boldsymbol{p})\hat{P}_z^{\rm cl}(\boldsymbol{p}) + \hat{R}_{az}^{\rm cl}(-\boldsymbol{p})\hat{R}_{az}^{\rm cl}(\boldsymbol{p})] \\ &- \frac{\pi}{8}\int d^2p V_X(\boldsymbol{p})\hat{\rho}^{\rm cl}(-\boldsymbol{p})\hat{\rho}^{\rm cl}(\boldsymbol{p}), \end{aligned} \tag{2.126}$$

with

$$V_{\rm X}^{\pm}(\boldsymbol{p}) = \frac{\sqrt{2\pi}e^2\ell_B}{8\pi\epsilon} I_0(\ell_B^2\boldsymbol{p}^2/4)e^{-\ell_B^2\boldsymbol{p}^2/4} \pm \frac{e^2\ell_B^2}{4\pi\epsilon}\int_0^\infty dk e^{-\frac{1}{2}\ell_B^2k^2 - kd} J_0(\ell_B^2|\boldsymbol{p}|k), \tag{2.127}$$

$$V_{\rm X} = V_{\rm X}^{+} + V_{\rm X}^{-}, \quad V_{\rm X}^{d} = V_{\rm X}^{+} - V_{\rm X}^{-}. \tag{2.128}$$

Here, $I_0(x)$ is the modified Bessel function, and $J_0(x)$ is the Bessel function of the first kind. We comment that a similar Hamiltonian has been derived based on the Schwinger boson mean-field theory [126]. When the SU(4) isospins are spontaneously polarized, with the homogeneous configuration, driven by the exchange Coulomb interaction, four energy levels are degenerate into ν energy states in the ground state. Such state is called the SU(4) QH ferromagnet.

The expectation value of the Coulomb Hamiltonian in (2.120) is taken by the state

$$|\chi\rangle = e^{iW}|\chi_0\rangle, \tag{2.129}$$

where W is an arbitrary element of the W_∞(N) algebra, and $|\chi_0\rangle$ given by

$$|\chi_0\rangle = \prod_{\mu n}\left[c_\mu^\dagger(n)\right]^{\nu_\mu(n)}|0\rangle. \tag{2.130}$$

Here $\nu_\mu(n)$ in (2.130) takes either 0 or 1, describing that the state with isospin μ at site n is occupied or not. e^{iW} is the local rotation for the isospins since it depends on the Landau-site n, and therefore, (2.129) represents the many-body state where the isospins are polarized into certain direction. The simplest example is the SU(2) QH ferromagnet in the monolayer QH systems, where all the spins are aligned in the same direction. Furthermore, the state (2.129) also describes the low-energy excitation modes. For instance, NG modes as the isospin waves, which are the perturbative excitation modes around the ground state.

We derive the effective Hamiltonian for the NG modes by making the derivative expansion, or equivalently, the momentum expansion for the exchange term [101]. This is because the exchange interaction $V_X(\boldsymbol{x})$ is a short-range potential, so that it becomes good approximation to make the derivative expansion for $V_{\rm X}(\boldsymbol{x})$. This is the term which induces the symmetry breaking and the associated NG modes.

We first discuss in the case of the monolayer SU(N) QH system to clearly understand the procedure for the derivation of the effective Hamiltonian. Its exchange Coulomb Hamiltonian

in the momentum space is given by (2.122). We expand the exchange potential $V_{\rm X}(\boldsymbol{p})$ as

$$V_{\rm X}(\boldsymbol{p}) = V_{\rm X}(0) - \frac{2J_s}{\pi\rho_\Phi^2}\boldsymbol{p}^2 + \mathcal{O}(\boldsymbol{p}^4), \tag{2.131}$$

where $\rho_\Phi = \rho_0/\nu$ is the density of states, and

$$V_{\rm X}(0) = 4l_B^2\epsilon_{\rm X}. \tag{2.132}$$

The parameter J_s describes the spin stiffness, and for the lowest Landau level we have

$$J_s = \frac{1}{8\pi}\epsilon_{\rm X} = \frac{1}{16\sqrt{2\pi}}E_{\rm C}^0. \tag{2.133}$$

Substituting (2.131) into (2.122) and performing the Fourier transformation with retaining the first nontrivial term, we have the effective Hamiltonian

$$H_{\rm X}^{\rm eff} = \frac{2J_s}{\rho_\Phi^2}\int d^2x \left[\partial_i \hat{I}_a^{\rm cl}(\boldsymbol{x})\partial_i \hat{I}_a^{\rm cl}(\boldsymbol{x}) + \frac{1}{2N}\hat{\rho}^{\rm cl}(\boldsymbol{x})\hat{\rho}^{\rm cl}(\boldsymbol{x})\right]. \tag{2.134}$$

As a result we derived the SU(N) nonlinear sigma model,

$$H_{\rm X}^{\rm eff} = 2J_s\int d^2x \partial_i\mathcal{I}_a(\boldsymbol{x})\partial_i\mathcal{I}_a(\boldsymbol{x}), \tag{2.135}$$

where $\mathcal{I}_a(\boldsymbol{x})$ is the normalized isospin density given by $I_a(\boldsymbol{x}) = \rho_\Phi\mathcal{I}_a(\boldsymbol{x})$. Hamiltonian (2.135) represents the exchange interaction between isospins $\mathcal{I}_a(\boldsymbol{x})$. Especially for N= 2, by including the Zeeman term in (2.135), we obtain the SU(2) effective Hamiltonian for the monolayer QH systems

$$H_{\rm X}^{\rm eff} = 2J_s\int d^2x \partial_i\mathcal{S}_a(\boldsymbol{x})\partial_i\mathcal{S}_a(\boldsymbol{x}) - \Delta_{\rm Z}\int d^2x\rho_\Phi\mathcal{S}_z(\boldsymbol{x}), \tag{2.136}$$

which describes the dynamics of spin wave.

With the similar analysis, we can derive the effective Hamiltonian for the bilayer QH systems with spin. The exchange interactions $V^\pm(\boldsymbol{p})$ are short ranged, and therefore, we make the derivative expansion for them. The exchange Coulomb potential $V_{\rm X}^\pm(\boldsymbol{p})$ is expanded as

$$V_{\rm X}^\pm(\boldsymbol{p}) = V_{\rm X}^\pm(0) - \frac{2J_s^\pm}{\pi\rho_\Phi^2}\boldsymbol{p}^2 + \mathcal{O}(\boldsymbol{p}^4), \tag{2.137}$$

with

$$J_s = J_s^+ + J_s^-, \quad J_s^d = J_s^+ - J_s^- \tag{2.138}$$

$$J_s^d = J_s\left[-\sqrt{\frac{2}{\pi}}\frac{d}{\ell_B} + \left(1 + \frac{d^2}{\ell_B^2}\right)e^{d^2/2\ell_B^2}\mathrm{erfc}\left(d/\sqrt{2}\ell_B\right)\right], \tag{2.139}$$

$$\epsilon_X^\pm = \frac{1}{2}\left[1 \pm e^{d^2/2\ell_B^2}\mathrm{erfc}\left(d/\sqrt{2}\ell_B\right)\right]\epsilon_X. \tag{2.140}$$

Then for the later analysis of NG modes, we set $\hat{\rho}^{\rm cl}(\boldsymbol{p}) = \rho_0$, $\hat{S}^{\rm cl}_a(\boldsymbol{p}) = \rho_\Phi \mathcal{S}_a(\boldsymbol{p})$, $\hat{P}^{\rm cl}_a(\boldsymbol{p}) = \rho_\Phi \mathcal{P}_a(\boldsymbol{p})$, and $\hat{R}^{\rm cl}_{ab}(\boldsymbol{p}) = \rho_\Phi \mathcal{R}_{ab}(\boldsymbol{p})$. Taking the nontrivial lowest order terms in the derivative expansion and including the $H_{\rm ZPZ}$ term, we obtain the SU(4) effective Hamiltonian density

$$\begin{aligned}\mathcal{H}^{\rm eff} &= J_s^d \left((\partial_k \mathcal{S}_a)^2 + (\partial_k \mathcal{P}_a)^2 + (\partial_k \mathcal{R}_{ab})^2)\right) + 2J_s^- \left((\partial_k \mathcal{S}_a)^2 + (\partial_k \mathcal{P}_z)^2 + (\partial_k \mathcal{R}_{az})^2\right) \\ &+ \rho_\phi [\epsilon_{\rm cap} (\mathcal{P}_z)^2 - (\epsilon_X^+ - \epsilon_X^-) \left(\left((\mathcal{S}_a)^2 + (\mathcal{P}_a)^2\right) + \sum_{a,b=x,y,z} (\mathcal{R}_{ab})^2 \right) \\ &- 2\epsilon_X^- \left((\mathcal{S}_a)^2 + (\mathcal{R}_{az})^2\right) - (\Delta_{\rm Z} \mathcal{S}_z + \Delta_{\rm SAS} \mathcal{P}_x + \Delta_{\rm bias} \mathcal{P}_z)], \end{aligned} \tag{2.141}$$

where the irrelevant constants are neglected and

$$\epsilon_D^- = \frac{d}{4\ell_B} E^0_{\rm C}, \quad \epsilon_{\rm cap} = 4\epsilon_D^- - 2\epsilon_X^-. \tag{2.142}$$

This Hamiltonian is valid at $\nu = 1, 2$ and 3. It is to be remarked that all potential terms vanish in the SU(4) invariant limit, where perturbative excitations are gapless. They are the NG modes associated with spontaneous breaking of the SU(4) symmetry. They get gapped in the actual system, since the SU(4) symmetry is explicitly broken. Nevertheless we call them the NG modes. We use (2.141) as the basic Hamiltonian for the study of the NG modes in the SU(4) QH ferromagnet.

In this thesis, we treat only the type of the states (2.129) where the lowest Landau levels are filled by electrons to describe " integer QH states". Thus the total filling factor ν is limited to integer values. In this way, we can calculate the expectation values of physical quantities in a mathematically rigorous way, and derive the effective Hamiltonian, the equations of motion for the expectation values of SU(4) isospins or electric currents, the existence of the CAF phase, the Josephson current and the associated QH effects, and the Josephson supercurrent, as shown in chapters 3,4, and 5. Although the analysis of impurity effects are beyond the scope of this thesis, these phenomena may expected to be realized in the realistic systems with impurities.

Chapter 3

Nambu-Goldstone Modes and the Josephson Supercurrent at $\nu = 1$

An interlayer phase coherence develops spontaneously in the bilayer quantum Hall systems at the filling factor $\nu = 1$, driven by the pseudospin wave as a NG mode with a linear dispersion in the zero tunneling-interaction limit. Then its phase field provokes a Josephson supercurrent in each layer, which is dissipationless as in superconductor. The Josephson supercurrent affects the Hall resistance leading to its anomalous behavior.

This chapter is organized as follows. In section 3.1, we discuss the ground state in $\nu = 1$ bilayer QH systems. In section 3.2, we derive the effective Hamiltonian for the NG modes. By taking account of the NG-mode spectrum such as the dispersions and coherence lengths, in section 3.3, we study the interlayer phase coherence developed by the psedudospin wave as a NG mode showing the linear dispersion. Then we analyze the Josephson supercurrent induced by the interlayer phase field. In section 3.4, we present the anomalous behavior of the Hall resistivity in the counterflow and drag geometries, driven by the Josephson supercurrent. We then compare our theoretical results with the experimental ones reported by [74, 75, 76, 77]. The description of this chapter is based on [59, 74, 75, 76, 77, 78, 79, 110].

3.1 Ground state structure

We introduce the CP^3 field based on the composite boson theory. An electron is converted into a composite boson by acquiring a flux quantum in the QH state. The CP^3 field emerges when composite bosons undergo Bose-Einstein condensation. The dimensionless SU(4) isospin

densities are given by [59]

$$\begin{aligned}\mathcal{S}_a(\boldsymbol{x}) &= \frac{1}{2}\boldsymbol{n}^\dagger \tau_a^{\mathrm{spin}} \boldsymbol{n},\\ \mathcal{P}_a(\boldsymbol{x}) &= \frac{1}{2}\boldsymbol{n}^\dagger \tau_a^{\mathrm{ppin}} \boldsymbol{n},\\ \mathcal{R}_{ab}(\boldsymbol{x}) &= \frac{1}{2}\boldsymbol{n}^\dagger \tau_a^{\mathrm{spin}} \tau_b^{\mathrm{ppin}} \boldsymbol{n},\end{aligned} \tag{3.1}$$

where $\boldsymbol{n}$ is the CP^3 field of the form $\boldsymbol{n}(\boldsymbol{x}) = \left(n^{\mathrm{f}\uparrow}, n^{\mathrm{f}\downarrow}, n^{\mathrm{b}\uparrow}, n^{\mathrm{b}\downarrow}\right)^t$.

At $\nu = 1$, the ground state is the bonding state with up-spin, where all the electrons belong to the unique one-body state. In the bonding-antibonding representation, the corresponding CP^3 field is described by

$$(n_g^{\mathrm{B}\uparrow}, n_g^{\mathrm{B}\downarrow}, n_g^{\mathrm{A}\uparrow}, n_g^{\mathrm{A}\downarrow}) = (1, 0, 0, 0), \tag{3.2}$$

and in the layer representation, it becomes

$$\begin{pmatrix} n_g^{\mathrm{f}\uparrow} \\ n_g^{\mathrm{f}\downarrow} \\ n_g^{\mathrm{b}\uparrow} \\ n_g^{\mathrm{b}\downarrow} \end{pmatrix} = \frac{1}{\sqrt{2}} \begin{pmatrix} \sqrt{1+\sigma_0} & 0 & \sqrt{1-\sigma_0} & 0 \\ 0 & \sqrt{1+\sigma_0} & 0 & \sqrt{1-\sigma_0} \\ \sqrt{1-\sigma_0} & 0 & -\sqrt{1+\sigma_0} & 0 \\ 0 & \sqrt{1-\sigma_0} & 0 & -\sqrt{1+\sigma_0} \end{pmatrix} \begin{pmatrix} n_g^{\mathrm{B}\uparrow} \\ n_g^{\mathrm{B}\downarrow} \\ n_g^{\mathrm{A}\uparrow} \\ n_g^{\mathrm{A}\downarrow} \end{pmatrix} = \begin{pmatrix} \sqrt{\frac{1+\sigma_0}{2}} \\ 0 \\ \sqrt{\frac{1-\sigma_0}{2}} \\ 0 \end{pmatrix}, \tag{3.3}$$

where σ_0 is the imbalanced configuration. The values of the isospin fields in the ground state are described in terms of the imbalanced configuration σ_0 as

$$\mathcal{S}_a^g = \frac{1}{2}\delta_{az}, \quad \mathcal{P}_a^g = \frac{1}{2}\left(\sqrt{1-\sigma_0^2}\delta_{ax} + \sigma_0\delta_{az}\right), \quad \mathcal{R}_{ab}^g = \frac{1}{2}\delta_{az}\left(\sqrt{1-\sigma_0^2}\delta_{bx} + \sigma_0\delta_{bz}\right), \tag{3.4}$$

and all others being zero, giving a unique phase. The ground state is invariant under U(3) transformation, and the symmetry breaking pattern becomes SU(4)→U(3), so that the target space becomes

$$\mathrm{CP}^3 = \mathrm{SU}(4)/\mathrm{U}(3) = \mathrm{U}(4)/[\mathrm{U}(1) \otimes \mathrm{U}(3)], \tag{3.5}$$

which is called the complex-projective (CP) space.

From (3.4) and (2.141), the ground state energy in $\nu = 1$, denoting $E_{\mathrm{g}}^{\nu=1}$, is expressed in terms of σ_0 as

$$E_{\mathrm{g}}^{\nu=1} = \rho_0 \left(\epsilon_{\mathrm{cap}}^{\nu=1}\left(\frac{\sigma_0}{2}\right)^2 - \Delta_{\mathrm{SAS}}\frac{\sqrt{1-\sigma_0^2}}{2} - \Delta_{\mathrm{bias}}\frac{\sigma_0}{2}\right), \tag{3.6}$$

where

$$\epsilon_{\mathrm{cap}}^{\nu=1} = 4(\epsilon_D^- - \epsilon_X^-). \tag{3.7}$$

The constant term which does not depend on σ_0 has been neglected in (3.6). By minimizing

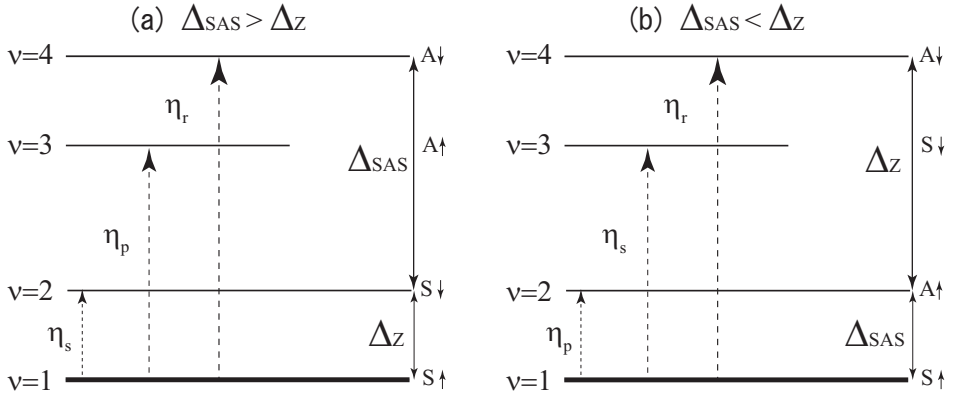

Fig. 3.1 In the bilayer QH systems, the lowest Landau level contains four energy levels separated by Zeeman and tunneling gap, due to two degrees of freedom of spin and pseudospin. We can consider two cases; (a) $\Delta_{\rm SAS} > \Delta_{\rm Z}$ and (b) $\Delta_{\rm SAS} < \Delta_{\rm Z}$. In both cases, all the electrons occupy the up-spin symmetric (bonding) states in the balanced (imbalanced) configurations at $\nu = 1$. Therefore, $\nu = 1$ shows the unique phase. There exist three small fluctuations as the NG modes, $\eta_{\rm s}$, $\eta_{\rm p}$, and $\eta_{\rm r}$, which are the excitations to the down-spin symmetric state, up-spin antisymmetric state, and down-spin antisymmetric state, respectively. Correspondingly, the excitation gaps are the Zeeman energy $\Delta_{\rm Z}$, the tunneling gap $\Delta_{\rm SAS}$, and the sum of Zeeman and tunneling gap $\Delta_{\rm Z} + \Delta_{\rm SAS}$. This picture is taken from [110].

the energy (3.6) with respect to σ_0, the bias voltage $\Delta_{\rm bias}$ is determined as

$$\Delta_{\rm bias} = \frac{\sigma_0}{\sqrt{1-\sigma_0^2}}\Delta_{\rm SAS} + \sigma_0 \epsilon_{\rm cap}^{\nu=1}. \tag{3.8}$$

3.2 Effective Hamiltonian for the NG modes

From the previous section, we see that the symmetry breaking pattern is given by (3.5), and therefore three complex NG modes emerge, which are described by the CP^3 fields[*1]. This also agrees with the one-body picture shown in Fig. 3.1. Since the ground state is up-spin bonding state $|{\rm B}\uparrow\rangle$, there exist three types of excitation modes: (i) the excitation mode from $|{\rm B}\uparrow\rangle$ to $|{\rm B}\downarrow\rangle$ with the excitation gap given by Zeeman gap $\Delta_{\rm Z}$, (ii) the excitation mode from $|{\rm B}\uparrow\rangle$ to $|{\rm A}\uparrow\rangle$ with the excitation gap given by tunneling gap $\Delta_{\rm SAS}$, (iii) the excitation mode from $|{\rm B}\uparrow\rangle$ to $|{\rm A}\downarrow\rangle$ with the excitation gap given by the sum of Zeeman and tunneling gap $\Delta_{\rm Z} + \Delta_{\rm SAS}$. Therefore, it is a good approximation to consider the NG modes as perturbative excitations around the ground state. In order to study the NG-mode spectrum, we first parameterize the

[*1] For the parametrization of the isospin fields in terms of NG modes in nonlinear representation, see Appendix C.

bonding-antibonding state as

$$n^{\mathrm{B}\uparrow} = \sqrt{1 - |\eta_{\mathrm{s}}|^2 - |\eta_{\mathrm{p}}|^2 - |\eta_{\mathrm{r}}|^2}, \quad n^{\mathrm{B}\downarrow} = \eta_{\mathrm{s}}, \quad n^{\mathrm{A}\uparrow} = \eta_{\mathrm{p}}, \quad n^{\mathrm{A}\downarrow} = \eta_{\mathrm{r}}, \tag{3.9}$$

with the commutation relations

$$\left[\eta_i(\boldsymbol{x}), \eta_j^\dagger(\boldsymbol{y})\right] = \rho_0^{-1}\delta_{ij}\delta(\boldsymbol{x} - \boldsymbol{y}), \tag{3.10}$$

required to satisfy the SU(4) algebraic relation. The fluctuation mode η_{s} describes the spin wave which is an excitation mode from $|\mathrm{B}\uparrow\rangle$ to $|\mathrm{B}\downarrow\rangle$, η_{p} the pseudospin wave an excitation from $|\mathrm{B}\uparrow\rangle$ to $|\mathrm{A}\uparrow\rangle$, and η_{r} the R-spin wave an excitation from the ground state to the highest level $|\mathrm{A}\downarrow\rangle$ [Fig. 3.1]. The transformation from the bonding-antibonding field to the layer field is given by

$$\begin{pmatrix} n^{\mathrm{f}\uparrow} \\ n^{\mathrm{f}\downarrow} \\ n^{\mathrm{b}\uparrow} \\ n^{\mathrm{b}\downarrow} \end{pmatrix} = \frac{1}{\sqrt{2}} \begin{pmatrix} \sqrt{1+\sigma_0} & 0 & \sqrt{1-\sigma_0} & 0 \\ 0 & \sqrt{1+\sigma_0} & 0 & \sqrt{1-\sigma_0} \\ \sqrt{1-\sigma_0} & 0 & -\sqrt{1+\sigma_0} & 0 \\ 0 & \sqrt{1-\sigma_0} & 0 & -\sqrt{1+\sigma_0} \end{pmatrix} \begin{pmatrix} n^{\mathrm{B}\uparrow} \\ n^{\mathrm{B}\downarrow} \\ n^{\mathrm{A}\uparrow} \\ n^{\mathrm{A}\downarrow} \end{pmatrix}. \tag{3.11}$$

The isospin fields can be expressed in terms of the excitation fields η_i. Since we consider η_i being small fluctuations around the ground state, we expand the field (3.9) in terms of η_i as

$$(n^{\mathrm{B}\uparrow}, n^{\mathrm{B}\downarrow}, n^{\mathrm{A}\uparrow}, n^{\mathrm{A}\downarrow}) = \left(1 - \frac{1}{2}\left(|\eta_{\mathrm{s}}|^2 + |\eta_{\mathrm{p}}|^2 + |\eta_{\mathrm{r}}|^2\right), \eta_{\mathrm{s}}, \eta_{\mathrm{p}}, \eta_{\mathrm{r}}\right) + \ldots, \tag{3.12}$$

and we have

$$\begin{aligned} n^{\mathrm{f}\uparrow} &= \sqrt{\frac{1+\sigma_0}{2}}\left(1 - \frac{1}{2}(|\eta_{\mathrm{s}}|^2 + |\eta_{\mathrm{p}}|^2 + |\eta_{\mathrm{r}}|^2)\right) + \eta_{\mathrm{p}}\sqrt{\frac{1-\sigma_0}{2}}, \quad n^{\mathrm{f}\downarrow} = \eta_{\mathrm{s}}\sqrt{\frac{1+\sigma_0}{2}} + \eta_{\mathrm{r}}\sqrt{\frac{1-\sigma_0}{2}}, \\ n^{\mathrm{b}\uparrow} &= \sqrt{\frac{1-\sigma_0}{2}}\left(1 - \frac{1}{2}(|\eta_{\mathrm{s}}|^2 + |\eta_{\mathrm{p}}|^2 + |\eta_{\mathrm{r}}|^2)\right) - \eta_{\mathrm{p}}\sqrt{\frac{1+\sigma_0}{2}}, \quad n^{\mathrm{b}\downarrow} = \eta_{\mathrm{s}}\sqrt{\frac{1-\sigma_0}{2}} - \eta_{\mathrm{r}}\sqrt{\frac{1+\sigma_0}{2}}. \end{aligned} \tag{3.13}$$

We then set

$$\eta_i(\boldsymbol{x}) = \frac{\sigma_i(\boldsymbol{x}) + i\vartheta_i(\boldsymbol{x})}{2}, \tag{3.14}$$

with i =s,p,r. Here $\rho_0\sigma_i(\boldsymbol{x})$ is the number density of the excitation mode η_i and $\vartheta_i(\boldsymbol{x})$ is the conjugate phase field, satisfying the commutation relation

$$\frac{\rho_0}{2}\left[\sigma_i(\boldsymbol{x}), \vartheta_j(\boldsymbol{y})\right] = i\delta_{ij}\delta(\boldsymbol{x} - \boldsymbol{y}). \tag{3.15}$$

The isospin fields are expressed in terms of the CP^3 field (3.13) as,

$$
\begin{aligned}
2\mathcal{S}_a &= \left(\sigma_{\rm s} + \frac{1}{2}\left(\sigma_{\rm p}\sigma_{\rm r} + \vartheta_{\rm p}\vartheta_{\rm r}\right), \vartheta_{\rm s} + \frac{1}{2}\left(\sigma_{\rm p}\vartheta_{\rm r} - \vartheta_{\rm p}\sigma_{\rm r}\right), 1 - 2|\eta_{\rm s}|^2 - 2|\eta_{\rm r}|^2\right), \\
2\mathcal{P}_a &= \left(p_x({\rm s,p,r}), -\vartheta_{\rm p} - \frac{1}{2}(\sigma_{\rm s}\vartheta_{\rm r} - \vartheta_{\rm s}\sigma_{\rm r}), p_z({\rm s,p,r})\right), \\
2\mathcal{R}_{xa} &= \left(r_{xx}({\rm s,p,r}), -\vartheta_{\rm r} + \frac{1}{2}(\sigma_{\rm p}\vartheta_{\rm s} - \vartheta_{\rm p}\sigma_{\rm s}), r_{xz}({\rm s,p,r})\right), \\
2\mathcal{R}_{ya} &= \left(r_{yx}({\rm s,p,r}), \sigma_{\rm r} - \frac{1}{2}(\sigma_{\rm s}\sigma_{\rm p} + \vartheta_{\rm s}\vartheta_{\rm p}), r_{yz}({\rm s,p,r})\right), \\
2\mathcal{R}_{za} &= \left(r_{zx}({\rm s,p,r}), -\vartheta_{\rm p} + \frac{1}{2}(\sigma_{\rm s}\vartheta_{\rm r} - \vartheta_{\rm s}\sigma_{\rm r}), r_{zz}({\rm s,p,r})\right),
\end{aligned}
\tag{3.16}
$$

with

$$
\begin{aligned}
p_x({\rm s,p,r}) &= \sqrt{1-\sigma_0^2} - \sigma_0\sigma_{\rm p} - 2\sqrt{1-\sigma_0^2}\left(|\eta_{\rm p}|^2 + |\eta_{\rm r}|^2\right) - \frac{\sigma_0}{2}(\sigma_{\rm s}\sigma_{\rm r} + \vartheta_{\rm s}\vartheta_{\rm r}), \\
p_z({\rm s,p,r}) &= \sigma_0 + \sqrt{1-\sigma_0^2}\sigma_{\rm p} - 2\sigma_0\left(|\eta_{\rm p}|^2 + |\eta_{\rm r}|^2\right) + \frac{\sqrt{1-\sigma_0^2}}{2}(\sigma_{\rm s}\sigma_{\rm r} + \vartheta_{\rm s}\vartheta_{\rm r}), \\
r_{xx}({\rm s,p,r}) &= \sqrt{1-\sigma_0^2}\sigma_{\rm s} - \sigma_0\sigma_{\rm r} - \frac{\sigma_0}{2}\left(\sigma_{\rm s}\sigma_{\rm p} + \vartheta_{\rm s}\vartheta_{\rm p}\right) - \frac{\sqrt{1-\sigma_0^2}}{2}\left(\sigma_{\rm p}\sigma_{\rm r} + \vartheta_{\rm p}\vartheta_{\rm r}\right), \\
r_{yx}({\rm s,p,r}) &= \sqrt{1-\sigma_0^2}\vartheta_{\rm s} - \sigma_0\vartheta_{\rm r} + \frac{\sigma_0}{2}\left(\sigma_{\rm s}\vartheta_{\rm p} - \vartheta_{\rm s}\sigma_{\rm p}\right) - \frac{\sqrt{1-\sigma_0^2}}{2}\left(\sigma_{\rm p}\vartheta_{\rm r} - \vartheta_{\rm p}\sigma_{\rm r}\right), \\
r_{xz}({\rm s,p,r}) &= \sigma_0\sigma_{\rm s} + \sqrt{1-\sigma_0^2}\sigma_{\rm r} - \frac{\sigma_0}{2}\left(\sigma_{\rm p}\sigma_{\rm r} + \vartheta_{\rm p}\vartheta_{\rm r}\right) + \frac{\sqrt{1-\sigma_0^2}}{2}\left(\sigma_{\rm s}\sigma_{\rm p} + \vartheta_{\rm s}\vartheta_{\rm p}\right), \\
r_{yz}({\rm s,p,r}) &= \sigma_0\vartheta_{\rm s} + \sqrt{1-\sigma_0^2}\vartheta_{\rm r} - \frac{\sigma_0}{2}\left(\sigma_{\rm p}\vartheta_{\rm r} - \vartheta_{\rm p}\sigma_{\rm r}\right) - \frac{\sqrt{1-\sigma_0^2}}{2}\left(\sigma_{\rm s}\vartheta_{\rm p} - \vartheta_{\rm s}\sigma_{\rm p}\right), \\
r_{zx}({\rm s,p,r}) &= \sqrt{1-\sigma_0^2} - \sigma_0\sigma_{\rm p} - 2\sqrt{1-\sigma_0^2}\left(|\eta_{\rm p}|^2 + |\eta_{\rm s}|^2\right) + \frac{\sigma_0}{2}(\sigma_{\rm s}\sigma_{\rm r} + \vartheta_{\rm s}\vartheta_{\rm r}), \\
r_{zz}({\rm s,p,r}) &= \sigma_0 + \sqrt{1-\sigma_0^2}\sigma_{\rm p} - 2\sigma_0\left(|\eta_{\rm p}|^2 + |\eta_{\rm s}|^2\right) - \frac{\sqrt{1-\sigma_0^2}}{2}(\sigma_{\rm s}\sigma_{\rm r} + \vartheta_{\rm s}\vartheta_{\rm r}).
\end{aligned}
\tag{3.17}
$$

By Substituting Eq. (3.16) and (3.17) into (2.141), we obtain the effective Hamiltonian for the NG modes

$$
\int d^2k\mathcal{H}_{\rm eff} = \int d^2k\mathcal{H}_{\rm ppin} + \int d^2k\mathcal{H}_{\rm mix}, \tag{3.18}
$$

with

$$\mathcal{H}_{\rm ppin} = \frac{(1-\sigma_0^2)J_s + \sigma_0^2 J_s^d}{2}(\partial_k \sigma_{\rm p})^2 + \frac{\rho_0}{4}\left[\epsilon_{\rm cap}^{\nu=1}(1-\sigma_0^2) + \frac{\Delta_{\rm SAS}}{\sqrt{1-\sigma_0^2}}\right]\sigma_{\rm p}^2 + \frac{1}{2}J_s^d(\partial_k \vartheta_{\rm p})^2 + \frac{\rho_0}{4}\frac{\Delta_{\rm SAS}}{\sqrt{1-\sigma_0^2}}\vartheta_{\rm p}^2, \tag{3.19}$$

$$\mathcal{H}_{\rm mix} = \frac{J_s^+ + \sigma_0 J_s^-}{2}\left[(\partial_k\sigma_1)^2 + (\partial_k\vartheta_1)^2\right] + \frac{\rho_0}{4}\left(\Delta_{\rm Z} + \frac{1}{2}\Delta_{\rm SAS}\frac{\sqrt{1-\sigma_0}}{\sqrt{1+\sigma_0}}\right)\left[\sigma_1^2 + \vartheta_1^2\right] + \frac{J_s^+ - \sigma_0 J_s^-}{2}\left[(\partial_k\sigma_2)^2 + (\partial_k\vartheta_2)^2\right] + \frac{\rho_0}{4}\left(\Delta_{\rm Z} + \frac{1}{2}\Delta_{\rm SAS}\frac{\sqrt{1-\sigma_0}}{\sqrt{1+\sigma_0}}\right)\left[\sigma_2^2 + \vartheta_2^2\right] - \frac{\rho_0}{4}\Delta_{\rm SAS}(\sigma_1\sigma_2 + \vartheta_1\vartheta_2), \tag{3.20}$$

where constant terms have been neglected and change the variables in (3.20) as

$$\eta_{\rm s} = \sqrt{\frac{1+\sigma_0}{2}}\eta_1 + \sqrt{\frac{1-\sigma_0}{2}}\eta_2, \quad \eta_{\rm r} = \sqrt{\frac{1-\sigma_0}{2}}\eta_1 - \sqrt{\frac{1+\sigma_0}{2}}\eta_2, \tag{3.21}$$

and Eqs. (3.7) and (3.8) was used for $\epsilon_{\rm cap}^{\nu=1}$ and $\Delta_{\rm bias}$, respectively. We see that the pseudospin mode is decoupled from other modes, and from (3.19) we have coherence lengths of the interlayer phase field $\vartheta_{\rm p}$ and the conjugate field $\sigma_{\rm p}$

$$\xi_{\rm ppin}^{\vartheta} = 2l_B\sqrt{\frac{\pi\sqrt{1-\sigma_0^2}J_s^d}{\Delta_{\rm SAS}}},$$
$$\xi_{\rm ppin}^{\sigma} = 2l_B\sqrt{\frac{\pi\left[1-\sigma_0^2 J_s + \sigma_0^2 J_s^d\right]}{\epsilon_{\rm cap}^{\nu=1}(1-\sigma_0^2) + \Delta_{\rm SAS}/\sqrt{1-\sigma_0^2}}}. \tag{3.22}$$

We see that in the limit $\Delta_{\rm SAS} \to 0$, the coherence length of interlayer phase mode $\vartheta_{\rm p}$ diverges which implies that it is gapless, while that for $\sigma_{\rm p}$ mode remains finite due to the capacitance term $\epsilon_{\rm cap}^{\nu=1}$. Indeed, the Hamiltonian (3.19) in the limit $\Delta_{\rm SAS} \to 0$ can be diagonalized as

$$H_{\rm ppin} = \int d^2k E_{\boldsymbol{k}} a_{\boldsymbol{k}}^\dagger a_{\boldsymbol{k}}, \tag{3.23}$$
$$E_{\boldsymbol{k}} = 2\sqrt{\lambda^{\sigma_{\rm p}}\lambda^{\vartheta_{\rm p}}} \tag{3.24}$$

where $a_{\boldsymbol{k}}$, $\lambda^{\sigma_{\rm p}}$, and $\lambda^{\vartheta_{\rm p}}$ given by

$$a_{\boldsymbol{k}} = \left(\frac{\rho_0}{4}\right)^{\frac{1}{2}}\left(\left(\frac{\lambda^{\sigma_{\rm p}}}{\lambda^{\vartheta_{\rm p}}}\right)^{\frac{1}{4}}\sigma_{\boldsymbol{k}}^{\rm p} + i\left(\frac{\lambda^{\vartheta_{\rm p}}}{\lambda^{\sigma_{\rm p}}}\right)^{\frac{1}{4}}\vartheta_{\boldsymbol{k}}^{\rm p}\right),$$
$$\lambda^{\vartheta_{\rm p}} = \frac{\boldsymbol{k}^2}{\rho_0}J_s^d, \quad \lambda^{\sigma_{\rm p}} = \frac{(\sigma_0^2 J_s^d + (1-\sigma_0^2)J_s)}{\rho_0}\boldsymbol{k}^2 + \frac{\epsilon_{\rm cap}^{\nu=1}(1-\sigma_0^2)}{2}, \tag{3.25}$$

respectively, obeying the commutation relation, $\left[a_{\boldsymbol{k}}, a_{\boldsymbol{k}'}^\dagger\right] = \delta(\boldsymbol{k}-\boldsymbol{k}')$. Eq. (3.24) shows the linear dispersion.

On the other hand, the two modes η_1 and η_2 are decoupled from (3.20) for $\Delta_{\rm SAS}=0$, and there exist no gapless modes in the Hamiltonian (3.20) unless $\Delta_{\rm Z}\neq 0$.

3.3 Interlayer Phase Coherence and Josephson Supercurrents

In this section, we discuss the interlayer phase coherence at $\nu=1$ bilayer QH systems. This is one of the main topics of the present thesis. The QH states are considered to be incompressible QH liquid states, where the total density is fixed. Since $\Delta N_{\rm tot}=0$, we cannot expect the emergence of macroscopic phase coherence for the monolayer systems. For bilayer systems, although the total density remains fixed, the density difference is not fixed in general. Thus, we may expect the emergence of the macroscopic phase coherence described by the canonical conjugate variable of the density difference. As we have seen in Fig. 2.7, one of the elements which determine if the system is in QH state or not is the ratio d/l_B. On the other hand, the realization of the bilayer QH state does not depend on the magnitude of $\Delta_{\rm SAS}$, or more precisely, $\Delta_{\rm SAS}/E_{\rm C}^0$. With d/l_B small enough, the bilayer QH state is realized even for $\Delta_{\rm SAS}/E_{\rm C}^0\to 0$, and this is the region where the interlayer phase coherence is spontaneously developed.

To describe the interlayer phase coherence quantitatively, we focus on the gapless mode in the limit $\Delta_{\rm SAS}\to 0$. We analyze the nonperturbative phase coherent phenomena, where the phase field $\vartheta(\boldsymbol{x})$ is essentially classical and may become large. To see its physical picture clearly, we parameterize the CP^3 field in terms of imbalanced field $\sigma(\boldsymbol{x})$ and its canonical conjugate interlayer phase field $\vartheta(\boldsymbol{x})$ as

$$\begin{pmatrix} n^{\mathrm{f}\uparrow}(\boldsymbol{x}) \\ n^{\mathrm{f}\downarrow}(\boldsymbol{x}) \\ n^{\mathrm{b}\uparrow}(\boldsymbol{x}) \\ n^{\mathrm{b}\downarrow}(\boldsymbol{x}) \end{pmatrix} = \frac{1}{\sqrt{2}} \begin{pmatrix} e^{i\vartheta(\boldsymbol{x})/2}\sqrt{1+\sigma(\boldsymbol{x})} \\ 0 \\ e^{-i\vartheta(\boldsymbol{x})/2}\sqrt{1-\sigma(\boldsymbol{x})} \\ 0 \end{pmatrix}. \tag{3.26}$$

Then we have the isospin fields expressed as

$$\begin{aligned} &\mathcal{S}_z(\boldsymbol{x})=\frac{1}{2},\quad \mathcal{P}_z(\boldsymbol{x})=\mathcal{R}_{zz}(\boldsymbol{x})=\frac{1}{2}\sigma(\boldsymbol{x}),\\ &\mathcal{P}_x(\boldsymbol{x})=\mathcal{R}_{zx}(\boldsymbol{x})=\frac{1}{2}\sqrt{1-\sigma^2(\boldsymbol{x})}\cos\vartheta(\boldsymbol{x}),\quad \mathcal{P}_y(\boldsymbol{x})=\mathcal{R}_{zy}(\boldsymbol{x})=-\frac{1}{2}\sqrt{1-\sigma^2(\boldsymbol{x})}\sin\vartheta(\boldsymbol{x}), \end{aligned} \tag{3.27}$$

with all others being zero. From (3.27) we obtain the effective Hamiltonian

$$\begin{aligned} \mathcal{H}_{\rm eff}=&\frac{J_s^d}{2}(1-\sigma^2(\boldsymbol{x}))(\partial_k\vartheta(\boldsymbol{x}))^2+\frac{1}{2}\left(J_s+\frac{\sigma^2(\boldsymbol{x})}{1-\sigma^2(\boldsymbol{x})}J_s^d\right)(\partial_k\sigma(\boldsymbol{x}))^2\\ &+\frac{\rho_0\epsilon_{\rm cap}^{\nu=1}}{4}\sigma^2(\boldsymbol{x})-\frac{\rho_0}{2}\left(\Delta_{\rm SAS}\sqrt{1-\sigma^2(\boldsymbol{x})}\cos\vartheta(\boldsymbol{x})+\Delta_{\rm bias}\sigma(\boldsymbol{x})\right). \end{aligned} \tag{3.28}$$

The canonical commutation relation is given by

$$\frac{\rho_0}{2}\left[\sigma(\boldsymbol{x}), \vartheta(\boldsymbol{x})\right] = i\delta(\boldsymbol{x}-\boldsymbol{y}). \tag{3.29}$$

From (3.28) and (3.29), the Heisenberg equations of motion can be calculated as

$$\begin{aligned}\hbar\partial_t\vartheta = {}& \frac{2}{\rho_0}\partial_k(J_{\mathrm{s}}^{\sigma}\partial_k\sigma) + \frac{2J_s^d}{\rho_0}\sigma\left[(\partial_k\vartheta)^2 - \frac{1}{1-\sigma^2}(\partial_k\sigma)^2\right] \\ & - \epsilon_{\mathrm{cap}}\sigma(\boldsymbol{x}) - \Delta_{\mathrm{SAS}}\frac{\sigma(\boldsymbol{x})\cos\vartheta(\boldsymbol{x})}{\sqrt{1-\sigma^2(\boldsymbol{x})}} + \Delta_{\mathrm{bias}},\end{aligned} \tag{3.30}$$

$$\hbar\partial_t\sigma = -\frac{2}{\rho_0}\partial_k(J_{\mathrm{s}}^{\vartheta}\partial_k\vartheta) + \sqrt{1-\sigma^2}\Delta_{\mathrm{SAS}}\sin\vartheta, \tag{3.31}$$

with

$$J_{\mathrm{s}}^{\vartheta} = (1-\sigma^2)J_s^d, \quad J_{\mathrm{s}}^{\sigma} = J_s + \frac{\sigma^2}{1-\sigma^2}J_s^d. \tag{3.32}$$

We analyze the solution for σ and ϑ in the ground state, which are the ground expectation values of them. By setting $\langle\sigma\rangle = \sigma_0$ and $\langle\vartheta\rangle = \vartheta_0 = 0$ in (3.30), we have

$$\Delta_{\mathrm{bias}} = \epsilon_{\mathrm{cap}}\sigma_0 + \frac{\Delta_{\mathrm{SAS}}\sigma_0}{\sqrt{1-\sigma_0^2}}, \tag{3.33}$$

which agrees with (3.8). The bias voltage Δ_{bias} is determined by the equations of motion for σ and ϑ in the ground state.

We now take $\Delta_{\mathrm{SAS}} \to 0$ in (3.28) and retain all the terms up to the second order in the field σ and ϑ, having

$$\mathcal{H}_{\mathrm{eff}} = \frac{J_s^d(\sigma_0)}{2}(\partial_k\vartheta(\boldsymbol{x}))^2 + \frac{J_{\mathrm{s}}^{\sigma}(\sigma_0)}{2}(\partial_k\sigma(\boldsymbol{x}))^2 + \frac{\rho_0\epsilon_{\mathrm{cap}}^{\nu=1}}{4}(\sigma(\boldsymbol{x})-\sigma_0)^2, \tag{3.34}$$

and therefore, by using the Heisenberg equations, we obtain the dispersion

$$E_{\boldsymbol{k}} = |\boldsymbol{k}|\sqrt{\frac{2J_{\mathrm{s}}^{\vartheta}(\sigma_0)}{\rho_0}\left(\frac{2J_{\mathrm{s}}^{\sigma}(\sigma_0)}{\rho_0}\boldsymbol{k}^2 + \epsilon_{\mathrm{cap}}^{\nu=1}\right)}, \tag{3.35}$$

which agrees with (3.24). The emergence of the linear mode represents the U(1) spontaneously symmetry breaking, due to its restoration in the limit $\Delta_{\mathrm{SAS}} \to 0$. For $\nu = 1$, it is the U(1) symmetry generated by T_{0z}. We can see this as follows: in the limit $\Delta_{\mathrm{SAS}} \to 0$, the effective Hamiltonian (2.141) is invariant under the unitary transformation $\exp(-i\vartheta_0 T_{0z})$, describing the $\mathrm{U}(1)_{T_{0z}}$ symmetry, while the ground state characterized by

$$\begin{aligned}&\mathcal{S}_z^g = \frac{1}{2}, \quad \mathcal{P}_z^g = \mathcal{R}_{zz}^g = \frac{1}{2}\sigma_0, \\ &\mathcal{P}_x^g = \mathcal{R}_{zx}^g = \frac{1}{2}\sqrt{1-\sigma_0^2}\cos\vartheta_0, \quad \mathcal{P}_y^g = \mathcal{R}_{zy}^g = -\frac{1}{2}\sqrt{1-\sigma_0^2}\sin\vartheta_0,\end{aligned} \tag{3.36}$$

is not invariant under $\mathrm{U}(1)_{T_{0z}}$. The order parameters (3.36) can be obtained from (3.27) by

using the expectation values $\langle\sigma\rangle = \sigma_0$ and $\langle\vartheta\rangle = \vartheta_0$. The interlayer coherence is spontaneously developed due to the $\mathrm{U}(1)_{T_{0z}}$ symmetry breaking in $\nu = 1$ bilayer QH systems.

We now study the electric Josephson supercurrent carried by the gapless mode $\vartheta(\boldsymbol{x})$. In general the total current consists of three types of current; the Josephson in-plane current $\mathcal{J}_i^{\mathrm{Jos}}$, the Josephson tunneling current $\mathcal{J}_z^{\mathrm{Jos}}$ proportional to Δ_{SAS}, and the Hall current $\mathcal{J}_i^{\mathrm{Hall}}$. What has been argued in [79] is that in the case of $\nu = 1$, there exists interlayer voltage V_{junc} and thus no dissipationless tunneling current $\mathcal{J}_z^{\mathrm{Jos}}$ exists, as long as $\sigma_0 \neq 0$. On the other hand the Josephson in-plane current which is dissipationless does exist, even for $\sigma_0 \neq 0$. Here we assume $\sigma_0 \neq 0$ and $\Delta_{\mathrm{SAS}} = 0$, so that there is no dissipationless tunneling current $\mathcal{J}_z^{\mathrm{Jos}}$ between the two layers.

The electron densities are $\rho_e^{\mathrm{f(b)}} = -e\rho_0\left(1/2 \pm \mathcal{P}_z\right) = -e\rho_0\left(1 \pm \sigma(\boldsymbol{x})\right)/2$ on each layer. Taking the time derivative and using (3.31) we find

$$\partial_t \rho_e^{\mathrm{f}} = -\partial_t \rho_e^{\mathrm{b}} = \frac{eJ_s^{\vartheta}}{\hbar}\nabla^2\vartheta(\boldsymbol{x}). \tag{3.37}$$

The time derivative of the charge is associated with the current via the continuity equation, $\partial_t \rho_e^{\mathrm{f(b)}} = -\partial_i \mathcal{J}_i^{\mathrm{f(b)}}$. We thus identify $\mathcal{J}_i^{\mathrm{f(b)}} = \pm\mathcal{J}_i^{\mathrm{Jos}}(\boldsymbol{x})$+constant, where

$$\mathcal{J}_i^{\mathrm{Jos}}(\boldsymbol{x}) \equiv -\frac{eJ_s^{\vartheta}}{\hbar}\partial_i\vartheta(\boldsymbol{x}). \tag{3.38}$$

Consequently, the current $\mathcal{J}_i^{\mathrm{Jos}}(\boldsymbol{x})$ flows when there exists inhomogeneity in the phase $\vartheta(\boldsymbol{x})$. Such a current is precisely the Josephson supercurrent. Indeed, it is a supercurrent because the coherent mode exhibits a linear dispersion relation.

3.4 Quantum Hall Effects

From section 3.1 to section 3.3, we have discussed the ground state structure of the bilayer QH state, where the electric current is not applied to the QH system, and therefore, no Hall electric field is created in the system. From now on, we consider the QH state in the bilayer system with the electric current. As we have seen in the previous argument, there emerge 3 complex NG modes, one gapless mode and two gapped modes. By taking account of this fact, we expect that the gapless NG mode becomes the carrier of the electric current when the interlayer phase difference is created and becomes spatially inhomogeneous. Thus, the current flowing in the QH system consists of the quantum Hall current and the Josephson supercurrent carried by the gapless NG mode[*2]

$$\mathcal{J}_i^{\mathrm{f(b)}}(\boldsymbol{x}) = \mp\frac{eJ_s^{\vartheta}}{\hbar}\partial_i\vartheta(\boldsymbol{x}) + \frac{e^2 l_B^2}{\hbar}\epsilon_{ij}E_j^{\mathrm{f(b)}}\rho_0^{\mathrm{f(b)}}. \tag{3.39}$$

In this section, we discuss the quantum Hall effect in the presence of the interlayer phase coherence. Concretely, we analyze the Hall resistivity affected by the Josephson supercurrent.

[*2] The detailed derivation of the currents (3.39) is derived in subsection 5.2.3

Then, in the end, we compare our theoretical results with the experimental results reported in [74, 75, 76, 77]. To understand the discussion well, we first discuss the QH effect when the interlayer phase coherence is negligible.

In the system, the homogeneous current density $\mathcal{J}_x^{\mathrm{f(b)}}$ is fed in to each layer. In the steady state, the Hall electric field $E_y^{\mathrm{f(b)}}$ is dynamically generated. Then the Hall current is given in terms of $E_y^{\mathrm{f(b)}}$ by

$$\begin{aligned} \mathcal{J}_x^{\mathrm{f}} &= \frac{\nu}{2R_{\mathrm{K}}}(1+\sigma_0)E_y^{\mathrm{f}}, \qquad \mathcal{J}_x^{\mathrm{b}} = \frac{\nu}{2R_{\mathrm{K}}}(1-\sigma_0)E_y^{\mathrm{b}}, \\ \rho_0^{\mathrm{f}} &= \frac{(1+\sigma_0)}{2}\rho_0, \qquad \rho_0^{\mathrm{b}} = \frac{(1-\sigma_0)}{2}\rho_0, \end{aligned} \tag{3.40}$$

where ν is the total filling factor which is equal to one in this case. All the dynamical variables, $E_y^{\mathrm{f(b)}}$, are determined by Eq. (3.40), and the Hall resistivity becomes

$$R_{\mathrm{Hall}}^{\mathrm{f}} \equiv \left|\frac{E_y^{\mathrm{f}}}{\mathcal{J}_x^{\mathrm{f}}}\right| = \frac{2R_{\mathrm{K}}}{(1+\sigma_0)}, \qquad R_{\mathrm{Hall}}^{\mathrm{b}} \equiv \left|\frac{E_y^{\mathrm{b}}}{\mathcal{J}_x^{\mathrm{b}}}\right| = \frac{2R_{\mathrm{K}}}{(1-\sigma_0)}. \tag{3.41}$$

On the other hand, when there exists the Josephson supercurrent, the total current is given by (3.39). In this case, we have three dynamical variables, $E_y^{\mathrm{f(b)}}$ and $\partial_x\vartheta(x)$, so that, we need the third equation to determine the dynamics. In this thesis, we introduce the third equation motivated by the experimental results shown in Figs. 1.2-1.5. First, from the experimental data in Fig. 1.4, which is the data of the drag geometry at the balanced configuration ($\sigma_0 = 0$), at the total filling factor $\nu = 1$, which is denoted as $\nu_{\mathrm{T}} = 1$, we see that $R_{\mathrm{Hall}}^{\mathrm{f}} = R_{\mathrm{Hall}}^{\mathrm{b}} = R_{\mathrm{K}}$. Thus by using the definition $|R_{\mathrm{Hall}}^{\mathrm{f(b)}} = E_y^{\mathrm{f(b)}}/\mathcal{J}_x^{\mathrm{f(b)}}|$, it implies that

$$E_y^{\mathrm{f}} = E_y^{\mathrm{b}}, \tag{3.42}$$

as reported in [76]. This is because the same amount of the currents were injected ($\mathcal{J}_x^{\mathrm{f}} = \mathcal{J}_x^{\mathrm{b}}$) in both the front and back layer. On the other hand, from Figs. 1.2 and 1.3 in the counterflow geometry at $\sigma_0 = 0$, we see that at $\nu = 1$, the Hall resistivity in one of the layers is zero. In such a situation, it may be considered that the Hall resistivity in both front and back layers satisfy $R_{\mathrm{Hall}}^{\mathrm{f}} = R_{\mathrm{Hall}}^{\mathrm{b}} = 0$, and thus, by using the condition for the current injection in the counterflow geometry $\mathcal{J}_x^{\mathrm{f}} = -\mathcal{J}_x^{\mathrm{b}}$), the condition

$$E_y^{\mathrm{f}} = E_y^{\mathrm{b}} = 0, \tag{3.43}$$

is realized. Consequently, from Eqs. (3.42) and (3.43), we may consider that when the interlayer phase coherence is developed in the bilayer QH system, the condition

$$E_y^{\mathrm{f}} = E_y^{\mathrm{b}} \equiv E_y, \tag{3.44}$$

is held. In the following argument, we analyze the Hall resistivity in the presence of the Josephson supercurrent for various geometries, based on Eq. (3.39) with the condition (3.44). We see later on that the result of $\nu = 1$ in the standard geometry at $\sigma_0 = 0$ in Fig. 1.2 and

the left side of Fig. 1.3, and the one in Fig. 1.5, which is the data for the drag geometry at $\sigma_0 = 1/3$, can also be explained in such a way.

First, for the standard geometry [Fig. 1.6 (a)] at $\sigma_0 = 0$, where the same amount of current is fed in both layers with the same direction, $\mathcal{J}_x^{\rm f} = \mathcal{J}_x^{\rm b}$, and we have $\mathcal{J}_x^{\rm Jos} = 0$. As a result, we have $R_{xy}^{\rm f} = R_{xy}^{\rm b} = 2R_{\rm K}$. By defining the "bilayer Hall resistance" R_{xy} as

$$R_{xy} \equiv \frac{E_y}{\mathcal{J}_x^{\rm f} + \mathcal{J}_x^{\rm b}} = \left(\frac{1}{R_{xy}^{\rm f}} + \frac{1}{R_{xy}^{\rm b}} \right)^{-1}, \tag{3.45}$$

we obtain the standard Hall resistance

$$R_{xy} = R_{\rm K}. \tag{3.46}$$

The emergence of the Josephson supercurrent is verified when the Hall resistance shows different behavior from the standard one.

We next apply these formulas to analyze the counterflow and drag experiments since they occur without tunneling. In the counterflow experiment [Fig. 1.6 (b)], we apply the current $\mathcal{J}_{\rm in}$ to both layers with the same amount but in the opposite direction. Since there is no tunneling we have $\mathcal{J}_x^{\rm b} = -\mathcal{J}_x^{\rm f} = -\mathcal{J}_{\rm in}$. Hence, it follows from (3.39) and (3.44) that $E_y = 0$, or

$$R_{\rm Hall}^{\rm f} \equiv \left| \frac{E_y^{\rm f}}{\mathcal{J}_x^{\rm f}} \right| = 0, \qquad R_{\rm Hall}^{\rm b} \equiv \left| \frac{E_y^{\rm b}}{\mathcal{J}_x^{\rm b}} \right| = 0. \tag{3.47}$$

All the input currents are carried by the Josephson supercurrent, $\mathcal{J}_x^{\rm Jos} = \mathcal{J}_{\rm in}$. It generates an inhomogeneous phase field that $\vartheta(\boldsymbol{x}) = -(\hbar/eJ_s^\vartheta)\mathcal{J}_{\rm in}x$.

In the drag experiment [Fig. 1.6 (c)], since the interlayer coherent tunneling is absent, no current flows on the back layer, or $\mathcal{J}_x^{\rm b} = 0$. Hence, it follows from (3.39) and (3.44) that $\mathcal{J}_{\rm in} = \mathcal{J}_x^{\rm f} = (\nu/R_{\rm K})E_y$, or

$$R_{\rm Hall}^{\rm f} \equiv \left| \frac{E_y^{\rm f}}{\mathcal{J}_x^{\rm f}} \right| = \frac{R_{\rm K}}{\nu}, \tag{3.48}$$

A part of the input current is carried by the Josephson supercurrent, $\mathcal{J}_x^{\rm Jos} = \frac{1}{2}(1 - \sigma_0)\mathcal{J}_{\rm in}$. The interesting point of the drag geometry is that although the electric current is not flowing in the back layer, the Hall electric field $E_y^{\rm b}$ emerges, as reported in [76]. This is because there exists the Josephson supercurrent in the back layer flowing in the opposite direction to the one in the front layer, and in order that the electric current in the back layer becomes zero, the Hall current must be also flowing so as to cancel out the Josephson current. As a result, the Hall electric field $E_y^{\rm b}$ also emerges with the same magnitude as the one in the front layer.

When the two QH systems become independent, the interlayer phase coherence is destroyed and the interlayer phase is not defined. For each layer, the Hall current

$$\mathcal{J}_x^\alpha = \frac{\nu_\alpha}{R_{\rm K}} E_y^\alpha, \qquad \mathcal{J}_y^\alpha = 0, \tag{3.49}$$

is flowing. Here $\nu_{\rm f(b)} = \nu(1 \pm \sigma_0)/2 = (1 \pm \sigma_0)/2$ is the filling factor in the front (back) layer.

For instance, when $\sigma_0 = 1/3$, we have

$$R_{\rm Hall}^{\rm f} = \frac{3}{2} R_{\rm K}. \tag{3.50}$$

We observe $\nu = 2/3$ fractional QH effect in the front layer. The results (3.46), (3.47), (3.48), and (3.50) are consistent with the results obtained in [74, 75, 76, 77] [see also Figs. 1.2-1.5]. Hence, it is appropriate to consider that the condition (3.44) is realized when the interlayer phase coherence is developed in the bilayer QH systems.

We end this chapter by noting that there is another description of the interlayer phase coherence which is considered to be physically equivalent to the pseudospin ferromagnetism called the exciton condensation [68, 69, 136], where an electron in one layer and a hole in the other layer form an electrically neutral boson and condensate. Such a state, for instance, in the balanced configuration ($\sigma_0 = 0$) is described by the wave function [69, 136]

$$|{\rm EC}\rangle = \prod_{\boldsymbol{k}} \frac{1}{\sqrt{2}} \left(1 + e^{i\varphi_0} c_{{\rm b}\boldsymbol{k}}^\dagger c_{{\rm f}\boldsymbol{k}}\right) |\tilde{0}\rangle, \tag{3.51}$$

where $|\tilde{0}\rangle$ is the state where the lowest Landau level is occupied by all the electrons in the front layer, and no electrons exist in the back layer. The operator $c_{{\rm b}\boldsymbol{k}}^\dagger c_{{\rm f}\boldsymbol{k}}$ in (3.51) describes the creation operator of exciton with momentum $\boldsymbol{k}$; hole with momentum $-\boldsymbol{k}$ is created in the front layer while the electron with momentum $\boldsymbol{k}$ is created in the back layer. The phase φ_0 in the (3.51) corresponds to the orientation-angle of the pseudospin ϑ_0.

It may be considered that the exciton condensate is not subjected to the force due to the magnetic field and the Hall electric field, provided that the Hall electric field in the front layer is equal to the one in the back layer. When $E_y^{\rm f} \neq E_y^{\rm b}$, exciton condensate make a motion so as to cancel the mismatch between $E_y^{\rm f}$ and $E_y^{\rm b}$, and as a result, the exciton condensate gather in the edge of the sample, realizing the situation $E_y^{\rm f} = E_y^{\rm b}$. Then the anomalous behavior of the Hall resistivity which we have seen in the previous argument can be explained by the supercurrent carried by the exciton condensate. It may be considered that the supercurrent carried by the exciton condensate corresponds to the Josephson supercurrent (3.38). This is because the electron which is a part of the exciton moves toward certain direction, say positive x direction, while the hole which is a part of the exciton moves toward opposite direction and in the different layer with those of the electron. Similarly, the Josephson supercurrent flow such that the current carried by the interlayer phase field flows along the positive x direction in one layer while the one carried by the interlayer phase field flows in the negative x direction in the other layer, as shown in Eq. (3.39). Although the exciton-condensate description provides a simple explanation for the realization of the condition (3.44), it still remains as merely a qualitative picture, and therefore, lacks the ability to describe the QH effect quantitatively in terms of the excitonic supercurrent.

On the other hand, the effective theory for NG modes shown in this chapter or in Refs. [78, 79] provides the quantitative argument. By analyzing the dispersions of NG modes, it is possible to construct the effective theory of the NG mode with the linear dispersion in terms of

the imbalanced density and the canonical conjugate interlayer phase field. Then the Josephson supercurrent, the Hall currents, and the Hall resistance for each layer are calculable. It shows clearly the creation of the interlayer phase coherence as shown in (3.26) and the associated QH effects. Indeed the Hall resistances given in Eqs. (3.46), (3.47), and (3.48), match with the experimental results shown in Figs. 1.2-1.5 at $\nu = 1$.

Chapter 4

Nambu-Goldstone Modes at $\nu = 2$

In $\nu = 2$ bilayer QH systems, there are three phases; the spin phase, the pseudospin phase, and the CAF phase. The CAF phase shows the most intriguing features, where spins in each layer have ferromagnetic correlations, whereas the spins between the layers are making the antiferromagnetic correlations.

This chapter is organized as follows. In section 4.1, we discuss the ground-state structure; the spin phase, the pseudospin phase, and the CAF phase, in $\nu = 2$ bilayer QH systems based on Ref. [104]. In concrete, the phase diagram described by $\Delta_{\rm Z}$-$\Delta_{\rm SAS}$ plane and the expectation values of the SU(4) isospin densities are shown. The original works of this thesis is written from section 4.2 to section 4.6 based on [110, 111]. In section 4.2, we construct the Grassmannian formalism in order to construct the effective theories for NG modes. In section 4.3, we study the NG-mode spectrum such as the dispersion relations and coherence lengths in the spin phase. In section 4.4, we study the dispersion relations and coherence lengths for the NG modes in the pseudospin phase. In section 4.5, we first study the effective Hamiltonian for the NG modes in the CAF phase. Then we take the tunneling gap $\Delta_{\rm SAS} \to 0$ to seek for the gapless modes. In section 4.6, by retaining only the gapless NG mode in the limit $\Delta_{\rm SAS} \to 0$, we investigate the effective Hamiltonian for the NG mode up to $\mathcal{O}(\Delta_{\rm SAS}^3)$.

4.1 Ground state structure

For $\nu = 2$, four out of two energy levels are filled up to the Fermi energy. Which two energy levels are occupied depends on the relative strength between the Zeeman and tunneling energy. In this section we present the essence of the ground-state structure for $\nu = 2$ following Ref. [104]. We first present the phase diagram as $\Delta_{\rm Z}$-$\Delta_{\rm SAS}$ plane. Then we show SU(4) order parameters, which are the ground-state expectation values of SU(4) operators. See Ref. [104] for the detailed discussion.

In the ground state at $\nu = 2$, the Landau site n is occupied by two electrons. The corre-

sponding wave functions can be expressed as

$$|g_{\nu=2}\rangle = \left(\prod_n \frac{1}{2} g_{\mu\nu}\right) c^\dagger_\mu(n) c^\dagger_\nu(n)|0\rangle, \tag{4.1}$$

where $g_{\mu\nu}$ is the complex 4×4 antisymmetric matrix, reflecting the Pauli principle, and n denoting the Landau-site index. The above states correspond to $|\chi\rangle$ in (2.129) at $\nu = 2$. The expectation values of the SU(4) isospins densities per one Landau site in the ground state are

$$\begin{aligned}
&\mathcal{S}^0_a = \langle g_{\nu=2}|S_a(n,n)|g_{\nu=2}\rangle, \quad \mathcal{P}^0_a = \langle g_{\nu=2}|S_a(n,n)|g_{\nu=2}\rangle, \quad \mathcal{R}^0_{ab} = \langle g_{\nu=2}|S_a(n,n)|g_{\nu=2}\rangle, \\
&S_a(n,n) = c^\dagger_\mu(n) \left(\frac{1}{2}\tau^{\rm spin}_a\right)_{\mu\nu} c_\nu(n), \quad P_a(n,n) = c^\dagger_\mu(n) \left(\frac{1}{2}\tau^{\rm spin}_a\right)_{\mu\nu} c_\nu(n), \\
&R_{ab}(n,n) = c^\dagger_\mu(n) \left(\frac{1}{2}\tau^{\rm spin}_a\right)_{\mu\nu} c_\nu(n).
\end{aligned} \tag{4.2}$$

We call the expectation values of SU(4) isospins as SU(4) order parameters. The SU(4) order parameters satisfy the condition

$$(\mathcal{S}^0_a)^2 + (\mathcal{P}^0_a)^2 + (\mathcal{R}^0_{ab})^2 = 1, \tag{4.3}$$

which originates from the the incompressibility condition

$$\rho(m,n)|g_{\nu=2}\rangle = \nu\delta_{mn}|g_{\nu=2}\rangle. \tag{4.4}$$

By using the the SU(4) order parameters (4.2), the ground-state Hamiltonian per Landau-site is expressed as

$$\begin{aligned}
\tilde{\mathcal{H}}_0 \equiv \frac{\mathcal{H}_0}{\rho_\Phi} &= \epsilon_{\rm cap}(\mathcal{P}^0_z)^2 - (\epsilon^+_X - \epsilon^-_X)\left((\mathcal{S}^0_a)^2 + (\mathcal{P}^0_a)^2 + (\mathcal{R}^0_{ab})^2\right) - 2\epsilon^-_X\left((\mathcal{S}^0_a)^2 + (\mathcal{R}^0_{az})^2\right) \\
&\quad - (\Delta_{\rm Z}\mathcal{S}^0_z + \Delta_{\rm SAS}\mathcal{P}^0_x + \Delta_{\rm bias}\mathcal{P}^0_z).
\end{aligned} \tag{4.5}$$

From now on, we neglect the irrelevant constant term $-\left(\epsilon^+_X + \epsilon^-_X\right)$ and the term $-\left(\epsilon^+_X - \epsilon^-_X\right)\left((\mathcal{S}^0_a)^2 + (\mathcal{P}^0_a)^2 + (\mathcal{R}^0_{ab})^2\right)$ since it also becomes constant due to Eq. (4.3). As a result, the ground-state Hamiltonian reduces to the form

$$\tilde{\mathcal{H}}_0 = \epsilon_{\rm cap}(\mathcal{P}^0_z)^2 - 2\epsilon^-_X\left((\mathcal{S}^0_a)^2 + (\mathcal{R}^0_{az})^2\right) - (\Delta_{\rm Z}\mathcal{S}^0_z + \Delta_{\rm SAS}\mathcal{P}^0_x + \Delta_{\rm bias}\mathcal{P}^0_z). \tag{4.6}$$

The Hamiltonian (4.6) is the one we are going to minimize. By minimizing this Hamiltonian we obtain the variational equations

$$\Delta^2_{\rm Z} = \frac{\Delta^2_{\rm SAS}}{1-\beta^2} - \frac{4\epsilon^-_X\left(\Delta^2_0 - \beta^2\Delta^2_{\rm SAS}\right)}{\Delta_0\sqrt{1-\beta^2}}, \tag{4.7}$$

$$\frac{\Delta_{\rm bias}}{\beta\Delta_{\rm SAS}} = \frac{4\left(\epsilon^-_X + 2\alpha^2(\epsilon^-_{\rm D} - \epsilon^-_X)\right)}{\Delta_0} + \frac{1}{\sqrt{1-\beta^2}}, \tag{4.8}$$

where α and β are real parameters satisfying

$$0 \leq \alpha \leq 1, \qquad 0 \leq |\beta| \leq 1, \tag{4.9}$$

and

$$\Delta_0 = \sqrt{\Delta_{\rm SAS}^2 \alpha^2 + \Delta_{\rm Z}^2 (1-\alpha^2)(1-\beta^2)}. \tag{4.10}$$

Due to the minimization of the Hamiltonian (4.6), the parameters α and β are determined in terms of the sample parameters such as the total density ρ_0, the layer separation d, and the tunneling gap $\Delta_{\rm SAS}$, through the above variational equations.

Let us determine the phase boundaries. It was shown that [104] there are three phases. They are called the spin phase, the pseudospin phase, and the canted antiferromagnetic (CAF) phase. We can show that the two phase boundaries are obtained by setting $\alpha = 0$ or 1 in the Eqs. (4.7) and (4.8). Then note that β is determined so as to satisfy (4.9).

First, by setting $\alpha = 0$, we have

$$\Delta_{\rm SAS}^2 = \Delta_{\rm Z}^2 + 4\epsilon_{\rm X}^- \Delta_{\rm Z} - \frac{\Delta_{\rm Z}\Delta_{\rm bias}^2}{\Delta_{\rm Z} + 4\epsilon_{\rm X}^-}, \tag{4.11}$$

which represents the spin-CAF phase boundary. Next, by setting $\alpha = 1$, we have a set of equations

$$\begin{aligned} \Delta_{\rm SAS} &= \sqrt{1-\beta^2}\left(\frac{\Delta_{\rm bias}}{\beta} - 2\epsilon_{\rm cap}\right), \\ \Delta_{\rm Z}^2 &= \left(\frac{\Delta_{\rm bias}}{\beta} - 2\epsilon_{\rm cap}\right)\left(\frac{\Delta_{\rm bias}}{\beta} - 8\epsilon_{\rm D}^- + 4\beta^2\epsilon_{\rm X}^-\right). \end{aligned} \tag{4.12}$$

which is mediated by the parameter β. It represents the pseudospin-CAF phase boundary. By using (4.11) and (4.12), we obtain the phase diagram for $\nu = 2$ bilayer QH state as the $\Delta_{\rm Z}$-$\Delta_{\rm SAS}$ plane. Here we show the phase diagrams for four different values of bias parameter $\Delta_{\rm bias}$ with setting $d = l_B$ in Fig. 4.1.

On the other hand the SU(4) order parameters are described in terms of three real variables α, β, and ω as

$$\begin{aligned} &\mathcal{S}_z^0 = \frac{\Delta_{\rm Z}}{\Delta_0}(1-\alpha^2)\sqrt{1-\beta^2}, \quad \mathcal{P}_x^0 = \frac{\Delta_{\rm SAS}}{\Delta_0}\alpha^2\sqrt{1-\beta^2}, \quad \mathcal{P}_z^0 = \frac{\Delta_{\rm SAS}}{\Delta_0}\alpha^2\beta, \\ &\mathcal{R}_{xx}^0 + i\mathcal{R}_{yx}^0 = -\frac{\Delta_{\rm SAS}}{\Delta_0}\alpha\sqrt{1-\alpha^2}\beta e^{i\omega}, \\ &\mathcal{R}_{yy}^0 - i\mathcal{R}_{xy}^0 = -\frac{\Delta_{\rm Z}}{\Delta_0}\alpha\sqrt{1-\alpha^2}\sqrt{1-\beta^2}e^{i\omega}, \\ &\mathcal{R}_{xz}^0 + i\mathcal{R}_{yz}^0 = \frac{\Delta_{\rm SAS}}{\Delta_0}\alpha\sqrt{1-\alpha^2}\sqrt{1-\beta^2}e^{i\omega}, \end{aligned} \tag{4.13}$$

with all others being zero. The physical meaning of the ω is discussed later on.

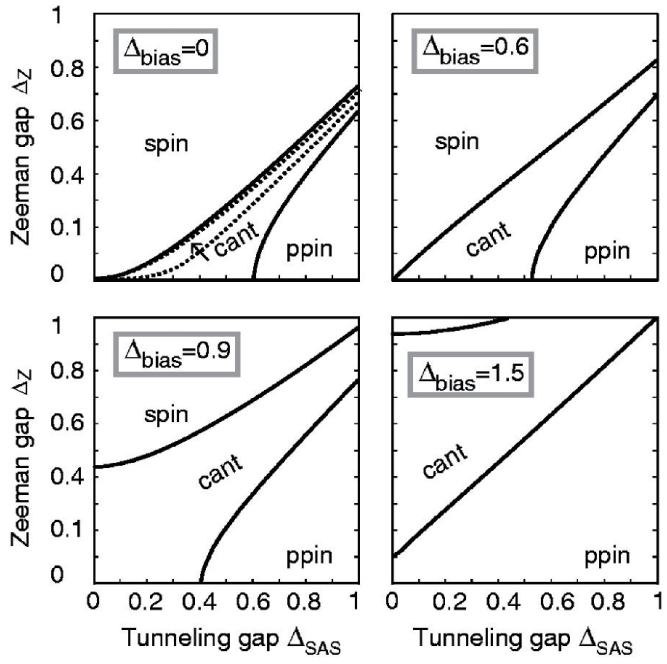

Fig. 4.1 The phase diagrams for $\nu = 2$ bilayer QH state, represented by $\Delta_{\rm Z}$-$\Delta_{\rm SAS}$ plane for four different values of bias parameter $\Delta_{\rm bias}$. Here the physical quantities having the dimension of energy, such as $\Delta_{\rm Z}$,$\Delta_{\rm SAS}$, and $\Delta_{\rm bias}$ is normalized in terms of Coulomb energy $E_{\rm C}^0 = e^2/4\pi\epsilon l_B^2$. Every diagrams are taken as $d = l_B$. The doted line in the diagram for $\Delta_{\rm bias} = 0$ is the result of exact due to exact diagonalization in Ref. [86]. This figure is taken from [104].

As a physical variable it is more convenient to use the imbalance parameter defined by

$$\sigma_0 \equiv \mathcal{P}_z^0 = \frac{\Delta_{\rm SAS}}{\Delta_0}\alpha^2\beta, \tag{4.14}$$

instead of the bias voltage $\Delta_{\rm bias}$. This is possible in the pseudospin and CAF phases. The bilayer system is balanced at $\sigma_0 = 0$, while all electrons are in the front layer at $\sigma_0 = 1$ and in the back layer at $\sigma_0 = -1$.

There are three phases in the bilayer QH system at $\nu = 2$. We discuss them in terms of α and β by using the SU(4) order parameters (4.13) in the following. The schematic illustration of the SU(4) isospin configurations for each phase are shown in Fig. 4.2.

When $\alpha = 0$, we have

$$\mathcal{S}_z^0 = 1, \tag{4.15}$$

and all others being zero. We see that only the z-component of the spin is polarized. For $\alpha = 0$, the spin phase is realized. From (4.6), the energy in the spin phase is

$$E^{\rm spin} = -(2\epsilon_X^- + \Delta_{\rm Z}). \tag{4.16}$$

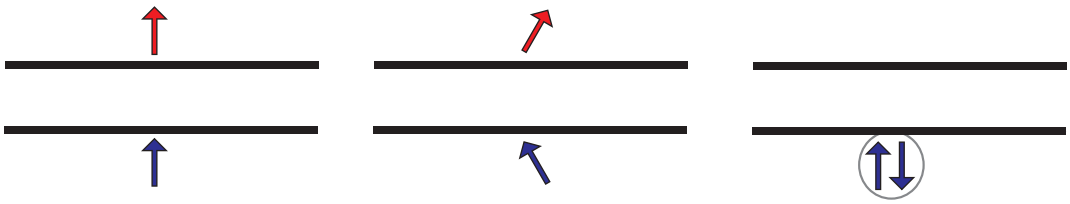

(a) Spin Phase (α=0) (b) CAF Phase (0<α<1) (c) Pseudospin Phase (α=1)

Fig. 4.2 The spin configurations in the front and back layers for each three phases. (a) For $\alpha = 0$, The ground state is the spin phase. All the spins in both layers align to the positive z axis. (b) When α increases from 0, the CAF phase is realized. In this phase not only the spin and pseudospin, but also the R-spin are polarized. As a result, the spins in both layers start to cant and make antiferromagnetic correlations between the two layers. (c) When α becomes 1 the ground state is in the pseudospin phase. The spins in each layer are in a spin-singlet state so that the magnitude of the spin becomes zero.

Next when $\alpha = 1$, the order parameters (4.13) becomes

$$\mathcal{P}_x^0 = \sqrt{1-\beta^2}, \qquad \mathcal{P}_z^0 = \beta = \sigma_0, \tag{4.17}$$

and rest of all being zero. In this case, only the pseudospin is polarized. For $\alpha = 1$, the ground state is the pseudospin phase. The energy in the pseudospin phase is given by

$$E^{\rm ppin} = \epsilon_{\rm cap}\sigma_0^2 - (\Delta_{\rm SAS}\sqrt{1-\sigma_0^2} + \Delta_{\rm bias}\sigma_0), \tag{4.18}$$

where $\Delta_{\rm bias}$ is given by (4.8) with $\alpha = 1$, or

$$\Delta_{\rm bias} = \sigma_0\Delta_{\rm SAS}\left(\frac{2\epsilon_{\rm cap}}{\Delta_0} + \frac{1}{\sqrt{1-\sigma_0^2}}\right), \tag{4.19}$$

Finally when α takes intermediate values ($0 < \alpha < 1$), the ground state is the CAF phase. In this phase from (4.13), we see that not only the spin and pseudospin but also some components of the R-spin are non-vanishing. The imbalanced configuration can be created by a bias voltage, as in the case of the pseudospin phase. The energy in the CAF phase is

$$E^{\rm CAF} = \epsilon_{\rm cap}(\mathcal{P}_z^0)^2 - 2\epsilon_X^-\left((\mathcal{S}_a^0)^2 + (\mathcal{R}_{az}^0)^2\right) - (\Delta_{\rm Z}\mathcal{S}_z^0 + \Delta_{\rm SAS}\mathcal{P}_x^0 + \Delta_{\rm bias}\mathcal{P}_z^0), \tag{4.20}$$

with $\mathcal{S}_a^0, \mathcal{P}_a^0$, and $\mathcal{R}_{ab}^0$ given by (4.13).

Let us now focus on spin-properties of the CAF phase. From (4.13), when the phase transits from the spin phase ($\alpha = 0$) to the CAF phase ($0 < \alpha < 1$), the R-spin starts to polarize, and subsequently, the spins begin to cant coherently and make antiferromagnetic correlations between the two layers. It can be verified from (4.13) with using the relation $2\mathcal{S}_a^{\rm f} = \mathcal{S}_a^0 + \mathcal{R}_{az}^0$

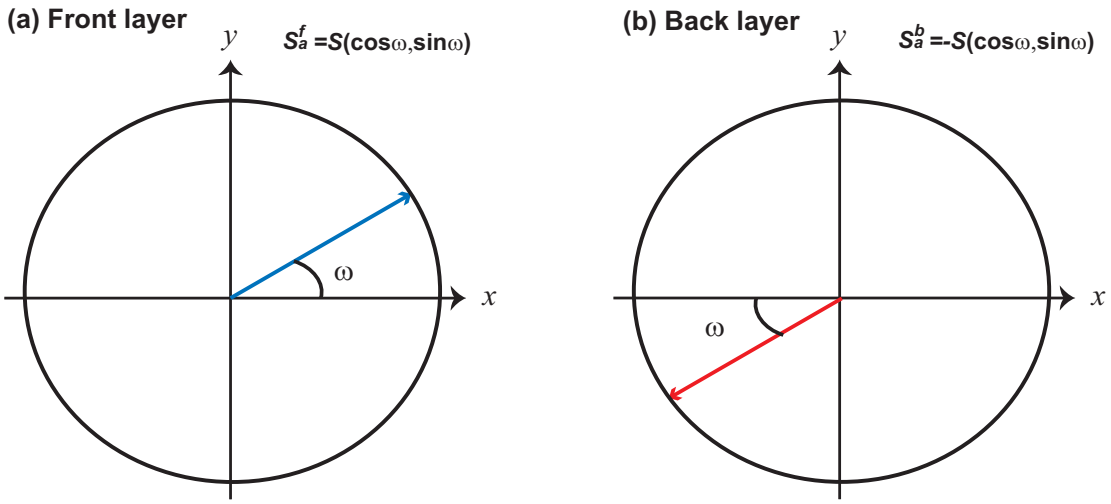

Fig. 4.3 The schematic illustration of the in-plane spin component in the CAF phase, given by the formula (4.21). The angle ω represents orientation angle of the in-plane spin component. It is determined by the U(1) spin rotational symmetry breaking generated by T_{z0}. Here we write $S = (\Delta_{\rm SAS}/2\Delta_0)\alpha\sqrt{1-\alpha^2}\sqrt{1-\beta^2}$.

and $2\mathcal{S}_a^{\rm b} = \mathcal{S}_a^0 - \mathcal{R}_{az}^0$, that

$$\begin{aligned}
\mathcal{S}_x^{\rm f} &= -\mathcal{S}_x^{\rm b} = \frac{1}{2}\frac{\Delta_{\rm SAS}}{\Delta_0}\alpha\sqrt{1-\alpha^2}\sqrt{1-\beta^2}\cos\omega, \\
\mathcal{S}_y^{\rm f} &= -\mathcal{S}_y^{\rm b} = \frac{1}{2}\frac{\Delta_{\rm SAS}}{\Delta_0}\alpha\sqrt{1-\alpha^2}\sqrt{1-\beta^2}\sin\omega, \\
\mathcal{S}_z^{\rm f} &= \mathcal{S}_z^{\rm b} = \frac{1}{2}\mathcal{S}_z^0.
\end{aligned} \tag{4.21}$$

Therefore from (4.21) we see that the in-plane component of the spin in the front layer $\mathcal{S}_a^{\rm f}$ is anti-parallel to that in the back layer $\mathcal{S}_a^{\rm b}$, which describes the antiferromagnetic correlation between the two layers. Hence it is called the canted antiferromagnetic phase. The meaning of ω now becomes clear. It represents the orientation angle of the in-plane spin component as schematically illustrated in Fig. 4.3. Moreover, the order parameters (4.13) are obtained by performing the rotation around $z0$ axis in the group space, $\exp[-iT_{z0}\omega]$, to the ones at $\omega = 0$, and the ground-state energy does not depend on ω. It implies that the CAF is the state where the $\mathrm{U}_{T_{z0}}(1)$ spin rotational symmetry is spontaneously broken. Therefore, the angle is not determined by the sample parameters but due to the spontaneous symmetry breaking. For the rest of this chapter, we set $\omega = 0$. It is the CAF phase that SU(4)-peculiarity is strongly reflected, since the R-spin ordering plays an important role for the realization of this phase. The possibility of the emergence of the entangled spin-pseudospin phenomena is expected for the CAF phase. The study of the CAF phase is the main theme of this thesis.

The interlayer phase coherence is an intriguing phenomenon in the bilayer QH systems. Since it is enhanced in the limit $\Delta_{\rm SAS} \to 0$, it is interesting to investigate the effective Hamiltonian in this limit also at $\nu = 2$. We need to know how the parameters α and β are expressed in

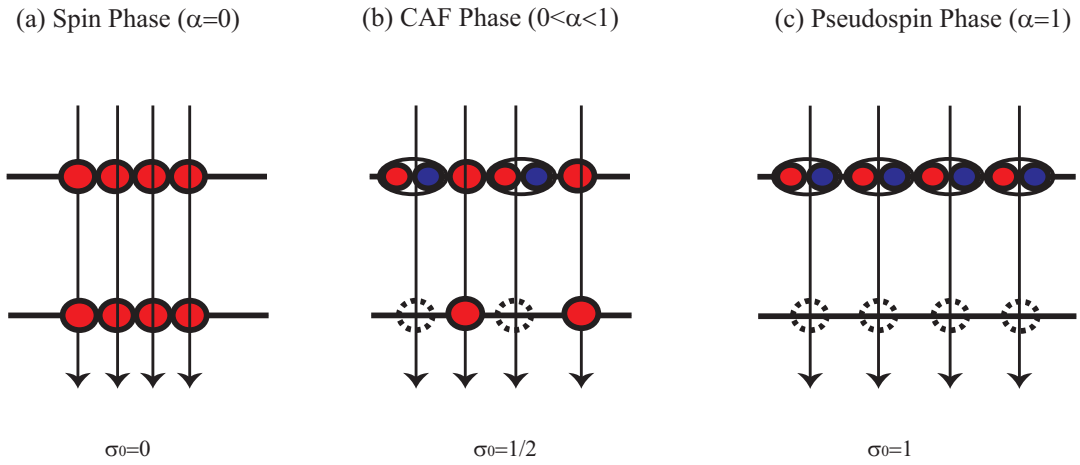

Fig. 4.4 The schematic illustration of the ground-state structure at $\nu = 2$ in the limit $\Delta_{\rm SAS} \to 0$. Here red (blue) disks denotes the up-spin (down-spin) electrons while an arrow indicates one unit of magnetic flux. In the bilayer QH systems, electrons in both the front and back layers are attached to magnetic flux. (a) In the spin phase, all electrons are in the up-spin states. It is realized at $\sigma_0 = 0$. (b) In the CAF phase, although the in-plane components of the real spin vanish, the R-spin is still polarized. It is realized at $0 < |\sigma_0| < 1$. Here we show the illustration of the CAF phase at $\sigma_0 = 1/2$. (c) In the pseudospin phase, all electrons are at front (back) layer while the other layer becomes empty. Here we show the illustration of the pseudospin phase at $\sigma_0 = 1$. This figure is adapted from [59].

terms of the physical variables. The solutions are

$$\beta = \pm\sqrt{1 - \left(\frac{\Delta_{\rm SAS}}{\Delta_{\rm Z}}\right)^2} + O(\Delta_{\rm SAS}^4), \tag{4.22}$$

with

$$\Delta_0 \to \Delta_{\rm SAS} + O(\Delta_{\rm SAS}^3), \tag{4.23}$$

for (4.10), as we shall derived in (4.125). By using (4.14) we have

$$\mathcal{P}_z^0 = \sigma_0 = \pm\alpha^2 + O(\Delta_{\rm SAS}^2). \tag{4.24}$$

The parameters α and β are simple functions of the physical variables $\Delta_{\rm SAS}/\Delta_{\rm Z}$ and σ_0 in the limit $\Delta_{\rm SAS} \to 0$. From (4.13), (4.22), (4.23), and (4.24), the SU(4) order parameters in the limit $\Delta_{\rm SAS} \to 0$ for each phase are given by

$$\text{Spin phase :} \quad \mathcal{S}_z^0 = 1, \tag{4.25}$$

$$\text{CAF phase :} \quad \mathcal{S}_z^0 = 1 - |\sigma_0|, \quad \mathcal{P}_z^0 = \sigma_0,$$

$$\mathcal{R}_{xx}^0 = \mathrm{sgn}(\sigma_0)\mathcal{R}_{yy}^0, \quad \mathcal{R}_{yy}^0 = -\sqrt{|\sigma_0|(1 - |\sigma_0|)}, \tag{4.26}$$

$$\text{Pseudospin phase :} \quad \mathcal{P}_z^0 = \pm 1. \tag{4.27}$$

The bilayer system becomes balanced in the spin phase and also near the spin-phase boundary in the CAF phase, since we have $\sigma_0 \to 0$ as $\alpha \to 0$ with all electron spins polarized into the positive z axis. On the other hand, in the pseudospin phase and also near the pseudospin-phase boundary in the CAF phase, one of the layers becomes empty since we have $\sigma_0 \to \pm 1$ as $\alpha \to 1$. For the CAF phase, from the phase diagram Fig. 4.1 and (4.11), we see that the CAF phase is realized in the limit $\Delta_{\rm SAS} \to 0$ under the condition $\Delta_{\rm bias} > 4\epsilon_{\rm X}^{-}$, and at the imbalanced-density configuration $0 < |\sigma_0| < 1$. In the CAF phase, although the in-plane components of the real spin vanish, the R-spin is still polarized, which are totally different characteristic from the ones in the spin and pseudospin phase. In Fig. 4.4, we show the schematic illustration of the ground-state structure at $\nu = 2$ in the limit $\Delta_{\rm SAS} \to 0$ in terms of electrons attached to magnetic flux.

4.2 Grassmannian Approach

In this section, we present the analysis of the physical spectrum of NG modes by taking account of the ground-state structure shown in the previous section.

We employ the Grassmannian formalism [59, 99, 109, 110] to make the physical picture of this NG mode clearer and to construct a theory which is valid nonperturbatively. The Grassmannian field $Z(\boldsymbol{x})$ consists of two CP^3 fields $\boldsymbol{n}_1(\boldsymbol{x})$ and $\boldsymbol{n}_2(\boldsymbol{x})$ at $\nu = 2$, since there are two electrons per one Landau site. From the Pauli exclusion principle, two CP^3 fields $\boldsymbol{n}_i(\boldsymbol{x})$ and $\boldsymbol{n}_j(\boldsymbol{x})$ satisfy the condition

$$\boldsymbol{n}_i^{\dagger}(\boldsymbol{x}) \cdot \boldsymbol{n}_j(\boldsymbol{x}) = \delta_{ij}, \tag{4.28}$$

with $i, j = 1, 2$. Based on the above normalization, we construct a 4×2 matrix field in terms of two CP^3 fields as

$$Z(\boldsymbol{x}) = (\boldsymbol{n}_1, \boldsymbol{n}_2), \tag{4.29}$$

satisfying the normalization condition $Z^{\dagger}Z = \mathbf{1}$. The above matrix field $Z(\boldsymbol{x})$ is the Grassmannian field. We note that the two fields $\boldsymbol{n}_1(\boldsymbol{x})$ and $\boldsymbol{n}_2(\boldsymbol{x})$ cannot be distinguished quantum mechanically since these two electrons belong to the same Landau site. Correspondingly, two fields $Z(\boldsymbol{x})$ and $Z'(\boldsymbol{x})$ become physically equivalent, and they are related by a local U(2) gauge transformation $U(\boldsymbol{x})$ as $Z'(\boldsymbol{x}) = Z(\boldsymbol{x})U(\boldsymbol{x})$. The Grassmannian field $Z(\boldsymbol{x})$ is the dynamical field on the Grassmann manifold $\mathrm{G}_{4,2}$ defined by

$$\mathrm{G}_{4,2} = \frac{\mathrm{SU}(4)}{\mathrm{U}(1) \otimes \mathrm{SU}(2) \otimes \mathrm{SU}(2)}. \tag{4.30}$$

The Grassmannian field $Z(\boldsymbol{x})$ is a new variable, which differs from just a set of two independent CP^3 fields, and described by eight real fields due to the normalization condition (4.28) or $Z^{\dagger}Z = \mathbf{1}$.

The dimensionless SU(4) isospin densities are given by

$$\mathcal{S}_a(\boldsymbol{x}) = \frac{1}{2}\mathrm{Tr}\left[Z^\dagger \tau_a^{\mathrm{spin}} Z\right] = \frac{1}{2}\sum_{i=1}^{2} \boldsymbol{n}_i^\dagger \tau_a^{\mathrm{spin}} \boldsymbol{n}_i,$$
$$\mathcal{P}_a(\boldsymbol{x}) = \frac{1}{2}\mathrm{Tr}\left[Z^\dagger \tau_a^{\mathrm{ppin}} Z\right] = \frac{1}{2}\sum_{i=1}^{2} \boldsymbol{n}_i^\dagger \tau_a^{\mathrm{ppin}} \boldsymbol{n}_i,$$
$$\mathcal{R}_{ab}(\boldsymbol{x}) = \frac{1}{2}\mathrm{Tr}\left[Z^\dagger \tau_a^{\mathrm{spin}} \tau_b^{\mathrm{ppin}} Z\right] = \frac{1}{2}\sum_{i=1}^{2} \boldsymbol{n}_i^\dagger \tau_a^{\mathrm{spin}} \tau_b^{\mathrm{ppin}} \boldsymbol{n}_i, \tag{4.31}$$

where $\boldsymbol{n}_i$ consists of the basis $\boldsymbol{n}_i(\boldsymbol{x}) = \left(n^{\mathrm{f}\uparrow}, n^{\mathrm{f}\downarrow}, n^{\mathrm{b}\uparrow}, n^{\mathrm{b}\downarrow}\right)^t$. The ground state is given by Eq. (4.13), which we express in terms of the two CP^3 fields $\boldsymbol{n}_i^g$. It is straightforward to show that it is given by $\boldsymbol{n}_i^g = U\bar{\boldsymbol{n}}_i^g$ with

$$U = \exp\left[-\frac{i}{2}\tau_y^{\mathrm{ppin}}(\theta_\beta + \frac{\pi}{2})\right]\exp\left[-\frac{i}{2}\tau_x^{\mathrm{spin}}\tau_y^{\mathrm{ppin}}\theta_\alpha\right]\exp\left[\frac{i}{2}\tau_y^{\mathrm{spin}}\tau_x^{\mathrm{ppin}}\theta_\delta\right]$$
$$= \begin{pmatrix} \cos\frac{(2\theta_\beta+\pi)}{4}\cos\frac{\theta_\delta-\theta_\alpha}{2} & -\sin\frac{(2\theta_\beta+\pi)}{4}\sin\frac{\theta_\delta+\theta_\alpha}{2} & -\sin\frac{(2\theta_\beta+\pi)}{4}\cos\frac{\theta_\delta+\theta_\alpha}{2} & \cos\frac{(2\theta_\beta+\pi)}{4}\sin\frac{\theta_\delta-\theta_\alpha}{2} \\ \sin\frac{(2\theta_\beta+\pi)}{4}\sin\frac{\theta_\delta-\theta_\alpha}{2} & \cos\frac{(2\theta_\beta+\pi)}{4}\cos\frac{\theta_\delta+\theta_\alpha}{2} & -\cos\frac{(2\theta_\beta+\pi)}{4}\sin\frac{\theta_\delta+\theta_\alpha}{2} & -\sin\frac{(2\theta_\beta+\pi)}{4}\cos\frac{\theta_\delta-\theta_\alpha}{2} \\ \sin\frac{(2\theta_\beta+\pi)}{4}\cos\frac{\theta_\delta-\theta_\alpha}{2} & \cos\frac{(2\theta_\beta+\pi)}{4}\sin\frac{\theta_\delta+\theta_\alpha}{2} & \cos\frac{(2\theta_\beta+\pi)}{4}\cos\frac{\theta_\delta+\theta_\alpha}{2} & \sin\frac{(2\theta_\beta+\pi)}{4}\sin\frac{\theta_\delta-\theta_\alpha}{2} \\ -\cos\frac{(2\theta_\beta+\pi)}{4}\sin\frac{\theta_\delta-\theta_\alpha}{2} & \sin\frac{(2\theta_\beta+\pi)}{4}\cos\frac{\theta_\delta+\theta_\alpha}{2} & -\sin\frac{(2\theta_\beta+\pi)}{4}\sin\frac{\theta_\delta+\theta_\alpha}{2} & \cos\frac{(2\theta_\beta+\pi)}{4}\cos\frac{\theta_\delta-\theta_\alpha}{2} \end{pmatrix}, \tag{4.32}$$

where θ_α, θ_β, and θ_δ are given by

$$\cos\theta_\alpha \equiv \sqrt{1-\alpha^2}, \quad \sin\theta_\alpha \equiv \alpha, \quad \cos\theta_\beta \equiv \sqrt{1-\beta^2}, \quad \sin\theta_\beta \equiv -\beta,$$
$$\cos\theta_\delta \equiv \frac{\Delta_Z\sqrt{1-\beta^2}}{\Delta_0}\sqrt{1-\alpha^2}, \quad \sin\theta_\delta \equiv \frac{\Delta_{\mathrm{SAS}}}{\Delta_0}\alpha, \tag{4.33}$$

and

$$\bar{\boldsymbol{n}}_1^g = (1,0,0,0)^t, \quad \bar{\boldsymbol{n}}_2^g = (0,0,1,0)^t. \tag{4.34}$$

We may introduce perturbative excitation modes η_i by introducing the two CP^3 fields $\boldsymbol{n}_i = U\bar{\boldsymbol{n}}_i$ with

$$\bar{\boldsymbol{n}}_1 = \begin{pmatrix} 1 - \frac{1}{2}|\eta_1|^2 - \frac{1}{2}|\eta_3|^2 \\ \eta_1 \\ -\frac{1}{2}\eta_4^\dagger\eta_1 - \frac{1}{2}\eta_2^\dagger\eta_3 \\ \eta_3 \end{pmatrix}, \quad \bar{\boldsymbol{n}}_2 = \begin{pmatrix} -\frac{1}{2}\eta_1^\dagger\eta_4 - \frac{1}{2}\eta_3^\dagger\eta_2 \\ \eta_4 \\ 1 - \frac{1}{2}|\eta_2|^2 - \frac{1}{2}|\eta_4|^2 \\ \eta_2 \end{pmatrix}, \tag{4.35}$$

where we parameterize as

$$\eta_i(\boldsymbol{x}) = \frac{\sigma_i(\boldsymbol{x}) + i\vartheta_i(\boldsymbol{x})}{\sqrt{2}}, \tag{4.36}$$

with $i = 1,2,3,4$, obeying the equal-time commutation relations between η_i and η_j, or

$$\left[\eta_i(\boldsymbol{x},t), \eta_j^\dagger(\boldsymbol{x},t)\right] = \frac{2}{\rho_0}\delta_{ij}\delta(\boldsymbol{x}-\boldsymbol{y}), \tag{4.37}$$

or

$$[\sigma_i(\boldsymbol{x},t),\vartheta_j(\boldsymbol{x},t)] = \frac{2i}{\rho_0}\delta_{ij}\delta(\boldsymbol{x}-\boldsymbol{y}). \tag{4.38}$$

From (4.32), (4.33), and (4.35), the explicit forms of isospin densities $\mathcal{S}^{\rm c}_a$, $\mathcal{P}^{\rm c}_a$, and $\mathcal{R}^{\rm c}_{ab}$ in terms of η_i are given by

$$\begin{aligned}
&\mathcal{I}^{\rm c}_{0x} = \mathrm{Re}\left[\eta_1^\dagger\eta_3 + \eta_4^\dagger\eta_2 - \eta_4^\dagger\eta_1 - \eta_2^\dagger\eta_3\right], \quad \mathcal{I}^{\rm c}_{0y} = \mathrm{Im}\left[\eta_1^\dagger\eta_3 + \eta_4^\dagger\eta_2 - \eta_4^\dagger\eta_1 - \eta_2^\dagger\eta_3\right],\\
&\mathcal{I}^{\rm c}_{0z} = |\eta_4|^2 - |\eta_3|^2,\\
&\mathcal{I}^{\rm c}_{x0} = \mathrm{Re}[\eta_1+\eta_2], \quad \mathcal{I}^{\rm c}_{xx} = \mathrm{Re}[\eta_3+\eta_4], \quad \mathcal{I}^{\rm c}_{xy} = \mathrm{Im}[\eta_3-\eta_4], \quad \mathcal{I}^{\rm c}_{xz} = \mathrm{Re}[\eta_1-\eta_2],\\
&\mathcal{I}^{\rm c}_{y0} = \mathrm{Im}[\eta_1+\eta_2], \quad \mathcal{I}^{\rm c}_{yx} = \mathrm{Im}[\eta_3+\eta_4], \quad \mathcal{I}^{\rm c}_{yy} = -\mathrm{Re}[\eta_3-\eta_4], \quad \mathcal{I}^{\rm c}_{yz} = \mathrm{Im}[\eta_1-\eta_2],\\
&\mathcal{I}^{\rm c}_{z0} = 1 - \sum_{i=1}^{4}|\eta_i|^2, \quad \mathcal{I}^{\rm c}_{zx} = -\mathrm{Re}\left[\eta_1^\dagger\eta_3 + \eta_4^\dagger\eta_2 + \eta_4^\dagger\eta_1 + \eta_2^\dagger\eta_3\right],\\
&\mathcal{I}^{\rm c}_{zy} = -\mathrm{Im}\left[\eta_1^\dagger\eta_3 + \eta_4^\dagger\eta_2 + \eta_4^\dagger\eta_1 + \eta_2^\dagger\eta_3\right], \quad \mathcal{I}^{\rm c}_{zz} = |\eta_2|^2 - |\eta_1|^2.
\end{aligned} \tag{4.39}$$

where we defined $\mathcal{I}_{a0} \equiv \mathcal{S}_a$, $\mathcal{I}_{0a} \equiv \mathcal{P}_a$, $\mathcal{I}_{ab} \equiv \mathcal{R}_{ab}$ and the relation between $\mathcal{I}_{\mu\nu}$ and $\mathcal{I}^{\rm c}_{\mu\nu}$ is

$$\begin{aligned}
\mathcal{I}_{0x} &= -\cos\theta_\alpha\sin\theta_\beta\mathcal{I}^{\rm c}_{0x} + \cos\theta_\alpha\cos\theta_\beta\cos\theta_\delta\mathcal{I}^{\rm c}_{0z} - \sin\theta_\alpha\cos\theta_\beta\cos\theta_\delta\mathcal{I}^{\rm c}_{xx} - \sin\theta_\alpha\sin\theta_\beta\mathcal{I}^{\rm c}_{xz}\\
&\quad - \cos\theta_\alpha\cos\theta_\beta\sin\theta_\delta\mathcal{I}^{\rm c}_{yy} + \sin\theta_\alpha\cos\theta_\beta\sin\theta_\delta\mathcal{I}^{\rm c}_{z0},\\
\mathcal{I}_{0y} &= \cos\theta_\delta\mathcal{I}^{\rm c}_{0y} + \sin\theta_\delta\mathcal{I}^{\rm c}_{yz},\\
\mathcal{I}_{0z} &= -\cos\theta_\alpha\cos\theta_\beta\mathcal{I}^{\rm c}_{0x} - \cos\theta_\alpha\sin\theta_\beta\cos\theta_\delta\mathcal{I}^{\rm c}_{0z} + \sin\theta_\alpha\sin\theta_\beta\cos\theta_\delta\mathcal{I}^{\rm c}_{xx} - \sin\theta_\alpha\cos\theta_\beta\mathcal{I}^{\rm c}_{xz}\\
&\quad + \cos\theta_\alpha\sin\theta_\beta\sin\theta_\delta\mathcal{I}^{\rm c}_{yy} - \sin\theta_\alpha\sin\theta_\beta\sin\theta_\delta\mathcal{I}^{\rm c}_{z0},\\
\mathcal{I}_{x0} &= \cos\theta_\delta\mathcal{I}^{\rm c}_{x0} - \sin\theta_\delta\mathcal{I}^{\rm c}_{zx},\\
\mathcal{I}_{xx} &= -\sin\theta_\alpha\cos\theta_\beta\mathcal{I}^{\rm c}_{0x} - \sin\theta_\alpha\sin\theta_\beta\cos\theta_\delta\mathcal{I}^{\rm c}_{0z} - \cos\theta_\alpha\sin\theta_\beta\cos\theta_\delta\mathcal{I}^{\rm c}_{xx} + \cos\theta_\alpha\cos\theta_\beta\mathcal{I}^{\rm c}_{xz}\\
&\quad + \sin\theta_\alpha\sin\theta_\beta\sin\theta_\delta\mathcal{I}^{\rm c}_{yy} + \cos\theta_\alpha\sin\theta_\beta\sin\theta_\delta\mathcal{I}^{\rm c}_{z0},\\
\mathcal{I}_{xy} &= \mathcal{I}^{\rm c}_{xy},\\
\mathcal{I}_{xz} &= \sin\theta_\alpha\sin\theta_\beta\mathcal{I}^{\rm c}_{0x} - \sin\theta_\alpha\cos\theta_\beta\cos\theta_\delta\mathcal{I}^{\rm c}_{0z} - \cos\theta_\alpha\cos\theta_\beta\cos\theta_\delta\mathcal{I}^{\rm c}_{xx} - \cos\theta_\alpha\sin\theta_\beta\mathcal{I}^{\rm c}_{xz}\\
&\quad + \sin\theta_\alpha\cos\theta_\beta\sin\theta_\delta\mathcal{I}^{\rm c}_{yy} + \cos\theta_\alpha\cos\theta_\beta\sin\theta_\delta\mathcal{I}^{\rm c}_{z0},\\
\mathcal{I}_{y0} &= \cos\theta_\alpha\mathcal{I}^{\rm c}_{y0} - \sin\theta_\alpha\mathcal{I}^{\rm c}_{zy},\\
\mathcal{I}_{yx} &= -\cos\theta_\beta\sin\theta_\delta\mathcal{I}^{\rm c}_{0y} - \sin\theta_\beta\mathcal{I}^{\rm c}_{yx} + \cos\theta_\beta\cos\theta_\delta\mathcal{I}^{\rm c}_{yz},\\
\mathcal{I}_{yy} &= \cos\theta_\alpha\sin\theta_\delta\mathcal{I}^{\rm c}_{0z} - \sin\theta_\alpha\sin\theta_\delta\mathcal{I}^{\rm c}_{xx} + \cos\theta_\alpha\cos\theta_\delta\mathcal{I}^{\rm c}_{yy} - \sin\theta_\alpha\cos\theta_\delta\mathcal{I}^{\rm c}_{z0},\\
\mathcal{I}_{yz} &= \sin\theta_\beta\sin\theta_\delta\mathcal{I}^{\rm c}_{0y} - \cos\theta_\beta\mathcal{I}^{\rm c}_{yx} - \sin\theta_\beta\cos\theta_\delta\mathcal{I}^{\rm c}_{yz},\\
\mathcal{I}_{z0} &= \sin\theta_\alpha\sin\theta_\delta\mathcal{I}^{\rm c}_{0z} + \cos\theta_\alpha\sin\theta_\delta\mathcal{I}^{\rm c}_{xx} + \sin\theta_\alpha\cos\theta_\delta\mathcal{I}^{\rm c}_{yy} + \cos\theta_\alpha\cos\theta_\delta\mathcal{I}^{\rm c}_{z0},\\
\mathcal{I}_{zx} &= -\sin\theta_\beta\sin\theta_\delta\mathcal{I}^{\rm c}_{x0} - \sin\theta_\beta\cos\theta_\delta\mathcal{I}^{\rm c}_{zx} + \cos\theta_\beta\mathcal{I}^{\rm c}_{zz},\\
\mathcal{I}_{zy} &= \sin\theta_\alpha\mathcal{I}^{\rm c}_{y0} + \cos\theta_\alpha\mathcal{I}^{\rm c}_{zy},\\
\mathcal{I}_{zz} &= -\cos\theta_\beta\sin\theta_\delta\mathcal{I}^{\rm c}_{x0} - \cos\theta_\beta\cos\theta_\delta\mathcal{I}^{\rm c}_{zx} - \sin\theta_\beta\mathcal{I}^{\rm c}_{zz}.
\end{aligned} \tag{4.40}$$

From (4.40), (4.39) and the equal time commutation relations (4.37), it can be verified that

the SU(4) algebraic relation

$$[\mathcal{I}_{\mu\nu}(\boldsymbol{x},t),\mathcal{I}_{\gamma\delta}(\boldsymbol{x},t)] = i\delta(\boldsymbol{x}-\boldsymbol{y})f_{\mu\nu,\gamma\delta,\mu'\nu'}\mathcal{I}_{\mu'\nu'}(\boldsymbol{y},t), \tag{4.41}$$

is held. The commutation relations (4.37) or (4.38) are required so the SU(4) algebraic relation (4.41) holds for $\mathcal{S}_a$, $\mathcal{P}_a$, and $\mathcal{S}_{ab}$.

As shown in Eq. (4.35) and Fig. 4.5, two lowest energy states are occupied at $\nu = 2$, denoting the states $|1\rangle$ and $|2\rangle$, and the rest of the higher energy states as $|3\rangle$ and $|4\rangle$. Correspondingly, four types of excitation modes could be considered; the excitations from $|1\rangle$ ($|2\rangle$) to $|3\rangle$ and from $|1\rangle$ ($|2\rangle$) to $|4\rangle$.

We use the isospin components (4.40) with the use of (4.39), and substitute them into the effective Hamiltonian (2.141), or

$$\begin{aligned}\mathcal{H}^{\rm eff} = {} & J_s^d\left((\partial_k\mathcal{S}_a)^2+(\partial_k\mathcal{P}_a)^2+(\partial_k\mathcal{R}_{ab})^2\right)+2J_s^-\left((\partial_k\mathcal{S}_a)^2+(\partial_k\mathcal{P}_z)^2+(\partial_k\mathcal{R}_{az})^2\right)\\ & +\rho_\phi\left[\epsilon_{\rm cap}(\mathcal{P}_z)^2-2\epsilon_X^-\left((\mathcal{S}_a)^2+(\mathcal{R}_{az})^2\right)-(\Delta_{\rm Z}\mathcal{S}_z+\Delta_{\rm SAS}\mathcal{P}_x+\Delta_{\rm bias}\mathcal{P}_z)\right],\end{aligned} \tag{4.42}$$

where the condition (4.3) was used and neglected the constant $-\left(\epsilon_X^+-\epsilon_X^-\right)$. In this way we obtain the effective Hamiltonian for η_i and is expressed in terms of parameter α, which classifies the phases at $\nu = 2$. Thus the obtained effective Hamiltonian is valid in all three phases. See Appendix C for the nonlinear representation for the isospin fields.

4.3 NG Modes in the Spin Phase

As an illustration we study the spin phase at $\sigma_0 = 0$, where the transformation (4.32) is given by

$$U = \frac{1}{\sqrt{2}}\begin{pmatrix}1&0&-1&0\\0&1&0&-1\\1&0&1&0\\0&1&0&1\end{pmatrix}, \tag{4.43}$$

by setting $\alpha, \beta = 0$. We note that

$$\bar{\boldsymbol{n}} = \begin{pmatrix}n^{\rm S\uparrow}\\n^{\rm S\downarrow}\\n^{\rm A\uparrow}\\n^{\rm A\downarrow}\end{pmatrix} = U^\dagger\begin{pmatrix}n^{\rm f\uparrow}\\n^{\rm f\downarrow}\\n^{\rm b\uparrow}\\n^{\rm b\downarrow}\end{pmatrix} = U^\dagger\boldsymbol{n}, \tag{4.44}$$

where

$$n^{{\rm S}\alpha} = \frac{1}{\sqrt{2}}(n^{{\rm b}\alpha}+n^{{\rm f}\alpha}), \quad n^{{\rm A}\alpha} = \frac{1}{\sqrt{2}}(n^{{\rm b}\alpha}-n^{{\rm f}\alpha}), \tag{4.45}$$

with $\alpha = \uparrow, \downarrow$. The lowest-energy one-body electron state is the up-spin symmetric state, and the second lowest energy state is the up-spin antisymmetric state. They are filled up at $\nu = 2$. The perturbative excitations η_i are illustrated in Fig. 4.5 (a).

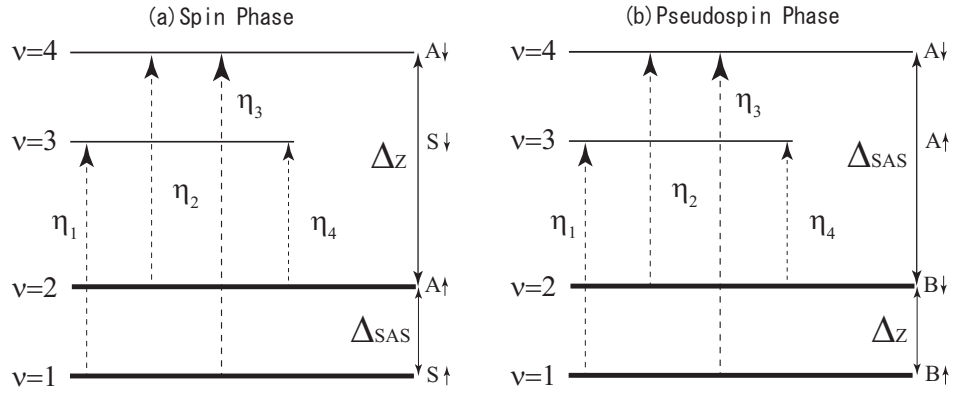

Fig. 4.5 The lowest two energy levels are occupied, described by the two thick lines, in the ground state at $\nu = 2$. Small four fluctuations are the NG modes η_1, η_2, η_3, and η_4. (a) For the spin phase η_1 and η_2 describe the fluctuation from the up-spin symmetric state to the down-spin symmetric state and from the up-spin antisymmetric state to the down-spin symmetric state, respectively. Their energy levels are degenerated with the Zeeman gap $\Delta_{\rm Z}$. On the other hand, η_3 and η_4, which are fluctuations from up-spin symmetric state to the down-spin antisymmetric state and from up-spin antisymmetric state to down-spin symmetric state, having a energy gap $\Delta_{\rm Z} \pm \Delta_{\rm SAS}$, respectively. (b) For the pseudospin phase η_1 and η_2 describe the fluctuation from the up-spin bonding state to the up-spin antibonding state and from the down-spin bonding state to the down-spin antibonding state, respectively. Their energy levels are degenerated with the tunneling gap $\Delta_{\rm SAS}$. On the other hand, η_3 and η_4, which are fluctuations from up-spin bonding state to the down-spin antibonding state and from down-spin bonding state to the up-spin antibonding state, having a energy gap $\Delta_{\rm SAS} \pm \Delta_{\rm Z}$, respectively. This picture is taken from [110].

It follows from (4.31), (4.32), and (4.35) that the isospin densities are explicitly given in terms of $\sigma_i(\boldsymbol{x})$ and $\vartheta_i(\boldsymbol{x})$ by

$$\begin{aligned}
&\mathcal{S}_x = \frac{\sigma_1 + \sigma_2}{\sqrt{2}} \equiv \tilde{\sigma}_1, \quad \mathcal{S}_y = \frac{\vartheta_1 + \vartheta_2}{\sqrt{2}} \equiv \tilde{\vartheta}_1, \quad \mathcal{R}_{xx} = \frac{\sigma_1 - \sigma_2}{\sqrt{2}} \equiv \tilde{\sigma}_2, \quad \mathcal{R}_{yx} = \frac{\vartheta_1 - \vartheta_2}{\sqrt{2}} \equiv \tilde{\vartheta}_2, \\
&\mathcal{R}_{yy} = \frac{\sigma_4 - \sigma_3}{\sqrt{2}} \equiv -\tilde{\sigma}_3, \quad \mathcal{R}_{xy} = \frac{\vartheta_3 - \vartheta_4}{\sqrt{2}} \equiv \tilde{\vartheta}_3, \quad \mathcal{R}_{xz} = -\frac{\sigma_4 + \sigma_3}{\sqrt{2}} \equiv \tilde{\sigma}_4, \quad \mathcal{R}_{yz} = -\frac{\vartheta_4 + \vartheta_3}{\sqrt{2}} \equiv \tilde{\vartheta}_4, \\
&\mathcal{S}_z = 1 - \sum_{i=1}^{4} \frac{\sigma_i^2 + \vartheta_i^2}{2} = 1 - \sum_{i=1}^{4} \frac{\tilde{\sigma}_i^2 + \tilde{\vartheta}_i^2}{2}, \quad \mathcal{P}_x = \tilde{\sigma}_3\tilde{\sigma}_4 + \tilde{\vartheta}_3\tilde{\vartheta}_4, \quad \mathcal{P}_y = \tilde{\sigma}_4\tilde{\vartheta}_2 - \tilde{\sigma}_2\tilde{\vartheta}_4, \\
&\mathcal{P}_z = -\left(\tilde{\sigma}_2\tilde{\sigma}_3 + \tilde{\vartheta}_2\tilde{\vartheta}_3\right), \quad \mathcal{R}_{zx} = -\left(\tilde{\sigma}_1\tilde{\sigma}_2 + \tilde{\vartheta}_1\tilde{\vartheta}_2\right), \quad \mathcal{R}_{zy} = \tilde{\sigma}_3\tilde{\vartheta}_1 - \tilde{\sigma}_1\tilde{\vartheta}_3, \quad \mathcal{R}_{zz} = -\left(\tilde{\sigma}_1\tilde{\sigma}_4 + \tilde{\vartheta}_1\tilde{\vartheta}_4\right).
\end{aligned} \tag{4.46}$$

Substituting them into (4.42), we obtain the effective Hamiltonian of the NG modes in terms

of the canonical sets of $\tilde{\sigma}_i$ and $\tilde{\vartheta}_i$ as

$$\mathcal{H}^{\rm spin} = \mathcal{H}_0^{\rm spin} + \mathcal{H}_{\rm NG}^{\rm spin}, \tag{4.47}$$

$$\mathcal{H}_0^{\rm spin} = -\frac{\rho_0}{2}\left(2\epsilon_X^- + \Delta_{\rm Z}\right), \tag{4.48}$$

$$\begin{aligned}\mathcal{H}_{\rm NG}^{\rm spin} = {} & J_s \sum_{a=1,4}\left[(\partial_k\tilde{\sigma}_a)^2 + (\partial_k\tilde{\vartheta}_a)^2\right] + J_s^d \sum_{a=2,3}\left[(\partial_k\tilde{\sigma}_a)^2 + (\partial_k\tilde{\vartheta}_a)^2\right] \\ & + \frac{\rho_0\Delta_{\rm Z}}{4}\sum_{=1,4}\left[\tilde{\sigma}_a^2 + \tilde{\vartheta}_a^2\right] + \left(\frac{\rho_0\Delta_{\rm Z}}{4} + \rho_0\epsilon_X^-\right)\sum_{a=2,3}\left[\tilde{\sigma}_a^2 + \tilde{\vartheta}_a^2\right] \\ & - \frac{\rho_0\Delta_{\rm SAS}}{2}\left[\tilde{\sigma}_3\tilde{\sigma}_4 + \tilde{\vartheta}_3\tilde{\vartheta}_4\right] + \frac{\rho_0\Delta_{\rm bias}}{2}\left[\tilde{\sigma}_2\tilde{\sigma}_3 + \tilde{\vartheta}_2\tilde{\vartheta}_3\right].\end{aligned} \tag{4.49}$$

We see that (4.48) matches with the energy in the spin phase (4.16)$\times\rho_0/2$. The annihilation operators are defined by

$$\eta_i^{\rm s}(\boldsymbol{x}) = \frac{\check{\sigma}_i(\boldsymbol{x}) + i\check{\vartheta}_i(\boldsymbol{x})}{\sqrt{2}}, \tag{4.50}$$

with

$$\check{\sigma}_i \equiv \rho_\Phi^{1/2}\tilde{\sigma}_i, \qquad \check{\vartheta}_i \equiv \rho_\Phi^{1/2}\tilde{\vartheta}_i, \tag{4.51}$$

and they satisfy the commutation relations,

$$\left[\check{\sigma}_i(\boldsymbol{x},t), \check{\vartheta}_j(\boldsymbol{y},t)\right] = i\delta_{ij}\delta(\boldsymbol{x}-\boldsymbol{y}), \tag{4.52}$$

or

$$\left[\eta_i^{\rm s}(\boldsymbol{x},t), \eta_j^{\rm s\dagger}(\boldsymbol{y},t)\right] = \delta_{ij}\delta(\boldsymbol{x}-\boldsymbol{y}), \tag{4.53}$$

with $i,j = 1,2,3,4$.

The effective Hamiltonian (4.49) reads in terms of the creation and annihilation variables (4.50) as

$$\begin{aligned}\mathcal{H}_{\rm NG}^{\rm spin} = {} & \frac{4J_s}{\rho_0}\sum_{a=1,4}\partial_k\eta_a^{\rm s\dagger}\partial_k\eta_a^{\rm s} + \frac{4J_s^d}{\rho_0}\sum_{a=2,3}\partial_k\eta_a^{\rm s\dagger}\partial_k\eta_a^{\rm s} + \Delta_{\rm Z}\sum_{a=1,4}\eta_a^{\rm s\dagger}\eta_a^{\rm s} + [\Delta_{\rm Z} + 4\epsilon_X^-]\sum_{a=2,3}\eta_a^{\rm s\dagger}\eta_a^{\rm s} \\ & + \Delta_{\rm bias}[\eta_2^{\rm s\dagger}\eta_3^{\rm s} + \eta_3^{\rm s\dagger}\eta_2^{\rm s}] - \Delta_{\rm SAS}[\eta_3^{\rm s\dagger}\eta_4^{\rm s} + \eta_4^{\rm s\dagger}\eta_3^{\rm s}].\end{aligned} \tag{4.54}$$

The variables $\eta_2^{\rm s}$, $\eta_3^{\rm s}$ and $\eta_4^{\rm s}$ are mixing by $\Delta_{\rm SAS}$ and $\Delta_{\rm bias}$.

In the momentum space the annihilation and creation operators are $\eta_{i,\boldsymbol{k}}^{\rm s}$ and $\eta_{i,\boldsymbol{k}}^{\rm s\dagger}$ together with the commutation relations,

$$\left[\eta_{i,\boldsymbol{k}}^{\rm s}, \eta_{j,\boldsymbol{k}'}^{\rm s\dagger}\right] = \delta_{ij}\delta(\boldsymbol{k}-\boldsymbol{k}'). \tag{4.55}$$

For the sake of the simplicity we consider the balanced configuration with $\Delta_{\rm bias} = 0$ in the

rest of this section. Then the Hamiltonian density is given by

$$H_{\rm NG}^{\rm spin} = \int d^2k\ \mathcal{H}_{\rm NG}^{\rm spin},$$
$$\mathcal{H}_{\rm NG}^{\rm spin} = \mathcal{H}_{\rm NG,1}^{\rm spin} + \mathcal{H}_{\rm NG,2}^{\rm spin} + \mathcal{H}_{\rm NG,3}^{\rm spin}, \tag{4.56}$$

where

$$\mathcal{H}_{\rm NG,1}^{\rm spin} = \left[\frac{4J_s}{\rho_0}\boldsymbol{k}^2 + \Delta_{\rm Z}\right]\eta_{1,\boldsymbol{k}}^{\rm s\dagger}\eta_{1,\boldsymbol{k}}^{\rm s}, \tag{4.57}$$

$$\mathcal{H}_{\rm NG,2}^{\rm spin} = \left[\frac{4J_s^d}{\rho_0}\boldsymbol{k}^2 + \Delta_{\rm Z} + 4\epsilon_X^-\right]\eta_{2,\boldsymbol{k}}^{\rm s\dagger}\eta_{2,\boldsymbol{k}}^{\rm s}, \tag{4.58}$$

$$\mathcal{H}_{\rm NG,3}^{\rm spin} = \left[\frac{4J_s^d}{\rho_0}\boldsymbol{k}^2 + \Delta_{\rm Z} + 4\epsilon_X^-\right]\eta_{3,\boldsymbol{k}}^{\rm s\dagger}\eta_{3,\boldsymbol{k}}^{\rm s} + \left[\frac{4J_s}{\rho_0}\boldsymbol{k}^2 + \Delta_{\rm Z}\right]\eta_{4,\boldsymbol{k}}^{\rm s\dagger}\eta_{4,\boldsymbol{k}}^{\rm s} - \Delta_{\rm SAS}\left[\eta_{3,\boldsymbol{k}}^{\rm s\dagger}\eta_{4,\boldsymbol{k}}^{\rm s} + \eta_{4,\boldsymbol{k}}^{\rm s\dagger}\eta_{3,\boldsymbol{k}}^{\rm s}\right]. \tag{4.59}$$

We first analyze the dispersion relation and the coherence length of $\eta_{1,\boldsymbol{k}}^{\rm s}$. From (4.57), we have

$$E_{\eta_1^{\rm s}}(\boldsymbol{k}) = \frac{4J_s}{\rho_0}\boldsymbol{k}^2 + \Delta_{\rm Z}, \tag{4.60}$$

$$\xi_{\eta_1^{\rm s}} = 2l_B\sqrt{\frac{\pi J_s}{\Delta_{\rm Z}}}. \tag{4.61}$$

The coherence length diverges in the limit $\Delta_{\rm Z} \to 0$. This mode is a pure spin wave since it describes the fluctuation of $\mathcal{S}_x$ and $\mathcal{S}_y$ as in (4.46). Indeed, the energy (4.60) as well as the coherence length (4.61) depend only on the Zeeman gap $\Delta_{\rm Z}$ and the intralayer stiffness J_s.

We next analyze those of $\eta_{2,\boldsymbol{k}}^{\rm s}$,

$$E_{\eta_2^{\rm s}}(\boldsymbol{k}) = \frac{4J_s^d}{\rho_0}\boldsymbol{k}^2 + \Delta_{\rm Z} + 4\epsilon_X^-, \tag{4.62}$$

$$\xi_{\eta_2^{\rm s}} = 2l_B\sqrt{\frac{\pi J_s^d}{\Delta_{\rm Z} + 4\epsilon_X^-}}. \tag{4.63}$$

They depend not only $\Delta_{\rm Z}$ but also on the exchange Coulomb energy ϵ_X^- and the interlayer stiffness originating in the interlayer Coulomb interaction. This mode is a R-spin wave since it describes the fluctuation of $\mathcal{R}_{xx}$ and $\mathcal{R}_{yx}$. From (4.60) and (4.62) we see that, in the one body picture, $\eta_1^{\rm s}$ and $\eta_2^{\rm s}$ have the same energy gap $\Delta_{\rm Z}$. Indeed they are described in terms of η_1 and η_2, having the same energy gap $\Delta_{\rm Z}$ [Fig. 4.5 (a)].

We finally analyze those of $\eta_{3,\boldsymbol{k}}^{\rm s}$ and $\eta_{4,\boldsymbol{k}}^{\rm s}$, which are coupled. Hamiltonian (4.59) can be written in the matrix form,

$$\mathcal{H}_{\rm NG,3}^{\rm spin} = \begin{pmatrix} \eta_{3,\boldsymbol{k}}^{\rm s} \\ \eta_{4,\boldsymbol{k}}^{\rm s} \end{pmatrix}^\dagger \begin{pmatrix} A_{\boldsymbol{k}} & -\Delta_{\rm SAS} \\ -\Delta_{\rm SAS} & B_{\boldsymbol{k}} \end{pmatrix} \begin{pmatrix} \eta_{3,\boldsymbol{k}}^{\rm s} \\ \eta_{4,\boldsymbol{k}}^{\rm s} \end{pmatrix}, \tag{4.64}$$

where

$$A_{\boldsymbol{k}} = \frac{4J_s^d}{\rho_0}\boldsymbol{k}^2 + \Delta_{\rm Z} + 4\epsilon_X^-, \quad B_{\boldsymbol{k}} = \frac{4J_s}{\rho_0}\boldsymbol{k}^2 + \Delta_{\rm Z}. \tag{4.65}$$

Hamiltonian (4.64) can be diagonalized as

$$\mathcal{H}_{\rm NG,3}^{\rm spin} = \begin{pmatrix} \tilde{\eta}_{3,\boldsymbol{k}}^{\rm s} \\ \tilde{\eta}_{4,\boldsymbol{k}}^{\rm s} \end{pmatrix}^\dagger \begin{pmatrix} E^{\tilde{\eta}_3^{\rm s}} & 0 \\ 0 & E^{\tilde{\eta}_4^{\rm s}} \end{pmatrix} \begin{pmatrix} \tilde{\eta}_{3,\boldsymbol{k}}^{\rm s} \\ \tilde{\eta}_{4,\boldsymbol{k}}^{\rm s} \end{pmatrix}, \tag{4.66}$$

where

$$E^{\tilde{\eta}_3^{\rm s}} = \frac{1}{2}\left[A_{\boldsymbol{k}} + B_{\boldsymbol{k}} + \sqrt{(A_{\boldsymbol{k}} - B_{\boldsymbol{k}})^2 + 4\Delta_{\rm SAS}^2}\right], \quad E^{\tilde{\eta}_4^{\rm s}} = \frac{1}{2}\left[A_{\boldsymbol{k}} + B_{\boldsymbol{k}} - \sqrt{(A_{\boldsymbol{k}} - B_{\boldsymbol{k}})^2 + 4\Delta_{\rm SAS}^2}\right], \tag{4.67}$$

and the annihilation operator $\tilde{\eta}_{i,\boldsymbol{k}}^{\rm s}$ $(i = 3, 4)$ given by the form

$$\begin{aligned} \tilde{\eta}_{3,\boldsymbol{k}}^{\rm s} &= \frac{\left(\sqrt{C_{\boldsymbol{k}}^2 + 4\Delta_{\rm SAS}^2} + C_{\boldsymbol{k}}\right)\eta_{3,\boldsymbol{k}} - 2\Delta_{\rm SAS}\eta_{4,\boldsymbol{k}}}{\sqrt{2\left(C_{\boldsymbol{k}}^2 + 4\Delta_{\rm SAS}^2 + C_{\boldsymbol{k}}\sqrt{C_{\boldsymbol{k}}^2 + 4\Delta_{\rm SAS}^2}\right)}}, \\ \tilde{\eta}_{4,\boldsymbol{k}}^{\rm s} &= \frac{\left(\sqrt{C_{\boldsymbol{k}}^2 + 4\Delta_{\rm SAS}^2} - C_{\boldsymbol{k}}\right)\eta_{3,\boldsymbol{k}} + 2\Delta_{\rm SAS}\eta_{4,\boldsymbol{k}}}{\sqrt{2\left(C_{\boldsymbol{k}}^2 + 4\Delta_{\rm SAS}^2 - C_{\boldsymbol{k}}\sqrt{C_{\boldsymbol{k}}^2 + 4\Delta_{\rm SAS}^2}\right)}}, \end{aligned} \tag{4.68}$$

with $C_{\boldsymbol{k}} = A_{\boldsymbol{k}} - B_{\boldsymbol{k}}$. The annihilation operators (4.68) satisfy the commutation relations

$$\left[\tilde{\eta}_{i,\boldsymbol{k}}^{\rm s}, \tilde{\eta}_{j,\boldsymbol{k}'}^{\rm s\dagger}\right] = \delta_{ij}\delta(\boldsymbol{k} - \boldsymbol{k}'), \tag{4.69}$$

with $i, j = 3, 4$. We obtain the dispersions for the modes $\tilde{\eta}_{i,\boldsymbol{k}}^{\rm s}$ $(i = 3, 4)$ from (4.65) and (4.67).

By taking the limit $\boldsymbol{k} \to 0$ in (4.67), we have two gaps

$$E_{\boldsymbol{k}=0}^{\tilde{\eta}_3^{\rm s}} = \Delta_{\rm Z} + 2\epsilon_X^- + \left[4(\epsilon_X^-)^2 + \Delta_{\rm SAS}^2\right]^{\frac{1}{2}}, \quad E_{\boldsymbol{k}=0}^{\tilde{\eta}_4^{\rm s}} = \Delta_{\rm Z} + 2\epsilon_X^- - \left[4(\epsilon_X^-)^2 + \Delta_{\rm SAS}^2\right]^{\frac{1}{2}}. \tag{4.70}$$

The gapless condition ($E_{\boldsymbol{k}=0}^{\tilde{\eta}_4^{\rm s}} = 0$) implies

$$\Delta_{\rm Z}(\Delta_{\rm Z} + 4\epsilon_X^-) - \Delta_{\rm SAS}^2 = 0, \tag{4.71}$$

which holds only along the boundary of the spin and CAF phases: See (4.17) in Ref. [104]. In the interior of the spin phase we have $\Delta_{\rm Z}(\Delta_{\rm Z} + 4\epsilon_X^-) - \Delta_{\rm SAS}^2 > 0$, as implies that there arise no gapless modes from $\tilde{\eta}_3^{\rm s}$ and $\tilde{\eta}_4^{\rm s}$. From (4.70), in the one body picture, $\tilde{\eta}_3^{\rm s}$ and $\tilde{\eta}_4^{\rm s}$ have the energy gap $\Delta_{\rm Z} \pm \Delta_{\rm SAS}$, respectively. Indeed they are described in terms of η_3 and η_4 [Fig. 4.5 (a)]. These excitation modes are R-spin waves coupled to the layer degree of freedom. There emerge four complex NG modes, one of which describing the spin wave ($\eta_1^{\rm s}$), and the other three the R-spin waves ($\eta_2^{\rm s}, \eta_3^{\rm s}, \eta_4^{\rm s}$).

4.4 NG Modes in the Pseudospin Phase

For the pseudospin phase, β is identified with the imbalanced parameter σ_0, as we have discussed in section 4.1 with (4.17). In this section, instead of β we express the effective Hamiltonian, the dispersions, and the coherence length in terms of σ_0, since it is a physical variable.

From (4.32), by setting $\alpha = 1$ we have

$$U = \frac{1}{\sqrt{2}} \begin{pmatrix} \sqrt{1+\sigma_0} & -\sqrt{1-\sigma_0} & 0 & 0 \\ 0 & 0 & -\sqrt{1+\sigma_0} & -\sqrt{1-\sigma_0} \\ \sqrt{1-\sigma_0} & \sqrt{1+\sigma_0} & 0 & 0 \\ 0 & 0 & -\sqrt{1-\sigma_0} & \sqrt{1+\sigma_0} \end{pmatrix}, \tag{4.72}$$

and

$$\bar{\boldsymbol{n}} = \begin{pmatrix} n^{\mathrm{B}\uparrow} \\ n^{\mathrm{A}\uparrow} \\ -n^{\mathrm{B}\downarrow} \\ n^{\mathrm{A}\downarrow} \end{pmatrix} = U^\dagger \begin{pmatrix} n^{\mathrm{f}\uparrow} \\ n^{\mathrm{f}\downarrow} \\ n^{\mathrm{b}\uparrow} \\ n^{\mathrm{b}\downarrow} \end{pmatrix} = U^\dagger \boldsymbol{n}, \tag{4.73}$$

where

$$n^{\mathrm{B}\alpha} = \frac{1}{\sqrt{2}}(\sqrt{1-\sigma_0} n^{\mathrm{b}\alpha} + \sqrt{1+\sigma_0} n^{\mathrm{f}\alpha}), \quad n^{\mathrm{A}\alpha} = \frac{1}{\sqrt{2}}(\sqrt{1+\sigma_0} n^{\mathrm{b}\alpha} - \sqrt{1-\sigma_0} n^{\mathrm{f}\alpha}), \tag{4.74}$$

with $\alpha = \uparrow, \downarrow$. The lowest-energy one-body electron state is the up-spin bonding state, and the second lowest energy state is the down-spin bonding state. They are filled up at $\nu = 2$. The perturbative excitations η_i are as illustrated in Fig. 4.5 (b).

We go on to derive the effective Hamiltonian governing these NG modes. From (4.31), (4.32), and (4.35), the isospin densities are given in terms of $\tilde{\sigma}_i(\boldsymbol{x})$ and $\tilde{\vartheta}_i(\boldsymbol{x})$ as

$$\begin{aligned}
&\mathcal{P}_x = \sigma_0 \tilde{\sigma}_2 + \sqrt{1-\sigma_0^2} \left(1 - \sum_{i=1}^{4} \frac{\tilde{\sigma}_i^2 + \tilde{\vartheta}_i^2}{2} \right), \qquad \mathcal{P}_z = -\sqrt{1-\sigma_0^2} \tilde{\sigma}_2 + \sigma_0 \left(1 - \sum_{i=1}^{4} \frac{\tilde{\sigma}_i^2 + \tilde{\vartheta}_i^2}{2} \right), \\
&\mathcal{S}_x = -\left(\tilde{\sigma}_1 \tilde{\sigma}_4 + \tilde{\vartheta}_1 \tilde{\vartheta}_4 \right), \quad \mathcal{S}_y = \tilde{\sigma}_1 \tilde{\vartheta}_3 - \tilde{\sigma}_3 \tilde{\vartheta}_1, \quad \mathcal{S}_z = \tilde{\sigma}_3 \tilde{\sigma}_4 + \tilde{\vartheta}_3 \tilde{\vartheta}_4, \\
&\mathcal{R}_{zy} = \tilde{\vartheta}_1, \qquad \mathcal{P}_y = \tilde{\vartheta}_2, \qquad \mathcal{R}_{xy} = \tilde{\vartheta}_3, \qquad \mathcal{R}_{yy} = \tilde{\sigma}_4, \\
&\mathcal{R}_{xx} = -\sqrt{1-\sigma_0^2} \left(\tilde{\sigma}_2 \tilde{\sigma}_3 + \tilde{\vartheta}_2 \tilde{\vartheta}_3 \right) + \sigma_0 \tilde{\sigma}_3, \ \mathcal{R}_{xz} = -\sigma_0 \left(\tilde{\sigma}_2 \tilde{\sigma}_3 + \tilde{\vartheta}_2 \tilde{\vartheta}_3 \right) - \sqrt{1-\sigma_0^2} \tilde{\sigma}_3, \\
&\mathcal{R}_{yx} = \sqrt{1-\sigma_0^2} \left(\tilde{\sigma}_2 \tilde{\vartheta}_4 - \tilde{\sigma}_4 \tilde{\vartheta}_2 \right) - \sigma_0 \tilde{\vartheta}_4, \ \mathcal{R}_{yz} = \sigma_0 \left(\tilde{\sigma}_2 \tilde{\vartheta}_4 - \tilde{\sigma}_4 \tilde{\vartheta}_2 \right) + \sqrt{1-\sigma_0^2} \tilde{\vartheta}_4, \\
&\mathcal{R}_{zx} = -\sqrt{1-\sigma_0^2} \left(\tilde{\sigma}_1 \tilde{\sigma}_2 + \tilde{\vartheta}_1 \tilde{\vartheta}_2 \right) + \sigma_0 \tilde{\sigma}_1, \ \mathcal{R}_{zz} = -\sigma_0 \left(\tilde{\sigma}_1 \tilde{\sigma}_2 + \tilde{\vartheta}_1 \tilde{\vartheta}_2 \right) - \sqrt{1-\sigma_0^2} \tilde{\sigma}_1
\end{aligned} \tag{4.75}$$

Now, we substitute the isospin densities (4.75) into the effective Hamiltonian (4.42). In this way we derive the effective Hamiltonian of the NG modes in terms of the canonical sets of $\tilde{\sigma}_i$ and $\tilde{\vartheta}_i$ (or with $\check{\sigma}_i$ and $\check{\vartheta}_i$).

In the momentum space it reads

$$\mathcal{H}^{\mathrm{ppin}} = \mathcal{H}_0^{\mathrm{ppin}} + \mathcal{H}_{\mathrm{NG}}^{\mathrm{ppin}}, \tag{4.76}$$

$$\mathcal{H}_0^{\mathrm{ppin}} = \frac{\rho_0}{2}\left(\epsilon_{\mathrm{cap}}\sigma_0^2 - (\Delta_{\mathrm{SAS}}\sqrt{1-\sigma_0^2} + \Delta_{\mathrm{bias}}\sigma_0)\right), \tag{4.77}$$

$$\int d^2k\mathcal{H}_{\mathrm{NG}}^{\mathrm{ppin}} = \int d^2k\mathcal{H}_{\mathrm{NG},1}^{\mathrm{ppin}} + \int d^2k\mathcal{H}_{\mathrm{NG},2}^{\mathrm{ppin}} + \int d^2k\mathcal{H}_{\mathrm{NG},3}^{\mathrm{ppin}}, \tag{4.78}$$

where

$$\mathcal{H}_{\mathrm{NG},1}^{\mathrm{ppin}} = A_{\boldsymbol{k}}^{\mathrm{p}}\check{\sigma}_{1,\boldsymbol{k}}^{\dagger}\check{\sigma}_{1,\boldsymbol{k}} + B_{\boldsymbol{k}}^{\mathrm{p}}\check{\vartheta}_{1,\boldsymbol{k}}^{\dagger}\check{\vartheta}_{1,\boldsymbol{k}}, \tag{4.79}$$

$$\mathcal{H}_{\mathrm{NG},2}^{\mathrm{ppin}} = C_{\boldsymbol{k}}^{\mathrm{p}}\check{\sigma}_{2,\boldsymbol{k}}^{\dagger}\check{\sigma}_{2,\boldsymbol{k}} + B_{\boldsymbol{k}}^{\mathrm{p}}\check{\vartheta}_{2,\boldsymbol{k}}^{\dagger}\check{\vartheta}_{2,\boldsymbol{k}}, \tag{4.80}$$

$$\mathcal{H}_{\mathrm{NG},3}^{\mathrm{ppin}} = (\vec{P}_{\boldsymbol{k}}^{\mathrm{p}})^{\dagger}\mathcal{M}^{\mathrm{p}}\vec{P}_{\boldsymbol{k}}^{\mathrm{p}}, \tag{4.81}$$

with $\check{\sigma}_{i,\boldsymbol{k}}$, and $\check{\vartheta}_{i,\boldsymbol{k}}$ given by (4.51) and

$$\begin{aligned}
&A_{\boldsymbol{k}}^{\mathrm{p}} = \frac{2J_1^{\sigma_0}}{\rho_0}k^2 + \frac{\Delta_{\mathrm{SAS}}}{2\sqrt{1-\sigma_0^2}} - 2\epsilon_X^{-}(1-\sigma_0^2), \quad B_{\boldsymbol{k}}^{\mathrm{p}} = \frac{2J_s^d}{\rho_0}k^2 + \frac{\Delta_{\mathrm{SAS}}}{2\sqrt{1-\sigma_0^2}},\\
&C_{\boldsymbol{k}}^{\mathrm{p}} = \frac{2J_1^{\sigma_0}}{\rho_0}k^2 + \frac{\Delta_{\mathrm{SAS}}}{2\sqrt{1-\sigma_0^2}} + \epsilon_{\mathrm{cap}}(1-\sigma_0^2), \quad J_1^{\sigma_0} = (1-\sigma_0^2)J_s + \sigma_0^2 J_s^d,\\
&\vec{P}_{\boldsymbol{k}}^{\mathrm{p}} = \begin{pmatrix} \check{\vartheta}_4 \\ \check{\vartheta}_3 \\ \check{\sigma}_3 \\ \check{\sigma}_4 \end{pmatrix}, \quad \mathcal{M}^{\mathrm{p}} = \begin{pmatrix} A_{\boldsymbol{k}}^{\mathrm{p}} & -\Delta_{\mathrm{Z}}/2 & 0 & 0 \\ -\Delta_{\mathrm{Z}}/2 & B_{\boldsymbol{k}}^{\mathrm{p}} & 0 & 0 \\ 0 & 0 & A_{\boldsymbol{k}}^{\mathrm{p}} & -\Delta_{\mathrm{Z}}/2 \\ 0 & 0 & -\Delta_{\mathrm{Z}}/2 & B_{\boldsymbol{k}}^{\mathrm{p}} \end{pmatrix}.
\end{aligned} \tag{4.82}$$

It can be verified that the Hamiltonian (4.77) matches with the energy in the pseudospin phase (4.18)$\times\rho_0/2$.

We first analyze the dispersions and the coherence lengths from (4.80), since it describes the pseudospin wave. It is diagonalized as,

$$H_{2,\mathrm{NG}}^{\mathrm{ppin}} = \int d^2k E_2^{\mathrm{p}}\eta_{2,\boldsymbol{k}}^{\mathrm{p}\dagger}\eta_{2,\boldsymbol{k}}^{\mathrm{p}} \tag{4.83}$$

with

$$E_{2,\boldsymbol{k}}^{\mathrm{p}} = 2\sqrt{B_{\boldsymbol{k}}^{\mathrm{p}}C_{\boldsymbol{k}}^{\mathrm{p}}}, \tag{4.84}$$

$$\eta_{2,\boldsymbol{k}}^{\mathrm{p}} = \frac{1}{\sqrt{2}}\left(\left(\frac{C_{\boldsymbol{k}}^{\mathrm{p}}}{B_{\boldsymbol{k}}^{\mathrm{p}}}\right)^{\frac{1}{4}}\check{\sigma}_{2,\boldsymbol{k}} + i\left(\frac{B_{\boldsymbol{k}}^{\mathrm{p}}}{C_{\boldsymbol{k}}^{\mathrm{p}}}\right)^{\frac{1}{4}}\check{\vartheta}_{2,\boldsymbol{k}}\right), \tag{4.85}$$

where $\eta_{2,\boldsymbol{k}}^{\mathrm{p}}$ satisfy the commutation relation

$$\left[\eta_{2,\boldsymbol{k}}^{\mathrm{p}}, \eta_{2,\boldsymbol{k}'}^{\mathrm{p}\dagger}\right] = \delta(\boldsymbol{k}-\boldsymbol{k}'). \tag{4.86}$$

Since the ground state is a squeezed coherent state due to the capacitance energy ϵ_{cap}, it is

more convenient [59] to use the dispersion and the coherence lengths of $\check{\sigma}_2$ and $\check{\vartheta}_2$ separately. The dispersion relations are given by

$$E_{\boldsymbol{k}}^{\check{\sigma}_2} = \frac{2J_1^{\sigma_0}}{\rho_0}\boldsymbol{k}^2 + \frac{\Delta_{\rm SAS}}{2\sqrt{1-\sigma_0^2}} + \epsilon_{\rm cap}(1-\sigma_0^2), \quad E_{\boldsymbol{k}}^{\check{\vartheta}_2} = \frac{2J_s^d}{\rho_0}\boldsymbol{k}^2 + \frac{\Delta_{\rm SAS}}{2\sqrt{1-\sigma_0^2}}, \tag{4.87}$$

and their coherence lengths are

$$\xi^{\check{\sigma}_2} = 2l_B\sqrt{\frac{\pi J_1^{\sigma_0}}{\frac{\Delta_{\rm SAS}}{\sqrt{1-\sigma_0^2}} + 2\epsilon_{\rm cap}(1-\sigma_0^2)}}, \quad \xi^{\check{\vartheta}_2} = 2l_B\sqrt{\frac{\pi J_s^d\sqrt{1-\sigma_0^2}}{\Delta_{\rm SAS}}}. \tag{4.88}$$

The similar analysis can be adopted for (4.79), diagonalized as,

$$H_{\rm 1,NG}^{\rm ppin} = \int d^2k E_1^{\rm p}\eta_{1,\boldsymbol{k}}^{\rm p\dagger}\eta_{1,\boldsymbol{k}}^{\rm p} \tag{4.89}$$

with

$$E_1^{\rm p} = 2\sqrt{B_{\boldsymbol{k}}^{\rm p}A_{\boldsymbol{k}}^{\rm p}}, \tag{4.90}$$

$$\eta_{1,\boldsymbol{k}}^{\rm p} = \frac{1}{\sqrt{2}}\left(\left(\frac{A_{\boldsymbol{k}}^{\rm p}}{B_{\boldsymbol{k}}^{\rm p}}\right)^{\frac{1}{4}}\check{\sigma}_{1,\boldsymbol{k}} + i\left(\frac{B_{\boldsymbol{k}}^{\rm p}}{A_{\boldsymbol{k}}^{\rm p}}\right)^{\frac{1}{4}}\check{\vartheta}_{1,\boldsymbol{k}}\right), \tag{4.91}$$

where $\eta_{1,\boldsymbol{k}}^{\rm p}$ satisfy the commutation relation

$$\left[\eta_{1,\boldsymbol{k}}^{\rm p}, \eta_{1,\boldsymbol{k}'}^{\rm p\dagger}\right] = \delta(\boldsymbol{k}-\boldsymbol{k}'). \tag{4.92}$$

The dispersion relations of the canonical sets of $\check{\sigma}_1$ and $\check{\vartheta}_1$ are given by

$$E_{\boldsymbol{k}}^{\check{\sigma}_1} = \frac{2J_1^{\sigma_0}}{\rho_0}\boldsymbol{k}^2 + \frac{\Delta_{\rm SAS}}{2\sqrt{1-\sigma_0^2}} - 2\epsilon_X^-(1-\sigma_0^2), \quad E_{\boldsymbol{k}}^{\check{\vartheta}_1} = \frac{2J_s^d}{\rho_0}\boldsymbol{k}^2 + \frac{\Delta_{\rm SAS}}{2\sqrt{1-\sigma_0^2}}. \tag{4.93}$$

Their coherence lengths are

$$\xi^{\check{\sigma}_1} = 2l_B\sqrt{\frac{\pi J_1^{\sigma_0}}{\frac{\Delta_{\rm SAS}}{\sqrt{1-\sigma_0^2}} - 4\epsilon_X^-(1-\sigma_0^2)}}, \quad \xi^{\check{\vartheta}_1} = 2l_B\sqrt{\frac{\pi J_s^d\sqrt{1-\sigma_0^2}}{\Delta_{\rm SAS}}}. \tag{4.94}$$

It appears that $\xi^{\check{\sigma}_1}$ is ill-defined for $\Delta_{\rm SAS} \to 0$ in (4.94). This is not the case due to the relation (4.96) in the pseudospin phase, which we mention later. We see that from (4.84) and (4.90), in the one body picture, $\eta_1^{\rm p}$ and $\eta_2^{\rm p}$ have the same energy gap $\Delta_{\rm SAS}$. They are described in terms of η_1 and η_2, having the same energy gap $\Delta_{\rm SAS}$ [Fig. 4.5 (b)].

Finally, making an analysis of the Hamiltonian (4.81) as in the case of the spin phase, we

obtain the condition for the existence of a gapless mode,

$$\frac{\Delta_{\rm SAS}}{\sqrt{1-\sigma_0^2}}\left[\frac{\Delta_{\rm SAS}}{\sqrt{1-\sigma_0^2}}-4\epsilon_X^-(1-\sigma_0^2)\right]-\Delta_{\rm Z}^2=0. \tag{4.95}$$

It occurs along the pseudospin-canted boundary: See (5.3) and (5.4) in Ref.[104]. Inside the pseudospin phase, since we have

$$\frac{\Delta_{\rm SAS}}{\sqrt{1-\sigma_0^2}}\left[\frac{\Delta_{\rm SAS}}{\sqrt{1-\sigma_0^2}}-4\epsilon_X^-(1-\sigma_0^2)\right]-\Delta_{\rm Z}^2>0, \tag{4.96}$$

there are no gapless modes.

4.5 NG Modes in the CAF Phase

We derive the effective Hamiltonian of the NG modes in terms of the canonical sets of $\check{\sigma}_i$ and $\check{\vartheta}_i$. This can be done by substituting (4.40) and (4.39) into the Hamiltonian (4.42). We first derive the Hamiltonian, without taking any limits. Since the expression becomes too extensive, we introduce the notation

$$c_{\theta_\alpha}\equiv\cos\theta_\alpha,\quad s_{\theta_\alpha}\equiv\sin\theta_\alpha,\quad c_{\theta_\beta}\equiv\cos\theta_\beta,\quad s_{\theta_\beta}\equiv\sin\theta_\beta,\quad c_{\theta_\delta}\equiv\cos\theta_\delta,\quad s_{\theta_\delta}\equiv\sin\theta_\delta. \tag{4.97}$$

to express the formula of the effective Hamiltonian in a simple way.

Working in the momentum space, the effective Hamiltonian reads,

$$H^{\rm c}=\int d^2k\mathcal{H}^{\rm c}=\int d^2k\mathcal{H}_1^{\rm c}+\int d^2k\mathcal{H}_2^{\rm c}, \tag{4.98}$$

where

$$\mathcal{H}^{\rm CAF}=\mathcal{H}_0^{\rm CAF}+\mathcal{H}_{\rm NG}^{\rm CAF}, \tag{4.99}$$

$$\mathcal{H}_0^{\rm CAF}=\frac{\rho_0}{2}\left(\epsilon_{\rm cap}(\mathcal{P}_z^0)^2-2\epsilon_X^-\left(\sum_a(\mathcal{S}_a^0)^2+(\mathcal{R}_{az}^0)^2\right)-(\Delta_{\rm Z}\mathcal{S}_z^0+\Delta_{\rm SAS}\mathcal{P}_x^0+\Delta_{\rm bias}\mathcal{P}_z^0)\right), \tag{4.100}$$

$$\mathcal{H}_{1,\rm NG}^{\rm CAF}=\left(\frac{2}{\rho_0}J_1^\alpha\boldsymbol{k}^2+\frac{\Delta_0c_{\theta_\beta}^{-1}}{2}\right)\check{\vartheta}_{1,\boldsymbol{k}}^\dagger\check{\vartheta}_{1,\boldsymbol{k}}+\left(\frac{2}{\rho_0}(c_{\theta_\delta}^2J_s+s_{\theta_\delta}^2J_1^\beta)\boldsymbol{k}^2+\frac{M-4(s_{\theta_\delta}^2c_{\theta_\beta}^2+c_{\theta_\delta}^2)\epsilon_X^-}{2}\right)\check{\sigma}_{1,\boldsymbol{k}}^\dagger\check{\sigma}_{1,\boldsymbol{k}}, \tag{4.101}$$

$$\mathcal{H}_{2,\rm NG}^{\rm CAF}=\vec{Q}_{\boldsymbol{k}}^{\rm c\dagger}\mathcal{M}_2^{\rm c}\vec{Q}_{\boldsymbol{k}}^{\rm c}, \tag{4.102}$$

with

$$J_1^\alpha = c_{\theta_\alpha}^2 J_s + s_{\theta_\alpha}^2 J_s^d, \quad M = 4c_{\theta_\alpha}^2 \epsilon_X^- + \Delta_0 c_{\theta_\beta}^{-1},$$
$$\vec{Q}_{\boldsymbol{k}}^{\rm c} = \begin{pmatrix} \check{\vartheta}_{2,\boldsymbol{k}} \\ \check{\vartheta}_{4,\boldsymbol{k}} \\ \check{\vartheta}_{3,\boldsymbol{k}} \\ \check{\sigma}_{2,\boldsymbol{k}} \\ \check{\sigma}_{4,\boldsymbol{k}} \\ \check{\sigma}_{3,\boldsymbol{k}} \end{pmatrix}, \quad \mathcal{M}_2^{\rm c} = \begin{pmatrix} A^{\rm c} & c^{\rm c} & -e^{\rm c} & 0 & 0 & 0 \\ c^{\rm c} & C^{\rm c} & -f^{\rm c} & 0 & 0 & 0 \\ -e^{\rm c} & -f^{\rm c} & F^{\rm c} & 0 & 0 & 0 \\ 0 & 0 & 0 & B^{\rm c} & a^{\rm c} & b^{\rm c} \\ 0 & 0 & 0 & a^{\rm c} & D^{\rm c} & d^{\rm c} \\ 0 & 0 & 0 & b^{\rm c} & d^{\rm c} & E^{\rm c} \end{pmatrix}. \tag{4.103}$$

The Matrix elements in (4.103) are given by

$$A^{\rm c} = \frac{2\boldsymbol{k}^2}{\rho_0}\left[c_{\theta_\delta}^2 J_3^\beta + s_{\theta_\delta}^2 J_s^d\right] + \frac{M}{2} - 2s_{\theta_\beta}^2 c_{\theta_\delta}^2 \epsilon_X^-, \quad B^{\rm c} = \frac{2\boldsymbol{k}^2}{\rho_0}\left[c_{\theta_\alpha}^2 J_3^\beta + s_{\theta_\alpha}^2 J_1^\beta\right] + \frac{\Delta_0}{2c_{\theta_\beta}} + \frac{c_{\theta_\beta}^2 \epsilon_\alpha}{2},$$
$$C^{\rm c} = \frac{2\boldsymbol{k}^2}{\rho_0} J_1^\beta + \frac{M}{2} - 2c_{\theta_\beta}^2 \epsilon_X^-, \quad D^{\rm c} = \frac{2\boldsymbol{k}^2}{\rho_0}\left[c_{\theta_\delta}^2\left(s_{\theta_\alpha}^2 J_3^\beta + c_{\theta_\alpha}^2 J_1^\beta\right) + s_{\theta_\delta}^2 J_1^\alpha\right] + \frac{\Delta_0}{2c_{\theta_\beta}} + \frac{c_{\theta_\delta}^2 s_{\theta_\beta}^2 \epsilon_\alpha}{2},$$
$$E^{\rm c} = \frac{2\boldsymbol{k}^2}{\rho_0}\left[s_{\theta_\delta}^2\left(c_{\theta_\alpha}^2 J_3^\beta + s_{\theta_\alpha}^2 J_1^\beta\right) + c_{\theta_\delta}^2 J_3^\alpha\right] + \frac{M}{2} + s_{\theta_\beta}^2 s_{\theta_\delta}^2 c_{\theta_\alpha}^2 \epsilon_{\rm cap} - 2(c_{\theta_\beta}^2 s_{\theta_\delta}^2 + c_{\theta_\delta}^2) s_{\theta_\alpha}^2 \epsilon_X^-,$$
$$F^{\rm c} = \frac{2\boldsymbol{k}^2}{\rho_0} J_s^d + \frac{M}{2}, \tag{4.104}$$

and

$$a^{\rm c} = \frac{2\boldsymbol{k}^2}{\rho_0} c_{\theta_\delta} c_{2\theta_\alpha} J_2^\beta + \frac{s_{2\theta_\beta} c_{\theta_\delta}}{4}\epsilon_\alpha, \quad b^{\rm c} = -\frac{2\boldsymbol{k}^2}{\rho_0} s_{\theta_\delta} s_{2\theta_\alpha} J_2^\beta + L + \frac{\Delta_{\rm SAS}}{4\Delta_0} c_{\theta_\alpha} s_{2\theta_\beta}\epsilon_\alpha,$$
$$c^{\rm c} = \frac{2\boldsymbol{k}^2}{\rho_0} c_{\theta_\delta} J_2^\beta + s_{2\theta_\beta} c_{\theta_\delta}\epsilon_X^-,$$
$$d^{\rm c} = -\frac{s_{2\theta_\alpha} s_{2\theta_\delta}}{4}\left[\frac{2\boldsymbol{k}^2}{\rho_0}\left(J_1^\beta + J_s^d - J_3^\beta - J_s\right) + s_{\theta_\beta}^2(2\epsilon_X^- - \epsilon_{\rm cap})\right] - \frac{N}{2},$$
$$e^{\rm c} = -\frac{L}{2}, \quad f^{\rm c} = \frac{N}{2}, \tag{4.105}$$

with

$$J_3^\alpha = c_{\theta_\alpha}^2 J_s^d + s_{\theta_\alpha}^2 J_s, \quad J_1^\beta = c_{\theta_\beta}^2 J_s + s_{\theta_\beta}^2 J_s^d, \quad J_2^\beta = \frac{s_{2\theta_\beta}}{2}(J_s^d - J_s), \quad J_3^\beta = c_{\theta_\beta}^2 J_s^d + s_{\theta_\beta}^2 J_s,$$
$$L = -\frac{s_{2\theta_\beta}}{2}\left[s_{\theta_\delta} s_{2\theta_\alpha}(2\epsilon_X^- - \epsilon_{\rm cap}) + c_{\theta_\alpha}\frac{\Delta_{\rm SAS}}{\Delta_0}\epsilon_\alpha\right], \quad \epsilon_\alpha = 4c_{\theta_\alpha}^2\epsilon_X^- + 2s_{\theta_\alpha}^2\epsilon_{\rm cap},$$
$$N = \frac{s_{2\theta_\delta} s_{2\theta_\alpha} s_{\theta_\beta}^2}{2}(2\epsilon_X^- - \epsilon_{\rm cap}) + \frac{\Delta_{\rm SAS}}{\Delta_0}(c_{\theta_\delta} c_{\theta_\alpha} s_{\theta_\beta}^2 \epsilon_\alpha + \Delta_Z), \tag{4.106}$$

where we denote $s_{2\theta_\alpha} = \sin 2\theta_\alpha$, $s_{2\theta_\beta} = \sin 2\theta_\beta$, and $s_{2\theta_\delta} = \sin 2\theta_\delta$. We see that Hamiltonian (4.100) matches with the energy in the CAF phase (4.20)$\times\rho_0/2$.

It can be verified that the effective Hamiltonian (4.101) and (4.102) reproduce the effective Hamiltonian in the spin phase (4.56), by taking the limit $\alpha, \beta \to 0$. On the other hand, we reproduce the effective Hamiltonian in the pseudospin phase (4.78), by taking the limit $\alpha \to 1$,

in (4.101) and (4.102).

The effective Hamiltonian in the CAF phase is too complicated to make further analysis. We take the limit $\Delta_{\rm SAS} \to 0$ to examine if some simplified formulas are obtained. In particular we would like to seek for gapless modes. Such gapless modes will play an important role to drive the interlayer coherence in the CAF phase. In this limit we have

$$\cos\theta_\beta = \frac{\Delta_{\rm SAS}}{\Delta_{\rm Z}}, \quad \sin\theta_\beta = \pm\sqrt{1-\left(\frac{\Delta_{\rm SAS}}{\Delta_{\rm Z}}\right)^2}, \quad \cos\theta_\delta = \cos\theta_\alpha, \quad \sin\theta_\delta = \sin\theta_\alpha,$$
$$\alpha^2 = |\sigma_0|. \tag{4.107}$$

From (4.13) and (4.107) the classical ground state reads

$$\mathcal{S}^0_z = 1-|\sigma_0|, \quad \mathcal{P}^0_z = \sigma_0, \quad \mathcal{R}^0_{xx} = {\rm sgn}(\sigma_0)\mathcal{R}^0_{yy}, \quad \mathcal{R}^0_{yy} = -\sqrt{|\sigma_0|(1-|\sigma_0|)}, \tag{4.108}$$

and all others being zero. We see that the above order parameters match with (4.26). We assume $\sigma_0 > 0$ for definiteness. The transformation (4.32) has a simple expression,

$$U^\dagger = \begin{pmatrix} 1 & 0 & 0 & 0 \\ 0 & \sqrt{1-|\sigma_0|} & \sqrt{|\sigma_0|} & 0 \\ 0 & -\sqrt{|\sigma_0|} & \sqrt{1-|\sigma_0|} & 0 \\ 0 & 0 & 0 & 1 \end{pmatrix}, \tag{4.109}$$

We find $\bar{\boldsymbol{n}} = U^\dagger \boldsymbol{n}$ is of the form $(n^{\rm f\uparrow}, n^{\rm S}_{\rm f\downarrow b\uparrow}, n^{\rm A}_{\rm f\downarrow b\uparrow}, n^{\rm b\downarrow})^t$, by setting

$$n^{\rm S}_{\rm f\downarrow b\uparrow} = (\sqrt{1-|\sigma_0|}n^{\rm f\downarrow} + \sqrt{|\sigma_0|}n^{\rm b\uparrow}), \quad n^{\rm A}_{\rm f\downarrow b\uparrow} = (-\sqrt{|\sigma_0|}n^{\rm f\downarrow} + \sqrt{1-|\sigma_0|}n^{\rm b\uparrow}). \tag{4.110}$$

Consequently, the ground state is such that $|n^{\rm f\uparrow}\rangle$ and $|n^{\rm A}_{\rm f\downarrow b\uparrow}\rangle$ are filled up: The NG modes η_1 and η_3 describe an excitation from the state $|n^{\rm f\uparrow}\rangle$ to $|n^{\rm S}_{\rm f\downarrow b\uparrow}\rangle$ and $|n^{\rm b\downarrow}\rangle$, respectively, while the NG modes η_2 and η_4 describe an excitation from the state $|n^{\rm A}_{\rm f\downarrow b\uparrow}\rangle$ to $|n^{\rm b\downarrow}\rangle$ and $|n^{\rm S}_{\rm f\downarrow b\uparrow}\rangle$, respectively. A similar analysis can be done for $\sigma_0 < 0$, $|n^{\rm b\uparrow}\rangle$ and $|n^{\rm S}_{\rm f\uparrow b\downarrow}\rangle$ are filled up, where

$$n^{\rm S}_{\rm f\uparrow b\downarrow} = (\sqrt{1-|\sigma_0|}n^{\rm f\uparrow} + \sqrt{|\sigma_0|}n^{\rm b\downarrow}), \quad n^{\rm A}_{\rm f\downarrow b\uparrow} = (-\sqrt{|\sigma_0|}n^{\rm f\uparrow} + \sqrt{1-|\sigma_0|}n^{\rm b\downarrow}). \tag{4.111}$$

and the gapless mode η_4 describes an excitation from the state $|n^{\rm S}_{\rm f\uparrow b\downarrow}\rangle$ to $|n^{\rm A}_{\rm f\uparrow b\downarrow}\rangle$.

By using (4.107) into (4.101) and (4.102) with (4.103), (4.104), (4.105), and (4.106) we have the Hamiltonian

$$H = \sum_{i=1}^{4} \int d^2k E_i \eta^{\rm c\dagger}_{i,\boldsymbol{k}} \eta^{\rm c}_{i,\boldsymbol{k}}, \tag{4.112}$$

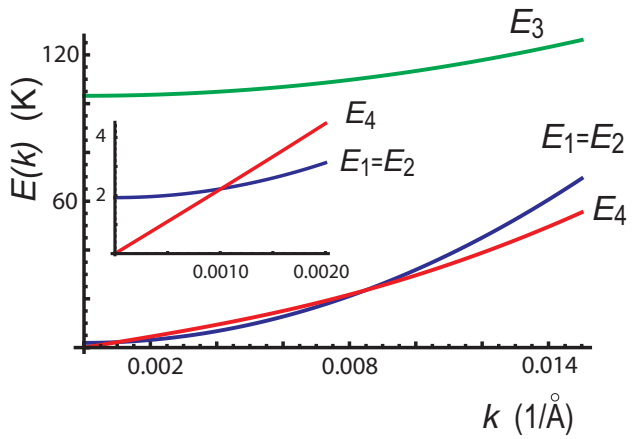

Fig. 4.6 Dispersion relations (4.113) for the four NG modes E_i. The sample parameters are $l_B = d \approx 231\mathring{A}$, $\rho_0 \approx 3.15 \times 10^{-5}\mathring{A}^{-2}$, and $\sigma_0 = 0.3572$. Inset: Dispersion relations near $k = 0$. It is clear that $E_4(k)$ is linear.

together with the dispersion relations

$$E_1 = E_2 = \frac{4\boldsymbol{k}^2}{\rho_0} J_1^{\alpha} + \Delta_{\mathrm{Z}}, \quad E_3 = \frac{4\boldsymbol{k}^2}{\rho_0} J_s^d + 2\Delta_{\mathrm{Z}} + 8\cos^2\theta_\alpha \epsilon_X^-,$$
$$E_4 = |\boldsymbol{k}| \sqrt{\frac{8J_s^d}{\rho_0}\left(\frac{2\boldsymbol{k}^2}{\rho_0}(\cos^2 2\theta_\alpha J_s^d + \sin^2 2\theta_\alpha J_s) + 2\sin^2 2\theta_\alpha(\epsilon_D^- - \epsilon_X^-)\right)}, \tag{4.113}$$

where $\eta_{i,\boldsymbol{k}}^{\mathrm{c}}$ $(i = 1, 2, 3, 4)$ are the annihilation operators

$$\eta_{1,\boldsymbol{k}}^{\mathrm{c}} = \frac{\check{\vartheta}_{1,\boldsymbol{k}} - i\check{\sigma}_{1,\boldsymbol{k}}}{\sqrt{2}}, \quad \eta_{2,\boldsymbol{k}}^{\mathrm{c}} = \frac{\check{\vartheta}_{2,\boldsymbol{k}} - i\check{\sigma}_{2,\boldsymbol{k}}}{\sqrt{2}}, \quad \eta_{3,\boldsymbol{k}}^{\mathrm{c}} = \left(\frac{\rho_0}{4}\right)^{\frac{1}{2}} (\sigma_{3,\boldsymbol{k}} + i\vartheta_{3,\boldsymbol{k}}),$$
$$\eta_{4,\boldsymbol{k}}^{\mathrm{c}} = \left(\frac{\rho_0}{4}\right)^{\frac{1}{2}} \left(\left(\frac{\lambda^{\sigma_4}}{\lambda^{\vartheta_4}}\right)^{\frac{1}{4}} \sigma_{4,\boldsymbol{k}} + i\left(\frac{\lambda^{\vartheta_4}}{\lambda^{\sigma_4}}\right)^{\frac{1}{4}} \vartheta_{4,\boldsymbol{k}}\right), \tag{4.114}$$

with

$$\lambda^{\vartheta_4} = \frac{2\boldsymbol{k}^2}{\rho_0} J_s^d, \quad \lambda^{\sigma_4} = \frac{2\boldsymbol{k}^2}{\rho_0}(\cos^2 2\theta_\alpha J_s^d + \sin^2 2\theta_\alpha J_s) + 2\sin^2 2\theta_\alpha(\epsilon_D^- - \epsilon_X^-). \tag{4.115}$$

The annihilation operators $\eta_{i,\boldsymbol{k}}$ satisfy the commutation relation,

$$\left[\eta_{i,\boldsymbol{k}}^{\mathrm{c}}, \eta_{j,\boldsymbol{k}'}^{\mathrm{c}\dagger}\right] = \delta_{ij}\delta(\boldsymbol{k} - \boldsymbol{k}'), \tag{4.116}$$

with $i, j = 1, 2, 3, 4$. We show graphically the dispersion relations (4.113) in Fig. 4.6.

We summarize the NG modes in the CAF phase in the limit $\Delta_{\mathrm{SAS}} \to 0$. It is to be emphasized that there emerges one gapless mode, $\eta_{4,\boldsymbol{k}}^{\mathrm{c}}$, reflecting the realization of the exact and its spontaneous breaking of the U(1) symmetry, which is a part of the SU(4) rotational symmetry, as in $\nu = 1$. Furthermore, it has the linear dispersion relation as in (4.113), and leads to a superfluidity associated with this gapless mode. All other modes are gapped.

4.6 CAF phase in $\Delta_{\rm SAS} \to 0$ up to $\mathcal{O}(\Delta_{\rm SAS}^3)$

We focus solely on the gapless mode η_4^c (or η_4) by neglecting all other gapped modes, and derive the effective Hamiltonian for η_4 up to $\mathcal{O}(\Delta_{\rm SAS}^3)$. We assume $\sigma_0 > 0$ for the simplicity.

The two CP^3 fields to be used in perturbation theory are given by $\bar{\boldsymbol{n}} = U^\dagger \boldsymbol{n}$ with (4.32) and (4.35), or

$$\bar{\boldsymbol{n}}_1 = \begin{pmatrix} 1 \\ 0 \\ 0 \\ 0 \end{pmatrix}, \quad \bar{\boldsymbol{n}}_2 = \begin{pmatrix} 0 \\ \eta_4 \\ 1 - \frac{1}{2}|\eta_4|^2 \\ 0 \end{pmatrix}, \tag{4.117}$$

Using (4.14) we can exactly solve β as

$$\beta^2 = \frac{\Delta_{\rm SAS}^2 \alpha^2 + \Delta_{\rm Z}^2(1-\alpha^2)}{\Delta_{\rm SAS}^2 \alpha^4 + \sigma_0^2 \Delta_{\rm Z}^2 (1-\alpha^2)} \sigma_0^2. \tag{4.118}$$

Note that in the limit $\Delta_{\rm SAS} \to 0$ we obtain $\beta \to 1$ which is in accord with our previous calculations. Substituting (4.118) into (4.7) we find

$$\Delta_{\rm Z}^2 = \frac{\Delta_{\rm SAS}^2 \alpha^4 + \sigma_0^2 \Delta_{\rm Z}^2 (1-\alpha^2)}{\alpha^2(\alpha^2 - \sigma_0^2)} + 4\epsilon_X^- \frac{\sigma_0^2 - \alpha^4}{\alpha^3} \frac{\sqrt{\Delta_{\rm SAS}^2 \alpha^2 + \Delta_{\rm Z}^2(1-\alpha^2)}}{\sqrt{\alpha^2 - \sigma_0^2}}. \tag{4.119}$$

The relation (4.119) determines the value of α^2 as a function of $\Delta_{\rm Z}$, $\Delta_{\rm SAS}$ and σ_0. Substituting this value into (4.118) we obtain β^2 as a function of $\Delta_{\rm Z}$, $\Delta_{\rm SAS}$, σ_0. We have thus summarized our problem into a single equation (4.119). When $\Delta_{\rm SAS}$ is exactly zero, (4.119) yields the relation $\alpha^2 = |\sigma_0|$. Therefore, for weak tunnelings we search for the solution of the form

$$\alpha^2 = |\sigma_0| + \lambda \Delta_{\rm SAS}^2 + \mathcal{O}(\Delta_{\rm SAS}^4), \tag{4.120}$$

where we expect λ to be a constant. In order to find the value of λ we use (4.120) and expand the relevant combinations in powers of $\Delta_{\rm SAS}^2$. In particular, for the first and the second terms of (4.119) we find

$$\begin{aligned} &\frac{\Delta_{\rm SAS}^2 \alpha^4 + \sigma_0^2 \Delta_{\rm Z}^2 (1-\alpha^2)}{\alpha^2(\alpha^2 - \sigma_0^2)} = \Delta_{\rm Z}^2 \left[1 + \frac{(1 - \lambda \Delta_{\rm Z}^2)\Delta_{\rm SAS}^2}{(1-|\sigma_0|)\Delta_{\rm Z}^2} - \frac{\lambda(2-|\sigma_0|)}{|\sigma_0|(1-|\sigma_0|)} \Delta_{\rm SAS}^2 \right] + \mathcal{O}(\Delta_{\rm SAS}^4), \\ &4\epsilon_X^- \frac{\sigma_0^2 - \alpha^4}{\alpha^3} \frac{\sqrt{\Delta_{\rm SAS}^2 \alpha^2 + \Delta_{\rm Z}^2(1-\alpha^2)}}{\sqrt{\alpha^2 - \sigma_0^2}} = -\lambda \frac{8\epsilon_X^- \Delta_{\rm Z}}{|\sigma_0|} \Delta_{\rm SAS}^2 + \mathcal{O}(\Delta_{\rm SAS}^4). \end{aligned} \tag{4.121}$$

Substituting these into (4.119) we obtain

$$\Delta_{\rm Z}^2 = \Delta_{\rm Z}^2 \left[1 + \frac{(1 - \lambda \Delta_{\rm Z}^2)\Delta_{\rm SAS}^2}{(1-|\sigma_0|)\Delta_{\rm Z}^2} - \frac{\lambda(2-|\sigma_0|)}{|\sigma_0|(1-|\sigma_0|)} \Delta_{\rm SAS}^2 \right] - \lambda \frac{8\epsilon_X^- \Delta_{\rm Z}}{|\sigma_0|} \Delta_{\rm SAS}^2 + \mathcal{O}(\Delta_{\rm SAS}^4). \tag{4.122}$$

The lowest terms $\Delta_{\rm SAS}^0$ disappear automatically. Requiring the $\Delta_{\rm SAS}^2$-terms to vanish we

obtain

$$\lambda = \frac{1}{\Delta_{\rm Z}} \frac{|\sigma_0|}{2(\Delta_{\rm Z} + 4\epsilon_X^-(1-|\sigma_0|))}, \tag{4.123}$$

and for α^2 we summarize as

$$\alpha^2 = |\sigma_0| \left(1 + \frac{\Delta_{\rm Z}}{2(\Delta_{\rm Z} + 4\epsilon_X^-(1-|\sigma_0|))} \frac{\Delta_{\rm SAS}^2}{\Delta_{\rm Z}^2} \right) + \mathcal{O}(\Delta_{\rm SAS}^4). \tag{4.124}$$

Using this in (4.118) we come to

$$\beta^2 = 1 - \frac{\Delta_{\rm SAS}^2}{\Delta_{\rm Z}^2} + \mathcal{O}(\Delta_{\rm SAS}^4). \tag{4.125}$$

Finally, using (4.124) and (4.125) in (4.33) and (4.8) we find

$$\sin^2\theta_\delta = |\sigma_0| \left(1 + \frac{\Delta_{\rm Z} + 8\epsilon_X^-(1-|\sigma_0|))}{2(\Delta_{\rm Z} + 4\epsilon_X^-(1-|\sigma_0|))} \frac{\Delta_{\rm SAS}^2}{\Delta_{\rm Z}^2} \right) + \mathcal{O}(\Delta_{\rm SAS}^4) \tag{4.126}$$

$$\Delta_{\rm bias} = {\rm sgn}(\sigma_0)\Delta_{\rm Z} \left[1 + \frac{4\epsilon_X^- + 8(\epsilon_D^- - \epsilon_X^-)|\sigma_0|}{\Delta_{\rm Z}} - \frac{1}{2}\frac{\Delta_{\rm SAS}^2}{\Delta_{\rm Z}^2} \right] + \mathcal{O}(\Delta_{\rm SAS}^4). \tag{4.127}$$

Then by using (4.124), (4.125), (4.126), (4.127) with (2.141), we obtain the effective Hamiltonian for the gapless mode η_4 (σ_4 and ϑ_4),

$$\mathcal{H} = \frac{J_{\vartheta_4}}{2}(\nabla\vartheta_4)^2 + \frac{J_{\sigma_4}}{2}(\nabla\sigma_4)^2 + 4\rho_0(\epsilon_D^- - \epsilon_X^-)|\sigma_0| \left(1 - |\sigma_0| - \frac{1}{2}\frac{\Delta_{\rm SAS}^2}{\Delta_{\rm Z}^2} \right), \tag{4.128}$$

with

$$J_{\vartheta_4} = 2\left(J_s^d + J_s^- \frac{\Delta_{\rm SAS}^2}{\Delta_{\rm Z}^2} \right), \quad J_{\sigma_4} = 2\left(J_s^d + 8J_s^-|\sigma_0|(1-|\sigma_0|) + J_s^-(1-4|\sigma_0|)\frac{\Delta_{\rm SAS}^2}{\Delta_{\rm Z}^2} \right). \tag{4.129}$$

Taking $\Delta_{\rm SAS}^2 = 0$, we reproduce the previously calculated expression (4.112) and (4.113).

Chapter 5

Entangled Spin-Pseudospin Phase Coherence and Spin Josephson Supercurrent at CAF Phase

The standard Hall resistance is given by $R^{\rm f}_{\rm Hall} = \frac{2}{\nu} R_{\rm K} = R_{\rm K}$ at $\nu = 2$. On the other hand, it is experimentally found [74, 75, 76] that $R^{\rm f}_{\rm Hall} = R_{\rm K}$ at $\nu = 2$. It seems that the interlayer phase coherence together with the supercurrent does not develop at $\nu = 2$. Note that the experiments [74, 75, 76] were performed at the balance point $\sigma_0 = 0$. As we now demonstrate, the entangled spin-pseudospin phase coherence develops only at the imbalance point $\sigma_0 \neq 0$ in the CAF phase. Furthermore, the spin Josephson current carries only the spins in the counterflow geometry.

This chapter is organized as follows. In section 5.1, we study the interlayer phase coherence in the CAF phase. It is the entangled spin-pseudospin phase coherence. We then study the Josephson supercurrent due to the development of the entangled spin-pseudospin phase coherence. In section 5.2, we show the detailed derivation of the electric current density flowing in the bilayer systems based on the Landau-Level Projection Formalism given in the subsection 2.2.4. In section 5.3, we study the quantum Hall effect in the presence of the entangled spin-pseudospin phase coherence, the effect from the Josephson supercurrent to the Hall resistivity in the counterflow and drag geometries in the CAF phase. Finally, in section 5.4, we study the spin Josephson current in the counterflow geometry in the CAF phase. We note that when we study the physics of the CAF phase, the limit $\Delta_{\rm SAS} \to 0$ is taken. The description of this chapter is based on [109, 110].

5.1 Entangled Spin-Pseudospin Phase Coherence

In this chapter we analyzed the phenomena generated by the linear dispersing NG mode in the CAF phase at $\Delta_{\rm SAS} \to 0$. We wish to derive the effective Hamiltonian for the nonperturbative

analysis of the phase field $\vartheta(\boldsymbol{x})$ so as to describe the interlayer phase coherence in the CAF phase. For this purpose, it is necessary to start with the parameterization of the Grassmannian field valid for arbitral value of $\vartheta(\boldsymbol{x})$. We make an ansatz,

$$\boldsymbol{n}_2 = \begin{pmatrix} 0 \\ -e^{+i\vartheta(\boldsymbol{x})}\sqrt{\sigma(\boldsymbol{x})} \\ \sqrt{1-\sigma(\boldsymbol{x})} \\ 0 \end{pmatrix} = e^{i\sigma_0\vartheta(\boldsymbol{x})} \begin{pmatrix} 0 \\ -e^{+i(1-\sigma_0)\vartheta(\boldsymbol{x})}\sqrt{\sigma(\boldsymbol{x})} \\ e^{-i\sigma_0\vartheta(\boldsymbol{x})}\sqrt{1-\sigma(\boldsymbol{x})} \\ 0 \end{pmatrix}. \tag{5.1}$$

We expand it around $\vartheta(\boldsymbol{x}) = 0$ and $\sigma(\boldsymbol{x}) = \sigma_0$ by setting $\delta\sigma(\boldsymbol{x}) \equiv \sigma(\boldsymbol{x}) - \sigma_0$. Up to the linear orders in $\vartheta(\boldsymbol{x})$ and $\delta\sigma(\boldsymbol{x})$, it is straightforward to show that

$$\begin{aligned} e^{+i(1-\sigma_0)\vartheta(\boldsymbol{x})}\sqrt{\sigma(\boldsymbol{x})} &= \sqrt{\sigma_0} - \sqrt{1-\sigma_0}\eta_4(\boldsymbol{x}), \\ e^{-i\sigma_0\vartheta(\boldsymbol{x})}\sqrt{1-\sigma(\boldsymbol{x})} &= \sqrt{1-\sigma_0} + \sqrt{\sigma_0}\eta_4(\boldsymbol{x}), \end{aligned} \tag{5.2}$$

where we have set

$$\eta_4(\boldsymbol{x}) = -\frac{\sigma(\boldsymbol{x}) - \sigma_0}{2\sqrt{\sigma_0(1-\sigma_0)}} - i\vartheta(\boldsymbol{x})\sqrt{\sigma_0(1-\sigma_0)}. \tag{5.3}$$

By requiring the commutation relation (4.37), we find

$$\frac{\rho_0}{2}\left[\sigma(\boldsymbol{x}), \vartheta(\boldsymbol{y})\right] = i\delta(\boldsymbol{x}-\boldsymbol{y}) \tag{5.4}$$

We have shown that the CP^3 field (5.1) is reduced to $\boldsymbol{n}_2$ in (4.117) in the linear order of the perturbation fields, apart from the U(1) factor $e^{-i\sigma_0\vartheta(\boldsymbol{x})}$. We may drop it off the parameterization since the CP^3 field is defined up to such a U(1) factor. Indeed, such a factor does not contribute to the isospin fields.

Here we parameterize the CP^3 fields as

$$\boldsymbol{n}_1 = \begin{pmatrix} n_{1,\mathrm{f}\uparrow} \\ n_{1,\mathrm{f}\downarrow} \\ n_{1,\mathrm{b}\uparrow} \\ n_{1,\mathrm{b}\downarrow} \end{pmatrix} = \begin{pmatrix} 1 \\ 0 \\ 0 \\ 0 \end{pmatrix}, \quad \boldsymbol{n}_2 = \begin{pmatrix} n_{2,\mathrm{f}\uparrow} \\ n_{2,\mathrm{f}\downarrow} \\ n_{2,\mathrm{b}\uparrow} \\ n_{2,\mathrm{b}\downarrow} \end{pmatrix} = \begin{pmatrix} 0 \\ -e^{+i\vartheta(\boldsymbol{x})/2}\sqrt{\sigma(\boldsymbol{x})} \\ e^{-i\vartheta(\boldsymbol{x})/2}\sqrt{1-\sigma(\boldsymbol{x})} \\ 0 \end{pmatrix}, \tag{5.5}$$

for $\sigma(\boldsymbol{x}) > 0$, and

$$\boldsymbol{n}_1 = \begin{pmatrix} n_{1,\mathrm{f}\uparrow} \\ n_{1,\mathrm{f}\downarrow} \\ n_{1,\mathrm{b}\uparrow} \\ n_{1,\mathrm{b}\downarrow} \end{pmatrix} \begin{pmatrix} 0 \\ 0 \\ 1 \\ 0 \end{pmatrix}, \quad \boldsymbol{n}_2 = \begin{pmatrix} n_{2,\mathrm{f}\uparrow} \\ n_{2,\mathrm{f}\downarrow} \\ n_{2,\mathrm{b}\uparrow} \\ n_{2,\mathrm{b}\downarrow} \end{pmatrix} = \begin{pmatrix} e^{+i\vartheta(\boldsymbol{x})/2}\sqrt{1+\sigma(\boldsymbol{x})} \\ 0 \\ 0 \\ e^{-i\vartheta(\boldsymbol{x})/2}\sqrt{-\sigma(\boldsymbol{x})} \end{pmatrix}. \tag{5.6}$$

for $\sigma(\boldsymbol{x}) < 0$. The isospin density fields are expressed in terms of $\sigma(\boldsymbol{x})$ and $\vartheta(\boldsymbol{x})$,

$$\begin{aligned}
&\mathcal{S}_z(\boldsymbol{x}) = 1 - |\sigma(\boldsymbol{x})|, \quad \mathcal{P}_z(\boldsymbol{x}) = \sigma(\boldsymbol{x}), \\
&\mathcal{R}_{yy}(\boldsymbol{x}) = \mathrm{sgn}(\sigma_0)\mathcal{R}_{xx}(\boldsymbol{x}) = -\sqrt{|\sigma(\boldsymbol{x})|(1-|\sigma(\boldsymbol{x})|)}\cos\vartheta(\boldsymbol{x}), \\
&\mathcal{R}_{yx}(\boldsymbol{x}) = -\mathrm{sgn}(\sigma_0)\mathcal{R}_{xy}(\boldsymbol{x}) = -\sqrt{|\sigma(\boldsymbol{x})|(1-|\sigma(\boldsymbol{x})|)}\sin\vartheta(\boldsymbol{x}),
\end{aligned} \tag{5.7}$$

with all others being zero. The ground-state expectation values are $\langle\sigma(\boldsymbol{x})\rangle = \sigma_0$, $\langle\vartheta(\boldsymbol{x})\rangle = 0$, with which the order parameters (4.26), or

$$\mathcal{S}_z^0 = 1 - |\sigma_0|, \quad \mathcal{P}_z^0 = \sigma_0, \quad \mathcal{R}_{xx}^0 = \mathrm{sgn}(\sigma_0)\mathcal{R}_{yy}^0, \quad \mathcal{R}_{yy}^0 = -\sqrt{|\sigma_0|(1-|\sigma_0|)}, \tag{5.8}$$

are reproduced from (5.7).

It is notable that the fluctuations of the phase field $\vartheta(\boldsymbol{x})$ affect both spin and pseudospin components of the R-spin. Indeed, from the two CP^3 fields (5.5) and (5.6), we see that the phase field $\vartheta(\boldsymbol{x})$ appears in the two components of the CP^3 field where both the spin and pseudospin are opposite; for $\sigma_0 > 0$, $\vartheta(\boldsymbol{x})$ appears in components $\alpha = \mathrm{f}\downarrow$ and $\mathrm{b}\uparrow$, while for $\sigma_0 < 0$, in components $\alpha = \mathrm{f}\uparrow$ and $\mathrm{b}\downarrow$. This is very different from the spin wave in the monolayer QH system or the pseudospin wave in the bilayer QH system at $\nu = 1$, since for example in $\nu = 1$ bilayer systems, from (3.26) we see that the phase field $\vartheta(\boldsymbol{x})$ appears in the two component having the same spin (up spin) but different pseudospin. Hence we call it the entangled spin-pseudospin phase field $\vartheta(\boldsymbol{x})$.

By substituting (5.7) into (2.141), apart from irrelevant constant terms the resulting effective Hamiltonian is

$$\mathcal{H}_{\mathrm{eff}} = \frac{J_\vartheta}{2}(\nabla\vartheta)^2 + \frac{J_\sigma}{2}(\nabla\sigma)^2 + \rho_\Phi\epsilon_{\mathrm{cap}}^{\nu=1}(\sigma-\sigma_0)^2, \tag{5.9}$$

where we have used

$$\Delta_{\mathrm{bias}} = \mathrm{sgn}(\sigma_0)\left[\Delta_{\mathrm{Z}} + 4\epsilon_X^- + 2\epsilon_{\mathrm{cap}}^{\nu=1}|\sigma_0|\right], \tag{5.10}$$

$$J_\sigma = 4J_s + \frac{(2|\sigma_0|-1)^2}{|\sigma_0|(1-|\sigma_0|)}J_s^d, \quad J_\vartheta = 4J_s^d|\sigma_0|(1-|\sigma_0|). \tag{5.11}$$

When we require the equal-time commutation relation,

$$\frac{\rho_0}{2}[\sigma(\boldsymbol{x}), \vartheta(\boldsymbol{y})] = i\delta(\boldsymbol{x}-\boldsymbol{y}), \tag{5.12}$$

the Hamiltonian (5.9) is second quantized, and it has the linear dispersion relation,

$$E_{\boldsymbol{k}} = |\boldsymbol{k}|\sqrt{\frac{2J_\vartheta}{\rho_0}\left(\frac{2J_\sigma}{\rho_0}\boldsymbol{k}^2 + 2\epsilon_{\mathrm{cap}}^{\nu=1}\right)}. \tag{5.13}$$

This agrees with E_4 in Eq. (4.113). It reflects the $\mathrm{U}_{T_{z0}}(1)$ spontaneous symmetry breaking which can be easily seen by adopting the similar discussion given in section 3.3 (see also the discussion in chapter 6). It should be emphasized that the effective Hamiltonian (5.9) is valid

in all orders of the phase field $\vartheta(\boldsymbol{x})$. It may be regarded as a classical Hamiltonian as well, where (5.12) should be replaced with the corresponding Poisson bracket.

The effective Hamiltonian (5.9) for $\vartheta(\boldsymbol{x})$ and $\sigma(\boldsymbol{x})$ reminds us of the one that governs the Josephson effect at $\nu = 1$. The main difference is the absence of the tunneling term, as implies that there exists no Josephson tunneling. We have shown that the effective Hamiltonian is correct up to $\mathcal{O}(\Delta_{\rm SAS}^3)$ as $\Delta_{\rm SAS} \to 0$. Nevertheless, the Josephson supercurrent is present within the layer.

By using the Hamiltonian (5.9) and the commutation relation (5.12), we obtain the equations of motion,

$$\hbar\partial_t\vartheta(\boldsymbol{x}) = \frac{2J_\sigma}{\rho_0}\nabla^2\sigma(\boldsymbol{x}) - 2\epsilon_{\rm cap}^{\nu=1}(\sigma(\boldsymbol{x}) - \sigma_0), \tag{5.14}$$

$$\hbar\partial_t\sigma(\boldsymbol{x}) = -\frac{2J_\vartheta}{\rho_0}\nabla^2\vartheta(\boldsymbol{x}). \tag{5.15}$$

We now study the electric Josephson supercurrent carried by the gapless mode $\vartheta(\boldsymbol{x})$ in the CAF phase, where the further analysis goes in parallel with that given at $\nu = 1$.

The electron densities for each layer are given by $\rho_e^{\rm f(b)} = -e\rho_0\left(1 \pm \sigma(\boldsymbol{x})\right)/2$, and by taking the time derivative with (5.15), we obtain the continuity equation for each layer, reading

$$\partial_t\rho_e^{\rm f} = -\partial_t\rho_e^{\rm b} = \frac{eJ_\vartheta}{\hbar}\nabla^2\vartheta(\boldsymbol{x}). \tag{5.16}$$

Therefore, we identify the current $\mathcal{J}_i^{\rm f(b)}$ flowing in each layer as the Josephson supercurrent $\pm\mathcal{J}_i^{\rm Jos}(\boldsymbol{x})$+constant, and we have

$$\mathcal{J}_i^{\rm Jos}(\boldsymbol{x}) \equiv -\frac{eJ_\vartheta}{\hbar}\partial_i\vartheta(\boldsymbol{x}). \tag{5.17}$$

From (5.8), we see that in the CAF phase at $\Delta_{\rm SAS} \to 0$, which is realized for $0 < |\sigma_0| < 1$, although the in-plane component of the spin in the front (back) layer $\mathcal{S}_{x,y}^{\rm f(b)}$ vanishes, the R-spins R_{xx} and R_{yy} are polarized. Since the NG mode ϑ is the fluctuation mode of these R-spins as we see from Eq. (5.7), the Josephson supercurrent flows in the CAF phase at $\Delta_{\rm SAS} \to 0$, even though $\mathcal{S}_{x,y}^{\rm f(b)}$ are zero.

Once again, we note that we call the current (5.17), which is carried by the interlayer phase field as " Josephson supercurrent". This is because this current is induced to decrease the phase difference, just like the dc-Josephson effect in the superconductivity.

It is intriguing that the Josephson supercurrent does not flow in the balanced system since $J_\vartheta = 0$ at $\sigma_0 = 0$ from Eq. (5.11).

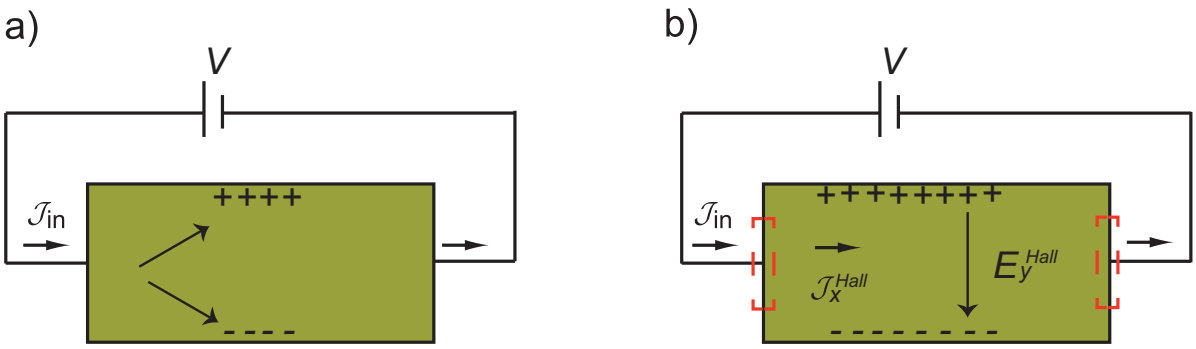

Fig. 5.1 The schematic illustration of the mechanism of the QH current in monolayer system. (a) When the current $\mathcal{J}_{\text{in}}$ is injected to the system, electrons in the sample move not only in the x direction but also in the y direction. At the beginning, electrons have both x and y-component velocity due to the Lorentz force. The electric current flows both in the x and y directions, $\mathcal{J}_x, \mathcal{J}_y \neq 0$. Electrons gather along the edge of the sample where as holes gather along the opposite side of the edge. (b) When the system is in the steady state, the Lorentz force is matching with the force derived by the electric field in the y direction (the Hall electric field E_y^{Hall}). Therefore, in the bulk of the sample, electrons are only flowing in the x direction. Furthermore, since σ_{xx} (or R_{xx}) is zero, the electric field in the x direction is zero, and as a result, the electric current in the bulk is flowing in the x direction without dissipation. This is the QH current. The voltage is consumed not in the bulk, but at the electrode enclosed by the red dotted line.

5.2 Quantum Hall Currents and Josephson Supercurrents at $\nu = 2$

5.2.1 Overview of Quantum Hall Currents and Josephson Supercurrents

To seek what kind of electric currents are flowing in the bilayer QH system, we analyze "the ground state of the bilayer QH state in the presence of the electric current", through the equations of motion for classical density fields such as the expectation values of the density and SU(4) isospin fields (or the imbalanced density and interlayer phase) in the ground state. Here we note that, we are not treating the electric current and the corresponding Hall electric field as perturbations to the "ground state of the bilayer QH systems without the electric current". The ground state of the QH systems with the electric current and the one without the electric current, which was discussed in chapter 3 and 4, must be clearly distinguished.

Especially at $\nu = 1$, when we consider the static solutions $\sigma = \sigma_0$ and $\partial_t \vartheta = 0$, and retaining up to the linear order in σ and ϑ in Eq. (3.31), the interlayer phase field ϑ satisfies the sine-Gordon equation

$$\partial_x^2 \vartheta(x) = \left(\frac{\rho_0 \Delta_{\text{SAS}}}{2\sqrt{1-\sigma_0^2} J_s^d} \right) \vartheta(x). \tag{5.18}$$

It has the trivial solution $\vartheta(x) = 0$ and sine-Gordon soliton solutions. It follows from (3.38) that there is no current flowing in the system for $\vartheta(x) = 0$, while there is a current flowing in the system for $\partial_x \vartheta(x) \neq 0$. Any nontrivial solution for (5.18) describes a topological state and cannot be connected perturbatively from the "ground state solution $\vartheta = 0$ of the QH systems without the electric current".

By taking account of this fact, we can consider that at $\nu = 2$ bilayer QH systems, the "ground state of the QH systems without the electric current" cannot be continuously connected to the "ground state of the bilayer QH state in the presence of the electric current".

We seek for the ground state with the electric current by solving the semiclassical equations of motion for the classical fields, which contains the information of the ground state of the QH systems.

We first review the essence of QH effect and present the overview of what kind of the electric currents flowing in both monolayer and bilayer systems. The detailed mathematical derivation of electric currents flowing in the QH systems is shown in the next subsection.

Let us first start considering the monolayer QH current in the Hall bar geometry. The electric current is injected to the system along the x direction. Since the magnetic field is applied to the system, the electrons in the sample flow into both the x and y directions due to the Lorentz force. As a result, some electrons gathered along the edge of the sample parallel to the x direction, as shown in Fig. 5.1 (a). As time goes by, the QH system is in the steady state. In such a situation, the force $-eE_y^{\rm Hall}$ due to electric field (the Hall electric field $E_y^{\rm Hall}$) in the y direction created by the electrons gathering in the edge, matching with the Lorentz force, and as a result, we have

$$\mathcal{J}_y = 0. \tag{5.19}$$

In the steady state, the electric current density does not flow into the y direction as schematically illustrated in Fig. 5.1 (b). We call Eq. (5.19) the geometrical condition for the Hall bar geometry. The creation of the electric field is expressed by the electric field Hamiltonian

$$H_{\rm E} = ec \int d^2q e^{-\boldsymbol{q}l_B^2/4} A_0(\boldsymbol{q}) \hat{\rho}(-\boldsymbol{q}), \tag{5.20}$$

where $cA_0(\boldsymbol{x}, z)$ is the scalar potential corresponding to the Hall electric field, and $e^{-\boldsymbol{q}l_B^2/4}$ the Landau-level form factor for the lowest Landau level. The electric field Hamiltonian has the two-dimensional form since the electron density has the form $\rho(\boldsymbol{x}, z) = \rho(\boldsymbol{x})\delta(z - z_0)$ in the real space. Here we consider that the QH system is located at $z = z_0$.

The relation between the electric current density and the electric field is given in terms of conductivity tensor as

$$\mathcal{J}_x = \sigma_{xx}E_x + \sigma_{xy}E_y, \qquad \mathcal{J}_y = \sigma_{yx}E_x + \sigma_{yy}E_y, \tag{5.21}$$

where $\sigma_{yy} = \sigma_{xx}$ and $\sigma_{xy} = -\sigma_{yx}$. Since $\sigma_{xx} = 0$ (or $R_{xx} = 0$) and $\sigma_{xy} \neq 0$ in the QH state,

from the geometrical condition (5.19), we have

$$E_x^{\rm Hall} = 0. \tag{5.22}$$

The quantum Hall current is given by

$$\mathcal{J}_x = \frac{\nu}{R_{\rm K}} E_y^{\rm Hall}, \tag{5.23}$$

which is derived in subsection 5.2.2. Thus, when we applied the current into the x direction $\mathcal{J}_x = \mathcal{J}_{\rm in}$, the Hall electric field is determined as $E_y^{\rm Hall} = \mathcal{J}_{\rm in} R_{\rm K}/\nu$. The Hall current flows into the x direction without dissipation. One might ask that there must be voltage consumption since the electric current is applied to the sample. In the QH system, the applied voltage is consumed at the electrode and not at the bulk, as represented by the red dotted lines in Fig. 5.1 (b).

We next consider the case where the current $\mathcal{J}_{\rm in}^{(\alpha)}$ ($\alpha = {\rm f}, {\rm b}$) is injected into the x direction of the bilayer sample in the Hall bar geometry. Similarly to the monolayer QH systems, in the steady state, the Hall electric field $E_y^{\rm f}$ and $E_y^{\rm b}$ is created so that the Hall current flows into the x direction. It is described by the Hamiltonian

$$H_{\rm E} = ec \int d^2 q e^{-\boldsymbol{q} l_B^2/4} \left(A_0^{\rm f}(\boldsymbol{q}) \hat{\rho}^{\rm f}(-\boldsymbol{q}) + A_0^{\rm b}(\boldsymbol{q}) \hat{\rho}^{\rm b}(-\boldsymbol{q}) \right), \tag{5.24}$$

where the scalar potential $cA_0(\boldsymbol{x}, z)$ satisfies

$$\partial_i c A_0(\boldsymbol{x}, z) = E_i(\boldsymbol{x}, z), \qquad \left(i = x, y, z, \quad |z| < \frac{d}{2} \right) \tag{5.25}$$

$$c A_0^{\rm f}(\boldsymbol{x}) = c A_0 \left(\boldsymbol{x}, z = d/2 \right), \quad c A_0^{\rm b}(\boldsymbol{x}) = c A_0 \left(\boldsymbol{x}, z = -d/2 \right), \tag{5.26}$$

$$\partial_i c A_0 \left(\boldsymbol{x}, z = \frac{d}{2} \right) = E_i^{\rm f}(\boldsymbol{x}), \quad \partial_i c A_0 \left(\boldsymbol{x}, z = -\frac{d}{2} \right) = E_i^{\rm b}(\boldsymbol{x}). \qquad (i = x, y) \tag{5.27}$$

For each layer the geometrical condition (5.19) is satisfied. It is represented as

$$\mathcal{J}_y^{(\alpha)} = 0, \tag{5.28}$$

with $\alpha =$f,b, and subsequently, we have

$$E_x^{(\alpha){\rm Hall}} = 0, \tag{5.29}$$

due to the QH effect $\sigma_{yy}^{\alpha} = \sigma_{xx}^{\alpha} = 0$ (or $R_{xx}^{\alpha} = 0$).

We discuss the Hall current in each layer. It is driven by the electric fields $E_y^{\rm f}$ and $E_y^{\rm b}$,

respectively, and flow into the x direction. They are given by

$$\mathcal{J}_x^{(\mathrm{f})\mathrm{Hall}} = \frac{e^2 l_B^2}{\hbar}\rho_0^{\mathrm{f}} E_y^{(\mathrm{f})\mathrm{Hall}} = \frac{\nu}{2R_{\mathrm{K}}}(1+\sigma_0)E_y^{\mathrm{fHall}},$$
$$\mathcal{J}_x^{(\mathrm{b})\mathrm{Hall}} = \frac{e^2 l_B^2}{\hbar}\rho_0^{\mathrm{b}} E_y^{(\mathrm{b})\mathrm{Hall}} = \frac{\nu}{2R_{\mathrm{K}}}(1-\sigma_0)E_y^{\mathrm{bHall}}, \tag{5.30}$$

and $\mathcal{J}_y^{(\mathrm{f})\mathrm{Hall}} = \mathcal{J}_y^{(\mathrm{b})\mathrm{Hall}} = 0$. Here we set the electron densities $\rho_0^{\mathrm{f}} = (1+\sigma_0)\rho_0/2$ and $\rho_0^{\mathrm{b}} = (1-\sigma_0)\rho_0/2$, since at very low temperature, the excitation for the imbalanced parameter $\delta\sigma(\boldsymbol{x}) = \sigma(\boldsymbol{x}) - \sigma_0$ is suppressed. This is because the energy gap of $\sigma(\boldsymbol{x})$ ($\sim \epsilon_{\mathrm{cap}}^{\nu=1}$) is large enough compared to the thermal energy, so that we may set $\sigma(\boldsymbol{x}) = \sigma_0$.

When the interlayer phase coherence is developed, the NG mode as an interlayer phase field also becomes the carrier of the electric current as the electric Josephson supercurrent, as we have discussed in section 3.4. In the ground state without the current, the interlayer phase field is homogeneous $\vartheta(\boldsymbol{x}) = \vartheta_0$. On the other hand, in the ground state with the current, the interlayer phase difference is created due to the applied current in the QH systems, and the Josephson supercurrent (5.17) is driven.

The x-component of the total in plane current is the sum of the standard QH current (5.30) and the Josephson supercurrent (5.17)[*1],

$$\mathcal{J}_x^{\mathrm{f}}(x) = \frac{\nu}{R_{\mathrm{K}}}\frac{\rho_0^{\mathrm{f}}}{\rho_0}E_y^{(\mathrm{f})\mathrm{Hall}} + \mathcal{J}_x^{\mathrm{Jos}}, \quad \mathcal{J}_x^{\mathrm{b}}(x) = \frac{\nu}{R_{\mathrm{K}}}\frac{\rho_0^{\mathrm{b}}}{\rho_0}E_y^{(\mathrm{b})\mathrm{Hall}} - \mathcal{J}_x^{\mathrm{Jos}}. \tag{5.31}$$

On the other hand, from the condition (5.28), for the y component we have

$$0 = \mathcal{J}_y^{(\mathrm{f})} = -\frac{\nu}{R_{\mathrm{K}}}\frac{\rho_0^{\mathrm{f}}}{\rho_0}\cdot 0 + \mathcal{J}_y^{\mathrm{Jos}}, \quad 0 = \mathcal{J}_y^{(\mathrm{b})} = -\frac{\nu}{R_{\mathrm{K}}}\frac{\rho_0^{\mathrm{b}}}{\rho_0}\cdot 0 - \mathcal{J}_y^{\mathrm{Jos}}, \tag{5.32}$$

and hence,

$$\partial_y \vartheta(\boldsymbol{x}) = 0. \tag{5.33}$$

Eq. (5.33) implies that the interlayer phase difference is created along the direction perpendicular to the one of the electric field. This is physically natural, because the Josephson supercurrent is current flowing without dissipation and does not flow into the direction where the dissipation occurs.

From now on, we omit the word "Hall" from the electric field $E_y^{(\alpha)\mathrm{Hall}}$. When the total current $\mathcal{J}_{\mathrm{in}}$ is applied to the bilayer systems, the electric field $E_y^{\mathrm{f(b)}}$ and the derivative of the interlayer phase field $\partial_x\vartheta(x)$ are determined dynamically, satisfying (5.31). In other words, there are three dynamical variables, the Hall electric field $E_y^{\mathrm{f(b)}}$ and the derivative of the interlayer phase field $\partial_x\vartheta(x)$. When the interlayer coherence is negligible in the QH systems, then we have two equations, which are (5.30), and the two dynamical variables $E_y^{\mathrm{f(b)}}$ are determined by them. On the other hand, when the interlayer coherence exists, we need one

[*1] We derive these formulas for the currents from the noncommutative quantum theory in subsection 5.2.3.

more equation besides (5.31) so as to determine the dynamics of the QH systems. Here we require the condition

$$E_y^{\rm f} = E_y^{\rm b} \equiv E_y, \tag{5.34}$$

when the interlayer coherence is developed as in the case of $\nu = 1$ (see Eq. (3.44)).

By using the relation (5.34), we can rewrite the basic formulas for the current as

$$\begin{aligned} \mathcal{J}_x^{\rm f}(x) = \frac{\nu_{\rm f}}{R_{\rm K}} E_y + \mathcal{J}_x^{\rm Jos}, \quad \mathcal{J}_x^{\rm b}(x) = \frac{\nu_{\rm b}}{R_{\rm K}} E_y - \mathcal{J}_x^{\rm Jos}, \\ \nu_{\rm f} = \frac{\nu}{2R_{\rm K}}(1+\sigma_0), \qquad \nu_{\rm b} = \frac{\nu}{2R_{\rm K}}(1-\sigma_0). \end{aligned} \tag{5.35}$$

We note that the current formulas (5.35) become invalid when d/l_B becomes large and the bilayer QH state is broken. Based on (5.35), we analyze the Hall resistance in each layer, for various geometries, the standard, the counterflow, and the drag geometries as shown in Fig. 1.6.

5.2.2 Electric Currents in Monolayer QH Systems

In this and next subsection, we show the detailed derivation of the electric currents flowing in the QH systems based on the Landau-Level Projection Formalism given in subsection 2.2.4. We start from the analysis of the monolayer systems to see clearly the essence of the argument. The electric current is constructed from the continuity equation,

$$\frac{d\hat{\rho}_e(\boldsymbol{x})}{dt} = -\partial_i \hat{\mathcal{J}}_i(\boldsymbol{x}), \tag{5.36}$$

where $\hat{\rho}_e(\boldsymbol{x}) = -e\hat{\rho}(\boldsymbol{x})$ denotes the electric charge density. The Heisenberg equation of motion for the bare operators reads,

$$i\hbar \frac{\hat{\rho}(\boldsymbol{x})}{dt} = [\hat{\rho}(\boldsymbol{x}), H]. \tag{5.37}$$

Here the total Hamiltonian H consists of the Coulomb term, the Zeeman term and the electric field term, $H = H_{\rm C} + H_{\rm Z} + H_{\rm E}$, where each term is given by

$$H_{\rm C} = \pi \int d^2q V_{\rm D} \hat{\rho}(-\boldsymbol{q})\hat{\rho}(\boldsymbol{q}), \tag{5.38}$$

$$H_{\rm Z} = -2\pi \Delta_{\rm Z} \hat{\mathcal{S}}_z(0) \tag{5.39}$$

$$H_{\rm E} = ec \int d^2q e^{-\frac{\boldsymbol{q}^2 l_B^2}{4}} A_0(-\boldsymbol{q})\hat{\rho}(\boldsymbol{q}). \tag{5.40}$$

Here $A_0(\boldsymbol{x})$ is the scalar potential and related to the electric field by $E_i(\boldsymbol{x}) = ec\partial_i A_0(\boldsymbol{x})$. What is observed in the experiments is the classic current $\mathcal{J}_i(\boldsymbol{x}) = \langle \hat{\mathcal{J}}_i(\boldsymbol{x}) \rangle$. Therefore, we analyze

the classical equation of motion for the classical electron density,

$$-\partial_i \mathcal{J}_i(\boldsymbol{x}) = -e\frac{\hat{\rho}^{\rm cl}(\boldsymbol{x})}{dt} = -e[\hat{\rho}^{\rm cl}(\boldsymbol{x}), H^{\rm cl}]_{\rm PB} = -e\left[\left(\int \frac{d^2k}{2\pi} e^{i\boldsymbol{k}\boldsymbol{x}}\hat{\rho}^{\rm cl}(\boldsymbol{k})\right), \int d^2k' \mathcal{H}^{\rm cl}(\boldsymbol{k}')\right]_{\rm PB}. \tag{5.41}$$

Here the total classical Hamiltonian is given by $H^{\rm cl} = H^{\rm cl}_{\rm C} + H^{\rm cl}_{\rm Z} + H^{\rm cl}_{\rm E}$,

$$H^{\rm cl}_{\rm C} = H^{\rm cl}_{\rm D} + H^{\rm cl}_{\rm X}, \tag{5.42}$$

$$H^{\rm cl}_{\rm D} = \pi \int d^2q V_{\rm D}(\boldsymbol{q})\hat{\rho}^{\rm cl}(-\boldsymbol{q})\hat{\rho}^{\rm cl}(\boldsymbol{q}), \tag{5.43}$$

$$H^{\rm cl}_{\rm X} = -\pi \int d^2q \left[V_{\rm X}(\boldsymbol{q})\hat{S}^{\rm cl}_a(-\boldsymbol{q})\hat{S}^{\rm cl}_a(\boldsymbol{q}) + \frac{1}{4}V_{\rm X}(\boldsymbol{q})\hat{\rho}^{\rm cl}(-\boldsymbol{q})\hat{\rho}^{\rm cl}(\boldsymbol{q})\right], \tag{5.44}$$

$$H^{\rm cl}_{\rm Z} = -2\pi\Delta_{\rm Z}\hat{S}^{\rm cl}_z(0), \tag{5.45}$$

$$H^{\rm cl}_{\rm E} = ec\int d^2q e^{-\frac{\boldsymbol{q}^2 l_B^2}{4}} A_0(-\boldsymbol{q})\hat{\rho}^{\rm cl}(\boldsymbol{q}). \tag{5.46}$$

In order to obtain the formula for $\mathcal{J}_i(\boldsymbol{x})$, we calculate the Poisson bracket in the right hand side of Eq. (5.41) by using the following Poisson bracket for the classical bare density operators,

$$\left[\hat{\rho}^{\rm cl}(\boldsymbol{p}), \hat{\rho}^{\rm cl}(\boldsymbol{q})\right]_{\rm PB} = \frac{1}{\pi\hbar}\hat{\rho}^{\rm cl}(\boldsymbol{p}+\boldsymbol{q})\sin\left(l_B^2\frac{\boldsymbol{p}\wedge\boldsymbol{q}}{2}\right), \tag{5.47}$$

$$\left[\hat{\rho}^{\rm cl}(\boldsymbol{p}), \hat{\mathcal{S}}^{\rm cl}_a(\boldsymbol{q})\right]_{\rm PB} = \frac{1}{\pi\hbar}\hat{\mathcal{S}}^{\rm cl}_a(\boldsymbol{p}+\boldsymbol{q})\sin\left(l_B^2\frac{\boldsymbol{p}\wedge\boldsymbol{q}}{2}\right), \tag{5.48}$$

$$\left[\hat{\mathcal{S}}^{\rm cl}_a(\boldsymbol{p}), \hat{\mathcal{S}}^{\rm cl}_b(\boldsymbol{q})\right]_{\rm PB} = \frac{1}{2\pi\hbar}\epsilon_{abc}\hat{\mathcal{S}}_c(\boldsymbol{p}+\boldsymbol{q})\cos\left(l_B^2\frac{\boldsymbol{p}\wedge\boldsymbol{q}}{2}\right) + \frac{1}{4\pi\hbar}\delta_{ab}\hat{\rho}^{\rm cl}(\boldsymbol{p}+\boldsymbol{q})\sin\left(l_B^2\frac{\boldsymbol{p}\wedge\boldsymbol{q}}{2}\right). \tag{5.49}$$

They are obtained from $\mathrm{W}_\infty(2)$ algebra (B.37)-(B.39), replacing the left hand side by the Poisson bracket and dividing the right hand side by $i\hbar$.

We can easily verify from (5.45) and (5.48) that there is no contribution from the Zeeman term to Eq. (5.41). We then calculate the Poisson bracket between $\hat{\rho}^{\rm cl}$ and Coulomb term. The Poisson brackets with the direct and exchange term are

$$\left[\hat{\rho}^{\rm cl}(\boldsymbol{p}), H^{\rm cl}_{\rm D}\right]_{\rm PB} = \frac{2}{\hbar}\int d^2q V_{\rm D}(\boldsymbol{q})\left\{\hat{\rho}^{\rm cl}(\boldsymbol{q}), \hat{\rho}^{\rm cl}(\boldsymbol{k}-\boldsymbol{q})\right\}\sin\left(l_B^2\frac{\boldsymbol{k}\wedge\boldsymbol{q}}{2}\right), \tag{5.50}$$

$$\begin{aligned}\left[\hat{\rho}^{\rm cl}(\boldsymbol{p}), H^{\rm cl}_{\rm X}\right]_{\rm PB} &= -\frac{1}{2\hbar}\int d^2q V_{\rm X}(\boldsymbol{k})\hat{\rho}^{\rm cl}(-\boldsymbol{q}), \hat{\rho}^{\rm cl}(\boldsymbol{k}+\boldsymbol{q})\sin\left(l_B^2\frac{\boldsymbol{k}\wedge\boldsymbol{q}}{2}\right)\\ &\quad - \frac{2}{\hbar}\int d^2q V_{\rm X}(\boldsymbol{q})\hat{\mathcal{S}}^{\rm cl}_a(-\boldsymbol{q})\hat{\mathcal{S}}^{\rm cl}_a(\boldsymbol{k}+\boldsymbol{q})\sin\left(l_B^2\frac{\boldsymbol{k}\wedge\boldsymbol{q}}{2}\right).\end{aligned} \tag{5.51}$$

The Poisson bracket from the direct term vanishes if we use the incompressibility condition

$$\hat{\rho}^{\rm cl}(\boldsymbol{p}) = 2\pi\rho_0\delta^2(\boldsymbol{p}). \tag{5.52}$$

On the other hand, the first term of the Poisson bracket from the exchange term, vanishes

from the incompressibility condition (5.52). For the second term, we treat it as follows: We make a derivative expansion of the potential $V_{\rm X}(\boldsymbol{q})$ and take the nontrivial lowest order term. Then by using the following formula, which holds for two arbitrary functions,

$$\int d^2q f(-\boldsymbol{q})g(\boldsymbol{k}+\boldsymbol{q})\sin\left(\boldsymbol{k}\wedge\boldsymbol{q}\right) = -\int d^2q f(\boldsymbol{k}+\boldsymbol{q})g(-\boldsymbol{q})\sin\left(\boldsymbol{k}\wedge\boldsymbol{q}\right), \tag{5.53}$$

the second term in (5.51) becomes

$$\begin{aligned}\int d^2q V_{\rm X}(\boldsymbol{q})\hat{\mathcal{S}}_a^{\rm cl}(-\boldsymbol{q})\hat{\mathcal{S}}_a^{\rm cl}(\boldsymbol{k}+\boldsymbol{q})\sin\left(l_B^2\frac{\boldsymbol{k}\wedge\boldsymbol{q}}{2}\right)& \\ \approx V_{\rm X}(0)\int d^2q\hat{\mathcal{S}}_a^{\rm cl}(-\boldsymbol{q})\hat{\mathcal{S}}_a^{\rm cl}(\boldsymbol{k}+\boldsymbol{q})\sin\left(l_B^2\frac{\boldsymbol{k}\wedge\boldsymbol{q}}{2}\right)&= 0.\end{aligned} \tag{5.54}$$

There is also no contribution from $H_{\rm X}^{\rm cl}$. Finally the Poisson bracket with the electric-field term $H_{\rm E}^{\rm cl}$ is

$$\left[\hat{\rho}^{\rm cl}(\boldsymbol{p}), H_{\rm E}^{\rm cl}\right]_{\rm PB} = \frac{ec}{\pi\hbar}\int d^2q e^{-\frac{\boldsymbol{q}^2 l_B^2}{4}}A_0(\boldsymbol{q})\hat{\rho}(\boldsymbol{k}-\boldsymbol{q})\sin\left(l_B^2\frac{\boldsymbol{k}\wedge\boldsymbol{q}}{2}\right). \tag{5.55}$$

By expanding $\sin\left(l_B^2(\boldsymbol{k}\wedge\boldsymbol{q})/2\right)$ in the above equation as,

$$\sin\left(l_B^2\frac{\boldsymbol{k}\wedge\boldsymbol{q}}{2}\right) = \frac{\epsilon_{ij}k_iq_j}{2}l_B^2 - \frac{1}{3!}\left(\frac{\epsilon_{ij}k_iq_j}{2}l_B^2\right)^3 + \cdots, \tag{5.56}$$

and using (5.41) with retaining only the nontrivial lowest order term, the classical electric current in the momentum space becomes

$$\mathcal{J}_i(\boldsymbol{k}) = i\frac{e^2l_B^2c}{2\pi\hbar}\int d^2q e^{-\frac{\boldsymbol{k}^2l_B^2}{4}}k_iq_jA_0(\boldsymbol{q})\hat{\rho}(\boldsymbol{k}-\boldsymbol{q}). \tag{5.57}$$

By using the relation between the electric field and the vector potential $A_0(\boldsymbol{q})$, $q_jcA_0(\boldsymbol{q}) = -2\pi iE_j(\boldsymbol{q})$ and the incompressibility condition (5.52), the electric current $\mathcal{J}_i(\boldsymbol{x})$ becomes

$$\mathcal{J}_i(\boldsymbol{x}) = \frac{e^2l_B^2}{\hbar}\epsilon_{ij}\rho_0E_j(\boldsymbol{x}) = \nu\frac{e^2}{2\pi\hbar}\epsilon_{ij}E_j(\boldsymbol{x}). \tag{5.58}$$

In the actual systems, it is considered that the homogeneous current is flowing in the sample. Hence, by setting $E_x = 0$, $E_y = E$ =const., we obtain the Hall current formula (2.60), or

$$\mathcal{J}_x^{\rm Hall} = \nu\frac{e^2}{2\pi\hbar}E_y, \quad \mathcal{J}_y^{\rm Hall} = 0. \tag{5.59}$$

Consequently, the total electric current consists solely of the Hall current, which is the contribution from the electric-field term. The Coulomb and Zeeman terms do not contribute to the electric current.

At the end of this subsection, we summarize that (i) in our calculation of electric currents, the total filling factor ν is limited to integer values, concretely 1 or 2. We have derived the

semi-classical equation of motion for the electric current (5.41) in the monolayer systems. In this equation, the expectation values of the electric currents are taken by the states (2.129) with (2.130), or

$$|\chi\rangle = e^{iW}|\chi_0\rangle, \qquad |\chi_0\rangle = \prod_{\mu n} \left[c_\mu^\dagger(n)\right]^{\nu_\mu(n)} |0\rangle. \tag{5.60}$$

They describe the states where ν $(= 1, 2)$ Landau levels are completely filled by electrons both in monolayer and bilayer systems. In our theory we use the states (5.60) to describe the $\nu = 1$ or 2 "quantum Hall states" in monolayer or bilayer systems. (ii) The impurity potential, which is responsible for the creation of the Hall plateau, is not included in this calculation. Even if the impurity potential is included, the Hall resistivity in (5.59) will not be changed. If the extended states could be constructed in a consistent way with the quantum theory [59, 101, 102, 103, 134], it would be possible to derive the Hall current corresponding to (5.59) generating Hall plateau.

5.2.3 Electric currents in Bilayer QH Systems

We extend the previous discussions to the bilayer QH systems. In this case we analyze the electric current flowing in the front and back layers. The basic equations are the continuity equations in each layer read [59, 78, 79]

$$\frac{d\hat{\rho}_e^{\mathrm{cl}(\alpha)}(\boldsymbol{x})}{dt} = -\partial_i \mathcal{J}_i^\alpha(\boldsymbol{x}) \tag{5.61}$$

where $\hat{\rho}_e^{\mathrm{cl}(\alpha)}(\boldsymbol{x})$ with α =f,b is given by

$$\hat{\rho}^{\mathrm{cl(f)}} = -e\left(\frac{1}{2}\hat{\rho}^{\mathrm{cl}} + \hat{P}_z^{\mathrm{cl}}\right), \quad \hat{\rho}^{\mathrm{cl(b)}} = -e\left(\frac{1}{2}\hat{\rho}^{\mathrm{cl}} - \hat{P}_z^{\mathrm{cl}}\right), \tag{5.62}$$

and $\mathcal{J}_z(\boldsymbol{x})$ denoting the tunneling current. The classical equations of motion for the electron densities in each layer read,

$$\frac{d\hat{\rho}_e^{\mathrm{cl}(\alpha)}(\boldsymbol{x})}{dt} = -e[\hat{\rho}^{\mathrm{cl}(\alpha)}, H^{\mathrm{cl}}]_{\mathrm{PB}} = -e\left[\left(\int \frac{d^2k}{2\pi} e^{i\boldsymbol{k}\boldsymbol{x}}\hat{\rho}^{\mathrm{cl}(\alpha)}(\boldsymbol{k})\right), \int d^2k' \mathcal{H}^{\mathrm{cl}}(\boldsymbol{k}')\right]_{\mathrm{PB}}, \tag{5.63}$$

where the total classical Hamiltonian is given by $H^{\rm cl} = H^{\rm cl}_{\rm D} + H^{\rm cl}_{\rm X} + H^{\rm cl}_{\rm Z} + H^{\rm cl}_{\rm T} + H^{\rm cl}_{\rm bias} + H^{\rm cl}_{\rm E}$, with each term having the form

$$
\begin{aligned}
H^{\rm cl}_{\rm D} &= \pi \int d^2q V^+_{\rm D} \hat{\rho}^{\rm cl}(-\boldsymbol{q})\hat{\rho}^{\rm cl}(\boldsymbol{q}) + 4\pi \int d^2q V^-_{\rm D} \hat{\mathcal{P}}^{\rm cl}_z(-\boldsymbol{q})\hat{\mathcal{P}}^{\rm cl}_z(\boldsymbol{q}), \qquad (5.64)\\
H^{\rm cl}_{\rm X} &= -\frac{\pi}{2}\int d^2q V^d_{\rm X}\left[\hat{\mathcal{S}}^{\rm cl}_a(-\boldsymbol{q})\hat{\mathcal{S}}^{\rm cl}_a(\boldsymbol{q}) + \hat{\mathcal{P}}^{\rm cl}_a(-\boldsymbol{q})\hat{\mathcal{P}}^{\rm cl}_a(\boldsymbol{q}) + \hat{\mathcal{R}}^{\rm cl}_{ab}(-\boldsymbol{q})\hat{\mathcal{R}}^{\rm cl}_{ab}(\boldsymbol{q})\right]\\
&\quad - \pi\int d^2q V^-_{\rm X}\left[\hat{\mathcal{S}}^{\rm cl}_a(-\boldsymbol{q})\hat{\mathcal{S}}^{\rm cl}_a(\boldsymbol{q}) + \hat{\mathcal{P}}^{\rm cl}_z(-\boldsymbol{q})\hat{\mathcal{P}}^{\rm cl}_z(\boldsymbol{q}) + \hat{\mathcal{R}}^{\rm cl}_{az}(-\boldsymbol{q})\hat{\mathcal{R}}^{\rm cl}_{az}(\boldsymbol{q})\right],\\
H^{\rm cl}_{\rm Z} &= -2\pi\Delta_{\rm Z}\hat{S}^{\rm cl}_z(0) \qquad (5.65)\\
H^{\rm cl}_{\rm T} &= -2\pi\Delta_{\rm SAS}\hat{P}^{\rm cl}_x(0), \qquad (5.66)\\
H^{\rm cl}_{\rm bias} &= -\int d^2p \Delta_{\rm bias}(-\boldsymbol{p})\hat{P}_z(\boldsymbol{p}), \qquad (5.67)\\
H^{\rm cl}_{\rm E} &= ec\int d^2q e^{-\frac{\boldsymbol{q}^2 l_B^2}{4}}\left[A^{\rm f}_0(-\boldsymbol{q})\hat{\rho}^{\rm cl(f)}(\boldsymbol{q}) + A^{\rm b}_0(-\boldsymbol{q})\hat{\rho}^{\rm cl(b)}(\boldsymbol{q})\right]. \qquad (5.68)
\end{aligned}
$$

Here we treat the bias term so that the bias voltage $\Delta_{\rm bias}$ has spatial dependence since it could depend on the coordinate when the current is injected to the system.[*2]

In the bilayer QH systems, not only the spin but also the pseudospin and R-spin become the dynamical variables. Therefore we need to consider the W_∞ algebra not only for the spin, but also for the pseudospin and R-spin. In order to obtain the formula for the current in each layer, we need to evaluate the Poisson brackets among the total Hamiltonian, the total bare electron density, and the z component of the bare pseudospin operator. The Poisson brackets to be used in the following calculations are

$$
\begin{aligned}
\left[\hat{\rho}^{\rm cl}(\boldsymbol{p}), \hat{S}^{\rm cl}_a(\boldsymbol{q})\right]_{\rm PB} &= \frac{1}{\pi\hbar}\hat{S}_a(\boldsymbol{p}+\boldsymbol{q})\sin\left(l_B^2\frac{\boldsymbol{p}\wedge\boldsymbol{q}}{2}\right),\\
\left[\hat{\rho}^{\rm cl}(\boldsymbol{p}), \hat{P}^{\rm cl}_a(\boldsymbol{q})\right]_{\rm PB} &= \frac{1}{\pi\hbar}\hat{P}_a(\boldsymbol{p}+\boldsymbol{q})\sin\left(l_B^2\frac{\boldsymbol{p}\wedge\boldsymbol{q}}{2}\right),\\
\left[\hat{\rho}^{\rm cl}(\boldsymbol{p}), \hat{R}^{\rm cl}_{ab}(\boldsymbol{q})\right]_{\rm PB} &= \frac{1}{\pi\hbar}\hat{R}_{ab}(\boldsymbol{p}+\boldsymbol{q})\sin\left(l_B^2\frac{\boldsymbol{p}\wedge\boldsymbol{q}}{2}\right),\\
\left[\hat{P}_z(\boldsymbol{k}), \hat{S}_a(\boldsymbol{k}')\right]_{\rm PB} &= \frac{1}{2\pi\hbar}\hat{R}_{az}(\boldsymbol{k}+\boldsymbol{k}')\sin\left(l_B^2\frac{\boldsymbol{k}\wedge\boldsymbol{k}'}{2}\right),\\
\left[\hat{P}_z(\boldsymbol{k}), \hat{P}_a(\boldsymbol{k}')\right]_{\rm PB} &= \frac{1}{2\pi\hbar}\epsilon_{zab}\cos\left(l_B^2\frac{\boldsymbol{k}\wedge\boldsymbol{k}'}{2}\right)\hat{P}_b(\boldsymbol{k}+\boldsymbol{k}') + \frac{1}{4\pi\hbar}\delta_{za}\sin\left(l_B^2\frac{\boldsymbol{k}\wedge\boldsymbol{k}'}{2}\right)\hat{\rho}(\boldsymbol{k}+\boldsymbol{k}'),\\
\left[\hat{P}_z(\boldsymbol{k}), \hat{R}_{ab}(\boldsymbol{k}')\right]_{\rm PB} &= \frac{1}{2\pi\hbar}\epsilon_{zbc}\cos\left(l_B^2\frac{\boldsymbol{k}\wedge\boldsymbol{k}'}{2}\right)\hat{R}_{ac}(\boldsymbol{k}+\boldsymbol{k}') + \frac{1}{2\pi\hbar}\delta_{zb}\sin\left(l_B^2\frac{\boldsymbol{k}\wedge\boldsymbol{k}'}{2}\right)\hat{S}_a(\boldsymbol{k}+\boldsymbol{k}').
\end{aligned}
\qquad (5.69)
$$

[*2] As we have seen in section 5.1, $\Delta_{\rm bias}$ is determined by the Zeeman gap $\Delta_{\rm Z}$, tunneling gap $\Delta_{\rm SAS}$, the Coulomb energy $(\epsilon^-_{\rm D}, \epsilon^-_{\rm X})$ and the ground expectation values σ_0 and ϑ_0 through the equations of motion for $\sigma(\boldsymbol{x})$ and $\vartheta(\boldsymbol{x})$ in the ground state. Both the ground state expectation value of $\sigma(\boldsymbol{x})$ and $\vartheta(\boldsymbol{x})$ are spatially homogeneous when the current is not injected into the system. When the current is injected, the ground state expectation value of $\sigma(\boldsymbol{x})$ is still spatially homogeneous ($\langle\sigma(\boldsymbol{x})\rangle = \sigma_0$) to a good accuracy, since the gap is large compared to the thermal energy. On the other hand, the ground state expectation value of $\vartheta(\boldsymbol{x})$ could depend on space, because the interlayer phase field $\vartheta(\boldsymbol{x})$ is gapless.

We also use the formulas

$$\sin\left(\frac{1}{2}l_B^2\boldsymbol{k}\wedge\boldsymbol{k}'\right)\simeq\frac{1}{2}l_B^2\boldsymbol{k}\wedge\boldsymbol{k}',\quad \cos\left(\frac{1}{2}l_B^2\boldsymbol{k}\wedge\boldsymbol{k}'\right)\simeq 1, \tag{5.70}$$

while setting $V_{\rm D}(\boldsymbol{k})=V_{\rm D}(\boldsymbol{0})$ and the derivative expansion for the exchange potential $V_{\rm X}^{\pm}(\boldsymbol{k})$ in the nontrivial lowest order.

By using the basic Poisson bracket (5.69), we see that there is no contribution to Eq. (5.63) from the Zeeman. Subsequently, from the conditions

$$\hat{\rho}^{\rm cl}(\boldsymbol{p})=2\pi\rho_0^{\rm cl}\delta(\boldsymbol{p}),\qquad \hat{P}_z(\boldsymbol{p})=\pi\rho_0\sigma_0\delta(\boldsymbol{p}). \tag{5.71}$$

or equivalently,

$$\hat{\rho}^{\rm f(b)cl}(\boldsymbol{p})=2\pi\rho_0^{\rm f(b)cl}\delta(\boldsymbol{p}), \tag{5.72}$$

there is also no contribution to Eq. (5.63) from the direct Coulomb term and the bias terms. The first equation in (5.71) indicates the incompressibility condition of the bilayer QH systems while the second equation in (5.71) is equivalent to $\sigma(\boldsymbol{x})=\sigma_0$. The solution $\sigma(\boldsymbol{x})=\sigma_0$ is adopted, because from (5.9) we see that the interlayer phase field ϑ is gapless, while the imbalanced-density field σ has the gap, which is in the order of $\epsilon_{\rm cap}^{\nu=1}$. It is large compared to the thermal energy. Therefore the excitation of $\sigma(\boldsymbol{x})$ is considered to be suppressed.

We next evaluate the contribution from the exchange Coulomb term $H_{\rm X}^{\rm cl}$. We note that the Poisson bracket between the density and the exchange Coulomb term, $[\hat{\rho}^{\rm cl},H_{\rm X}^{\rm cl}]_{\rm PB}$, is zero due to (5.72) and (5.53). On the other hand, for the Poisson bracket with $\hat{P}_z^{\rm cl}$, we have

$$\left[\hat{P}_z^{\rm cl}(\boldsymbol{k}),H_{\rm X}^{\rm cl}\right]_{\rm PB}=-\frac{\epsilon_{zbc}}{2\hbar}\int d^2k'V_{\rm X}^d(\boldsymbol{k}')\cos\left(l_B^2\frac{\boldsymbol{k}\wedge\boldsymbol{k}'}{2}\right)\left[\hat{P}_b^{\rm cl}(-\boldsymbol{k}')\hat{P}_c^{\rm cl}(\boldsymbol{k}+\boldsymbol{k}')+\hat{R}_{ab}^{\rm cl}(-\boldsymbol{k}')\hat{R}_{ac}^{\rm cl}(\boldsymbol{k}+\boldsymbol{k}')\right]. \tag{5.73}$$

In Eq. (5.73), we have only retained the terms which contributes to the Poisson bracket $\left[\hat{P}_z^{\rm cl}(\boldsymbol{k}),H_{\rm X}^{\rm cl}\right]_{\rm PB}$. Then by using the derivative expansion (2.137) for $V_{\rm X}^d(\boldsymbol{k}')$ and the formula (5.70) for $\cos\left(l_B^2(\boldsymbol{k}\wedge\boldsymbol{k}')/2\right)$ in the above equation, we obtain

$$\mathcal{J}_i^{\rm Jos(f)}(\boldsymbol{x})=-\mathcal{J}_i^{\rm Jos(b)}(\boldsymbol{x})=-\frac{2eJ_s^d}{\hbar}\epsilon_{zbc}\left(\partial_i\mathcal{P}_b^{\rm cl}(\boldsymbol{x})\cdot\mathcal{P}_c^{\rm cl}(\boldsymbol{x})+\partial_i\mathcal{R}_{ab}^{\rm cl}(\boldsymbol{x})\cdot\mathcal{R}_{ac}^{\rm cl}(\boldsymbol{x})\right), \tag{5.74}$$

We re-express the current (5.74) by using the parametrization (5.7), or

$$\begin{aligned}
&\mathcal{S}_z^{\rm cl}(\boldsymbol{x})=1-|\sigma(\boldsymbol{x})|,\quad \mathcal{P}_z^{\rm cl}(\boldsymbol{x})=\sigma(\boldsymbol{x}),\\
&\mathcal{R}_{yy}^{\rm cl}(\boldsymbol{x})=\mathrm{sgn}(\sigma_0)\mathcal{R}_{xx}^{\rm cl}(\boldsymbol{x})=-\sqrt{|\sigma(\boldsymbol{x})|(1-|\sigma(\boldsymbol{x})|)}\cos\vartheta(\boldsymbol{x}),\\
&\mathcal{R}_{yx}^{\rm cl}(\boldsymbol{x})=-\mathrm{sgn}(\sigma_0)\mathcal{R}_{xy}^{\rm cl}(\boldsymbol{x})=-\sqrt{|\sigma(\boldsymbol{x})|(1-|\sigma(\boldsymbol{x})|)}\sin\vartheta(\boldsymbol{x}),
\end{aligned} \tag{5.75}$$

and all other components being zero[*3]. In the ground state without the current, the interlayer phase field is homogeneous $\vartheta(\boldsymbol{x}) = \vartheta_0$, and the current (5.74) does not flow in this situation. On the other hand, the ground state with the current, the interlayer phase difference is considered to be created, and as a result, the inplane current (5.74) is driven, which is expressed in terms of the interlayer phase field

$$\mathcal{J}_i^{\mathrm{Jos}}(\boldsymbol{x}) = \mathcal{J}_i^{\mathrm{Jos(f)}}(\boldsymbol{x}) = -\mathcal{J}_i^{\mathrm{Jos(b)}}(\boldsymbol{x}) = -\frac{eJ_\vartheta}{\hbar}\partial_i\vartheta(\boldsymbol{x}). \tag{5.76}$$

It is the Josephson inplane current, which has exactly the same formula as (5.17). The Josephson inplane current flows in order to diminish the energy of the system since it becomes higher than the ground state, where the interlayer phase field is homogeneous, due to the kinetic energy $\sim J_s^d(\partial_i\vartheta(\boldsymbol{x}))^2$, as well as the inhomogeneity of the interlayer phase field. We can see clearly from Eq. (5.74) that the interlayer phase coherence and the associated Josephson current is driven by the interlayer exchange Coulomb interaction.

Finally, the contribution from the electric-field term H_{E} is

$$[\hat{\rho}^{\mathrm{cl}(\alpha)}(\boldsymbol{k}), H_{\mathrm{E}}^{\mathrm{cl}}]_{\mathrm{PB}} = \frac{ec}{\pi\hbar}\int d^2q e^{-\frac{ql_B^2}{4}} A_0^\alpha(\boldsymbol{q})\hat{\rho}^{\mathrm{cl}(\alpha)}(\boldsymbol{k}-\boldsymbol{q})\sin\left(\frac{1}{2}l_B^2\boldsymbol{k}\wedge\boldsymbol{q}\right), \tag{5.77}$$

which has the similar form as the monolayer one. By imposing the condition (5.72), we obtain in each layer,

$$\mathcal{J}_i^{\alpha(\mathrm{E})}(\boldsymbol{x}) = \frac{e^2l_B^2}{\hbar}\epsilon_{ij}E_j^\alpha\rho_0^\alpha = \frac{\nu}{R_{\mathrm{K}}}\epsilon_{ij}E_j^\alpha\frac{\rho_0^\alpha}{\rho_0}. \tag{5.78}$$

It is the standard formula for the Hall current in the bilayer systems. Here we assumed that the electric field E_j^α is spatially homogeneous.

Taking all together with the condition (5.34), the total in-plane current is given by the sum of the Josephson in-plane current and the Hall current,

$$\mathcal{J}_i^{\mathrm{f}}(\boldsymbol{x}) = -\frac{eJ_\vartheta}{\hbar}\partial_i\vartheta(\boldsymbol{x}) + \frac{e^2l_B^2}{\hbar}\epsilon_{ij}E_j^{\mathrm{f}}\rho_0^{\mathrm{f}}, \tag{5.79}$$

$$\mathcal{J}_i^{\mathrm{b}}(\boldsymbol{x}) = \frac{eJ_\vartheta}{\hbar}\partial_i\vartheta(\boldsymbol{x}) + \frac{e^2l_B^2}{\hbar}\epsilon_{ij}E_j^{\mathrm{b}}\rho_0^{\mathrm{b}}, \tag{5.80}$$

which match to the basic formulas for the current (5.35), when the current is flowing in the x direction.

In this thesis we have neglected the tunneling current, since we have focused on the limit $\Delta_{\mathrm{SAS}} \to 0$. When Δ_{SAS} is finite, it gives the Josephson tunneling current. For the detailed discussion about the Josephson tunneling current, see e.g. [79].

We note that $\Delta_{\mathrm{SAS}} \to 0$ does not imply $\langle\mathcal{P}_{x,y}\rangle = 0$. In other words, the expectation value $\langle\mathcal{P}_{x,y}\rangle$ becoming finite does not mean the frequency of the tunneling process from one layer to the other layer, but it just means that both the x and y components of the pseudospin are

[*3] We note that by using the (3.27) with (5.74), we obtain the total in-plane current for $\nu = 1$

polarized. This can be easily understood from the following fact. When both the x and y components of the real spin have finite expectation values, it does not mean that there is a spin flip-flop process occurring, but just describing that both the x and y components of the real spin are polarized. Indeed, in the ground state at $\nu = 1$ with $\sigma_0 = 0$, the pseudospin $\mathcal{P}_x$ is spontaneously polarized in the limit $\Delta_{\rm SAS} \to 0$, while the tunneling process does not occur.

We note once again that the integer QH effect in the bilayer is realized by the two-dimensional electrons possessing the pseudospin degree of freedom, because electrons in the front and back layers are indistinguishable. The bilayer system as a whole system exhibits the QH effect as if it were the monolayer system. It is not equivalent to two independent QH monolayer systems. The "total" filling factor of the bilayer QH system $\nu = 2\pi\rho_0 l_B^2$ with ρ_0 the "total" electron density, takes the integer values.

Although electrons in the front and back layers are indistinguishable, the average densities $\rho_0^{\rm f}$ and $\rho_0^{\rm b}$ are physical observables. They contribute to the Hall currents as in (5.78). Consequently, for layer α (=f,b), the Hall resistivity R_{xy}^{α} is given in terms of the total filling factor ν and the imbalance parameter σ_0 as

$$R_{xy}^{\rm f,b} = \frac{R_{\rm K}}{\nu_{\rm f,b}}, \qquad \nu_{\rm f,b} = \frac{(1 \pm \sigma_0)}{2}\nu. \tag{5.81}$$

For example, at $\nu = 2$ with $\sigma_0 = 0$, we have

$$R_{xy}^{\rm f} = R_{xy}^{\rm b} = R_{\rm K}, \tag{5.82}$$

while at $\nu = 1$ with $\sigma_0 = 0$, we have

$$R_{xy}^{\rm f} = R_{xy}^{\rm b} = 2R_{\rm K}. \tag{5.83}$$

The filling factors $\nu_{\rm f,b}$ are the function of σ_0 and does not necessary take integer values. In other words, it does not mean that when the system is realizing the integer ν bilayer QH effect, both Hall conductivities in the front and back layers always take integer values in the unit of $R_{\rm K}$.

By looking at the experimental results shown in the top part of Fig. 1.2, we can see that both the Hall conductivities in the front and back layers do not take integer values in the unit of $R_{\rm K}$. As wee see, when the total filling factor of the bilayer system becomes one (see the region indicated as $\nu_{\rm T} = 1$ with the black arrow), the Hall resistivity in one of the layers becomes $2R_{\rm K}$, which mathces with Eq. (5.83). What is remarkable is that even the filling factor of each layer takes $1/2 \pm \delta$ with δ a real number, the plateau is created. This phenomenon cannot be understand when we think that the bilayer QH system is composed of two independent monolayer QH systems. Indeed the filling factor 1/2 monolayer QH effect has not been observed experimentally. This result is obviously inconsistent with the statement such that both the Hall conductivities in the front and back layers take integer values in the unit of $R_{\rm K}$ in the bilayer QH system. In this case, the plateau is created because the systems is showing the $\nu = 1$ bilayer QH effect. These experimental facts support the correctness of

the formula for the Hall current for each layer (5.78). Furthermore the experimental results Fig. 2.8 show clearly that the bilayer QH effects are realized by electrons with the pseudospin degree of freedom as if it were the monolayer QH effects. This is because the Hall resistivity $R_{\rm K}/\nu$ of the bilayer system remains invariant under the change of the imbalance parameter σ_0. The plateau is created under the change of σ_0 for $\nu = 1 \pm \delta$ and $2 \pm \delta$. In such situations, the imbalance parameter is changed by the bias voltage with the total filling factor ν being fixed.

Although the calculations including the impurity potential is beyond the scope of our analysis, we may expect that the QH effects in the presence of the interlayer phase coherence in the CAF phase, which are analyzed based on the current formulas (5.79) and (5.80), are realized even if there are impurities. When the interlayer phase coherence is realized by the interlayer exchange Coulomb interaction between electrons in the extended states, then we may expect that the Josephson supercurrent (5.76) is induced with its present form remained unchanged. With the same reason the spin Josephson supercurrent is expected to be realized even if there are impurities. Indeed at $\nu = 1$, the theoretical results of the Hall resistance in Eqs. (3.46), (3.47), and (3.48), match with the experimental results Figs. 1.2-1.5, where the plateaus are formed.

In the monolayer case, there is no contribution to the current from the exchange term $H_{\rm X}^{\rm cl}$ as we have discussed before. On the other hand, in the bilayer systems, the contribution from the exchange term $H_{\rm X}^{\rm cl}$ arises from the interlayer exchange potential $V_{\rm X}^{d}$ in the bilayer systems. Indeed, the Josephson supercurrent has J_s^d dependency, carried by the interlayer phase field $\vartheta(\boldsymbol{x})$. The development of the interlayer phase coherence and the associated Josephson supercurrent are among the most peculiar phenomena in the bilayer QH systems, in contrast to the monolayer systems.

5.3 Quantum Hall Effects in the CAF phase

We consider the case where the current $\mathcal{J}_{\rm in}$ is applied into the x direction and the system being homogeneous in the y direction. By applying the same argument given in section 3.4, we show the anomalous Hall resistance behavior affected by the phase coherence in the CAF phase. The total current for each layer is

$$\mathcal{J}_x^{\rm f}(x) = \frac{\nu}{R_{\rm K}}\frac{\rho_0^{\rm f}}{\rho_0}E_y + \mathcal{J}_x^{\rm Jos}, \quad \mathcal{J}_x^{\rm b}(x) = \frac{\nu}{R_{\rm K}}\frac{\rho_0^{\rm b}}{\rho_0}E_y - \mathcal{J}_x^{\rm Jos}, \tag{5.84}$$

which are given by the sum of the Hall current and the Josephson current. Here we have used the condition (5.34).

We analyze the behavior of Hall resistance in the standard, counterflow and drag geometries without tunneling by using (5.84).

First for the standard geometry, by using (5.84) with the condition $\mathcal{J}_x^{\rm f} = \mathcal{J}_x^{\rm b} = \mathcal{J}_{\rm in}$, we have

$$R_{\rm Hall}^{\rm f} \equiv \left|\frac{E_y^{\rm f}}{\mathcal{J}_x^{\rm f}}\right| = R_{\rm Hall}^{\rm b} \equiv \left|\frac{E_y^{\rm b}}{\mathcal{J}_x^{\rm b}}\right| = R_{\rm K}. \tag{5.85}$$

The Josephson supercurrent flows as

$$\mathcal{J}_x^{\rm Jos} = -\sigma_0 \mathcal{J}_{\rm in}, \tag{5.86}$$

in the imbalanced configuration.

For the counterflow geometry, with the same argument given in 3.4 we have

$$R_{\rm Hall}^{\rm f} \equiv \left| \frac{E_y^{\rm f}}{\mathcal{J}_x^{\rm f}} \right| = 0, \qquad R_{\rm Hall}^{\rm b} \equiv \left| \frac{E_y^{\rm b}}{\mathcal{J}_x^{\rm b}} \right| = 0, \tag{5.87}$$

and therefore, implying that all the input current is the Josephson supercurrent,

$$\mathcal{J}_x^{\rm Jos} = \mathcal{J}_{\rm in}, \tag{5.88}$$

with generating an inhomogeneous phase field $\vartheta(\boldsymbol{x}) = -(\hbar/eJ_\vartheta)\mathcal{J}_{\rm in}x$.

In the drag geometry, we have $\mathcal{J}_{\rm in} = \mathcal{J}_x^{\rm f} = (\nu/R_{\rm K})E_y$, or

$$R_{\rm Hall}^{\rm f} \equiv \left| \frac{E_y^{\rm f}}{\mathcal{J}_x^{\rm f}} \right| = \frac{R_{\rm K}}{\nu} = \frac{1}{2}R_{\rm K} \qquad \text{at} \quad \nu = 2. \tag{5.89}$$

In this case, the input current is partially carried by the Josephson supercurrent

$$\mathcal{J}_x^{\rm Jos} = \frac{1}{2}(1-\sigma_0)\mathcal{J}_{\rm in}. \tag{5.90}$$

In conclusion, we predict the anomalous Hall resistance (5.87) and (5.89) in the CAF phase at $\nu = 2$ in the counterflow and drag geometries due to Kellogg *et al.* and Tutuc *et al* [74, 75, 76], in imbalanced configuration ($\sigma_0 \neq 0$).

5.4 Spin Josephson Supercurrent in the CAF phase

An intriguing feature of the CAF phase is that the phase field $\vartheta(\boldsymbol{x})$ describes the entangled spin-pseudospin coherence according to the basic formula (5.7).

The spin density in each layer is defined as $\rho_\alpha^{\rm spin}(\boldsymbol{x}) \equiv s_\alpha \psi_\alpha^\dagger \psi_\alpha$, where $s_\alpha = \frac{1}{2}\hbar$ for $\alpha = {\rm f}\uparrow, {\rm b}\uparrow$ and $s_\alpha = -\frac{1}{2}\hbar$ for $\alpha = {\rm f}\downarrow, {\rm b}\downarrow$. By using the formula

$$\begin{pmatrix} \rho_{{\rm f}\uparrow}(\boldsymbol{x}) \\ \rho_{{\rm f}\downarrow}(\boldsymbol{x}) \\ \rho_{{\rm b}\uparrow}(\boldsymbol{x}) \\ \rho_{{\rm b}\downarrow}(\boldsymbol{x}) \end{pmatrix} = \frac{1}{4} \begin{pmatrix} 1 & 1 & 1 & 1 \\ 1 & -1 & 1 & -1 \\ 1 & 1 & -1 & -1 \\ 1 & -1 & -1 & 1 \end{pmatrix} \begin{pmatrix} \rho_0 \\ 2S_z(\boldsymbol{x}) \\ 2P_z(\boldsymbol{x}) \\ 2R_{zz}(\boldsymbol{x}) \end{pmatrix}, \tag{5.91}$$

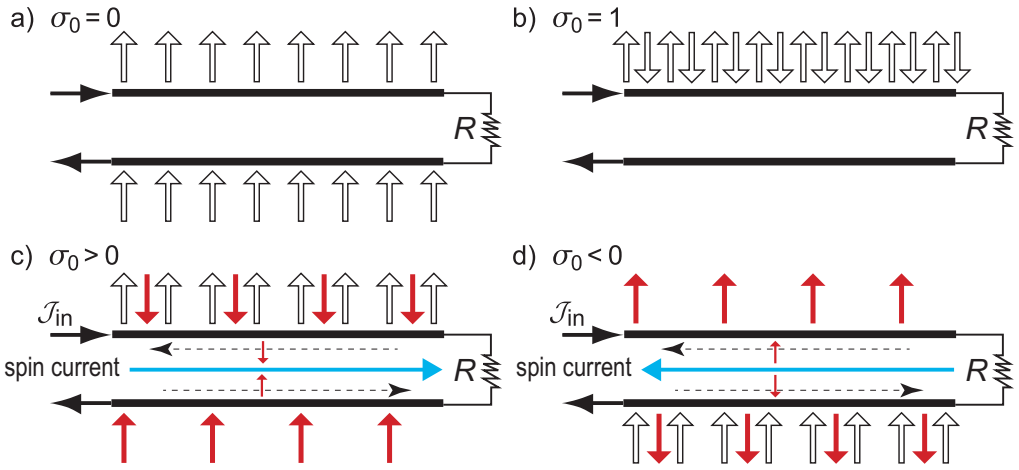

Fig. 5.2 Schematic illustration of the spin supercurrent flowing along the x-axis in the counterflow geometry. (a) All spins are polarized into the positive z axis due to the Zeeman effect at $\sigma_0 = 0$. No spin current flows. (b) All electrons belong to the front layer at $\sigma_0 = 1$. No spin current flows. (c) In the CAF phase for $\sigma_0 > 0$, some up-spin electrons are moved from the back layer to the front layer by flipping spins. There appears a NG mode associated with this charge-spin transfer. The interlayer phase difference $\vartheta(\boldsymbol{x})$ is created by feeding a charge current $\mathcal{J}_{\rm in}$ to the front layer, which also drives the spin current. Electrons flow in each layer as indicated by the dotted horizontal arrows, and the spin current flows as indicated by the solid horizontal arrow. (d) In the CAF phase for $\sigma_0 < 0$, similar phenomena occur but the direction of the spin current becomes opposite. This picture is taken from[110].

up to $\mathcal{O}((\sigma - \sigma_0)^2)$, we have $\mathcal{S}_z = 1 - |\sigma(\boldsymbol{x})|$, and we obtain

$$\partial_t \rho^{\rm spin}_{\rm b\uparrow} = \partial_t \rho^{\rm spin}_{\rm f\downarrow} = \frac{J_\vartheta}{4}[1 + {\rm sgn}(\sigma_0)]\partial_x^2 \vartheta(\boldsymbol{x}), \tag{5.92}$$

$$\partial_t \rho^{\rm spin}_{\rm f\uparrow} = \partial_t \rho^{\rm spin}_{\rm b\downarrow} = -\frac{J_\vartheta}{4}[1 - {\rm sgn}(\sigma_0)]\partial_x^2 \vartheta(\boldsymbol{x}). \tag{5.93}$$

From the continuity equation for the spin density, $\partial_t \rho^{\rm spin}_\alpha(\boldsymbol{x}) = -\partial_x \mathcal{J}^{\rm spin}_\alpha(\boldsymbol{x})$, for each α, we have

$$\mathcal{J}^{\rm spin}_{\rm b\uparrow}(\boldsymbol{x}) = \mathcal{J}^{\rm spin}_{\rm f\downarrow}(\boldsymbol{x}) = -\frac{J_\vartheta}{2}\partial_x \vartheta(\boldsymbol{x}), \quad \text{for } \sigma_0 > 0, \tag{5.94}$$

$$\mathcal{J}^{\rm spin}_{\rm f\uparrow}(\boldsymbol{x}) = \mathcal{J}^{\rm spin}_{\rm b\downarrow}(\boldsymbol{x}) = \frac{J_\vartheta}{2}\partial_x \vartheta(\boldsymbol{x}), \quad \text{for } \sigma_0 < 0. \tag{5.95}$$

The spin current $\mathcal{J}^{\rm spin}_\alpha(\boldsymbol{x})$ flows in order to decrease the inhomogeneity of the phase difference $\vartheta(\boldsymbol{x})$ along the the x-axis.

In the counterflow experiment, the total charge current along the x-axis is zero, $\mathcal{J}^{\rm f}_x(\boldsymbol{x}) + \mathcal{J}^{\rm b}_x(\boldsymbol{x}) = 0$. Consequently, the input current generates a pure spin current along the x-axis,

$$\mathcal{J}^{\rm spin}_x = \mathcal{J}^{\rm spin}_{\rm f\uparrow} + \mathcal{J}^{\rm spin}_{\rm f\downarrow} + \mathcal{J}^{\rm spin}_{\rm b\uparrow} + \mathcal{J}^{\rm spin}_{\rm b\downarrow} = {\rm sgn}(\sigma_0)\frac{\hbar}{e}\mathcal{J}_{\rm in}. \tag{5.96}$$

This current is dissipationless since the dispersion relation is linear. It is appropriate to call it

a *spin Josephson supercurrent*. It should be noted that the spin current flows in the opposite directions for $\sigma_0 > 0$ and $\sigma_0 < 0$, as illustrated in Fig. 5.2. Comment is in order: The spin current only flows within the sample, since spins are scattered in the resistor R and spin directions become random outside the sample.

System	QH current	Josephson supercurrent	Spin Josephson supercurrent
Spin phase ($\nu = 2$)	Yes	No	No
Pseudospin phase ($\nu = 2$)	Yes	No	No
CAF phase ($\nu = 2$)	Yes	Yes	Yes
Bilayer $\nu = 1$	Yes	Yes	No
Monolayer Integer ν	Yes	No	No

Table. 5.1 The currents flowing in various QH systems are shown. We denote "Yes" when the corresponding current exist in the system, where as "No" when the corresponding current does not exist.

System	Standard	Counterflow	Drag
Spin phase ($\nu = 2$)	$R^{\rm f}_{xy} = R^{\rm b}_{xy} = R_{\rm K}$	$R^{\rm f}_{xy} = R^{\rm b}_{xy} = R_{\rm K}$	$R^{\rm f}_{xy} = R^{\rm b}_{xy} = R_{\rm K}$
Pseudospin phase ($\nu = 2$)	$R^{\rm f}_{xy} = \frac{R_{\rm K}}{\nu_{\rm f}},\ R^{\rm f}_{xy} = \frac{R_{\rm K}}{\nu_{\rm b}}$	$R^{\rm f}_{xy} = \frac{R_{\rm K}}{\nu_{\rm f}},\ R^{\rm f}_{xy} = \frac{R_{\rm K}}{\nu_{\rm b}}$	$R^{\rm f}_{xy} = \frac{R_{\rm K}}{\nu_{\rm f}},\ R^{\rm f}_{xy} = \frac{R_{\rm K}}{\nu_{\rm b}}$
CAF phase ($\nu = 2$)	$R^{\rm f}_{xy} = R^{\rm b}_{xy} = R_{\rm K}$	$R^{\rm f}_{xy} = R^{\rm b}_{xy} = 0$	$R^{\rm f}_{xy} = R^{\rm b}_{xy} = R_{\rm K}/2$
Bilayer $\nu = 1$	$R^{\rm f}_{xy} = R^{\rm b}_{xy} = 2R_{\rm K}$	$R^{\rm f}_{xy} = R^{\rm b}_{xy} = 0$	$R^{\rm f}_{xy} = R^{\rm b}_{xy} = R_{\rm K}$

Table. 5.2 The values of Hall resistivity for bilayer systems in different are summarized. Here we defined the Hall resistivity of the layer α (= f,b) as $R^{\alpha}_{xy} \equiv |E^{\alpha}_{y}/\mathcal{J}^{\alpha}_{x}|$ so that the Hall resistivity becomes positive. Here we have defined $\nu_{\rm f} = \nu(1+\sigma_0)/2, \nu_{\rm b} = \nu(1-\sigma_0)/2$ with ν the total filling factor.

5.5 Summary

At the end of this chapter, we summarize the types of currents flowing and the value of Hall resistivity in the $\nu = 2$ bilayer QH systems for each phase, comparing with the ones in the $\nu = 1$ bilayer QH systems and integer monolayer QH systems in Table 5.1 and 5.2.

In the integer monolayer QH systems and the spin and pseudospin phases in the $\nu = 2$ bilayer QH systems, the gapless NG mode does not emerge, and hence, the interlayer phase coherence is not created. Only the Hall current (for spin phase $\sigma_0 = 0$, while for pseudospin phase $0 \leq |\sigma_0| \leq 1$) is flowing. Thus, neither the Josephson supercurrent nor spin Josephson supercurrent flow and the Hall resistivity does not depend on the geometry of current injection shown in Fig. 1.6. On the other hand, in the CAF phase with the interlayer phase coherence, both the Hall current and Josephson supercurrent are flowing. The total current is given by the sum of the Hall current and Josephson supercurrent. The Hall resistivity show various values by changing the geometry such as the counterflow geometry or drag geometry. Although the interlayer phase coherence emerges both in the CAF phase and the $\nu = 1$ bilayer systems, the spin Josephson supercurrent only flows in the CAF phase. This is because only the electron with up spin component becomes the carrier of the Josephson supercurrent, while electrons with both up and down spin components become the carriers of the Josephson supercurrent, reflecting the emergence of the entangled spin-pseudospin phase coherence. The creation of spin Josephson supercurrent plainly reflects the emergence of "entangled spin-pseudospin phase coherence phenomena" in the bilayer QH systems.

At the end of this section, we make a comparison between our theory and the exciton-

condensate description. It is possible that the spin Josephson supercurrent shown in Fig. 5.2 is the excitonic supercurrent, which may be realized by creating the exciton condensate from the spin phase. However, the mechanism of the creation of the exciton condensate and the wave function corresponding to (3.51) in the CAF phase is unclear. Indeed, the study of the QH effects in the CAF phase due to the exciton-condensate description has not been done yet. At this stage, it is difficult to make the quantitative comparison between the exciton-condensate description and our theory.

On the other hand, the effective theory of the NG mode with linear dispersion enables us to describe quantitatively and clearly the creation of the interlayer phase coherence and the associated QH effects in the CAF phase, as done for $\nu = 1$ in chapter 3 or in Refs. [78, 79]. Concretely, we have first analyzed the dispersion relations for NG modes in all three phases. We have found that one linear mode emerges in the CAF phase at $\Delta_{\rm SAS} \to 0$, describing the realization of the interlayer phase coherence in the CAF phase, the entangled spin-pseudospin phase coherence. Then by constructing the effective theory of this NG mode in terms of the fields σ and ϑ, we have calculated the values of the Josephson supercurrents given by (5.88) and (5.90), the Hall current for each layer, and the Hall resistance for each layer in various geometry. Quantitatively, we obtain the values of the Hall resistances in the front and back layers in the drag geometry, $R^{\rm f}_{xy} = R^{\rm b}_{xy} = R_{\rm K}/2$. In this way, we can also make a comparison between the interlayer phase coherence and the associated QH effects in the CAF phase and that at $\nu = 1$. It enables us to understand uniformly the physics of interlayer phase coherence in the integer bilayer QH systems. Moreover, the effective theory based on the NG mode is also valid from the experimental points of view, since the existence of the NG mode has been studied experimentally by measuring the nuclear spin relaxation with the RD-NMR [105, 106, 107, 125].

Consequently, we have derived the new phenomena in the CAF phase, the entangled spin-pseudospin phase coherence, the QH effects in the presence of the entangled spin-pseudospin phase coherence shown in Table 5.2, and the spin Josephson supercurrent. All these phenomena are realized at $\sigma_0 \neq 0$ ($0 < |\sigma_0| < 1$), and therefore, have not been observed yet from the experimental results shown in Figs. 1.2-1.4, which are results at $\sigma_0 = 0$.

Chapter 6

Summary and Conclusion

In this thesis we have investigated the Nambu-Goldstone (NG) spectrum and the Josephson supercurrent in $\nu = 1, 2$ bilayer quantum Hall (QH) systems in order to study the entangled spin-pseudospin phenomena in the bilayer QH systems.

After the introduction in chapter 1, we have summarized the QH effect in both monolayer and bilayer systems in chapter 2, and the Landau-level projection formalism and derivation of SU(4) effective Hamiltonian.

In chapter 3, we have presented the effective Hamiltonian for the NG modes and their spectrum; the dispersion relations and coherence length for $\nu = 1$. Then we investigated the interlayer phase coherence, the associated Josephson current, and its effect on the Hall resistivity in counterflow and drag geometries.

For $\nu = 1$, the ground state is the bonding state with up-spin and six NG modes emerge. We have derived the effective Hamiltonian, the dispersion relations and coherence length for the NG modes with both the Grassmaniann formalism and the SU(4) nonlinear representation. We have seen that the pseudospin wave shows the linear dispersion in the limit $\Delta_{\rm SAS} \to 0$.

We then have studied the interlayer coherence induced by the above pseudospin wave with the Grassmannian formalism, since it shows a clear physical picture of the spontaneous development of an interlayer phase coherence. It is to be emphasized that the Grassmannian formalism enables us to analyze the nonperturbative phase coherent phenomena such as the Josephson supercurrent. It has been argued [59] that the interlayer coherence is due to the Bose-Einstein condensation of composite bosons, which are single electrons bound to magnetic flux quanta. Such composite bosons are described by the complex projective (CP^3) fields which are directly related to the Grassmannian field in this thesis. For $\nu = 1$, the interlayer phase coherence is developed spontaneously due to the $U_{T_{0z}}(1)$ symmetry breaking . It is described in terms of the density difference field $\sigma(\boldsymbol{x})$ and its conjugate field $\vartheta(\mathbf{x})$. Driven by the Josephson supercurrent, the Hall resistivity show the anomalous behavior; the Hall resistivity vanishes in the counterflow geometry, whereas in the drag geometry, the Hall resistivity becomes $R^{\rm f}_{\rm Hall} = R_{\rm K} \neq R_{\rm K}/2$. This is different from the one in the standard geometry. Our theoretical results were consistent with the experimental ones obtained in [74, 75, 76, 77].

In chapter 4, we have presented the effective Hamiltonian, the dispersion relations and coherence length for the NG modes in all the three phases; the spin phase, the pseudospin phase, and the CAF phase, for $\nu = 2$. Then in chapter 5, we investigated the entangled spin-pseudospin

phase coherence, the associated Josephson current, and its effect on the Hall resistivity in the canted antiferromagnetic (CAF) phase. Moreover, we have shown that Josephson supercurrent carries solely spins without dissipation flows in the counterflow geometry.

In the spin phase, the spins in both layers are pointing to the positive z axis by the Zeeman effect, whereas the pseudospins are polarized in the pseudospin phase. In the CAF phase, not only the spin and pseudospin but also the R-spins become polarized. Thus, the spins are canted coherently, and the spins in each layer make the ferromagnetic correlations while the spins between the layers make the antiferromagnetic correlations, described by Eq. (4.21). This phase is the most interesting in $\nu = 2$ bilayer QH systems. We have next analyzed the SU(4) symmetry breaking pattern, the effective Hamiltonian for the accociated NG modes, the dispersions, and coherence lengths for all three phases. In the spin phase, there emerge four complex NG modes, one spin wave and three R-spin wave, while one pseudospin wave and three R-spin wave emerge in the pseudospin wave, and all of them are gapped. As we have seen in chapter 3, the interlayer phase coherence and the Josephson effect are the most intriguing phenomena in the $\nu = 1$ bilayer QH systems. They are enhanced in the limit $\Delta_{\rm SAS} \to 0$. Then it is natural to seek for similar phenomena in the $\nu = 2$ bilayer QH systems. We may naively expect them to occur in the pseudospin phase. However, we have shown that almost all electrons are moved to one of the layers in the above limit. This is not the case in the CAF phase, where the electron densities can be controlled arbitrarily in both layers. In the CAF phase we have investigated the dispersion relations and the coherence length in the limit $\Delta_{\rm SAS} \to 0$. We have found one coherent mode whose coherence length diverges. Furthermore it has the linear dispersion relation, so that it would be responsible to the interlayer phase coherence.

We have then presented an effective theory describing the interlayer coherence in the CAF phase at $\nu = 2$. It is the entangled spin-pseudospin phase coherence, and is governed by the NG mode $\vartheta(\boldsymbol{x})$, describing the R-spin according to the formula (5.7). Moreover, as mentioned in section 5.1, the entangled spin-pseudospin phase coherence reflects the spin $U_{T_{z0}}(1)$ symmetry breaking in the following way. In chapter 5, we have taken the expectation value of the interlayer phase field to be zero. Suppose that the interlayer phase field takes finite ground state-expectation value $\langle\vartheta(\boldsymbol{x})\rangle = \vartheta_0$, for $\sigma(\boldsymbol{x}) > 0$, we obtain from (5.7),

$$\begin{aligned} &\mathcal{S}^0_z = 1 - |\sigma_0|, \quad \mathcal{P}^0_z = \sigma_0, \quad \mathcal{R}^0_{xx} = \mathcal{R}^0_{yy} = -\sqrt{|\sigma_0|(1-|\sigma_0|)}\cos\vartheta_0, \\ &\mathcal{R}^0_{yx} = -\mathcal{R}^0_{xy} = -\sqrt{|\sigma_0|(1-|\sigma_0|)}\sin\vartheta_0, \end{aligned} \tag{6.1}$$

while from (4.13), the SU(4) order parameters in $\Delta_{\rm SAS} \to 0$ are

$$\begin{aligned} &\mathcal{S}^0_z = 1 - |\sigma_0|, \quad \mathcal{P}^0_z = \sigma_0, \quad \mathcal{R}^0_{xx} = \mathcal{R}^0_{yy} = -\sqrt{|\sigma_0|(1-|\sigma_0|)}\cos\omega, \\ &\mathcal{R}^0_{yx} = -\mathcal{R}^0_{xy} = -\sqrt{|\sigma_0|(1-|\sigma_0|)}\sin\omega. \end{aligned} \tag{6.2}$$

Thus, we can identify the angle ϑ_0 with ω, describing the orientation angle for in-plane spin component. On the other hand the Hamiltonian (2.141) is invariant under the spin transfor-

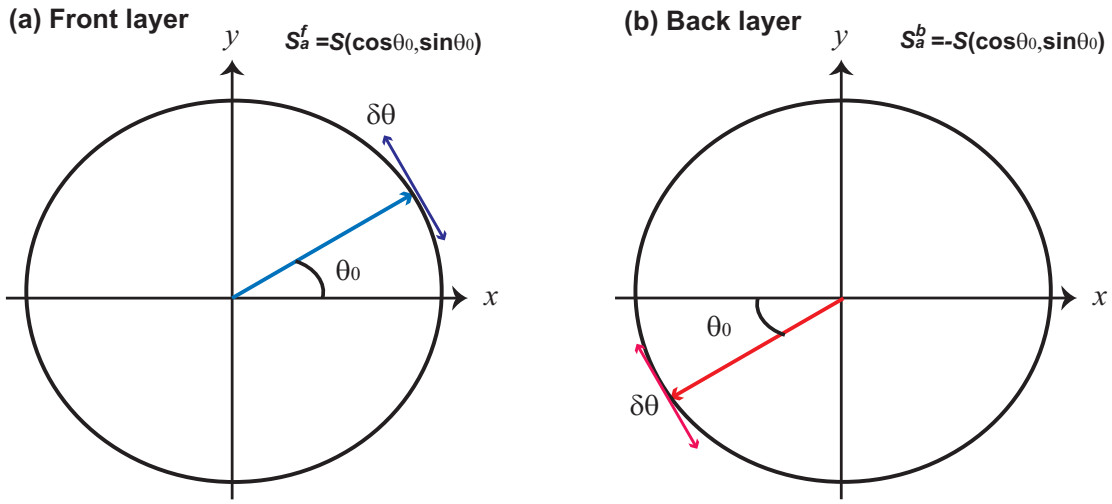

Fig. 6.1 The schematic illustration of the in-plane spin component in the CAF phase in terms of ϑ_0, corresponding to Fig. 4.3 . We can identify $\langle\vartheta(\boldsymbol{x})\rangle = \mathrm{sgn}(\sigma_0)\vartheta_0$ as a orientation angle ω, and the NG mode $\delta\vartheta(\boldsymbol{x})$ describes the fluctuation of the orientation angle. It reflects the U(1) spin rotational symmetry breaking generated by T_{z0}.

mation $\exp(-iT_{z0}\omega)$, implying that the ground state does not depend on the orientation of in-plane spin component. Consequently, we can interpret the fluctuation mode $\delta\vartheta(\boldsymbol{x}) = \vartheta(\boldsymbol{x}) - \vartheta_0$ as the fluctuation of in-plane spin orientation angle. Indeed, as shown in Fig. 6.1, the NG mode $\delta\vartheta(\boldsymbol{x})$ and the associated entangled spin-pseudospin phase coherence reflect the $U_{T_{z0}}(1)$ rotational symmetry breaking. The similar analysis can be done for $\sigma(\boldsymbol{x}) < 0$, by identifying $\langle\vartheta(\boldsymbol{x})\rangle$ with $-\omega$.

Recently, the nuclear spin relaxation in $\nu = 2$ bilayer QH systems using the resistivity -detected nuclear magnetic resonance has been experimentaly studied [107, 125]. In this experiment, the nuclear spin relaxation in the CAF phase shows the fastest relaxation rate, compared to the ones in other two phases. Since the NG mode in the CAF phase has linear dispersion, there is a possibility that nuclear spins may couple to the NG mode in the CAF phase, although nuclear spin has low-Larmor frequency in the order of MHz per Tesla. In fact, this NG mode describing the fluctuation of in-plane spin component may couple to nuclear spins through the flip-flop interaction of s-wave type hyperfine interaction $A(I^+S- + I^-S-)$, where A, I, and S denote the hyperfine coupling, the nuclear spin, and the electron spin, respectively. Such a coupling would drive the nuclear spin relaxation. Thus, we may consider such nuclear spin relaxation as a hall mark for the existence of NG mode.

We have predicted the anomalous Hall resistivity in the counterflow and drag experiments in the CAF phase. We have shown that they exhibit precisely the same behavior as the ones for $\nu = 1$. The difference between them is that the supercurrent flows both in the balanced and imbalanced systems at $\nu = 1$ but only in imbalanced systems in the CAF phase. Furthermore, the spin Josephson supercurrent appears in the CAF phase in the counterflow geometry, but not for $\nu = 1$. In other words, the net spin current is nonzero for the CAF phase, while it is zero for $\nu = 1$. This is due to the fact that the spins are canted coherently and making

antiferromagnetic correlations between the two layers at $\nu = 2$, while the spin is actually frozen and therefore all of the spins are pointing to the positive z axis in both layers at $\nu = 1$ in the limit $\Delta_{\rm SAS} \to 0$.

In this thesis we analyzed the interlayer coherence and the associated Josephson supercurrent in the Hall bar geometry. Related to this works, recently, there are research for the detection of the interlayer phase coherence and supercurrent in the bilayer QH systems using the Corbino genometry, which has been proposed theoretically [135] and has been conducted experimentally [69, 136, 137, 138, 139]. Theory of bilayer QH systems in the Corbino geometry would be one of the next steps to generalize the works presented in this thesis.

In conclusion, we showed that the entangled spin-pseudospin phenomena are realized in the CAF phase. It is triggered by the NG mode as a SU(4) R-spin wave. The most interesting phenomenon is the emergence of the spin Josephson supercurrent, where spins are transported without dissipation. We hope that our predictions on the spin Josephson supercurrent can be tested experimentally in the future. As we have seen, physics of entangled spin-pseudospin is extremely rich and shows intriguing phenomena due to the coupling (or entangling) of the spin and pseudospin degrees of freedom. Entangled spin-pseudospin behaves as a new degree of freedom, which is totally different from spin or pseudospin.

Throughout this thesis, we have studied the entangled spin-pseudospin phenomena driven by the symmetry breaking and the associated NG mode. It may be very interesting to analyze the the entangled spin-pseudospin phenomena from the topological points of view, for instance, the entangled spin-pseudospin phenomena induced by the skyrmions and the associated transport phenomena. We expect that our investigation can be extended to other many-body systems possessing spin and pseudospin, such as graphene, magnets, ultracold atomic systems, quantum spin Hall systems, and so on. Furthermore, we expect that the entangled spin-pseudospin phenomena can be applied to establish new type of engineering and quantum computation, which may be called *spin-pseudospintronics*.

Acknowledgments

I would like to express my deepest gratitude to my supervisor, Prof. Tetsuo Hatsuda, for carefully reading the manuscript of this thesis, fruitful discussions, and helpful encouragements on all the things during my graduate-school life. I learned from Dr. Yoshimasa Hidaka, the physics of spontaneous symmetry breaking and techniques for the effective theory for Nambu-Goldstone modes and usage of Mathematica. I appreciate Prof. George Tsitsishvili for helped and supported me with my calculation for the investigation for Nambu-Goldstone mode in bilayer QH system. I really appreciate Prof. Zyun F. Ezawa for giving me an opportunity to do the research of bilayer quantum Hall system. I have learned from him the physics of bilayer QH system, as well as how to write the research paper, and the importance of the comparison between the theory and experiment, when doing the research of physics. I really appreciate Prof. Naoto Nagaosa for giving me a chance to have a fruitful discussion and very valuable advice about my research.

I would also like to appreciate Prof. Yoshiro Hirayama, Dr. M. H. Fauzi, Prof. Shuichi Murakami, Dr. Minoru Kawamura, Prof. Kae Nemoto, Dr. Norio Kumada, Dr. Kouji Muraki, Prof. Katsushi Hashimoto, Dr. Akira Furusaki, Prof. Takeo Kato, Mr. Kazuhiro Watanabe, Dr. Yasufumi Araki, Prof. Kei Iida, Prof. Yuki Kawaguchi, Mr. Taro Kanao, Mr. Takahiro Mikami, Mr. Takehiro yamaguchi, Miss. Miho Arai, Dr. Kazunori Itakura, Mr. Shinpei Endo, Mr. Arakawa Naoya, Dr. Tomoki Ozawa, Dr. Takahiro Morimoto, Prof. Shoichi Sasaki, Dr. Bohm-Jung Yang, Dr. Aron Beekman, and Dr. Wataru Koshibae for fruitful discussions and comments on my research.

I also would like to thank all my colleagues in Theoretical Hadron Physics group at the University of Tokyo and Quantum Hadron Groups in RIKEN.

I have really enjoyed my research life for five years in University of Tokyo, and for two years in RIKEN. My research life during the five-years Ph. D. course was, though I sometimes felt difficulties, it was really fascinating, challenging and exciting one.

Finally, I would like to express my heartfelt appreciation to my family and deceased grandfather, for the physical, financial and mental support, and really encouraged me on working on the research.

All my research was supported in part by JSPS Research Fellowships for Young Scientists and Global COE Program "the Physical Sciences Frontier", MEXT, Japan.

Appendix A

A.1 Physical Quantities in Quantum Hall Systems

In this appendix we list the basic physical quantities and their numerical quantities in QH systems [54, 57, 58, 59]. We adopt the MKSA unit. The physical constants used in this thesis are

$$\begin{aligned}
&\text{elementary charge}: \quad e = 1.60217657 \times 10^{-19}\ [\mathrm{C}],\\
&\text{the background dielectric constant}: \quad \epsilon_0 \approx 8.8542 \times 10^{-12}\left[\mathrm{C}^2/\mathrm{N}\cdot\mathrm{m}^2\right],\\
&\text{Plank's constant}: \quad \hbar = 1.05457 \times 10^{-34}[\mathrm{J}\cdot\mathrm{sec}],\\
&\text{Boltzmann constant}: \quad k_{\mathrm{B}} = 1.3806 \times 10^{-23}\,[\mathrm{J/K}],\\
&\text{Effective mass of electron in GaAs}: \quad M \simeq 0.067 \times 9.10930291 \times 10^{-31}[\mathrm{kg}].
\end{aligned} \tag{A.1}$$

In the QH systems, the magnetic field is applied in the order of Tesla. The physical quantities are described by the units of magnetic length and associated Coulomb energy. They are given by

$$l_B = \sqrt{\frac{\hbar}{eB_\perp}} \approx \frac{257}{\sqrt{B_\perp(\mathrm{T})}}\ [\mathring{A}], \tag{A.2}$$

$$E_{\mathrm{C}}^0 \approx 50.5\sqrt{B_\perp(\mathrm{T})}\ [\mathrm{K}]. \tag{A.3}$$

In the QH systems, we take E_{C}^0 and l_B as the energy and length unit, respectively. The physical quantities having the dimension of energy or length is described based on E_{C}^0 or l_B. For instance, the numerical constant ϵ_{X} is given by (B.52), or

$$\epsilon_{\mathrm{X}} = \frac{1}{2}\sqrt{\frac{\pi}{2}}E_{\mathrm{C}}^0 \approx 31.6\sqrt{B_\perp(\mathrm{T})}\ [\mathrm{K}], \tag{A.4}$$

and correspondingly, the spin stiffness is

$$J_s = \frac{1}{16\sqrt{2\pi}}E_{\mathrm{C}}^0 \approx 1.26\sqrt{B_\perp(\mathrm{T})}\ [\mathrm{K}]. \tag{A.5}$$

The magnetic length and the associated Coulomb energy can also be expressed in terms of

the filling factor ν as

$$l_B = \sqrt{\frac{\nu}{2\pi\rho_0}}\ [\mathring{A}], \tag{A.6}$$

$$E_{\rm C}^0 = \frac{e^2}{4\pi\epsilon}\sqrt{\frac{2\pi\rho_0}{\nu}}\ [\rm K], \tag{A.7}$$

where $\rho_0 = n \times 10^{15}[\rm m^{-2}]$ is the total electron density of the system. By combining (A.2) and (A.6), we obtain

$$B_\perp = \frac{h\rho_0}{e\nu}. \tag{A.8}$$

In order to realize the filling factor ν QH state with the total electron density fixed by ρ_0 experimentally, we applied constant magnetic field $B_\perp$ following (A.8).

The basic quantities of energy due to the magnetic field are the cyclotron (or the energy gap between two Landau levels) and Zeeman energy,

$$\hbar\omega_{\rm c} = \frac{\hbar e B_\perp}{M} \approx 20.0 B_\perp({\rm T})\ [\rm K], \qquad \Delta_{\rm Z} \equiv |g^*\mu_{\rm B}B_\perp| \approx 0.296 B({\rm T})\ [\rm K], \tag{A.9}$$

where $g^* \approx -0.44$ is the g-factor in a GaAs semiconductor, and $\mu_{\rm B} \approx 9.274 \times 10^{-24}$ [J/T] the Bohr magneton. Since the g-factor in a GaAs semiconductor is very small compared to that in the vacuum ($= 2$), the Zeeman energy in a GaAs semiconductor is extensively small compared to the cyclotron energy, $\Delta_{\rm Z} \approx \hbar\omega_{\rm c}/66$.

In the bilayer QH systems, besides the Zeeman energy, the tunneling energy also arises, which is the energy gap between symmetric and antisymmetric state. The typical values are

$$\Delta_{\rm SAS} \approx 1 \sim 10\ [\rm K]. \tag{A.10}$$

It is comparable with the Zeeman energy. There exist bilayer QH samples having enormously small tunneling gap, for example, $\Delta_{\rm SAS} \approx 0.1$mK [74].

A.2 Wave Functions for the Landau Levels in the Symmetric Gauge

In this section, we construct the wave function for the Landau state (2.37) by taking the gauge potential so called the *symmetric gauge* [54, 57, 58, 59, 61]. In this gauge, the vector potential is described as

$$A_x = \frac{B_\perp y}{2}, \quad A_y = -\frac{B_\perp x}{2}, \tag{A.11}$$

and correspondingly, the covariant momentum and the guiding center in the symmetric gauge (A.11) are described as

$$\Pi_x = -i\hbar\frac{\partial}{\partial x} + \frac{\hbar}{2l_B^2}y, \quad \Pi_y = -i\hbar\frac{\partial}{\partial y} - \frac{\hbar}{2l_B^2}x, \tag{A.12}$$

$$X = \frac{x}{2} - il_B^2\frac{\partial}{\partial y}, \quad Y = \frac{y}{2} + il_B^2\frac{\partial}{\partial x}. \tag{A.13}$$

Here we consider the case where the constant magnetic field is only applied in the z direction. Then the z component of the angular-momentum is conserved, $[H_{\rm K}, L_z] = 0$, and therefore, it is convenient to take a gauge potential so that the Landau site n in (2.37) can be identified with the magnetic quantum number. To see this explicitly, we rewrite the angular-momentum operator L_z in terms of the harmonic oscillator operators b and $b^\dagger$ in (2.35), which becomes

$$L_z = xp_y - yp_x = \frac{eB_\perp}{2}(X^2 + Y^2) - \frac{1}{2eB_\perp}(P_x^2 + P_y^2) = (b^\dagger b - a^\dagger a)\hbar, \tag{A.14}$$

From (A.14), we see that the diagonalizing L_z is equivalent to diagonalizing both $H_{\rm K}$ ($\sim a^\dagger a$) and $X^2 + Y^2 (\sim b^\dagger b)$. The state $|N, n\rangle$ can be identified as a simultaneous eigenfunctions for $H_{\rm K}$ and L_z. By operating the angular-momentum (A.14) to the state (2.37), we obtain

$$L_z|N, n\rangle = (b^\dagger b - a^\dagger a)\hbar|N, n\rangle = (n - N)\hbar|N, n\rangle. \tag{A.15}$$

We see that the state $|N, n\rangle$ has the angular momentum $(n - N)\hbar$, and b and $b^\dagger$ become the raising and lowering operator for the angular momentum. We now construct the wave function of the state $|N, n\rangle$. To do this, it is convenient to express the coordinate of electrons in terms of the complex number z, described as

$$z = \frac{1}{2l_B}(x + iy), \quad z^* = \frac{1}{2l_B}(x - iy). \tag{A.16}$$

Simultaneously, the harmonic oscillator operators $a, a^\dagger$ and $b, b^\dagger$ in (2.34) and (2.35), respec-

tively, are described in terms of z and z^* as

$$a = -\frac{i}{\sqrt{2}}\left(z + \frac{\partial}{\partial z^*}\right), \quad a^\dagger = \frac{i}{\sqrt{2}}\left(z^* - \frac{\partial}{\partial z}\right), \tag{A.17}$$

$$b = \frac{1}{\sqrt{2}}\left(z^* + \frac{\partial}{\partial z}\right), \quad b^\dagger = \frac{1}{\sqrt{2}}\left(z - \frac{\partial}{\partial z^*}\right). \tag{A.18}$$

We first consider the wave functions for the lowest Landau level state $|0,0\rangle$, and write it as $\langle \boldsymbol{x}|0,0\rangle = \chi^{\rm sym}_{0,0}(\boldsymbol{x})$. Since the lowest Landau level state $|0,0\rangle$ satisfies the condition $a|0,0\rangle = b|0,0\rangle = 0$, we have

$$\begin{aligned}\langle \boldsymbol{x}|a|0,0\rangle &= a(\boldsymbol{x})\langle \boldsymbol{x}|0,0\rangle = -\frac{i}{\sqrt{2}}\left(z + \frac{\partial}{\partial z^*}\right)\chi^{\rm sym}_{0,0}(\boldsymbol{x}) = 0,\\ \langle \boldsymbol{x}|b|0,0\rangle &= b(\boldsymbol{x})\langle \boldsymbol{x}|0,0\rangle = \frac{1}{\sqrt{2}}\left(z^* + \frac{\partial}{\partial z}\right)\chi^{\rm sym}_{0,0}(\boldsymbol{x}) = 0,\end{aligned} \tag{A.19}$$

The solution for Eq. (A.19) becomes

$$\chi^{\rm sym}_{0,0}(\boldsymbol{x}) = \frac{1}{\sqrt{2\pi l_B^2}} e^{-|z|^2} = \frac{1}{\sqrt{2\pi l_B^2}} \exp\left(-\frac{r^2}{4l_B^2}\right). \tag{A.20}$$

Subsequently, the wave function for the state $|0,n\rangle$ can be easily obtained from $\chi^{\rm sym}_{0,0}(\boldsymbol{x})$ as

$$\chi^{\rm sym}_{0,n}(\boldsymbol{x}) = \langle \boldsymbol{x}|0,n\rangle = \sqrt{\frac{1}{n!}}(b^\dagger)^n \chi^{\rm sym}_{0,0}(\boldsymbol{x}) = \sqrt{\frac{2^n}{2\pi l_B^2 n!}} z^n e^{-|z|^2}, \tag{A.21}$$

and obeys the orthonormality condition

$$\langle 0,n|0,m\rangle = \int d^2x \langle 0,n|\boldsymbol{x}\rangle\langle \boldsymbol{x}|0,m\rangle = \int d^2x \chi^{\rm sym*}_{0,n}(\boldsymbol{x})\chi^{\rm sym}_{0,m}(\boldsymbol{x}) = \delta_{nm}. \tag{A.22}$$

From (A.21), the probability of electron in the state $|0,n\rangle$ is

$$|\chi^{\rm sym}_{0,n}(\boldsymbol{x})|^2 = \frac{2^n}{2\pi l_B^2 n!}|z|^{2n} e^{-2|z|^2} \propto r^{2n} \exp\left(-\frac{r^2}{2l_B^2}\right), \tag{A.23}$$

and we see that it becomes maximum at $r = r_n = \sqrt{2n} l_B$. The electrons in the state $|0,n\rangle$ makes cyclotron motion with the radius l_B, where the center coordinate is on the circumference with radius $r_n = \sqrt{2n} l_B$. The Landau site in the symmetric gauge is represented by the ring, and the nth circle corresponds to the state $|0,n\rangle$, having the momentum $n\hbar$.

For $\nu = 1$, the construction of $N_{\rm e}$ $(= N_\Phi)$-body wave function is straightforward. It is given by the Slater determinant in terms of the one-body wave function (A.21), reading

$$\chi_{N_\mathrm{e}}(\boldsymbol{x}_1,\ldots,\boldsymbol{x}_{N_\mathrm{e}}) = \begin{vmatrix} \chi_1(\boldsymbol{x}_1) & \chi_1(\boldsymbol{x}_2) & \cdots & \chi_1(\boldsymbol{x}_{N_\mathrm{e}}) \\ \chi_2(\boldsymbol{x}_1) & \chi_2(\boldsymbol{x}_2) & \cdots & \chi_2(\boldsymbol{x}_{N_\mathrm{e}}) \\ \vdots & \vdots & \ddots & \vdots \\ \chi_{N_\mathrm{e}}(\boldsymbol{x}_1) & \chi_{N_\mathrm{e}}(\boldsymbol{x}_2) & \cdots & \chi_{N_\mathrm{e}}(\boldsymbol{x}_{N_\mathrm{e}}) \end{vmatrix} = A\prod_{i>j}(z_i - z_j)e^{-\sum_{i=1}^{N_\mathrm{e}}|z_i|^2}, \tag{A.24}$$

where A is the normalization constant. With a same argument, the wave function for a general Landau level state $|N,n\rangle$ is

$$\chi^{\mathrm{sym}}_{N,n}(\boldsymbol{x}) = \langle \boldsymbol{x}|N,n\rangle = \sqrt{\frac{1}{N!n!}}(a^\dagger)^N(b^\dagger)^n\chi^{\mathrm{sym}}_{0,0}(\boldsymbol{x}), \tag{A.25}$$

with using (A.17) and (A.18) for $a, a^\dagger$ and $b, b^\dagger$, respectively.

A.3 Group SU(4)

Group SU(4) consists of 4×4 unitary matrices satisfying the condition $\det U = 1$, where U denotes an arbitrary element of SU(4). It is generated by 15 Hermitian and traceless matrices. One of the representation for SU(4) generators is given by the following matrices λ_a [59, 129],

$$\lambda_1 = \begin{pmatrix} 0 & 1 & 0 & 0 \\ 1 & 0 & 0 & 0 \\ 0 & 0 & 0 & 0 \\ 0 & 0 & 0 & 0 \end{pmatrix}, \ \lambda_2 = \begin{pmatrix} 0 & -i & 0 & 0 \\ i & 0 & 0 & 0 \\ 0 & 0 & 0 & 0 \\ 0 & 0 & 0 & 0 \end{pmatrix}, \ \lambda_3 = \begin{pmatrix} 1 & 0 & 0 & 1 \\ 0 & -1 & 0 & 1 \\ 0 & 0 & 0 & 1 \\ 0 & 0 & 0 & 1 \end{pmatrix},$$

$$\lambda_4 = \begin{pmatrix} 0 & 0 & 1 & 0 \\ 0 & 0 & 0 & 0 \\ 1 & 0 & 0 & 0 \\ 0 & 0 & 0 & 0 \end{pmatrix}, \ \lambda_5 = \begin{pmatrix} 0 & 0 & -i & 0 \\ 0 & 0 & 0 & 0 \\ i & 0 & 0 & 0 \\ 0 & 0 & 0 & 0 \end{pmatrix}, \ \lambda_6 = \begin{pmatrix} 0 & 0 & 0 & 0 \\ 0 & 0 & 1 & 0 \\ 0 & 1 & 0 & 0 \\ 0 & 0 & 0 & 0 \end{pmatrix},$$

$$\lambda_7 = \begin{pmatrix} 0 & 0 & 0 & 0 \\ 0 & 0 & -i & 0 \\ 0 & i & 0 & 0 \\ 0 & 0 & 0 & 0 \end{pmatrix}, \ \lambda_8 = \frac{1}{\sqrt{3}} \begin{pmatrix} 1 & 0 & 0 & 0 \\ 0 & 1 & 0 & 0 \\ 0 & 0 & -2 & 0 \\ 0 & 0 & 0 & 0 \end{pmatrix}, \lambda_9 = \begin{pmatrix} 0 & 0 & 0 & 1 \\ 0 & 0 & 0 & 0 \\ 0 & 0 & 0 & 0 \\ 1 & 0 & 0 & 0 \end{pmatrix},$$

$$\lambda_{10} = \begin{pmatrix} 0 & 0 & 0 & i \\ 0 & 0 & 0 & 0 \\ 0 & 0 & 0 & 0 \\ -i & 0 & 0 & 0 \end{pmatrix}, \ \lambda_{11} = \begin{pmatrix} 0 & 0 & 0 & 0 \\ 0 & 0 & 0 & 1 \\ 0 & 0 & 0 & 0 \\ 0 & 1 & 0 & 0 \end{pmatrix}, \ \lambda_{12} = \begin{pmatrix} 0 & 0 & 0 & 0 \\ 0 & 0 & 0 & i \\ 0 & 0 & 0 & 0 \\ 0 & -i & 0 & 0 \end{pmatrix},$$

$$\lambda_{13} = \begin{pmatrix} 0 & 0 & 0 & 0 \\ 0 & 0 & 0 & 0 \\ 0 & 0 & 0 & 1 \\ 0 & 0 & 1 & 0 \end{pmatrix}, \ \lambda_{14} = \begin{pmatrix} 0 & 0 & 0 & 0 \\ 0 & 0 & 0 & 0 \\ 0 & 0 & 0 & i \\ 0 & 0 & -i & 0 \end{pmatrix}, \ \lambda_{15} = \frac{1}{\sqrt{6}} \begin{pmatrix} 1 & 0 & 0 & 0 \\ 0 & 1 & 0 & 0 \\ 0 & 0 & 1 & 0 \\ 0 & 0 & 0 & -3 \end{pmatrix}. \quad \text{(A.26)}$$

This representation, however, is not convenient for the study of bilayer QH physics, because it is not clear how the operators generated by (A.26) is related to spin or pseudospin operators. Since we describe the electron in the bilayer systems with the four-component electron field as, $\Psi = (\psi^{\mathrm{f}\uparrow}, \psi^{\mathrm{f}\downarrow}, \psi^{\mathrm{b}\uparrow}, \psi^{\mathrm{b}\downarrow})$, we choose the SU(4) generators, where the spin operators are generated by

$$\tau_a^{\mathrm{spin}} = \begin{pmatrix} \tau_a & 0 \\ 0 & \tau_a \end{pmatrix}, \quad \text{(A.27)}$$

where $a = x, y, z$ and τ_a the Pauli matrices. The generators (A.27) satisfy the $\mathrm{SU}_{\mathrm{spin}}(2)$

algebra. On the other hand, generators for pseudospin operators are given by

$$\tau_x^{\rm ppin} = \begin{pmatrix} 0 & \mathbf{1}_2 \\ \mathbf{1}_2 & 0 \end{pmatrix}, \quad \tau_y^{\rm ppin} = \begin{pmatrix} 0 & -i\mathbf{1}_2 \\ i\mathbf{1}_2 & 0 \end{pmatrix},$$
$$\tau_z^{\rm ppin} = \begin{pmatrix} \mathbf{1}_2 & 0 \\ 0 & -\mathbf{1}_2 \end{pmatrix}, \tag{A.28}$$

where $\mathbf{1}_2$ is the unit matrix in two dimensions. (A.28) satisfies the $\mathrm{SU}_{\rm ppin}(2)$ algebra. Nine remaining matrices are given by the products of the spin and pseudospin generators:

$$\tau_a^{\rm spin}\tau_x^{\rm ppin} = \begin{pmatrix} 0 & \tau_a \\ \tau_a & 0 \end{pmatrix}, \quad \tau_a^{\rm spin}\tau_y^{\rm ppin} = \begin{pmatrix} 0 & -i\tau_a \\ i\tau_a & 0 \end{pmatrix},$$
$$\tau_a^{\rm spin}\tau_z^{\rm ppin} = \begin{pmatrix} \tau_a & 0 \\ 0 & -\tau_a \end{pmatrix}. \tag{A.29}$$

They generate the R-spin operators. We see that (A.27)-(A.29) are constructed so that $\mathrm{SU}_{\rm spin}(2) \times \mathrm{SU}_{\rm ppin}(2)$ is embedded into SU(4). Their explicit forms are given by

$$\tau_x^{\rm spin} = \begin{pmatrix} 0 & 1 & 0 & 0 \\ 1 & 0 & 0 & 0 \\ 0 & 0 & 0 & 1 \\ 0 & 0 & 1 & 0 \end{pmatrix}, \ \tau_y^{\rm spin} = \begin{pmatrix} 0 & -i & 0 & 0 \\ i & 0 & 0 & 0 \\ 0 & 0 & 0 & -i \\ 0 & 0 & i & 0 \end{pmatrix}, \ \tau_z^{\rm spin} = \begin{pmatrix} 1 & 0 & 0 & 0 \\ 0 & -1 & 0 & 0 \\ 0 & 0 & 1 & 0 \\ 0 & 0 & 0 & -1 \end{pmatrix},$$
$$\tau_x^{\rm ppin} = \begin{pmatrix} 0 & 0 & 1 & 0 \\ 0 & 0 & 0 & 1 \\ 1 & 0 & 0 & 0 \\ 0 & 1 & 0 & 0 \end{pmatrix}, \ \tau_y^{\rm ppin} = \begin{pmatrix} 0 & 0 & -i & 0 \\ 0 & 0 & 0 & -i \\ i & 0 & 0 & 0 \\ 0 & i & 0 & 0 \end{pmatrix}, \ \tau_z^{\rm ppin} = \begin{pmatrix} 1 & 0 & 0 & 0 \\ 0 & 1 & 0 & 0 \\ 0 & 0 & -1 & 0 \\ 0 & 0 & 0 & -1 \end{pmatrix},$$
$$\tau_x^{\rm spin}\tau_x^{\rm ppin} = \begin{pmatrix} 0 & 0 & 0 & 1 \\ 0 & 0 & 1 & 0 \\ 0 & 1 & 0 & 0 \\ 1 & 0 & 0 & 0 \end{pmatrix}, \tau_x^{\rm spin}\tau_y^{\rm ppin} = \begin{pmatrix} 0 & 0 & 0 & -i \\ 0 & 0 & -i & 0 \\ 0 & i & 0 & 0 \\ i & 0 & 0 & 0 \end{pmatrix}, \tau_x^{\rm spin}\tau_z^{\rm ppin} = \begin{pmatrix} 0 & 1 & 0 & 0 \\ 1 & 0 & 0 & 0 \\ 0 & 0 & 0 & -1 \\ 0 & 0 & -1 & 0 \end{pmatrix},$$
$$\tau_y^{\rm spin}\tau_x^{\rm ppin} = \begin{pmatrix} 0 & 0 & 0 & -i \\ 0 & 0 & i & 0 \\ 0 & -i & 0 & 0 \\ i & 0 & 0 & 0 \end{pmatrix}, \tau_y^{\rm spin}\tau_y^{\rm ppin} = \begin{pmatrix} 0 & 0 & 0 & -1 \\ 0 & 0 & 1 & 0 \\ 0 & 1 & 0 & 0 \\ -1 & 0 & 0 & 0 \end{pmatrix}, \tau_y^{\rm spin}\tau_z^{\rm ppin} = \begin{pmatrix} 0 & -i & 0 & 0 \\ i & 0 & 0 & 0 \\ 0 & 0 & 0 & i \\ 0 & 0 & -i & 0 \end{pmatrix},$$
$$\tau_z^{\rm spin}\tau_x^{\rm ppin} = \begin{pmatrix} 0 & 0 & 1 & 0 \\ 0 & 0 & 0 & -1 \\ 1 & 0 & 0 & 0 \\ 0 & -1 & 0 & 0 \end{pmatrix}, \tau_z^{\rm spin}\tau_y^{\rm ppin} = \begin{pmatrix} 0 & 0 & -i & 0 \\ 0 & 0 & 0 & i \\ i & 0 & 0 & 0 \\ 0 & -i & 0 & 0 \end{pmatrix}, \tau_x^{\rm spin}\tau_y^{\rm ppin} = \begin{pmatrix} 1 & 0 & 0 & 0 \\ 0 & -1 & 0 & 0 \\ 0 & 0 & -1 & 0 \\ 0 & 0 & 0 & 1 \end{pmatrix}. \tag{A.30}$$

The matrices or (A.27)-(A.29) or (A.30) are the another representation for the SU(4) genera-

tors, and the relation between (A.26) and (A.30) are given by

$$\begin{aligned}
\tau_x^{\rm spin} &= \lambda_1 + \lambda_{13},\ \tau_y^{\rm spin} = \lambda_2 - \lambda_{14},\ \tau_z^{\rm spin} = \lambda_3 - \frac{1}{\sqrt{3}}\lambda_8 + \frac{\sqrt{6}}{3}\lambda_{15}, \\
\tau_x^{\rm ppin} &= \lambda_4 + \lambda_{11},\ \tau_y^{\rm ppin} = \lambda_5 - \lambda_{12},\ \tau_z^{\rm ppin} = \frac{2}{\sqrt{3}}\lambda_8 + \frac{2}{\sqrt{6}}\lambda_{15}, \\
\tau_x^{\rm spin}\tau_x^{\rm ppin} &= \lambda_9 + \lambda_6,\ \tau_x^{\rm spin}\tau_y^{\rm ppin} = \lambda_7 - \lambda_{10},\ \tau_x^{\rm spin}\tau_z^{\rm ppin} = \lambda_1 - \lambda_{13}, \\
\tau_y^{\rm spin}\tau_x^{\rm ppin} &= -(\lambda_7 + \lambda_{10}),\ \tau_y^{\rm spin}\tau_y^{\rm ppin} = \lambda_9 - \lambda_6,\ \tau_y^{\rm spin}\tau_z^{\rm ppin} = \lambda_2 + \lambda_{14}, \\
\tau_z^{\rm spin}\tau_x^{\rm ppin} &= \lambda_4 - \lambda_{11},\ \tau_z^{\rm spin}\tau_y^{\rm ppin} = \lambda_5 + \lambda_{12},\ \tau_z^{\rm spin}\tau_z^{\rm ppin} = \frac{2}{\sqrt{3}}\lambda_8 + \frac{2}{\sqrt{6}}\lambda_{15}.
\end{aligned} \tag{A.31}$$

We denote the generators (A.27)-(A.29) as $T_{a0} \equiv \frac{1}{2}\tau_a^{\rm spin}$, $T_{0a} \equiv \frac{1}{2}\tau_a^{\rm ppin}$, $T_{ab} \equiv \frac{1}{2}\tau_a^{\rm spin}\tau_b^{\rm ppin}$. They satisfy the normalization condition

$$\mathrm{Tr}(T_{\mu\nu}T_{\gamma\delta}) = \delta_{\mu\gamma}\delta_{\nu\delta}, \tag{A.32}$$

and the commutation relations

$$[T_{\mu\nu}, T_{\gamma\delta}] = i f_{\mu\nu,\gamma\delta,\mu'\nu'}T_{\mu'\nu'}, \tag{A.33}$$

where $f_{\mu\nu,\gamma\delta,\mu\prime\nu\prime}$ are the SU(4) structure constants in the basis (A.27)-(A.29). Greek indices run over $0, x, y, z$. Writing (A.33) explicitly, we have

$$[T_{a\mu}, T_{b\mu}] = i\epsilon_{abc}T_{c0}, \qquad [T_{\mu a}, T_{\mu b}] = i\epsilon_{abc}T_{0c}, \tag{A.34}$$

where ϵ_{abc} is the SU(2) structure constant, and $a, b, c = x, y, z$.

Appendix B

B.1 Quantum Theory in Noncommutative Geometry

When the high magnetic field is applied to the QH systems, the cyclotron energy becomes large enough to prohibit the excitations across the Landau levels. Electrons are confined in a single Landau level; such a situation is constructed by the Landau-level projection formalism. The electrons are described by the Landau sites, associated with the guiding center (X, Y), representing the noncommutativity $[X, Y] = -il_B^2$. Then the physics of QH effect is described by the quantum theory in this noncommutative geometry. It reveals the essence of the QH states and enables us to study the low energy excitation modes such as NG modes in the QH systems. In this appendix, we present the noncommutative quantum theory based on [59, 101, 102, 103, 134]. Based on this quantum theory, we present the detailed discussion for the Landau-level projection formalism. We also show the detailed discussion for the projected Coulomb Hamiltonian and the classical Coulomb Hamiltonian, which yields the effective Hamiltonian for the NG modes (2.141).

B.1.1 Basic Formalisms

In order to construct a noncommutative quantum theory based on commutation relation

$$[X, Y] = -il_B^2, \tag{B.1}$$

and describe a c-number function $f(\boldsymbol{x})$, with $\boldsymbol{x} = \boldsymbol{X} + \boldsymbol{R}$, by this theory, we introduce the quantity, which has an one to one corresponds to a function $f(\boldsymbol{x})$ in the noncommutative plane (B.1). Such an operator is called the Weyl operator $W[f]$, given by

$$f(\boldsymbol{x}) \Rightarrow W[f] = \frac{1}{(2\pi)^2} \int d^2q d^2x e^{-i\boldsymbol{q}(\boldsymbol{x}-\boldsymbol{X})} f(\boldsymbol{x}) = \frac{1}{2\pi} \int d^2q e^{i\boldsymbol{q}\boldsymbol{X}} f(\boldsymbol{q}). \tag{B.2}$$

The function $f(\boldsymbol{x})$ is called the symbol of $W[f]$ in this theory. Its inversion formula is given by

$$f(\boldsymbol{q}) = l_B^2 \sum_{n=0}^{\infty} \langle n | e^{-i\boldsymbol{q}\boldsymbol{X}} W[f] | n \rangle. \tag{B.3}$$

A simple example for the Weyl operator $W[f]$, which we use later, is the Weyl operator for the plane wave $e^{i\boldsymbol{p}\boldsymbol{x}}$. By using (B.2) with $f(\boldsymbol{x}) = e^{i\boldsymbol{p}\boldsymbol{x}}$, we obtain

$$W[e^{i\boldsymbol{p}\boldsymbol{x}}] = e^{i\boldsymbol{p}\boldsymbol{X}}. \tag{B.4}$$

The Weyl symbol for the plane wave (B.4) forms different algebraic structure from the one in the ordinary geometry. The plane wave in the ordinary geometry satisfy

$$e^{i\boldsymbol{p}\boldsymbol{x}}e^{i\boldsymbol{q}\boldsymbol{x}} = e^{i(\boldsymbol{p}+\boldsymbol{q})\boldsymbol{x}}. \tag{B.5}$$

On the other hand, the Weyl symbol for the plane wave has the algebraic structure,

$$e^{i\boldsymbol{p}\boldsymbol{X}}e^{i\boldsymbol{q}\boldsymbol{X}} = e^{i(\boldsymbol{p}+\boldsymbol{q})\boldsymbol{X}}\exp\left[\frac{i}{2}l_B^2\boldsymbol{p}\wedge\boldsymbol{q}\right], \tag{B.6}$$

where we have used the Baker-Campbell-Hausdorff formula

$$e^{\hat{A}}e^{\hat{B}} = e^{[\hat{A},\hat{B}]}e^{\hat{B}}e^{\hat{A}} = e^{\frac{[\hat{A},\hat{B}]}{2}}e^{\hat{A}+\hat{B}}, \tag{B.7}$$

which holds when the commutator between A and B is the c-number.

The additional phase factor $\exp[(i/2)l_B^2\boldsymbol{p}\wedge\boldsymbol{q}]$ arises in the noncommutative geometry. We can interpret its physical meaning as follows. Plane wave $e^{i\boldsymbol{p}\boldsymbol{x}}$ is the generator of the translational group. In the ordinary geometry, the trivial transformation, $1 = e^{i\boldsymbol{p}\boldsymbol{x}}e^{i\boldsymbol{q}\boldsymbol{x}}e^{-i\boldsymbol{q}\boldsymbol{x}}e^{-i\boldsymbol{p}\boldsymbol{x}}$, represents that it is the translation going back to the original position. However, in the noncommutative geometry, we have

$$e^{i\boldsymbol{p}\boldsymbol{X}}e^{i\boldsymbol{q}\boldsymbol{X}}e^{-i\boldsymbol{q}\boldsymbol{X}}e^{-i\boldsymbol{p}\boldsymbol{X}} = \exp\left[\frac{i}{2}l_B^2\boldsymbol{p}\wedge\boldsymbol{q}\right] \neq \mathbf{1}. \tag{B.8}$$

Therefore the phase factor $\exp[(i/2)l_B^2\boldsymbol{p}\wedge\boldsymbol{q}]$ is the Aharonov-Bohm phase.

Weyl operator $W[f]$ can also be represented in a matrix form. By using the completeness condition (2.90), or

$$\sum_n |n\rangle\langle n| = 1. \tag{B.9}$$

Weyl operator $W[f]$ is expressed as

$$W[f] = \sum_{mn} f_{mn}|m\rangle\langle n|, \tag{B.10}$$

$$f_{mn} = \langle m|W[f]|n\rangle = \frac{1}{2\pi}\int d^2q\langle m|e^{i\boldsymbol{q}\boldsymbol{X}}|n\rangle f(\boldsymbol{q}). \tag{B.11}$$

Corresponding to (B.3), the inversion formula for $W[f]$ in a matrix representation is given by

$$f(\boldsymbol{q}) = l_B^2\sum_n\langle n|e^{-i\boldsymbol{q}\boldsymbol{X}}W[f]|n\rangle = l_B^2\sum_{mn}\langle n|e^{-i\boldsymbol{q}\boldsymbol{X}}|m\rangle f_{mn}. \tag{B.12}$$

The Weyl operator for the derivative $\partial_i f$ is obtained from the definition (B.2), the Baker-Campbell-Hausdorff formula (B.7), and (B.1):

$$W[\partial_i f] = \frac{1}{i(2\pi l_B)^2}\epsilon_{ij}\int d^2q \left[X_j, e^{i\boldsymbol{q}\boldsymbol{X}}\right] f(\boldsymbol{q}) = \frac{1}{il_B^2}\epsilon_{ij}\left[X_j, W[f]\right]. \tag{B.13}$$

We also list the two formulas,

$$\mathrm{Tr}\left(e^{i\boldsymbol{p}\boldsymbol{X}}\right) \equiv \sum_{n=0}^{\infty}\langle n|e^{i\boldsymbol{p}\boldsymbol{X}}|n\rangle = \frac{2\pi}{l_B^2}\delta(\boldsymbol{p}), \tag{B.14}$$

$$\int d^2p\langle m|e^{-i\boldsymbol{p}\boldsymbol{X}}|n\rangle\langle i|e^{i\boldsymbol{p}\boldsymbol{X}}|j\rangle = \frac{2\pi}{l_B^2}\delta_{ni}\delta_{mj}, \tag{B.15}$$

which are used later on.

We now consider the Weyl operator for the density in the second-quantized form. The corresponding classical density is given by [134]

$$\rho^{\mathrm{cl}}(\boldsymbol{x},\boldsymbol{r}) = \delta(\boldsymbol{x}-\boldsymbol{r}), \tag{B.16}$$

where $\boldsymbol{x}$ denotes the position of the particle and $\boldsymbol{r}$ the coordinate of the plane. Substituting the above equation to (B.2), we have

$$W[\rho^{\mathrm{cl}}(\boldsymbol{x},\boldsymbol{r})] = \frac{1}{(2\pi)^2}\int d^2qd^2xe^{-i\boldsymbol{q}(\boldsymbol{x}-\boldsymbol{X})}\delta(\boldsymbol{x}-\boldsymbol{r}) = \frac{1}{2\pi}\int d^2qe^{i\boldsymbol{q}(\boldsymbol{r}-\boldsymbol{X})}. \tag{B.17}$$

Then from (B.17), we obtain the Weyl operator for the density in the second-quantized form,

$$\rho^{\mathrm{FT}}(\boldsymbol{r}) = \frac{1}{(2\pi)^2}\int d^2qd^2xd^2ye^{-i\boldsymbol{q}\boldsymbol{r}}\psi^\dagger(\boldsymbol{x})\langle\boldsymbol{y}|e^{i\boldsymbol{q}\boldsymbol{X}}|\boldsymbol{x}\rangle\psi(\boldsymbol{y}). \tag{B.18}$$

It can be easily verified that in the ordinary commutative plane $[X,Y]=0$, we obtain the ordinary formula for the density operator $\rho^{\mathrm{FT}}(\boldsymbol{r}) \to \psi^\dagger(\boldsymbol{r})\psi(\boldsymbol{r})$.

The electron field operator $\psi(\boldsymbol{x})$ can be expressed in terms of the Landau site $|N,n\rangle$ as [59]

$$\psi(\boldsymbol{x}) = \sum_{N,n}\langle\boldsymbol{x}|N,n\rangle c_N(n) = \sum_{N,n}\chi_{N,n}(\boldsymbol{x})c_N(n), \tag{B.19}$$

where $c_N(n)$ is the annihilation operator for electron in the Landau site $|N,n\rangle$, satisfying the anti-commutation relation

$$\{c_N(n), c_M^\dagger(m)\} = \delta_{NM}\delta_{nm}. \tag{B.20}$$

Here we neglect the internal degrees of freedom for the electrons for the sake of simplicity. Substituting (B.19) into (B.18), and setting $\rho^{\mathrm{FT}}(\boldsymbol{r}) = \hat{\rho}(\boldsymbol{r})$, we obtain the Weyl operator for

the density in the second-quantized form,

$$\hat{\rho}(\boldsymbol{r}) = \frac{1}{(2\pi)^2}\int d^2q e^{-i\boldsymbol{q}\boldsymbol{r}}\left[\sum_{NMnm}\langle M,m|e^{i\boldsymbol{q}\boldsymbol{X}}|N,n\rangle\rho_{NM}(n,m)\right], \tag{B.21}$$

where $\rho_{NM}(n,m) = c_M^\dagger(m)c_N(n)$, and its Fourier transformation given by

$$\hat{\rho}(\boldsymbol{q}) = \frac{1}{2\pi}\sum_{NMnm}\langle M,m|e^{-i\boldsymbol{q}\boldsymbol{X}}|N,n\rangle\rho_{NM}(n,m). \tag{B.22}$$

B.1.2 Landau Level Projection Formalism

In order to construct the electron field operator projected to the Nth Landau-level, we fix the Landau-level index in (B.19). Then we obtain

$$\psi_N(\boldsymbol{x}) = \sum_n \langle \boldsymbol{x}|N,n\rangle c_N(n) = \sum_n \chi_{N,n}(\boldsymbol{x})c_N(n). \tag{B.23}$$

We next construct the density and SU(4) isospin operators projected to the Nth Landau level, since the physical operators in the QH systems are expressed in terms of them. At first, we neglect the internal degrees of freedom for electrons, such as spin or pseudospin degrees of freedom for the sake of simplicity, and construct the projected density operator. From (B.23), the projected density operator to the Nth Landau level is,

$$\rho_N(\boldsymbol{x}) = \Psi_N^\dagger(\boldsymbol{x})\Psi_N(\boldsymbol{x}) = \sum_{mn}\langle N,m|\boldsymbol{x}\rangle\langle \boldsymbol{x}|N,n\rangle c_N^\dagger(m)c_N(n), \tag{B.24}$$

and its Fourier transformation given by

$$\begin{aligned}\rho_N(\boldsymbol{q}) &= \frac{1}{2\pi}\int d^2x e^{-i\boldsymbol{q}\boldsymbol{x}}\left(\sum_{mn}\langle N,m|\boldsymbol{x}\rangle\langle \boldsymbol{x}|N,n\rangle c_N^\dagger(m)c_N(n)\right)\\ &= \frac{1}{2\pi}\sum_{mn}\langle N|e^{-i\boldsymbol{q}\boldsymbol{R}}|N\rangle\langle m|e^{-i\boldsymbol{q}\boldsymbol{X}}|n\rangle c_N^\dagger(m)c_N(n) = F_N(\boldsymbol{q})\hat{\rho}_N(\boldsymbol{q}),\end{aligned} \tag{B.25}$$

where we have

$$\hat{\rho}(\boldsymbol{q}) = \frac{1}{2\pi}\sum_{mn}\langle m|e^{-i\boldsymbol{q}\boldsymbol{X}}|n\rangle c_N^\dagger(m)c_N(n) = \frac{1}{2\pi}\sum_{mn}\langle m|e^{-i\boldsymbol{q}\boldsymbol{X}}|n\rangle\rho(n,m), \tag{B.26}$$

$$F_N(\boldsymbol{q}) = \langle N|e^{-i\boldsymbol{q}\boldsymbol{R}}|N\rangle = L_N\left(\frac{l_B^2\boldsymbol{q}^2}{2}\right)e^{-\frac{l_B^2\boldsymbol{q}^2}{4}}, \qquad \rho(n,m) = c_N^\dagger(m)c_N(n), \tag{B.27}$$

The bare density (B.26) satisfies the algebra

$$[\hat{\rho}(\boldsymbol{p}),\hat{\rho}(\boldsymbol{q})] = \frac{i}{\pi}\hat{\rho}(\boldsymbol{p}+\boldsymbol{q})\sin\left(l_B^2\frac{\boldsymbol{p}\wedge\boldsymbol{q}}{2}\right), \tag{B.28}$$

which can be derived from the algebra

$$[\rho(m,n),\rho(i,j)] = \delta_{mj}\rho(i,n) - \delta_{in}\rho(m,j), \tag{B.29}$$

and the algebra (B.6). Eq. (B.28) is isomorphic to the W_∞ algebra [128, 132, 133]. We discuss the role of the bare density later on. By comparing with (B.22), we see that the bare density (B.26) is the Weyl operator for the density operator.

We now take into account the internal degrees of freedom for electrons, and consider SU(N) theory; N= 2 corresponds to monolayer QH systems with spins or spinless bilayer QH systems, while N= 4 corresponds to bilayer QH systems with spins. We call the N internal degrees of freedom of the electrons as the SU(N) isospin. The electron field operator in the Nth Landau level with N components is given by (2.93), or

$$\Psi_{N,\mu}(\boldsymbol{x}) = \sum_n \langle \boldsymbol{x}|N,n\rangle c_{N,\mu}(n), \tag{B.30}$$

with μ the isospin index. The creation and annihilation operators $c_{N,\mu}(n)$ and $c^\dagger_{N,\mu}(n)$ satisfy the anti-commutation relation

$$\{c_{N,\mu}(n), c_{N,\nu}(m)\} = \delta_{nm}\delta_{\mu\nu}. \tag{B.31}$$

From (B.30) the projected density and isospin density operator into the Nth Landau level are

$$\rho_N(\boldsymbol{x}) = \Psi^\dagger_{N,\mu}(\boldsymbol{x})\Psi_{N,\mu}(\boldsymbol{x}), \quad I_{N,a}(\boldsymbol{x}) = \Psi^\dagger_{N,\mu}(\boldsymbol{x})\left(\frac{\lambda_a}{2}\right)_{\mu\nu}\Psi_{N,\nu}(\boldsymbol{x}), \tag{B.32}$$

where λ_a denote the SU(N) generators. Correspondingly, we obtain the bare density and the bare isospin density

$$\hat\rho(\boldsymbol{q}) = \frac{1}{2\pi}\sum_{mn}\langle n|e^{-i\boldsymbol{q}\boldsymbol{X}}|m\rangle\rho(m,n), \quad \hat I_a(\boldsymbol{q}) = \frac{1}{2\pi}\sum_{mn}\langle n|e^{-i\boldsymbol{q}\boldsymbol{X}}|m\rangle I_a(m,n), \tag{B.33}$$

where

$$\rho(m,n) = c^\dagger_{N,\mu}(n)c_{N,\mu}(m), \quad I_a(m,n) = c^\dagger_{N,\mu}(n)\left(\frac{\lambda_a}{2}\right)_{\mu\nu}c_{N,\nu}(m). \tag{B.34}$$

By using (B.6) and the anticommutation relation (B.31), we obtain

$$\begin{aligned}
[\rho(m,n),\rho(i,j)] &= \delta_{mj}\rho(i,n) - \delta_{in}\rho(m,j),\\
[\rho(m,n),I_a(i,j)] &= \delta_{mj}I_a(i,n) - \delta_{in}i_a(m,j),\\
[I_a(m,n),I_b(i,j)] &= \frac{i}{2}f_{abc}\left[\delta_{mj}I_c(i,n) + \delta_{in}I_c(m,j)\right] + \frac{1}{2}d_{abc}\left[\delta_{mj}I_c(i,n) - \delta_{in}I_c(m,j)\right]\\
&\quad + \frac{1}{2\mathrm{N}}\delta_{ab}\left[\delta_{mj}\rho(i,n) - \delta_{in}\rho(m,j)\right]
\end{aligned} \tag{B.35}$$

and simultaneously,

$$
\begin{aligned}
[\hat{\rho}(\boldsymbol{p}), \hat{\rho}(\boldsymbol{q})] &= \frac{i}{\pi}\hat{\rho}(\boldsymbol{p}+\boldsymbol{q})\sin\left(\frac{l_B^2}{2}\boldsymbol{p}\wedge\boldsymbol{q}\right), \\
\left[\hat{\rho}(\boldsymbol{p}), \hat{I}_a(\boldsymbol{q})\right] &= \frac{i}{\pi}\hat{I}_a(\boldsymbol{p}+\boldsymbol{q})\sin\left(\frac{l_B^2}{2}\boldsymbol{p}\wedge\boldsymbol{q}\right), \\
\left[\hat{I}_a(\boldsymbol{p}), \hat{I}_b(\boldsymbol{q})\right] &= \frac{i}{2\pi}f_{abc}\hat{I}_c(\boldsymbol{p}+\boldsymbol{q})\cos\left(\frac{l_B^2}{2}\boldsymbol{p}\wedge\boldsymbol{q}\right) + \frac{i}{2\pi}d_{abc}\hat{I}_c(\boldsymbol{p}+\boldsymbol{q})\sin\left(\frac{l_B^2}{2}\boldsymbol{p}\wedge\boldsymbol{q}\right) \\
&\quad + \frac{i}{2\pi N}\delta_{ab}\hat{\rho}(\boldsymbol{p}+\boldsymbol{q})\sin\left(\frac{l_B^2}{2}\boldsymbol{p}\wedge\boldsymbol{q}\right),
\end{aligned}
\tag{B.36}
$$

with f_{abc} and d_{abc} the structure constants for SU(N) algebra. The algebra (B.36) is the W_∞(N) algebra [102, 103, 134]. For example in the case of monolayer QH system (N= 2), (B.36) becomes

$$
[\hat{\rho}(\boldsymbol{p}), \hat{\rho}(\boldsymbol{q})] = \frac{i}{\pi}\hat{\rho}(\boldsymbol{p}+\boldsymbol{q})\sin\left(l_B^2\frac{\boldsymbol{p}\wedge\boldsymbol{q}}{2}\right), \tag{B.37}
$$

$$
\left[\hat{\rho}(\boldsymbol{p}), \hat{S}_a(\boldsymbol{q})\right] = \frac{i}{\pi}\hat{S}_a(\boldsymbol{p}+\boldsymbol{q})\sin\left(l_B^2\frac{\boldsymbol{p}\wedge\boldsymbol{q}}{2}\right), \tag{B.38}
$$

$$
\left[\hat{S}_a(\boldsymbol{p}), \hat{S}_b^{\mathrm{cl}}(\boldsymbol{q})\right] = \frac{i}{2\pi}\epsilon_{abc}\hat{S}_c(\boldsymbol{p}+\boldsymbol{q})\cos\left(l_B^2\frac{\boldsymbol{p}\wedge\boldsymbol{q}}{2}\right) + \frac{i}{4\pi}\delta_{ab}\hat{\rho}(\boldsymbol{p}+\boldsymbol{q})\sin\left(l_B^2\frac{\boldsymbol{p}\wedge\boldsymbol{q}}{2}\right). \tag{B.39}
$$

The projected density and the isospin operators are obtained by performing the Fourier transformation of bare operators (B.33) with the Landau-level form factor $F_N(\boldsymbol{q})$ multiplied. In the real space, the projected density in the lowest-Landau level is expressed by the bare density as [102]

$$
\rho(\boldsymbol{x}) = e^{l_B^2\frac{\nabla^2}{4}}\hat{\rho}(\boldsymbol{x}) = \frac{1}{\pi l_B^2}\int d^2y e^{-\frac{|\boldsymbol{x}-\boldsymbol{y}|^2}{l_B^2}}\hat{\rho}(\boldsymbol{y}), \tag{B.40}
$$

representing that the projected density, which is the physical quantity, is unlocalized object characterized by the magnetic length l_B, whereas the bare density is the localized one. However, for the lowest Landau level $N = 0$ in the low energy limit $\boldsymbol{q} \to 0$, we have $F_0(\boldsymbol{q}) \to 1$. Therefore, the projected density and isospin operators can be identified with the bare density and isospin operators. It is convenient to use the bare density and isospin operators, rather than the projected density and isospin operators, since they are localized quantities, so that mathematical operations such as the derivative and the integral become well-defined. Thus, instead of the projected operators, which are the actual physical quantities, we treat the bare quantities.

At the end of this subsection, we comment on the incompressibility condition for the ground state. It implies the homogeneity of the density with some of the Landau levels being filled. In the noncommutative quantum theory, it is expressed as [104]

$$
\rho(n,m)|\mathrm{g}\rangle = \sum_\sigma c_\sigma^\dagger(m)c_\sigma(n)|\mathrm{g}\rangle = \nu\delta_{nm}|\mathrm{g}\rangle, \tag{B.41}
$$

or, in the momentum space, with usage of (B.14), we have

$$\hat{\rho}(\boldsymbol{q})|\mathrm{g}\rangle = 2\pi\rho_0\delta(\boldsymbol{q})|\mathrm{g}\rangle. \tag{B.42}$$

B.1.3 Projected Coulomb Interaction in the Lowest-Landau Level

We first discuss in the case of monolayer QH systems. In the following argument, we omit the index 0 in the operators. The projected Coulomb interaction in the lowest-Landau level is given by (2.112), or

$$H_{\mathrm{C}} = \pi \int d^2q V(\boldsymbol{q}) \left(F_0(-\boldsymbol{q})\hat{\rho}(-\boldsymbol{q})\right) \left(F_0(\boldsymbol{q})\hat{\rho}(\boldsymbol{q})\right) = \pi \int d^2q V_{\mathrm{D}}(\boldsymbol{q})\hat{\rho}(-\boldsymbol{q})\hat{\rho}(\boldsymbol{q}), \tag{B.43}$$

where

$$V_{\mathrm{D}}(\boldsymbol{q}) \equiv V_0^{\mathrm{eff}}(\boldsymbol{q}) = V(\boldsymbol{q})F_0(-\boldsymbol{q})F_0(\boldsymbol{q}) = \frac{e^2}{4\pi\epsilon|\boldsymbol{q}|}e^{-\frac{l_B^2\boldsymbol{q}^2}{2}}. \tag{B.44}$$

By using the expression (B.33) for the density operator $\hat{\rho}(\boldsymbol{q})$ in (B.43), the Coulomb Hamiltonian is also expressed in the Landau-site representation,

$$H_{\mathrm{C}} = \sum_{mnij} V_{mnij} \sum_{\sigma\tau} c_\sigma^\dagger(m)c_\sigma(n)c_\tau^\dagger(i)c_\tau(j) = \sum_{mnij} V_{mnij}\rho(n,m)\rho(j,i), \tag{B.45}$$

where

$$V_{mnij} = \frac{1}{4\pi}\int d^2k V_{\mathrm{D}}(\boldsymbol{k})\langle m|e^{i\boldsymbol{X}\boldsymbol{k}}|n\rangle\langle i|e^{-i\boldsymbol{X}\boldsymbol{k}}|j\rangle. \tag{B.46}$$

The above integral satisfies the relation $V_{mnij} = V_{ijmn} = V_{nmji}$, and also has the properties

$$V_{mnij} = V_{nnjj}\delta_{mn}, \quad V_{mnij} = V_{jnnj}\delta_{mj}, \tag{B.47}$$

due to the angular momentum conservation. Here V_{nnjj} and V_{jnnj} are

$$V_{nnjj} = \frac{1}{4\pi}\int d^2k V_{\mathrm{D}}(\boldsymbol{k})\langle n|e^{i\boldsymbol{X}\boldsymbol{k}}|n\rangle\langle j|e^{-i\boldsymbol{X}\boldsymbol{k}}|j\rangle, \tag{B.48}$$

$$V_{njjn} = \frac{1}{4\pi}\int d^2k V_{\mathrm{D}}(\boldsymbol{k})\langle n|e^{i\boldsymbol{X}\boldsymbol{k}}|j\rangle\langle j|e^{-i\boldsymbol{X}\boldsymbol{k}}|n\rangle. \tag{B.49}$$

The integrals (B.48) and (B.49) are the direct and exchange integrals in terms of the Landau site $|n\rangle$, respectively. From (B.14), (B.48), and (B.49), we obtain the numerical constants

$$\epsilon_{\mathrm{D}} \equiv \sum_j V_{nnjj} = \frac{1}{4\pi l_B^2}\int d^2x V_{\mathrm{D}}(\boldsymbol{x}) = \frac{1}{2l_B^2}V_{\mathrm{D}}(\boldsymbol{q}=0), \tag{B.50}$$

$$\epsilon_{\mathrm{X}} \equiv \sum_j V_{njjn} = \frac{1}{4\pi}\int d^2k V_{\mathrm{D}}(\boldsymbol{k}) = \frac{1}{4l_B^2}V_{\mathrm{X}}(\boldsymbol{q}=0), \tag{B.51}$$

where $V_{\rm X}(\boldsymbol{q})$ is the exchange potential defined later by (B.78). In particular, (B.51) for the lowest-Landau level becomes

$$\epsilon_{\rm X} = \frac{1}{4\pi}\int d^2k V(\boldsymbol{k}) e^{-\frac{\boldsymbol{k}^2 l_B^2}{2}} = \frac{1}{2}\sqrt{\frac{\pi}{2}} E_{\rm C}^0. \tag{B.52}$$

The projected Coulomb Hamiltonian in the bilayer QH systems is given by (2.117), or

$$H_{\rm C} = \pi\int d^2q V_{\rm D}^{+}(\boldsymbol{q})\hat{\rho}(-\boldsymbol{q})\hat{\rho}(\boldsymbol{q}) + 4\pi\int d^2q V_{\rm D}^{-}(\boldsymbol{q})\hat{P}_z(-\boldsymbol{q})\hat{P}_z(\boldsymbol{q}), \tag{B.53}$$

where

$$V_{\rm D}^{\pm}(\boldsymbol{q}) = \frac{e^2}{8\pi\epsilon|\boldsymbol{q}|}\left(1 \pm e^{-|\boldsymbol{q}|d}\right) e^{-\frac{1}{2}l_B^2\boldsymbol{q}^2}. \tag{B.54}$$

In the Landau-site representation (B.53) becomes

$$H_{\rm C} = \sum_{mnij}\left[V_{mnij}^{+}\rho(n,m)\rho(j,i) + 4V_{mnij}^{-}P_z(n,m)P_z(j,i)\right]. \tag{B.55}$$

B.1.4 Classical Coulomb Hamiltonian

In this subsection, we derive the classical Coulomb Hamiltonian in the QH systems. Consequently, it has the form [101]

$$\langle\chi|H_{\rm C}|\chi\rangle = H_{\rm D}^{\rm cl} + H_{\rm X}^{\rm cl}. \tag{B.56}$$

Here $H_{\rm D}^{\rm cl}$ is the one obtained by replacing the bare density operator in (B.43) with their expectation values,

$$H_{\rm D}^{\rm cl} = \pi \int d^2q V_{\rm D}(\boldsymbol{q})\hat{\rho}^{\rm cl}(-\boldsymbol{q})\hat{\rho}^{\rm cl}(\boldsymbol{q}), \tag{B.57}$$

as well as for the Hamiltonian in the Landau-site representation, we have

$$H_{\rm D}^{\rm cl} = \sum_{mnij} V_{mnij}\rho^{\rm cl}(n,m)\rho^{\rm cl}(j,i). \tag{B.58}$$

We call $H_{\rm D}^{\rm cl}$ the direct-interaction form. On the other hand, $H_{\rm X}^{\rm cl}$ is the peculiar one in the quantum theory due to the exchange integral. We call this the exchange-interaction form. Formula (B.56) holds for bilayer systems too, although the formulas of $H_{\rm D}^{\rm cl}$ and $H_{\rm X}^{\rm cl}$ become complicated compared to those in the monolayer systems. The state $|\chi\rangle$ in (B.56) is given by (2.129), or

$$|\chi\rangle = e^{iW}|\chi_0\rangle, \tag{B.59}$$

where

$$|\chi_0\rangle = \prod_{\mu n}\left[c_\mu^\dagger(n)\right]^{\nu_\mu(n)}|0\rangle. \tag{B.60}$$

In the following discussion, we prove the formula (B.56) following the procedure given in [102, 103].

In order to calculate the expectation value of the Coulomb Hamiltonian by the state (B.60), we have to calculate two and four-body averages for annihilation and creation operator $c_\mu(m)$ and $c_\mu^\dagger(m)$. For doing this, it is convenient to introduce the the multi-index $M \equiv (\mu, m)$, where $M = 1, 2, \ldots, NN_\Phi$, by combining the isospin index ($\mu = 1, 2, \ldots, N$) and the Landau-site index ($m = 0, 1, \ldots, N_\Phi - 1$). By using the above multi-index M, we first rewrite the state (B.60) as

$$|\chi_0\rangle = \sum_{M=1}^{NN_\Phi}\left[c_M^\dagger\right]^{\nu_M}|0\rangle. \tag{B.61}$$

Here we analyze a system with a finite number of Landau sites ($m = 0, 1, \ldots, N_\Phi - 1$) and take the limit $N_\Phi \to \infty$ at the end. In the limit $N_\Phi \to \infty$, the algebra $\mathrm{U(NN_\Phi)}$ becomes identical

to the $W_\infty(N)$ algebra. From (B.59), we have to consider the electron field operators in the Landau site $c_\mu(n)$ rotated by the $W_\infty(N)$ algebra. This treatment becomes much simpler in the limit $N_\Phi \to \infty$, since we can discuss in terms of the unitary transformation $U(NN_\Phi)$. The electron field operators $c_\mu(n)$ and $c^\dagger_\mu(n)$ rotate under the $U(NN_\Phi)$ algebra as

$$e^{-iW} c_M e^{iW} = U_{MM'} c_{M'}, \quad e^{-iW} c^\dagger_M e^{iW} = c^\dagger_{M'} U^\dagger_{M'M}, \tag{B.62}$$

where U is an element of $U(NN_\Phi)$. By using the properties (B.62), for two-body average, we have

$$\langle\chi|c^\dagger_M c_N|\chi\rangle = U^\dagger_{KM} U_{NL} \langle\chi_0|c^\dagger_K c_L|\chi_0\rangle = \nu_K U_{NK} U^\dagger_{KM}, \tag{B.63}$$

where we have used $\langle\chi_0|c^\dagger_K c_L|\chi_0\rangle = \nu_K \delta_{KL}$. By using the relation $\nu^2_K = \nu_K$, the two-body average (B.63) can be rewritten as

$$\langle\chi|c^\dagger_M c_N|\chi\rangle = \langle\chi|c^\dagger_M c_K|\chi\rangle\langle\chi|c^\dagger_K c_N|\chi\rangle, \tag{B.64}$$

or, by using both the isospin and the Landau-site index, (B.64) is expressed as

$$\langle\chi|c^\dagger_\mu(m) c_\kappa(k)|\chi\rangle\langle\chi|c^\dagger_\kappa(k) c_\nu(n)|\chi\rangle = \langle\chi|c^\dagger_\mu(m) c_\nu(n)|\chi\rangle. \tag{B.65}$$

We next calculate the four-body averages by applying the similar analysis as in the case of two-body average. We obtain

$$\begin{aligned}\langle\chi|c^\dagger_M c^\dagger_S c_T c_N|\chi\rangle &= U^\dagger_{KM} U^\dagger_{IS} U_{TJ} U_{NL} \langle\chi_0|c^\dagger_K c^\dagger_I c_J c_L|\chi_0\rangle \\ &= \nu_J \nu_L U^\dagger_{KM} U^\dagger_{IS} U_{TJ} U_{NL} (\delta_{IJ}\delta_{KL} - \delta_{IL}\delta_{KJ}),\end{aligned} \tag{B.66}$$

where the the formula $\langle\chi_0|c^\dagger_K c^\dagger_I c_J c_L|\chi_0\rangle = \nu_J\nu_L(\delta_{IJ}\delta_{KL} - \delta_{IL}\delta_{KJ})$ was used in the above equation. Then by using (B.63) and (B.66), we obtain

$$\langle\chi|c^\dagger_M c^\dagger_S c_T c_N|\chi\rangle = \langle\chi|c^\dagger_M c_N|\chi\rangle\langle\chi|c^\dagger_S c_T|\chi\rangle - \langle\chi|c^\dagger_M c_T|\chi\rangle\langle\chi|c^\dagger_S c_N|\chi\rangle, \tag{B.67}$$

and subsequently, we have

$$\begin{aligned}\langle\chi|c^\dagger_\sigma(m) c^\dagger_\tau(i) c_\tau(j) c_\sigma(n)|\chi\rangle &= \langle\chi|c^\dagger_\sigma(m) c_\sigma(n)|\chi\rangle\langle\chi|c^\dagger_\tau(i) c_\tau(j)|\chi\rangle \\ &\quad - \langle\chi|c^\dagger_\sigma(m) c_\tau(j)|\chi\rangle\langle\chi|c^\dagger_\tau(i) c_\sigma(n)|\chi\rangle.\end{aligned} \tag{B.68}$$

The first term in the right hand side of Eq. (B.68) gives the direct term, whereas the second

term gives the exchange term. From (B.68), we obtain

$$\rho^{\rm cl}(n,m)\rho^{\rm cl}(j,i) = \sum_{\sigma,\tau}\langle\chi|\left(c^\dagger_\sigma(m)c^\dagger_\tau(i)c_\tau(j)c_\sigma(n) + \delta_{\sigma\tau}\delta_{ni}c^\dagger_\sigma(m)c_\tau(i)\right)|\chi\rangle$$
$$= \sum_{\sigma,\tau}\left(\langle\chi|c^\dagger_\sigma(m)c_\sigma(n)|\chi\rangle\langle\chi|c^\dagger_\tau(i)c_\tau(j)|\chi\rangle - \langle\chi|c^\dagger_\sigma(m)c_\tau(j)|\chi\rangle\langle\chi|c^\dagger_\tau(i)c_\sigma(n)|\chi\rangle\right) + \delta_{ni}\rho^{\rm cl}(j,m), \tag{B.69}$$

and by multiplying $\sum_{mnij} V_{mnij}$ to the (B.69) from the left side, with using the formula

$$c^\dagger_\mu(m)c_\nu(n) = \frac{\delta_{\nu\mu}}{\rm N}\rho(n,m) + (\lambda_a)_{\nu\mu}I_a(n,m), \tag{B.70}$$

we finally obtain the decomposition formula in monolayer QH systems,

$$H^{\rm cl}_{\rm C} \equiv \langle\chi|H_{\rm C}|\chi\rangle = H^{\rm cl}_{\rm D} + H^{\rm cl}_{\rm X}, \tag{B.71}$$

with

$$H^{\rm cl}_{\rm D} = \sum_{mnij} V_{mnij}\rho^{\rm cl}(n,m)\rho^{\rm cl}(j,i), \tag{B.72}$$

$$H^{\rm cl}_{\rm X} = -2\sum_{mnij} V_{mnij}\left[I^{\rm cl}_a(j,m)I^{\rm cl}_a(n,i) + \frac{1}{2N}\rho^{\rm cl}(j,m)\rho^{\rm cl}(n,i)\right]. \tag{B.73}$$

Here the constant term $\epsilon_{\rm X}N_{\rm e}$ has been neglected, coming from the term $\delta_{ni}\rho^{\rm cl}(j,m)$ in (B.69). In the momentum space we have

$$H^{\rm cl}_{\rm D} = \pi\int d^2q V_{\rm D}(\boldsymbol{q})\hat\rho^{\rm cl}(-\boldsymbol{q})\hat\rho^{\rm cl}(\boldsymbol{q}), \tag{B.74}$$

$$H^{\rm cl}_{\rm X} = -\pi\int d^2k V_{\rm X}(\boldsymbol{k})\left[\hat I^{\rm cl}_a(-\boldsymbol{k})\hat I^{\rm cl}_a(\boldsymbol{k}) + \frac{1}{2N}\hat\rho^{\rm cl}(-\boldsymbol{k})\hat\rho^{\rm cl}(\boldsymbol{k})\right], \tag{B.75}$$

where we have used the inversion formulas for $\rho(n,m)$ and $I_a(n,m)$ and the formula [59],

$$\rho(n,m) = l_B^2\int d^2q\langle n|e^{i\boldsymbol{q}\boldsymbol{X}}|m\rangle\hat\rho(\boldsymbol{q}), \quad I_a(n,m) = l_B^2\int d^2q\langle n|e^{i\boldsymbol{q}\boldsymbol{X}}|m\rangle\hat I_a(\boldsymbol{q}), \tag{B.76}$$

$$\sum_n\langle n|e^{-i\boldsymbol{k}\boldsymbol{X}}e^{i\boldsymbol{p}\boldsymbol{X}}e^{i\boldsymbol{k}\boldsymbol{X}}e^{i\boldsymbol{q}\boldsymbol{X}}|n\rangle = \frac{2\pi}{l_B^2}\delta(\boldsymbol{p}+\boldsymbol{q})\exp\left(il_B^2\boldsymbol{p}\wedge\boldsymbol{k}\right). \tag{B.77}$$

Here the exchange potential $V_{\rm X}$ is given by,

$$V_{\rm X}(\boldsymbol{q}) = \frac{l_B^2}{\pi}\int d^2k e^{-il_B^2\boldsymbol{p}\wedge\boldsymbol{k}}V_{\rm D}(\boldsymbol{k}) \quad V_{\rm X}(\boldsymbol{x}) = \frac{1}{2\pi}\int d^2p e^{i\boldsymbol{p}\boldsymbol{x}}V_{\rm X}(\boldsymbol{p}). \tag{B.78}$$

In the lowest-Landau level, (B.78) has the form

$$V_{\rm X}(\boldsymbol{q}) = \frac{e^2\sqrt{2\pi}l_B}{4\pi\epsilon}I_0\left(\frac{l_B^2\boldsymbol{p}^2}{4}\right)e^{-\frac{l_B^2\boldsymbol{p}^2}{4}}, \quad V_{\rm X}(\boldsymbol{x}) = 2V(\boldsymbol{x})e^{-\frac{\boldsymbol{x}^2}{2l_B^2}}. \tag{B.79}$$

With a similar analysis given for the monolayer systems, the decomposition formula in the bilayer QH systems can also be obtained. For $H_{\rm C}^{+}$, by taking exactly the same procedure that we did in the monolayer systems, we obtain

$$H_{\rm D}^{+{\rm cl}} = \sum_{mnij} V_{mnij}^{+} \rho^{\rm cl}(n,m)\rho^{\rm cl}(j,i),$$
$$H_{\rm X}^{+{\rm cl}} = -2\sum_{mnij} V_{mnij}^{+}\left[\sum_{a=1}^{15} I_a^{\rm cl}(j,m)I_a^{\rm cl}(n,i) + \frac{1}{8}\rho^{\rm cl}(j,m)\rho^{\rm cl}(n,i)\right]. \tag{B.80}$$

For $H_{\rm C}^{-}$, we have to calculate the expectation value of $4P_z(n,m)P_z(j,i)$ in order to obtain the classical Hamiltonian. By using (B.67), (B.70), and the relations between the SU(4) generators (A.31), it is calculated as

$$\langle\chi|4P_z(n,m)P_z(j,i)|\chi\rangle = \sum_{\alpha\beta\gamma\delta}\left(\tau_z^{\rm ppin}\right)_{\alpha\beta}\left(\tau_z^{\rm ppin}\right)_{\gamma\delta}\langle\chi|c_\alpha^\dagger(m)c_\beta(n)c_\gamma^\dagger(i)c_\delta(j)|\chi\rangle$$
$$= 4P_z^{\rm cl}(n,m)P_z^{\rm cl}(j,i) - 2\sum_{a,b}^{15} M_{ab}I_a^{\rm cl}(j,m)I_b^{\rm cl}(n,i) - \frac{1}{4}\rho^{\rm cl}(j,m)\rho^{\rm cl}(n,i) + \rho^{\rm cl}(j,m)\delta_{ni}, \tag{B.81}$$

where M_{ab} is given by

$$M_{ab} = \frac{1}{2}{\rm Tr}\left(\lambda_a\tau_z^{\rm p}\lambda_b\tau_z^{\rm p}\right) = \xi_a\delta_{ab}, \tag{B.82}$$

and $\xi_{1,2,3,8,13,14,15} = +1$ or $\xi_{4,5,6,7,9,10,11,12} = -1$. We neglect the contribution from the term $\rho^{\rm cl}(j,m)\delta_{ni}$ in (B.81), leading to the numerical constant $\epsilon_{\rm X}N_{\rm e}$. Then by multiplying $\sum_{mnij} V_{mnij}$ to the (B.81) from the left side, we obtain the direct and exchange form of $H_{\rm C}^{-}$,

$$H_{\rm D}^{-{\rm cl}} = 4\sum_{mnij} V_{mnij}^{-} P_z^{\rm cl}(n,m)P_z^{\rm cl}(j,i)$$
$$H_{\rm X}^{-{\rm cl}} = -2\sum_{mnij} V_{mnij}^{-}\left[\sum_{a=1}^{15}\xi_a I_a^{\rm cl}(j,m)I_a^{\rm cl}(n,i) + \frac{1}{8}\rho^{\rm cl}(j,m)\rho^{\rm cl}(n,i)\right]. \tag{B.83}$$

Consequently, from (B.80) and (B.83), the direct and exchange form in the bilayer systems become,

$$H_{\rm D}^{\rm cl} = \sum_{mnij}\left[V_{mnij}^{+}\rho^{\rm cl}(n,m)\rho^{\rm cl}(j,i) + 4V_{mnij}^{-}P_z^{\rm cl}(n,m)P_z^{\rm cl}(j,i)\right], \tag{B.84}$$
$$H_{\rm X}^{\rm cl} = -\sum_{mnij} V_{mnij}^{d}\left[S_a^{\rm cl}(j,m)S_a^{\rm cl}(n,i) + P_a^{\rm cl}(j,m)P_a^{\rm cl}(n,i) + R_{ab}^{\rm cl}(j,m)R_{ab}^{\rm cl}(n,i)\right]$$
$$- 2\sum_{mnij} V_{mnij}^{-}\left[S_a^{\rm cl}(j,m)S_a^{\rm cl}(n,i) + P_z^{\rm cl}(j,m)P_z^{\rm cl}(n,i) + R_{az}^{\rm cl}(j,m)R_{az}^{\rm cl}(n,i)\right]$$
$$- \frac{1}{4}\sum_{mnij} V_{mnij}\rho^{\rm cl}(j,m)\rho^{\rm cl}(n,i), \tag{B.85}$$

where $V_{mnij} = V^+_{mnij} + V^-_{mnij}$ and $V^d_{mnij} = V^+_{mnij} - V^-_{mnij}$. We have expressed the Hamiltonian $H^{\rm cl}_{\rm X}$ by S_a, P_a and R_{ab}, instead of I_a. In the momentum space, (B.84) and (B.85) become

$$H^{\rm cl}_{\rm D} = \pi \int d^2q V^+_{\rm D}(\boldsymbol{q}) \hat{\rho}^{\rm cl}(-\boldsymbol{q}) \hat{\rho}^{\rm cl}(\boldsymbol{q}) + 4\pi \int d^2q V^-_{\rm D}(\boldsymbol{q}) \hat{P}^{\rm cl}_z(-\boldsymbol{q}) \hat{P}^{\rm cl}_z(\boldsymbol{q}), \tag{B.86}$$

$$\begin{aligned} H^{\rm cl}_{\rm X} = & -\frac{\pi}{2} \int d^2p V^d_X(\boldsymbol{p}) [\hat{S}^{\rm cl}_a(-\boldsymbol{p}) \hat{S}^{\rm cl}_a(\boldsymbol{p}) + \hat{P}^{\rm cl}_a(-\boldsymbol{p}) \hat{P}^{\rm cl}_a(\boldsymbol{p}) + \hat{R}^{\rm cl}_{ab}(-\boldsymbol{p}) \hat{R}^{\rm cl}_{ab}(\boldsymbol{p})] \\ & - \pi \int d^2p V^-_X(\boldsymbol{p}) [\hat{S}^{\rm cl}_a(-\boldsymbol{p}) \hat{S}^{\rm cl}_a(\boldsymbol{p}) + \hat{P}^{\rm cl}_z(-\boldsymbol{p}) \hat{P}^{\rm cl}_z(\boldsymbol{p}) + \hat{R}^{\rm cl}_{az}(-\boldsymbol{p}) \hat{R}^{\rm cl}_{az}(\boldsymbol{p})] \\ & - \frac{\pi}{8} \int d^2p V_X(\boldsymbol{p}) \hat{\rho}^{\rm cl}(-\boldsymbol{p}) \hat{\rho}^{\rm cl}(\boldsymbol{p}). \end{aligned} \tag{B.87}$$

Here the direct potential $V^{\pm}_{\rm D}$ and exchange potential $V^{\pm}_{\rm X}$ are given by (2.118) and (2.127), respectively, or

$$V^{\pm}_{\rm D}(\boldsymbol{q}) = \frac{e^2}{8\pi\epsilon|\boldsymbol{q}|} \left(1 \pm e^{-|\boldsymbol{q}|d}\right) e^{-\frac{1}{2}l_B^2 \boldsymbol{q}^2}, \tag{B.88}$$

$$V^{\pm}_{\rm X}(\boldsymbol{p}) = \frac{\sqrt{2\pi} e^2 \ell_B}{8\pi\epsilon} I_0(\ell_B^2 \boldsymbol{p}^2/4) e^{-\ell_B^2 \boldsymbol{p}^2/4} \pm \frac{e^2 \ell_B^2}{4\pi\epsilon} \int_0^\infty dk e^{-\frac{1}{2}\ell_B^2 k^2 - kd} J_0(\ell_B^2 |\boldsymbol{p}| k), \tag{B.89}$$

with $V_{\rm X} = V^+_{\rm X} + V^-_{\rm X}$ and $V^d_{\rm X} = V^+_{\rm X} - V^-_{\rm X}$.

As we have shown in subsection 2.2.4, by making the derivative expansion for the exchange Coulomb Hamiltonian (B.87), we obtain the basic Hamiltonian for the NG modes (2.141).

Appendix C

C.1 Effective Theories for Nambu Goldstone Modes in SU(4) Nonlinear Representation

In this appendix we show another systematic method for the analysis for the effective theory for the NG modes besides the Grassmannian formalism based on [108]. This method was originally developed in particle and nuclear physics [130, 131].

Most general excitations around the classical ground state are described by the operator

$$\mathcal{I}_{\mu\nu}(x) = \mathcal{I}(x) \left[\exp\left(i \sum_{\gamma\delta} \pi_{\gamma\delta} T_{\gamma\delta} \right) \right]_{\mu\nu}^{\mu'\nu'} \mathcal{I}^0_{\mu'\nu'}, \tag{C.1}$$

where $\mathcal{I}^0_{\mu'\nu'}$ is the SU(4) order parameter which characterizes the ground state structure, $T_{\gamma\delta}$ are the matrices of the broken SU(4) generators in the adjoint representation of SU(4), each of which is a 15×15 matrix. The greek indices run over $0, x, y, z$. The phase field $\pi_{\gamma\delta}(x)$ are the NG modes associated with the broken generators, and the coefficient $\mathcal{I}(x)$ is the amplitude function corresponding to the "sigma" field in the linear sigma model. Since we are only interested in an effective low energy theory of the NG modes, we set $\mathcal{I}(x) = 1$. Then we may identify

$$\mathcal{S}_a = \mathcal{I}_{a0}, \qquad \mathcal{P}_a = \mathcal{I}_{0a}, \qquad \mathcal{R}_{ab} = \mathcal{I}_{ab}, \tag{C.2}$$

and express various physical variables in terms of the NG modes $\pi_{\gamma\delta}(x)$.

We expand the formula (C.1) in $\pi_{\gamma\delta}$,

$$\mathcal{I}_{\mu\nu}(x) = \mathcal{I}^0_{\mu\nu} + \mathcal{I}^{(1)}_{\mu\nu}(x) + \mathcal{I}^{(2)}_{\mu\nu}(x) + \cdots, \tag{C.3}$$

where $\mathcal{I}^{(n)}_{\mu\nu}(x)$ is the nth order term in the NG mode $\pi_{\gamma\delta}$. Up to the second order, they are

$$\mathcal{I}^{(1)}_{\mu\nu}(x) = -f_{\mu\nu,\gamma\delta,\mu'\nu'} \pi_{\gamma\delta} \mathcal{I}^0_{\mu'\nu'}, \tag{C.4}$$

$$\mathcal{I}^{(2)}_{\mu\nu}(x) = \frac{1}{2!} f_{\mu\nu,\gamma\delta,\mu''\nu''} f_{\mu''\nu'',\gamma'\delta',\mu\nu} \pi_{\gamma\delta} \pi_{\gamma'\delta'} \mathcal{I}^0_{\mu\nu}, \tag{C.5}$$

where $f_{\mu\nu,\gamma\delta,\mu'\nu'}$ are the structure constant of SU(4),

$$(T_{\gamma\delta})^{\mu'\nu'}_{\mu\nu} = i f_{\mu\nu,\gamma\delta,\mu'\nu'}, \tag{C.6}$$

about which we explain in Appendix A Eq. (A.33).

The key observation is that the first order term $\mathcal{I}^{(1)}_{\mu\nu}(x)$ contains all information about the symmetry breaking pattern and the associated NG modes, yielding their kinematic terms. On the other hand, the second order term $\mathcal{I}^{(2)}_{\mu\nu}(x)$ provides them with gaps. We apply the basic formula (C.1) to obtain the effective theories for the NG modes in $\nu = 1$ and all three phases in $\nu = 2$ bilayer QH systems.

C.1.1 $\nu = 1$ Bilayer QH Systems

We first analyze the $\nu = 1$ bilayer QH systems. The order parameters are given by (3.4), or

$$\mathcal{I}^{0}_{\mu\nu} = \frac{1}{2}\left(\delta_{\mu z}\delta_{\nu 0} + \sqrt{1-\sigma_0^2}(\delta_{\mu 0}\delta_{\nu x} + \delta_{\mu z}\delta_{\nu x}) + \sigma_0(\delta_{\mu 0}\delta_{\nu z} + \delta_{\mu z}\delta_{\nu z})\right). \tag{C.7}$$

We rotate this vector around the $0y$ axis so that only three components become nonzero. We can show that

$$\mathcal{I}^{\mathrm{r}(0)}_{\mu\nu} \equiv [V_{\sigma_0}(\theta_{\sigma_0})]^{\mu'\nu'}_{\mu\nu}\, \mathcal{I}^{(0)}_{\mu'\nu'} = \frac{1}{2}\left(\delta_{\mu z}\delta_{\nu 0} + \delta_{\mu 0}\delta_{\nu x} + \delta_{\mu z}\delta_{\nu x}\right), \tag{C.8}$$

by choosing the rotation as

$$V_{\sigma_0}(\theta_{\sigma_0}) = \exp(i\theta_{\sigma_0} T_{0y}), \tag{C.9}$$

with $\cos\theta_{\sigma_0} = \sqrt{1-\sigma_0^2}$ and $\sin\theta_{\sigma_0} = -\sigma_0$.

Let us relate the variables in the rotated system to the original variables in the formula (C.1). The SU(4) isospin operator after the rotation is given by

$$\mathcal{I}^{\mathrm{r}}_{\mu\nu}(x) = [V_{\sigma_0}(\theta_{\sigma_0})]^{\mu'\nu'}_{\mu\nu}\, \mathcal{I}_{\mu'\nu'}(x), \tag{C.10}$$

with the use of (C.9). We substitute (C.1) into this formula to find

$$\mathcal{I}^{\mathrm{r}}_{\mu\nu}(x) = \left[\exp\left(i\sum_{a=1}^{6}\pi_a T_a\right)\right]^{\mu'\nu'}_{\mu\nu} \mathcal{I}^{\mathrm{r}(0)}_{\mu'\nu'}, \tag{C.11}$$

where T_a are the broken generators given by

$$\begin{aligned} T_1 &= \frac{T_{x0}+T_{xx}}{2}, \quad T_2 = -\frac{T_{y0}+T_{yx}}{2}, \quad T_3 = \frac{T_{0y}+T_{zy}}{2}, \\ T_4 &= \frac{T_{0z}+T_{zz}}{2}, \quad T_5 = \frac{T_{xy}-T_{yz}}{2}, \quad T_6 = \frac{T_{xz}+T_{yy}}{2}, \end{aligned} \tag{C.12}$$

and (C.8) was used.

We go on to express the original SU(4) isospins in terms of these NG modes. The first step is to convert the relation (C.10) to express the original fields in terms of those in the rotated

system. Explicitly we have

$$\begin{aligned}
\mathcal{I}_{\mu x} &= \cos\theta_{\sigma_0}\mathcal{I}^{\rm r}_{\mu x} + \sin\theta_{\sigma_0}\mathcal{I}^{\rm r}_{\mu z},\\
\mathcal{I}_{\mu z} &= -\sin\theta_{\sigma_0}\mathcal{I}^{\rm r}_{\mu x} + \cos\theta_{\sigma_0}\mathcal{I}^{\rm r}_{\mu z},\\
\mathcal{I}_{a0} &= \mathcal{I}^{\rm r}_{a0}, \quad \mathcal{I}_{\mu y} = \mathcal{I}^{\rm r}_{\mu y}.
\end{aligned} \tag{C.13}$$

The second step is to expand (C.11) in terms of π_a,

$$\begin{aligned}
2\mathcal{I}^{\rm r}_{a0} &= \left(\pi_2 + \frac{1}{2}\left(\pi_3\pi_5 + \pi_4\pi_6\right), \pi_1 + \frac{1}{2}\left(\pi_3\pi_6 - \pi_4\pi_5\right), 1 - \frac{1}{2}\left(\pi_1^2 + \pi_2^2 + \pi_5^2 + \pi_6^2\right)\right),\\
2\mathcal{I}^{\rm r}_{0a} &= \left(p^{\rm r}_x({\rm s,p,r}), -\pi_2 - \frac{1}{2}(\pi_2\pi_6 - \pi_1\pi_5), p^{\rm r}_z({\rm s,p,r})\right),\\
2\mathcal{I}^{\rm r}_{xa} &= \left(r^{\rm r}_{xx}({\rm s,p,r}), -\pi_6 + \frac{1}{2}(\pi_3\pi_1 - \pi_4\pi_2), r^{\rm r}_{xz}({\rm s,p,r})\right),\\
2\mathcal{I}^{\rm r}_{ya} &= \left(r^{\rm r}_{yx}({\rm s,p,r}), \pi_5 - \frac{1}{2}(\pi_2\pi_3 + \pi_1\pi_4), r^{\rm r}_{yz}({\rm s,p,r})\right),\\
2\mathcal{I}^{\rm r}_{za} &= \left(r^{\rm r}_{zx}({\rm s,p,r}), -\pi_4 + \frac{1}{2}(\pi_2\pi_6 - \pi_1\pi_5), r_{zz}({\rm s,p,r})\right),
\end{aligned} \tag{C.14}$$

with

$$\begin{aligned}
&p^{\rm r}_x({\rm s,p,r}) = 1 - \frac{1}{2}\left(\pi_3^2 + \pi_4^2 + \pi_2^5 + \pi_2^6\right), \quad p^{\rm r}_z({\rm s,p,r}) = \pi_3 + \frac{1}{2}(\pi_2\pi_5 + \pi_1\pi_6),\\
&r^{\rm r}_{xx}({\rm s,p,r}) = \pi_2 - \frac{1}{2}\left(\pi_3\pi_5 + \pi_4\pi_6\right), \quad r^{\rm r}_{yx}({\rm s,p,r}) = \pi_1 - \frac{1}{2}\left(\pi_3\pi_6 - \pi_4\pi_5\right),\\
&r^{\rm r}_{xz}({\rm s,p,r}) = \pi_5 + \frac{1}{2}\left(\pi_2\pi_3 + \pi_1\pi_4\right), \quad r^{\rm r}_{yz}({\rm s,p,r}) = \pi_6 - \frac{1}{2}\left(\pi_2\pi_4 - \pi_1\pi_3\right),\\
&r^{\rm r}_{zx}({\rm s,p,r}) = 1 - \frac{1}{2}\left(\pi_2^1 + \pi_2^2 + \pi_2^5 + \pi_2^6\right), \quad r^{\rm r}_{zz}({\rm s,p,r}) = \pi_3 - \frac{1}{2}(\pi_2\pi_5 + \pi_1\pi_6).
\end{aligned} \tag{C.15}$$

The SU(4) isospin density fields $\mathcal{I}^{\rm r}_{\mu\nu}$ satisfy the SU(4) algebraic relations

$$\left[\mathcal{I}^{\rm r}_{\mu a}(\boldsymbol{x},t), \mathcal{I}^{\rm r}_{\mu b}(\boldsymbol{y},t)\right] = i\epsilon_{abc}\rho_\Phi^{-1}\mathcal{I}^{\rm r}_{0c}(\boldsymbol{x},t)\delta(\boldsymbol{x}-\boldsymbol{y}), \tag{C.16}$$

from which we obtain the canonical commutation relations for the NG modes,

$$\frac{\rho_0}{2}\left[\pi_2(\boldsymbol{x},t), \pi_1(\boldsymbol{y},t)\right] = i\delta(\boldsymbol{x}-\boldsymbol{y}), \quad \frac{\rho_0}{2}\left[\pi_{2a-1}(\boldsymbol{x},t), \pi_{2a}(\boldsymbol{y},t)\right] = i\delta(\boldsymbol{x}-\boldsymbol{y}), \tag{C.17}$$

with $a = 2, 3$.

By using a replacement

$$\begin{aligned}
&\pi_1 \to \vartheta_{\rm s}, \quad \pi_2 \to \sigma_{\rm s}, \quad \pi_3 \to \sigma_{\rm p},\\
&\pi_4 \to \vartheta_{\rm p}, \quad \pi_5 \to \sigma_{\rm r} \quad \pi_6 \to \vartheta_{\rm r},
\end{aligned} \tag{C.18}$$

in (C.14) with using (C.13), we obtain (3.16).

C.1.2 Spin Phase

We analyze the spin phase in $\nu = 2$ bilayer QH system. Setting $\alpha = 0$ in the order parameters (4.13), we obtain

$$\mathcal{I}^0_{\mu\nu} = \delta_{\mu z}\delta_{\nu 0}. \tag{C.19}$$

With the use of this, it is straighforward to calculate the first order term $\mathcal{I}^{(1)}_{\mu\nu}(x)$ in (C.4),

$$\mathcal{I}^{(1)}_{x\mu} = -\pi_{y\mu},\ \mathcal{I}^{(1)}_{y\mu} = \pi_{x\mu}. \tag{C.20}$$

There are eight fields $\pi_{y\mu}$ and $\pi_{x\mu}$ with $\mu = 0, x, y$ and z, which are the NG modes. Since they emerge in eight directions, $x\mu$ and $y\mu$, the broken generators are $T_{x\mu}$, and $T_{y\mu}$, implying that the unbroken generators are T_{z0}, $(T_{0a} + T_{za})/2$ and $(T_{0a} - T_{za})/2$.

We require (C.1) to satisfy the SU(4) algebraic relation

$$[\mathcal{I}_{a\mu}(\boldsymbol{x}, t), \mathcal{I}_{b\mu}(\boldsymbol{y}, t)] = i\epsilon_{abc}\rho_\Phi^{-1}\mathcal{I}_{c0}(\boldsymbol{x}, t)\delta(\boldsymbol{x} - \boldsymbol{y}), \tag{C.21}$$

so that the field $\mathcal{I}_{\mu\nu}$ describes the SU(4) isospin. From (C.21), we obtain the equal-time commutation relations for the NG modes,

$$[\tilde{\pi}_{x\mu}(\boldsymbol{x}, t), \tilde{\pi}_{y\mu}(\boldsymbol{y}, t)] = i\delta(\boldsymbol{x} - \boldsymbol{y}), \tag{C.22}$$

with $\tilde{\pi}_{\gamma\delta} = \rho_\Phi^{1/2}\pi_{\gamma\delta}$. Equivalently, we may construct a Lagrangian formalism so that (C.22) is the canonical commutation relation.

It follows from (C.2) and (C.20) that the eight NG modes are explicitly given by

$$\mathcal{S}_x = -\pi_{y0}, \quad \mathcal{S}_y = \pi_{x0}, \quad \mathcal{R}_{xa} = -\pi_{ya}, \quad \mathcal{R}_{ya} = \pi_{xa}, \tag{C.23}$$

and the other SU(4) isospins are described in terms of these eight NG fields as

$$\begin{aligned}
\mathcal{I}_{0y} &= \frac{\pi_{xz}\pi_{yx} + \pi_{yx}\pi_{xz} - \pi_{yz}\pi_{xx} - \pi_{xx}\pi_{yz}}{2} + \mathcal{O}(\pi^3),\\
\mathcal{I}_{0z} &= \frac{\pi_{xx}\pi_{yy} + \pi_{yy}\pi_{xx} - \pi_{xy}\pi_{yx} - \pi_{yx}\pi_{xy}}{2} + \mathcal{O}(\pi^3),\\
\mathcal{I}_{zx} &= -\frac{\pi_{yx}\pi_{y0} + \pi_{y0}\pi_{yx} + \pi_{xx}\pi_{x0} + \pi_{x0}\pi_{xx}}{2} + \mathcal{O}(\pi^3),\\
\mathcal{I}_{zy} &= -\frac{\pi_{yy}\pi_{y0} + \pi_{y0}\pi_{yy} + \pi_{xy}\pi_{x0} + \pi_{x0}\pi_{xy}}{2} + \mathcal{O}(\pi^3),\\
\mathcal{I}_{zz} &= -\frac{\pi_{yz}\pi_{y0} + \pi_{y0}\pi_{yz} + \pi_{xz}\pi_{x0} + \pi_{x0}\pi_{xz}}{2} + \mathcal{O}(\pi^3),\\
\mathcal{I}_{0x} &= \frac{\pi_{xy}\pi_{yz} + \pi_{yz}\pi_{xy} - \pi_{yy}\pi_{xz} - \pi_{xz}\pi_{yy}}{2} + \mathcal{O}(\pi^3),\\
\mathcal{I}_{z0} &= 1 - \sum_{\mu=0,x,y,z}\frac{(\pi_{x\mu})^2 + (\pi_{y\mu})^2}{2} + \mathcal{O}(\pi^3).
\end{aligned} \tag{C.24}$$

By using a replacement

$$\pi_{x0} \to \tilde{\vartheta}_1, \quad \pi_{y0} \to -\tilde{\sigma}_1, \quad \pi_{xx} \to \tilde{\vartheta}_2, \quad \pi_{yx} \to -\tilde{\sigma}_2,$$
$$\pi_{yy} \to -\tilde{\vartheta}_3, \quad \pi_{xy} \to -\tilde{\sigma}_3, \quad \pi_{xz} \to \tilde{\vartheta}_4, \quad \pi_{yz} \to -\tilde{\sigma}_4, \tag{C.25}$$

in (C.23) and (C.24), we see that Eq. (4.46) is reproduced.

C.1.3 Pseudospin Phase

We next analyze the pseudospin phase. Setting $\alpha = 1$ in the order parameters (4.13), we obtain

$$\mathcal{I}^0_{\mu\nu} = \sqrt{1-\beta^2}\delta_{\mu 0}\delta_{\nu x} + \beta\delta_{\mu 0}\delta_{\nu z}. \tag{C.26}$$

In order to determine the symmetry breaking pattern, we rotate this vector around the $0y$ axis as we have done in the analysis for $\nu = 1$, so that only one component becomes nonzero. We can show that

$$\mathcal{I}^{\mathrm{p}(0)}_{\mu\nu} \equiv [V_\beta(\theta_\beta)]^{\mu'\nu'}_{\mu\nu}\, \mathcal{I}^{(0)}_{\mu'\nu'} = \delta_{\mu 0}\delta_{\nu x}, \tag{C.27}$$

by choosing

$$V_\beta(\theta_\beta) = \exp(i\theta_\beta T_{0y}), \tag{C.28}$$

with $\cos\theta_\beta = \sqrt{1-\beta^2}$ and $\sin\theta_\beta = -\beta$.

In the rotated basis the order parameter has a single nonzero component just as (C.19) in the case of the spin phase. Therefore the further analysis goes in parallel with that given in the previous analysis. Namely, there are eight NG fields,

$$\mathcal{I}^{\mathrm{p}(1)}_{\mu y} = -\pi^{\mathrm{p}}_{\mu z}, \quad \mathcal{I}^{\mathrm{p}(1)}_{\mu z} = \pi^{\mathrm{p}}_{\mu y}. \tag{C.29}$$

The unbroken generators are T_{0x}, $(T_{a0}+T_{ax})/2$, and $(T_{a0}-T_{ax})/2$.

We relate the variables in the rotated system to the original variables in the formula (C.1). The SU(4) isospin operator after the rotation is given by

$$\mathcal{I}^{\mathrm{p}}_{\mu\nu}(x) = [V_\beta(\theta_\beta)]^{\mu'\nu'}_{\mu\nu}\, \mathcal{I}_{\mu'\nu'}(x), \tag{C.30}$$

with the use of (C.28). We substitute (C.1) into this formula to find

$$\mathcal{I}^{\mathrm{p}}_{\mu\nu}(x) = \left[\exp\left(i\sum_{\gamma\delta}\pi^{\mathrm{p}}_{\gamma\delta}T_{\gamma\delta}\right)\right]^{\mu'\nu'}_{\mu\nu} \mathcal{I}^{\mathrm{p}(0)}_{\mu'\nu'}, \tag{C.31}$$

with (C.27), where $\pi^{\mathrm{p}}_{\gamma\delta}$ is defined by

$$\pi^{\mathrm{p}}_{\gamma\delta} = [V_\beta(\theta_\beta)]^{\gamma'\delta'}_{\gamma\delta}\, \pi_{\gamma'\delta'}, \tag{C.32}$$
$$\mathcal{I}^{\mathrm{p}(0)}_{\gamma\delta} = [V_\beta(\theta_\beta)]^{\gamma'\delta'}_{\gamma\delta}\, \mathcal{I}^0_{\gamma'\delta'}, \tag{C.33}$$

while $\mathcal{I}^{\mathrm{p}(0)}_{\gamma\delta}$ has been used by (C.27). Here, we have used the formula of the SU(N) group,

$$\sum_b T_b \Phi'_b = \sum_b T_b \left[\exp i\theta_a \mathrm{Ad}(T_a)\right]^c_b \Phi_c = \exp\left[i\theta_a T_a\right] \Phi_b T_b \exp\left[-i\theta_a T_a\right], \tag{C.34}$$

where Φ_b is an arbitrary adjoint vector with $a, b, c = 1, \ldots,$ dim SU(N), and $\exp\left[i\theta_a T_a\right]$ is the element of SU(N). Here we have N= 4 and Φ_b corresponds to $\pi_{\mu\nu}$.

The SU(4) isospin density fields $\mathcal{I}^{\mathrm{p}}_{\mu\nu}$ satisfy the SU(4) algebraic relations

$$\left[\mathcal{I}^{\mathrm{p}}_{\mu a}(\boldsymbol{x}, t), \mathcal{I}^{\mathrm{p}}_{\mu b}(\boldsymbol{y}, t)\right] = i\epsilon_{abc}\rho_\Phi^{-1}\mathcal{I}^{\mathrm{p}}_{0c}(\boldsymbol{x}, t)\delta(\boldsymbol{x} - \boldsymbol{y}), \tag{C.35}$$

from which we obtain the canonical commutation relations for the NG modes,

$$\left[\tilde{\pi}^{\mathrm{p}}_{\mu y}(\boldsymbol{x}, t), \tilde{\pi}^{\mathrm{p}}_{\mu z}(\boldsymbol{y}, t)\right] = i\delta(\boldsymbol{x} - \boldsymbol{y}), \tag{C.36}$$

with $\tilde{\pi}^{\mathrm{p}}_{\mu\nu} = \rho_\Phi^{1/2}\pi^{\mathrm{p}}_{\mu\nu}$.

By applying the same argument given in the analysis for $\nu = 1$, the SU(4) isospins are expressed in terms of $\pi^{\mathrm{p}}_{\mu\nu}$ as

$$\begin{aligned}
\mathcal{I}_{\mu x} &= \cos\theta_\beta \mathcal{I}^{\mathrm{p}}_{\mu x} + \sin\theta_\beta \mathcal{I}^{\mathrm{p}}_{\mu z}, \\
\mathcal{I}_{\mu z} &= -\sin\theta_\beta \mathcal{I}^{\mathrm{p}}_{\mu x} + \cos\theta_\beta \mathcal{I}^{\mathrm{p}}_{\mu z}, \\
\mathcal{I}_{a0} &= \mathcal{I}^{\mathrm{p}}_{a0}, \quad \mathcal{I}_{\mu y} = \mathcal{I}^{\mathrm{p}}_{\mu y}.
\end{aligned} \tag{C.37}$$

where $\mathcal{I}^{\mathrm{p}}_{\mu\nu}$ are given by

$$\begin{aligned}
\mathcal{I}^{\mathrm{p}}_{\mu y} &= -\pi^{\mathrm{p}}_{\mu z} + \mathcal{O}(\pi^2),\ \mathcal{I}^{\mathrm{p}}_{\mu z} = \pi^{\mathrm{p}}_{\mu y} + \mathcal{O}(\pi^2), \\
\mathcal{I}^{\mathrm{p}}_{x0} &= \frac{\pi^{\mathrm{p}}_{zz}\pi^{\mathrm{p}}_{yy} + \pi^{\mathrm{p}}_{yy}\pi^{\mathrm{p}}_{zz} - \pi^{\mathrm{p}}_{zy}\pi^{\mathrm{p}}_{yz} - \pi^{\mathrm{p}}_{yz}\pi^{\mathrm{p}}_{zy}}{2} + \mathcal{O}(\pi^3), \\
\mathcal{I}^{\mathrm{p}}_{y0} &= \frac{\pi^{\mathrm{p}}_{zy}\pi^{\mathrm{p}}_{xz} + \pi^{\mathrm{p}}_{xz}\pi^{\mathrm{p}}_{zy} - \pi^{\mathrm{p}}_{zz}\pi^{\mathrm{p}}_{xy} - \pi^{\mathrm{p}}_{xy}\pi^{\mathrm{p}}_{zz}}{2} + \mathcal{O}(\pi^3), \\
\mathcal{I}^{\mathrm{p}}_{z0} &= \frac{\pi^{\mathrm{p}}_{xy}\pi^{\mathrm{p}}_{yz} + \pi^{\mathrm{p}}_{yz}\pi^{\mathrm{p}}_{xy} - \pi^{\mathrm{p}}_{yy}\pi^{\mathrm{p}}_{xz} - \pi^{\mathrm{p}}_{xz}\pi^{\mathrm{p}}_{yy}}{2} + \mathcal{O}(\pi^3), \\
\mathcal{I}^{\mathrm{p}}_{xx} &= -\frac{\pi^{\mathrm{p}}_{xz}\pi^{\mathrm{p}}_{0z} + \pi^{\mathrm{p}}_{0z}\pi^{\mathrm{p}}_{xz} + \pi^{\mathrm{p}}_{xy}\pi^{\mathrm{p}}_{0y} + \pi^{\mathrm{p}}_{0y}\pi^{\mathrm{p}}_{xy}}{2} + \mathcal{O}(\pi^3), \\
\mathcal{I}^{\mathrm{p}}_{yx} &= -\frac{\pi^{\mathrm{p}}_{yz}\pi^{\mathrm{p}}_{0z} + \pi^{\mathrm{p}}_{0z}\pi^{\mathrm{p}}_{yz} + \pi^{\mathrm{p}}_{yy}\pi^{\mathrm{p}}_{0y} + \pi^{\mathrm{p}}_{0y}\pi^{\mathrm{p}}_{yy}}{2} + \mathcal{O}(\pi^3), \\
\mathcal{I}^{\mathrm{p}}_{zx} &= -\frac{\pi^{\mathrm{p}}_{zz}\pi^{\mathrm{p}}_{0z} + \pi^{\mathrm{p}}_{0z}\pi^{\mathrm{p}}_{zz} + \pi^{\mathrm{p}}_{zy}\pi^{\mathrm{p}}_{0y} + \pi^{\mathrm{p}}_{0y}\pi^{\mathrm{p}}_{zy}}{2} + \mathcal{O}(\pi^3), \\
\mathcal{I}^{\mathrm{p}}_{0x} &= 1 - \sum_{\mu=0,x,y,z} \frac{(\pi^{\mathrm{p}}_{\mu y})^2 + (\pi^{\mathrm{p}}_{\mu z})^2}{2} + \mathcal{O}(\pi^3).
\end{aligned} \tag{C.38}$$

Using the following replacement

$$\begin{aligned}
&\pi^{\rm p}_{zz} \to -\tilde{\vartheta}_1, \quad \pi^{\rm p}_{zy} \to -\tilde{\sigma}_1, \quad \pi^{\rm p}_{0z} \to -\tilde{\vartheta}_2, \quad \pi^{\rm p}_{0y} \to -\tilde{\sigma}_2, \\
&\pi^{\rm p}_{xz} \to -\tilde{\vartheta}_3, \quad \pi^{\rm p}_{xy} \to -\tilde{\sigma}_3, \quad \pi^{\rm p}_{yy} \to \tilde{\vartheta}_4, \quad \pi^{\rm p}_{yz} \to -\tilde{\sigma}_4,
\end{aligned} \tag{C.39}$$

in (C.38) with using (C.2), we obtain (4.75).

C.1.4 CAF Phase

Finally we analyze the CAF phase. This phase is characterized by the order parameters (4.13), which we may rewrite as

$$\begin{aligned}
\mathcal{I}^{(0)}_{\mu\nu} &= c_{\theta_\delta} c_{\theta_\alpha} \delta_{\mu z}\delta_{\nu 0} + s_{\theta_\delta} s_{\theta_\alpha} \left(c_{\theta_\beta}\delta_{\mu 0}\delta_{\nu x} - s_{\theta_\beta}\delta_{\mu 0}\delta_{\nu z}\right) \\
&\quad + s_{\theta_\delta} c_{\theta_\alpha} s_{\theta_\beta}\delta_{\mu x}\delta_{\nu x} - c_{\theta_\delta} s_{\theta_\alpha}\delta_{\mu y}\delta_{\nu y} + s_{\theta_\delta} c_{\theta_\alpha} c_{\theta_\beta}\delta_{\mu x}\delta_{\nu z},
\end{aligned} \tag{C.40}$$

where

$$\begin{aligned}
c_{\theta_\alpha} &\equiv \cos\theta_\alpha = \sqrt{1-\alpha^2}, \quad s_{\theta_\alpha} \equiv \sin\theta_\alpha = \alpha, \\
c_{\theta_\beta} &\equiv \cos\theta_\beta = \sqrt{1-\beta^2}, \quad s_{\theta_\beta} \equiv \sin\theta_\beta = -\beta, \\
c_{\theta_\delta} &\equiv \cos\theta_\delta = \frac{\Delta_Z\sqrt{1-\beta^2}}{\Delta_0}\sqrt{1-\alpha^2}, \quad s_{\theta_\delta} \equiv \sin\theta_\delta = \frac{\Delta_{\rm SAS}}{\Delta_0}\alpha.
\end{aligned} \tag{C.41}$$

The order parameter $\mathcal{I}^{(0)}_{\mu\nu}$ is quite complicated. Nevertheless, the problem is just to find an appropriate rotation in the SU(4) space so that the order parameter has only a single nonzero component after the rotation.

There are two ways. One is by choosing the rotational transformation as

$$U^s_{\alpha,\beta} = \exp[i\theta_\delta T_{yz}]\exp[i\theta_\alpha T_{xy}]V_\beta(\theta_\beta), \tag{C.42}$$

with V_β given by (C.28), and we obtain

$$\mathcal{I}^{{\rm sc}(0)}_{\mu\nu} \equiv \left[U^s_{\alpha,\beta}\right]^{\mu'\nu'}_{\mu\nu} \mathcal{I}^{(0)}_{\mu'\nu'} = \delta_{\mu z}\delta_{\nu 0}. \tag{C.43}$$

In this rotated basis, the further analysis goes in parallel with that given in the spin phase. Another choice of the rotational transformation is given by

$$\begin{aligned}
U^p_{\alpha,\beta} &= \exp\left[i\left(\theta_\delta - \frac{\pi}{2}\right)T_{yz}\right]\exp\left[i\left(\theta_\alpha - \frac{\pi}{2}\right)T_{xy}\right]V_\beta(\theta_\beta), \\
&= \exp\left[-i\frac{\pi}{2}T_{yz}\right]\exp\left[-i\frac{\pi}{2}T_{xy}\right]U^s_{\alpha,\beta},
\end{aligned} \tag{C.44}$$

obtaining

$$\mathcal{I}^{{\rm pc}(0)}_{\mu\nu} \equiv \left[U^p_{\alpha,\beta}\right]^{\mu'\nu'}_{\mu\nu} \mathcal{I}^{(0)}_{\mu'\nu'} = \delta_{\mu 0}\delta_{\nu x}. \tag{C.45}$$

In this rotated basis, the further analysis goes in parallel with that given in the pseudospin

phase. We call the rotated basis of the SU(4) group given by (C.42), the s-coordinate, and the rotated basis given by (C.44), the p-coordinate. They give the identical results.

We make an analysis by employing the s-coordinate. Namely, we define the SU(4) isospin operator in the s-coordinate by

$$\begin{aligned}\mathcal{I}^{\rm sc}_{\mu\nu}(x) &= \left[U^{s}_{\alpha,\beta}\right]^{\mu'\nu'}_{\mu\nu}\mathcal{I}_{\mu'\nu'}(x) \\ &= \left[\exp\left(i\sum_{\gamma\delta}\pi^{\rm sc}_{\gamma\delta}T_{\gamma\delta}\right)\right]^{\mu'\nu'}_{\mu\nu}\mathcal{I}^{\rm sc(0)}_{\mu'\nu'},\end{aligned} \tag{C.46}$$

where

$$\pi^{\rm sc}_{\gamma\delta} = \left[U^{s}_{\alpha,\beta}\right]^{\gamma'\delta'}_{\gamma\delta}\pi_{\gamma'\delta'} \tag{C.47}$$

with (C.1) and (C.34).

The eight NG fields are,

$$\mathcal{I}^{\rm sc(1)}_{x\mu} = -\pi^{\rm sc}_{y\mu}, \quad \mathcal{I}^{\rm sc(1)}_{y\mu} = \pi^{\rm sc}_{x\mu}. \tag{C.48}$$

Here we remark how the NG modes in the CAF phase are transformed into those in spin/pseudospin phase at the phase boundary. On one hand, the field $\pi^{\rm sc}_{\mu\nu}$ shifts smoothly to the field (C.23), by the inverse transformation of (C.42), or by taking the limit $\alpha, \beta \to 0$, as

$$\pi^{\rm sc}_{\mu\nu} \to \pi_{\mu\nu}, \tag{C.49}$$

so that subscript of $\pi^{\rm sc}_{\mu\nu}$ perfectly matches with $\pi_{\mu\nu}$ for each $\mu\nu$ in the spin phase. On the other hand, $\pi^{\rm sc}_{\mu\nu}$ shifts smoothly to (C.32), by the inverse transformation of $\exp(i\theta_\delta T_{yz})\exp(i\theta_\alpha T_{xy})$, or taking the limit $\alpha \to 1$ as

$$\begin{aligned}&\pi^{\rm sc}_{x0} \to -\pi^{\rm p}_{zz}, \quad \pi^{\rm sc}_{y0} \to \pi^{\rm p}_{zy}, \\ &\pi^{\rm sc}_{xx} \to -\pi^{\rm p}_{0z}, \quad \pi^{\rm sc}_{yx} \to \pi^{\rm p}_{0y}, \\ &\pi^{\rm sc}_{xz} \to \pi^{\rm p}_{yy}, \quad \pi^{\rm sc}_{yz} \to \pi^{\rm p}_{yz}, \\ &\pi^{\rm sc}_{xy} \to \pi^{\rm p}_{xy}, \quad \pi^{\rm sc}_{yy} \to \pi^{\rm p}_{xz},\end{aligned} \tag{C.50}$$

for the fields in the pseudopin phase.

We require (C.46) to satisfy the SU(4) algebraic relation,

$$\left[\mathcal{I}^{\rm sc}_{x\mu}(\boldsymbol{x},t), \mathcal{I}^{\rm sc}_{y\mu}(\boldsymbol{y},t)\right] = i\rho_\Phi^{-1}\mathcal{I}^{\rm sc}_{z0}(\boldsymbol{x},t)\delta(\boldsymbol{x}-\boldsymbol{y}), \tag{C.51}$$

from which we obtain the canonical commutation relation,

$$\left[\tilde{\pi}^{\rm sc}_{x\mu}(\boldsymbol{x},t), \tilde{\pi}^{\rm sc}_{y\mu}(\boldsymbol{y},t)\right] = i\delta(\boldsymbol{x}-\boldsymbol{y}), \tag{C.52}$$

with $\tilde{\pi}^{\rm sc}_{\mu\nu} = \rho_\Phi^{1/2}\pi^{\rm sc}_{\mu\nu}$.

We express the rotated isospin fields $\mathcal{I}^{\rm sc}_{\mu\nu}$ in terms of the eight NG fields $\pi^{\rm sc}_{\mu\nu}$ up to the second order,

$$\begin{aligned}
\mathcal{I}^{\rm sc}_{x\mu} &= -\pi^{\rm sc}_{y\mu} + \mathcal{O}(\pi^2),\ \mathcal{I}^{\rm sc}_{y\mu} = \pi^{\rm sc}_{x\mu} + \mathcal{O}(\pi^2),\\
\mathcal{I}^{\rm sc}_{0y} &= \frac{\pi^{\rm sc}_{xz}\pi^{\rm sc}_{yx} + \pi^{\rm sc}_{yx}\pi^{\rm sc}_{xz} - \pi^{\rm sc}_{yz}\pi^{\rm sc}_{xx} - \pi^{\rm sc}_{xx}\pi^{\rm sc}_{yz}}{2} + \mathcal{O}(\pi^3),\\
\mathcal{I}^{\rm sc}_{0z} &= \frac{\pi^{\rm sc}_{xx}\pi^{\rm sc}_{yy} + \pi^{\rm sc}_{yy}\pi^{\rm sc}_{xx} - \pi^{\rm sc}_{xy}\pi^{\rm sc}_{yx} - \pi^{\rm sc}_{yx}\pi^{\rm sc}_{xy}}{2} + \mathcal{O}(\pi^3),\\
\mathcal{I}^{\rm sc}_{zx} &= -\frac{\pi^{\rm sc}_{yx}\pi^{\rm sc}_{y0} + \pi^{\rm sc}_{y0}\pi^{\rm sc}_{yx} + \pi^{\rm sc}_{xx}\pi^{\rm sc}_{x0} + \pi^{\rm sc}_{x0}\pi^{\rm sc}_{xx}}{2} + \mathcal{O}(\pi^3),\\
\mathcal{I}^{\rm sc}_{zy} &= -\frac{\pi^{\rm sc}_{yy}\pi^{\rm sc}_{y0} + \pi^{\rm sc}_{y0}\pi^{\rm sc}_{yy} + \pi^{\rm sc}_{xy}\pi^{\rm sc}_{x0} + \pi^{\rm sc}_{x0}\pi^{\rm sc}_{xy}}{2} + \mathcal{O}(\pi^3),\\
\mathcal{I}^{\rm sc}_{zz} &= -\frac{\pi^{\rm sc}_{yz}\pi^{\rm sc}_{y0} + \pi^{\rm sc}_{y0}\pi^{\rm sc}_{yz} + \pi^{\rm sc}_{xz}\pi^{\rm sc}_{x0} + \pi^{\rm sc}_{x0}\pi^{\rm sc}_{xz}}{2} + \mathcal{O}(\pi^3),\\
\mathcal{I}^{\rm sc}_{0x} &= \frac{\pi^{\rm sc}_{xy}\pi^{\rm sc}_{yz} + \pi^{\rm sc}_{yz}\pi^{\rm sc}_{xy} - \pi^{\rm sc}_{yy}\pi^{\rm sc}_{xz} - \pi^{\rm sc}_{xz}\pi^{\rm sc}_{yy}}{2} + \mathcal{O}(\pi^3),\\
\mathcal{I}^{\rm sc}_{z0} &= 1 - \sum_{\mu=0,x,y,z} \frac{(\pi^{\rm sc}_{x\mu})^2 + (\pi^{\rm sc}_{y\mu})^2}{2} + \mathcal{O}(\pi^3).
\end{aligned} \tag{C.53}$$

We next give the relation between the original isospin field $\mathcal{I}_{\mu\nu}$ and the rotated field $\mathcal{I}^{\rm sc}_{\mu\nu}$ in

the s-coordinate of the CAF phase. It is given by

$$
\begin{aligned}
\mathcal{I}_{0x} &= \cos\theta_\alpha \cos\theta_\beta \cos\theta_\delta \mathcal{I}^{\rm sc}_{0x} + \cos\theta_\alpha \sin\theta_\beta \mathcal{I}^{\rm sc}_{0z} - \sin\theta_\alpha \sin\theta_\beta \mathcal{I}^{\rm sc}_{xx} + \sin\theta_\alpha \cos\theta_\beta \cos\theta_\delta \mathcal{I}^{\rm sc}_{xz} \\
&\quad - \cos\theta_\alpha \cos\theta_\beta \sin\theta_\delta \mathcal{I}^{\rm sc}_{yy} + \sin\theta_\alpha \cos\theta_\beta \sin\theta_\delta \mathcal{I}^{\rm sc}_{z0}, \\
\mathcal{I}_{0y} &= \cos\theta_\delta \mathcal{I}^{\rm sc}_{0y} + \sin\theta_\delta \mathcal{I}^{\rm sc}_{yx}, \\
\mathcal{I}_{0z} &= -\cos\theta_\alpha \sin\theta_\beta \cos\theta_\delta \mathcal{I}^{\rm sc}_{0x} + \cos\theta_\alpha \cos\theta_\beta \mathcal{I}^{\rm sc}_{0z} - \sin\theta_\alpha \cos\theta_\beta \mathcal{I}^{\rm sc}_{xx} - \sin\theta_\alpha \sin\theta_\beta \cos\theta_\delta \mathcal{I}^{\rm sc}_{xz} \\
&\quad + \cos\theta_\alpha \sin\theta_\beta \sin\theta_\delta \mathcal{I}^{\rm sc}_{yy} - \sin\theta_\alpha \sin\theta_\beta \sin\theta_\delta \mathcal{I}^{\rm sc}_{z0}, \\
\mathcal{I}_{x0} &= \cos\theta_\delta \mathcal{I}^{\rm sc}_{x0} + \sin\theta_\delta \mathcal{I}^{\rm sc}_{zz}, \\
\mathcal{I}_{xx} &= -\sin\theta_\alpha \sin\theta_\beta \cos\theta_\delta \mathcal{I}^{\rm sc}_{0x} + \sin\theta_\alpha \cos\theta_\beta \mathcal{I}^{\rm sc}_{0z} + \cos\theta_\alpha \cos\theta_\beta \mathcal{I}^{\rm sc}_{xx} + \cos\theta_\alpha \sin\theta_\beta \cos\theta_\delta \mathcal{I}^{\rm sc}_{xz} \\
&\quad + \sin\theta_\alpha \sin\theta_\beta \sin\theta_\delta \mathcal{I}^{\rm sc}_{yy} + \cos\theta_\alpha \sin\theta_\beta \sin\theta_\delta \mathcal{I}^{\rm sc}_{z0}, \\
\mathcal{I}_{xy} &= \mathcal{I}^{\rm sc}_{xy}, \\
\mathcal{I}_{xz} &= -\sin\theta_\alpha \cos\theta_\beta \cos\theta_\delta \mathcal{I}^{\rm sc}_{0x} - \sin\theta_\alpha \sin\theta_\beta \mathcal{I}^{\rm sc}_{0z} - \cos\theta_\alpha \sin\theta_\beta \mathcal{I}^{\rm sc}_{xx} + \cos\theta_\alpha \cos\theta_\beta \cos\theta_\delta \mathcal{I}^{\rm sc}_{xz} \\
&\quad + \sin\theta_\alpha \cos\theta_\beta \sin\theta_\delta \mathcal{I}^{\rm sc}_{yy} + \cos\theta_\alpha \cos\theta_\beta \sin\theta_\delta \mathcal{I}^{\rm sc}_{z0}, \\
\mathcal{I}_{y0} &= \cos\theta_\alpha \mathcal{I}^{\rm sc}_{y0} - \sin\theta_\alpha \mathcal{I}^{\rm sc}_{zy}, \\
\mathcal{I}_{yx} &= -\cos\theta_\beta \sin\theta_\delta \mathcal{I}^{\rm sc}_{0y} + \cos\theta_\beta \cos\theta_\delta \mathcal{I}^{\rm sc}_{yx} + \sin_{\theta_\beta} \mathcal{I}^{\rm sc}_{yz}, \\
\mathcal{I}_{yy} &= \cos\theta_\alpha \sin\theta_\delta \mathcal{I}^{\rm sc}_{0x} + \sin\theta_\alpha \sin\theta_\delta \mathcal{I}^{\rm sc}_{xz} + \cos\theta_\alpha \cos\theta_\delta \mathcal{I}^{\rm sc}_{yy} - \sin\theta_\alpha \cos\theta_\delta \mathcal{I}^{\rm sc}_{z0}, \\
\mathcal{I}_{yz} &= \sin\theta_\beta \sin_{\theta_\delta} \mathcal{I}^{\rm sc}_{0y} - \sin\theta_\beta \cos\theta_\delta \mathcal{I}^{\rm sc}_{yx} + \cos\theta_\beta \mathcal{I}^{\rm sc}_{yz}, \\
\mathcal{I}_{z0} &= \sin\theta_\alpha \sin\theta_\delta \mathcal{I}^{\rm sc}_{0x} - \cos\theta_\alpha \sin\theta_\delta \mathcal{I}^{\rm sc}_{xz} + \sin\theta_\alpha \cos\theta_\delta \mathcal{I}^{\rm sc}_{yy} + \cos\theta_\alpha \cos\theta_\delta \mathcal{I}^{\rm sc}_{z0}, \\
\mathcal{I}_{zx} &= -\sin\theta_\beta \sin\theta_\delta \mathcal{I}^{\rm sc}_{x0} + \cos\theta_\beta \mathcal{I}^{\rm sc}_{zx} + \sin\theta_\beta \cos\theta_\delta \mathcal{I}^{\rm sc}_{zz}, \\
\mathcal{I}_{zy} &= \sin\theta_\alpha \mathcal{I}^{\rm sc}_{y0} + \cos\theta_\alpha \mathcal{I}^{\rm sc}_{zy}, \\
\mathcal{I}_{zz} &= -\cos\theta_\beta \sin\theta_\delta \mathcal{I}^{\rm sc}_{x0} - \sin\theta_\beta \mathcal{I}^{\rm sc}_{zx} + \cos\theta_\beta \cos\theta_\delta \mathcal{I}^{\rm sc}_{zz},
\end{aligned}
\tag{C.54}
$$

with (C.41).

By using the correspondence

$$
\begin{aligned}
&\pi^{\rm sc}_{x0} \to \tilde{\vartheta}_1, \quad \pi^{\rm sc}_{y0} \to -\tilde{\sigma}_1, \quad \pi^{\rm sc}_{xx} \to \tilde{\vartheta}_2, \quad \pi^{\rm sc}_{yx} \to -\tilde{\sigma}_2, \\
&\pi^{\rm sc}_{yy} \to -\tilde{\vartheta}_3, \quad \pi^{\rm sc}_{xy} \to -\tilde{\sigma}_3, \quad \pi^{\rm sc}_{xz} \to \tilde{\vartheta}_4, \quad \pi^{\rm sc}_{yz} \to -\tilde{\sigma}_4,
\end{aligned}
\tag{C.55}
$$

with (C.54), we reproduce (4.39).

Bibliography

[1] S. Chikazumi, *Physics of Ferromagnetism*, (Oxford University Press, USA, 2009).

[2] T. Oguchi, *Statistical Theory of Magnetism*, (Syōkabō, Tokyo, 1970).

[3] S. Murakami, N. Nagaosa, and S.-C. Zhang, Science **301**, 1348 (2003).

[4] S. Murakami, N. Nagaosa, and S.-C. Zhang, Phys. Rev. Lett. **93**, 156804 (2004).

[5] J. Sinova, D. Culcer, Q. Niu, N. A. Sinitsyn, T. Jungwirth, and A. H. MacDonald, Phys. Rev. Lett. **92**, 126603 (2004).

[6] J. Wunderlich, B. Kaestner, J. Sinova, and T. Jungwirth, Phys. Rev. Lett. **94**, 047204 (2005).

[7] C. L. Kane and E. J. Mele, Phys. Rev. Lett. **95**, 226801 (2005).

[8] N. Nagaosa, J. Sinova, S. Onoda, A. H. MacDonald, and N. P. Ong, Rev. Mod. Phys. **82**, 1539 (2010).

[9] I. Žutić, J. Fabian, and S. D. Sarma, Rev. Mod. Phys. **76**, 323 (2004).

[10] D. D. Awschalom and M. E. Flatté, Nature. Phys. **3**, 153 (2007).

[11] S. Hikino and S. Yunoki, Phys. Rev. Lett. **110**, 237003 (2013).

[12] R. Matsumoto and S. Murakami, Phys. Rev. B **84**, 184406 (2011).

[13] J. H. Smet R. A. Deutschmann, F. Ertl, W. Wegscheider, G. Abstreiter, & K. von Klitzing, Nature **415**, 281 (2002).

[14] Y. Hirayama, G. Yusa, K. Hashimoto, N. Kumada, T. Ota, and K. Muraki, Semicond. Sci. Technol. **24,** 023001 (2009).

[15] K. Nomura, and A. H. MacDonald, Phys. Rev. Lett. **96**, 256602 (2006).

[16] K. Yang, S. Das Sarma, and A. H. MacDonald, Phys. Rev. B **74**, 075423 (2006).

[17] B. Douçot, M. O. Goerbig, P. Lederer, and R. Moessner, Phys. Rev. B **78**, 195327 (2008).

[18] M. Kharitonov, Phys. Rev. B **85**, 155439 (2012).

[19] E. Minamitani, N. Tsukahara, D. Matsunaka, Y. Kim, N. Takagi, and M. Kawai, Phys. Rev. Lett. **109**. 086602 (2012).

[20] C. L. Kane and E. J. Mele, Phys. Rev. Lett. **95**. 146802 (2005).

[21] L. Fu and C. L. Kane, Phys. Rev. B. **76**. 045302 (2007).

[22] J. E. Moore and L. Balents, Phys. Rev. B. **75**. 121306(R) (2007).

[23] L. Fu, C. L. Kane, and E. J. Mele, Phys. Rev. Lett. **98**. 106803 (2007).

[24] M. König, S. Wiedmann, C. Brüne, A. Roth, H. Buhmann, L. W. Molenkamp, X.-L. Qi, and S.-C. Zhang, Science **318**. 766 (2007).

[25] S. Murakami and S. Kuga, Phys. Rev. B. **78**. 165313 (2008).

[26] X.-L. Qi, T. L. Hughes, and S.-C. Zhang, Phys. Rev. B. **78**. 195424 (2008).

[27] A. Roth, C. Brüne, H. Buhmann, L. W. Molenkamp, J. Maciejko, X.-L. Qi, and S.-C.

Zhang, Science **325**, 294 (2009).

[28] P. Cheng, C. Song, T. Zhang, Y. Zhang, Y. Wang, J.-F. Jia, J. Wang, Y. Wang, B.-F. Zhu, X. Chen, X. Ma, K. He, L. Wang, X. Dai, Z. Fang, X. Xie, X.-L. Qi, C.-X. Liu, S.-C. Zhang, and Q.-K. Xue, Phys. Rev. Lett. **105**. 076801 (2010).

[29] T. Hanaguri, K. Igarashi, M. Kawamura, H. Takagi, and T. Sagawa, Phys. Rev. B. **82**, 081305(R) (2010).

[30] M. Z. Hasan and C. L. Kane, Rev. Mod. Phys. **82**, 3045 (2010).

[31] X.-L. Qi and S.-C. Zhang, Rev. Mod. Phys. **83**, 1057 (2011).

[32] Y. Ando, J. Phys. Soc. Jpn. **82**, 102001 (2013).

[33] Y. Zheng and T. Ando, Phys. Rev. B **65**, 245420 (2002).

[34] K. S. Novoselov, A. K. Geim, S. V. Morozov, D. Jiang, M. I. Katsnelson, I. V. Grigorieva, S. V. Dubonos, and A. A. Firsov, Nature **438**, 197 (2005).

[35] Y. Zhang, Y. W. Tan, H. L. Stormer, and P. Kim, Nature **438**, 201 (2005).

[36] V. P. Gusynin and S. G. Sharapov, Phys. Rev. Lett. **95**, 146801 (2005).

[37] A. H. Castro Neto, F. Guinea, N. M. R. Peres, K. S. Novoselov, and A. K. Geim, Rev. Mod. Phys. **81**, 109 (2009).

[38] M. O. Goerbig, Rev. Mod. Phys. **83**, 1193 (2011).

[39] K. S. Novoselov, E. McCann, S. V. Morozov, V. I. Fal'ko, M. I. Katsnelson, U. Zeitler, D. Jiang, F. Schedin, and A. K. Geim, Nature. Phys. **2**, 177 (2006).

[40] E. McCann and V. I. Fal'ko, Phys. Rev. Lett. **96**, 086805 (2006).

[41] M. Koshino and T. Ando, Phys. Rev. B **73**, 245403 (2006).

[42] A. Pikovski, M. Klawunn, G. V. Shlyapnikov, and L. Santos, Phys. Rev. Lett. **105**, 215302 (2010).

[43] R. M. Lutchyn, E. Rossi, and S. D. Sarma, Phys. Rev. A **82**, 061604(R) (2010).

[44] R. Tamagaki and T. Takatsuka, Prog. Theor. Phys. **56**, 1340 (1976).

[45] T. Kunihiro, Prog. Theor. Phys. **60**, 1229 (1978).

[46] T. H. R. Skyrme, Proc. Roy. Soc. (London) **A260**, 127 (1961).

[47] S. L. Sondhi, A. Karlhede, S. A. Kivelson, and E. H. Reyazi, Phys. Rev. B. **47**, 16419 (1993).

[48] S. E. Barrett, G. Dabbagh, L. N. Pfeiffer, K. W. West, and R. Tycko, Phys. Rev. Lett. **74**, 5112 (1995).

[49] H. A. Fertig, L. Brey, R. Côté, A. H. MacDonald, A. Karlhede, and S. L. Sondhi, Phys. Rev. B. **55**, 10671 (1997).

[50] H. A. Fertig, L. Brey, R. Côté, and A. H. MacDonald, Phys. Rev. B. **50**, 11018 (1997).

[51] Z. F. Ezawa, Phys. Rev. Lett. **82**, 3512 (1999).

[52] N. Kumada, A. Sawada, Z. F. Ezawa, S. Nagahama, H. Azuhata, K. Muraki, T. Saku, and Y. Hirayama, J. Phys. Soc. Jpn. **69**, 3178 (2000).

[53] D. Terasawa, M. Morino, K. Nakada, S. Kozumi, A. Sawada, Z. F. Ezawa, N. Kumada, K. Muraki, T. Saku, and Y. Hirayama, Physica. E **22**, 52 (2004).

[54] S. M. Girvin, arXiv:cond-mat/9907002v1 (1999).

[55] S. M. Girvin, Phys. Scripta **102**, 112 (2002).

[56] S. Q. Murphy, J. P. Eisenstein, G. S. Boebinger, L. N. Pfeiffer, and K. W. West, Phys.

Rev. Lett. **72**, 728 (1994).
[57] T. Nakajima and H. Aoki, *Theory of Interacting Electrons, vol. III Fractional Quantum Hall Effect*, (University of Tokyo Press, Tokyo, 1999).
[58] D. Yoshioka, *Quantum Hall effects* (Springer, Berlin, 2002).
[59] Z. F. Ezawa, *Quantum Hall effects: Field theoretical approach and related topics, Third Edition* (World Scientific, Singapore, 2013).
[60] *Perspectives in Quantum Hall Effects,* edited by S. Das Sarma and A. Pinczuk (Wiley, New york, 1997).
[61] K. Ishikawa, *Banoryoushirikigaku*, (BAIFUKAN CO.,LTD, Tokyo, 2006).
[62] Z. F. Ezawa and A. Iwazaki, Int. J. Mod. Phys. B **6**, 3205 (1992).
[63] Z. F. Ezawa and A. Iwazaki, Phys. Rev. B **47**, 7295 (1993).
[64] Z. F. Ezawa and A. Iwazaki, Phys. Rev. B **48**, 15189 (1993).
[65] X.-G. Wen and A. Zee, Phys. Rev. Lett. **69**, 1811 (1992).
[66] X.-G. Wen and A. Zee, Phys. Rev. B **47**, 2265 (1993).
[67] K. Yang, K. Moon, L. Belkhir, H. Mori, S. M. Girvin, A. H. MacDonald, L. Zheng, and D. Yoshioka, Phys. Rev. B **54**, 11644 (1996).
[68] J.P. Eisenstein and A.H. MacDonald, Nature **432**, 691 (2004).
[69] J. P. Eisenstein, arXiv:cond-mat/13060584v1 (2013).
[70] I. B. Spielman, J. P. Eisenstein, L. N. Pfeiffer, and K. W. West, Phys. Rev. Lett. **84**, 5808 (2000).
[71] L. Tiemann, W. Dietsche, M. Hauser, and K. von Klitzing, New. J. Phys. **10**, 045018 (2008).
[72] L. Tiemann, Y. Yoon, W. Dietsche, K. von Klitzing, and W. Wegscheider, Phys. Rev. B **80**, 165120 (2009).
[73] Y. Yoon, L. Tiemann, S. Schmult, W. Dietsche, K. von Klitzing, and W. Wegscheider Phys. Rev. Lett. **104**, 116802 (2010).
[74] M. Kellogg, J. P. Eisenstein, L. N. Pfeiffer, and K. W. West, Phys. Rev. Lett. **93**, 036801 (2004).
[75] E. Tutuc, M. Shayegan, and D. A. Huse, Phys. Rev. Lett. **93**, 036802 (2004).
[76] M. Kellogg, I. B. Spielman, J. P. Eisenstein, L. N. Pfeiffer, and K. W. West, Phys. Rev. Lett. **88**, 126804 (2002).
[77] A. R. Champagne, A. D. K. Finck, J. P. Eisenstein, L. N. Pfeiffer, and K. W. West, Phys. Rev. B **78**, 205310 (2008).
[78] Z. F. Ezawa, S. Suzuki and G. Tsitsishvili, Phys. Rev. B **76**, 045307 (2007).
[79] Z. F. Ezawa, G. Tsitsishvili, and A. Sawada, Eur. Phys. J. B **85**, 270 (2012).
[80] L. Zheng, R. J. Radtke, and S. Das Sarma, Phys. Rev. Lett. **78**, 2453 (1997).
[81] S. Das Sarma, S. Sachdev, and L. Zheng, Phys. Rev. B **58**, 4672 (1998).
[82] E. Demler and S. Das Sarma, Phys. Rev. Lett. **82**, 3895 (1999).
[83] K. Yang, Phys. Rev. B **60**, 15578 (1999).
[84] A. H. MacDonald, R. Rajaraman, and T. Jungwirth, Phys. Rev. B **60**, 8817 (1999).
[85] L. Brey, E. Demler, and S. Das Sarma, Phys. Rev. Lett. **83**, 168 (1999).
[86] J. Schliemann and A. H. MacDonald, Phys. Rev. Lett. **84**, 4437 (2000).

[87] M. F. Yang and M. C. Chang, Phys. Rev. B **61**, 2429(R) (2000).
[88] Y. Shimoda, T. Nakajima, and A. Sawada, Physica E **22**, 56 (2004).
[89] A. Lopatnikova, S. H. Simon, and E. Demler, Phys. Rev. B **70**, 115325 (2004).
[90] A. Lopatnikova, S. H. Simon, and E. Demler, Phys. Rev. B **70**, 115326 (2004).
[91] V. Pellegrini, A. Pinczuk, B. S. Dennis, A. S. Plaut, L. N. Pfeiffer, and K. W. West, Phys. Rev. Lett. **78**, 310 (1997).
[92] V. Pellegrini, A. Pinczuk, B. S. Dennis, A. S. Plaut, L. N. Pfeiffer, and K. W. West, Science **281**, 779 (1998).
[93] A. Sawada, Z. F. Ezawa, H. Ohno, Y. Horikoshi, Y. Ohno, S. Kishimoto, F. Matsukura, M. Yasumoto, and A. Urayama, Phys. Rev. Lett. **80**, 4534 (1998).
[94] A. Sawada, Z. F. Ezawa, H. Ohno, Y. Horikoshi, A. Urayama, Y. Ohno, S. Kishimoto, F. Matsukura, and N. Kumada, Phys. Rev. B **59**, 14888 (1999).
[95] V. S. Khrapai, E. V. Deviatov, A. A. Shashkin, V. T. Dolgopolov, F. Hastreiter, A. Wixforth, K. L. Campman, and A. C. Gossard, Phys. Rev. Lett. **84**, 725 (2000).
[96] S. J. Geer, A. G. Davies, C. H. W. Barnes, K. R. Zolleis, M. Y. Simmons, and D. A. Ritchie, Phys. Rev. B **66**, 045318 (2002).
[97] N. Kumada, D. Terasawa, M. Morino, K. Tagashira, A. Sawada, Z. F. Ezawa, K. Muraki, Y. Hirayama, and T. Saku, Phys. Rev. B **69**, 155319 (2004).
[98] A. Fukuda, A. Sawada, S. Kozumi, D. Terasawa, Y. Shimoda, and Z. F. Ezawa, N. Kumada, and Y. Hirayama, Phys. Rev. B **73**, 165304 (2006).
[99] K. Hasebe and Z. F. Ezawa, Phys. Rev. B **66**, 155318 (2002).
[100] K. Hasebe, Physics Letters A **319**, 544 (2003).
[101] Z. F. Ezawa and G. Tsitsishvili, Phys. Rev. B **70**, 125304 (2004).
[102] G. Tsitsishvili and Z. F. Ezawa, Phys. Rev. B **72**, 115306 (2005)
[103] Z. F. Ezawa and G. Tsitsishvili, Phys. Rev. D **72**, 085002 (2005).
[104] Z. F. Ezawa, M. Eliashvili and G. Tsitsishvili, Phys. Rev. B **71**, 125318 (2005).
[105] N. Kumada, K. Muraki, and Y. Hirayama, Science **313**, 329 (2006).
[106] N. Kumada, K. Muraki, and Y. Hirayama, Phys. Rev. Lett. **99**, 076805 (2007).
[107] M. H. Fauzi, S. Watanabe, and Y. Hirayama, Phys. Rev. B **90**, 235308 (2014).
[108] Y. Hama, Y. Hidaka, G. Tsitsishvili, and Z. F. Ezawa, Eur. Phys. J. B (2012) **85**: 368.
[109] Y. Hama, G. Tsitsishvili, and Z. F. Ezawa, Phys. Rev. B **87**, 104516 (2013).
[110] Y. Hama, G. Tsitsishvili, and Z. F. Ezawa, Prog. Theor. Exp. Phys, **2013**, 053I01.
[111] Y. Hama, Y. Hidaka, G. Tsitsishvili, and Z. F. Ezawa, Journal of Physics: Conference Series **456**, 012012 (2013).
[112] E. H. Hall, Am. J. Math **2**, 287 (1879).
[113] T. Ando, Y. Matsumoto, and Y. Uemura, J. Phys. Soc. Jpn. **39**, 279 (1975).
[114] K. v. Klitzing, G. Dorda, and M. Pepper, Phys. Rev. Lett. **45**, 494 (1980).
[115] D. C. Tsui, H. L. Stormer, and A. C. Gossard, Phys. Rev. Lett. **48**, 1559 (1982).
[116] R. B. Laughlin, Phys. Rev. B **23**, 5632(R) (1981).
[117] R. B. Laughlin, Phys. Rev. Lett. **50**, 1395 (1983).
[118] J. K. Jain, Phys. Rev. Lett. **63**, 199 (1989).
[119] R. E. Prange and S. M. Girvin (eds), *The Quantum Hall Effect* (Springer, New York,

1990) 2nd ed..
[120] B. I. Halperin, Phys. Rev. B **25**, 2185 (1982).
[121] D. J. Thouless, M. Kohmoto, M. P. Nightingale, and M. den Nijs, Phys. Rev. Lett. **49**, 405 (1982).
[122] D. J. Thouless, *Topological Quantum Numbers in Nonrelativistic Physics*, (World Scientific 1998).
[123] F. D. M. Haldane, Phys. Rev. Lett. **61**, 2015 (1988).
[124] K. Muraki, N. Kumada, T. Saku, and Y. Hirayama, Jpn. J. Appl. Phys. **39**, 2444 (2000).
[125] M. H. Fauzi, *Electron-Nuclear Spin Dynamics in a GaAs Two Dimensional System*, PhD. thesis (2013).
[126] A. A. Burkov and A. H. MacDonald, Phys. Rev. B **66**, 115320 (2002).
[127] S. M. Girvin and T. Jach, Phys. Rev. B **29**, 5617 (1984).
[128] S. M. Girvin, A. H. MacDonald, and P. M. Platzman, Phys. Rev. B **33**, 2481 (1986).
[129] D. B. Lichtenberg, *Unitary Symmetry and Elementary Particles*, (Academic Press, New York, 1978).
[130] S. R. Coleman, J. Wess, and B. Zumino, Phys. Rev. **177**, 2239 (1969).
[131] C. G. Callan, Jr., S. R. Coleman, J. Wess, and B. Zumino, Phys. Rev. **177**, 2247 (1969).
[132] S. Iso, D. Karabali, and B. Sakita, Phys. Lett. B **296**, 143 (1992).
[133] S. A. Parameswaran, R. Roy, and S. L. Sondhi, Phys. Rev. B **85**, 241308(R) (2012).
[134] Z. F. Ezawa, G. Tsitsishvili, and K. Hasebe, Phys. Rev. B **67**, 125314 (2003).
[135] J-J. Su and A. H. MacDonald, Nature. Physics **4**, 799 (2008).
[136] L. Tiemann, *Phase Coherence in the Regime of Bilayer Exciton Condensation*, PhD. thesis (2008).
[137] L. Tiemann, J. G. S. Lok, W. Dietsche, K. von Klitzing, K. Muraki, D. Schuh, and W. Wegscheider, Phys. Rev. B **77**, 033306 (2008).
[138] A. D. K. Finck, J. P. Eisenstein, L. N. Pfeiffer, and K. W. West, Phys. Rev. Lett. **106**, 236807 (2011).
[139] D. Nandi, A. D. K. Finck, J. P. Eisenstein, L. N. Pfeiffer, and K. W. West, Nature. **488**, 481 (2012).